UNIVERSITÀ DEGLI STUDI DI PALERMO

Dottorato di Ricerca in Biomedicina e Neuroscienze

Dipartimento di Biomedicina, Neuroscienze e Diagnostica avanzata (BiND)
SSD BIO/16

THE ROLE OF LIPIDS IN THE PATHOGENESIS OF NEUROHIV

LA CANDIDATA
Dott.ssa Daniela D'Amico

IL COORDINATORE
Chiar.mo Prof. Fabio Bucchieri

IL CO-TUTOR
Chiar.mo Prof. Eliseo Eugenin

LA TUTOR
Chiar.ma Prof.ssa Valentina Di Felice

CICLO XXXII
ANNO CONSEGUIMENTO TITOLO 2018/2019

Table of Contents

Page

Acknowledgments

It is my pleasure to acknowledge several people who were essential for the completion of my Italian Ph.D. research. First, I wish to thank Professor Fabio Bucchieri as the coordinator of the doctoral course and to all the committee members of the Biomedicine and Neuroscience Graduate Program, Department of Biomedicine, Neuroscience and advanced diagnostics, University of Palermo, Italy.

I wish to particularly thank Professor Eliseo Eugenin, Professor Brendan Prideaux and Professor Valentina Di Felice, as my thesis tutors and responsible for my research activity, for giving me the opportunity to perform my research activity in my Country at the Department of Biomedicine, Neuroscience and advanced diagnostics in Palermo (Unipa) before and in the United States at the Department of Neuroscience, Cell Biology, and Anatomy in Galveston (UTMB) later.

These acknowledgements would not be complete without mentioning all the Post Docs (Dr. Anna Maria Gorska, Dr. Silvana Valdebenito, Dr. Maribel Donoso, Dr. David Ajasin, and Dr. Matthias Holzlechner) in Dr. Eugenin's laboratory for being friends and supporting me during my research activity and in the realization of this work. I want also to thank Dr. Rosario Barone and Dr. Antonella Marino for providing me the scientific rigor when I was only an ungraduated student and for their precious scientific and personal advices.

A friendly thanks to my UTMB Italian research colleagues and my Unipa research colleagues, who were so close in encouragement.

Finally, I wish to express a deep gratefulness to the most important people in my life, that allow me to reach this important achievement, full of troubles but very satisfying. To my husband Gabriele for his inestimable presence, his daily love, his tireless patience and for his crazy attitude to come with me to Texas and assisting me in this amazing experience. To my family and my best friends, indispensable presence in my life, who were thousand kilometers far, but they have never made me feel alone.

List of Abbreviations

aWM - abnormal white matter

aCDase - acid ceramidase

aSMase - acid sphingomyelinase

AD - Alzheimer's disease

AH - aconitase

AP-1 - activator protein 1

AML - acute myeloid leukemia

AIDS - Acquired Immunodeficiency Syndrome

ADP - adenosine diphosphate

ATP - adenosine triphosphate

AGA - 18-α-glycerritenic acid

α-KG - α-ketoglutarate

9-AA - 9-aminoacridine

AA - arachidonic acid

ASL - arterial spin labeling

ANI - asymptomatic neurocognitive impairment

Bcl-2 - B cell Lymphoma 2 gene

BAX - Bcl-2-associated protein X

BBB - blood brain barrier

BOLD - MRI for blood oxygen level dependent imaging

BSA - bovine serum albumin

$cPLA_2$ - cytosolic phospholipases A2

CL - cardiolipin

cFLIP - cellular FLICE (FADD-like IL-1β-converting enzyme)-inhibitory protein

CNS - Central Nervous System

CHARTER - CNS HIV Antiretroviral Therapy Effects Research

Cer - ceramide

CGT - ceramide galactosyltransferase

Cer1-P - ceramide-1 phosphate

CerS - ceramide synthase

CERT - ceramide transfer protein

CSF - cerebrospinal fluid

CST - cerebroside sulfotransferase

CHO - choline

CCL5 - CC chemokine ligand 5

CCL2 - Monocyte Chemoattractant Protein-1

CS - citrate synthase

cART - combined AntiRetroviral Therapies

cDNA - complementary DNA

STORM - Stochastic Optical Resolution microscopy

Cx - connexin

Cr - creatine

COX - cyclooxygenase

CytC - Cytochrome C

DNA - deoxyribonucleic acid

DAG - diacyloglycerol

DAN - 1,5-diaminonaphthalene

DKK1 - dickkopf-1 protein

dhCer - dihydroceramide

DES - dihydroceramide desaturase

dihydroCS - (dihydro)ceramide synthase

dhSph - dihydrosphingosine

DHB - 2,5-dihydroxybenzoic acid

DA - dopamine

DAT - dopamine transporter

dsDNA - double stranded DNA

DMEM - Dulbecco's modified Eagle's medium

EP- E-prostanoid

ETC - electron transport chain

ER - endoplasmic reticulum

Env - envelope polyprotein

EAAT - excitatory amino acid transporter

ERK1/2 - Extracellular signal-regulated protein kinases 1 and 2

FADD - Fas-associated protein with death domain

FBS - fetal bovine serum

FAD - flavin adenine dinucleotide

FAPP2 - four-phosphate adaptor protein 2

FH - fumarate hydratase

fMRI - functional magnetic resonance imaging

FCCP - p-trifluoremethoxyphenylhydrazone

GMs - gangliosides

GJ - gap junction

GFAP - glial fibrillary acidic protein

Glut1 - glucose transporter-1

G6PDH - glucose-6-phosphate dehydrogenase

Glu - glutamate

GLX - glutamate-glutamine

GLUD - glutamate dehydrogenase

Gln - glutamine

GLS - glutaminase

GS - glutamine synthase

GSL - glycosphingolipid

GluCer - glucosylceramide

GTP - guanosine triphosphate

H&E - hematoxylin and eosin stain

HDL - high density lipoprotein

HDAC - histone deacetylases

HIV - Human Immunodeficiency Virus

HAD - HIV-associated dementia

HAND - HIV-associated neurocognitive disorders

HIVE - HIV encephalitic

H-MRS - proton-magnetic resonance spectroscopy

IPA - Ingenuity Pathway Analysis

ICAM5 - Intercellular adhesion molecule-5

IFN-α - Interferon Alpha

IP-10 - Interferon-γ-Inducible Protein

IL - interleukin

IP_3 - inositol triphosphate

INSTI - integrase strand transfer inhibitors

Iba-1 - ionized calcium-binding adapter molecule 1

IDH2/3 - isocitrate dehydrogenase

KGDHC - α-ketoglutarate dehydrogenase complex

3KdhSph - 3-keto-dihydrosphingosine

3KSR - 3-keto-dihydrosphingosine reductase

LRA - latency reversing agent

LO - leukotriene

LPS - lipopolysaccharide

LRP - lipoprotein receptor-related protein

LTR - long terminal repeat

LDL - low density lipoprotein

L-ser - L-serine

MSI - Mass spectrometry imaging

MDH - malate dehydrogenase

m/z - mass-to-charge

MALDI - matrix-assisted laser desorption/ionization

mRNA - messenger RNA

MND - mild neurocognitive disorder

p38MAPK - p38 mitogen-activated protein kinases

Mcl-1 - myeloid cell leukemia 1

MI - myoinositol

NMDA - N-methyl-d-aspartic acid

NAA - N-acetylaspartate

Nef - negative factor

nNOS - neuronal nitric oxide synthase

NAD - nicotinamide adenine dinucleotide

NNRTI - non-nucleoside reverse transcriptase inhibitor

NRM - norharmane

NF-κB - nuclear factor κB

NFAT - nuclear factor of activated T-cells

NPC - nuclear pore complex

NRTI - nucleoside reverse transcriptase inhibitor

NP - unphosphorylated isoform

ORF - open reding frames

OXPHOS - oxidative phosphorylation

OCR - oxygen consumption rate

PalmitylCoA - palmityl coenzyme A

PFA - Paraformaldehyde

PPP - pentose phosphate pathway

PBMCs - Peripheral Blood Mononuclear Cells

PMA - phorbol myristate acetate

PBS - Phosphate-buffered saline

PLC - Phospholipase-C

PA - phosphatidic acid

PC - phosphatidylcholine

PD - Parkinson’s disease

PE - phosphatidylethanolamine

PS - phosphatidylserine

PI - phosphatidylinositol

PG - phosphatidylglycerol

P1 - phosphorylated isoform

PHA - Phytohaemagglutinin

PET - positron emission tomography

PSD-95 - postsynaptic density protein-95

PIC - pre-integration complex

PGE_2 - prostaglandin E_2

PI - protease inhibitor

PUFA - polyunsaturated fatty acids

PKC - protein kinase C

PDH - pyruvate dehydrogenase

QVOA - Quantitative Viral Outgrowth Assay

qRT-PCR - quantitative Real Time- Polymerase Chain Reaction

Rev - regulator of expression of viral protein

rsfMRI - resting-state of functional MRI

RNA - ribonucleic acid

S - serine

SPT - serine palmitoyltransferase

SIV - Simian Immunodeficiency Virus

SPECT - single photon emission computer tomography

SM - sphingomyelin

SMase - Sphingomyelinases

Sph - sphingosine

SK - sphingosine kinase

S1P - sphingosine-1-phosphate

SCS - succinyl-CoA synthase

SDH - succinate dehydrogenase

TILDA - Tat/rev Induced Limiting Dilution Assay

TC - total cholesterol

TAR element - trans-activation response element

Tat - trans-activator of transcription protein

tRNA - transfer RNA

TCA - tricarboxylic acid

TBS - Tris Buffered Saline

TNF-α - Tumor Necrosis Factor Alpha

TNT - tunneling nanotube

uHPLC - ultra-high-performance liquid chromatography

uHCs - unopposed hemichannels

Vif - virion infectivity factor

Vpr - viral protein R

Vpu - viral protein U

ZO-1 - Zonula occludens-1

XPO1 - exportin 1

List of Figures

Chapter 1 **Page**

Chapter 2

Chapter 3

Chapter 4

Chapter 5

Chapter 6

Chapter 7

List of Tables

Page

Abstract

A critical comorbidity of HIV infection is HIV-associated neurocognitive disorders (HAND). Although combined antiretroviral therapy (cART) is an effective treatment in blocking systemic viral replication, it is unsuccessful in reducing the incidence of HAND. HIV CNS damage, in the current cART era, can be associated to the presence of latently HIV-infected cells including microglia/macrophages and a small population of astrocytes. This Ph.D. thesis focuses on identifying, localizing, and quantifying viral reservoirs using an improved staining and microscopy technique. Although in low amount, our data confirmed that microglia/macrophages and a small population of astrocytes are still infected. These cells synthetize and secrete viral proteins generating a bystander damage in the CNS. Viral proteins are also involved in lipid dysregulation. We demonstrated by Mass Spectrometry Imaging (MSI) that in the brain of HIV-infected individuals with HAND lipids including sulfatide play a key role in bystander damage. Sulfatide is dysregulated in several neurocognitive diseases such as Alzheimer's disease and Parkinson's disease. Thus, we propose that sulfatide as a potential biomarker of neurocognitive disorders.

We demonstrated that sulfatide secretion can be regulated by HIV proteins and we evaluated sulfatide effects *in vitro*, focusing on cell-to-cell communication and mitochondrial metabolism, all parameters altered in NeuroHIV.

Therefore, this thesis provides specific tools and unique data to a better understanding the neuropathogenesis of HAND in the current cART-era and may lead to the identification of new molecular targets for preventing or curing HIV neurological decline.

Chapter 1: General introduction

Part I – Human Immunodeficiency Virus

Epidemiology

Human Immunodeficiency Virus (HIV) is a major public health concern with 37.9 million infected individuals worldwide in 2018. 1.7 million people were newly infected, and 770,000 people died from AIDS-related illnesses (http://www.unaids.org/en/, 2019). In developed countries, 90% of individuals have access to combined antiretroviral therapy (cART) resulting in extended lifespan. Although clinically successful, cART is not a cure. Most ARTs are potent small molecules targeting entry, reverse transcriptase, protease maturation and integration steps of the HIV life cycle (Reeves and Piefer 2005), but not viral genome transcription and translation. Even though cART suppresses systemic virus replication, decreases the risk of transmission, and restores the immune competence, it cannot deplete circulating or tissue associated HIV reservoirs which remains one of the main obstacles for curing HIV infection (Vanhamel et al. 2019).

HIV classification

HIV was identified in 1983 (Barre-Sinoussi et al. 1983) and it was considered the causative agent of acquired immunodeficiency syndrome (AIDS), which was first diagnosed in 1981 in the USA (Gottlieb et al. 1981). It is accepted that the origin of HIV occurred by a cross-species adaptation, which started from simian immunodeficiency virus (SIV) infected monkeys and progressed to great apes and ultimately humans (Sharp and Hahn 2011). Two types of HIV have been identified, HIV-1 and HIV-2, with comparable structure, tropism and transmission pathophysiology. HIV-1 is more virulent, responsible of 95% infection worldwide. HIV-1 strains are subdivided into four groups: M, N, O, and P. The M group, or "Major" group, is the responsible for the global HIV epidemy. Within the group M, there are 9 genetically distinct and phylogenetically equidistant clades (A, B, C, D, F, G, H, J, and K) (Hemelaar 2012). From them, the clade C is globally dominant and responsible for approximately 50% of infections especially in South Africa and India (McCutchan 2006). On another hand, HIV-1 N group consists in a recombinant virus between two ancestral strains, one ancestor related to HIV-1 group M and one related to SIV chimpanzee strains found in Cameroon (Simon et al. 1998). This group is not so common in the global

population, and all the cases identified are from Cameroon (Mourez et al. 2013). The O group is present in the 1-2% of the population, especially in Cameroon and some European countries (Belgium, France and Spain) (Bush and Tebit 2015). The last group is the P group that accounts for just 0.06% of infection in the global population (Vallari et al. 2011). In contrast to HIV-1, HIV-2 is mostly asymptomatic, and predominately found in West Africa. HIV-2 can be classified into nine groups (A to I), which derive from 9 different cross-species transmission involving SIV (Marlink 1996). The groups A and B are the most common in the population, and the other seven groups account for just one patient each (Visseaux et al. 2016).

Time course of HIV infection

HIV transmission is principally due to sharing of biological fluids including mucosal and blood (Shaw and Hunter 2012). The progression of HIV infection can be divided into 4 phases: primary infection, acute infection, chronic or latent infection, and AIDS (Figure 1.1) (Coffin and Swanstrom 2013). As indicated in Figure 1.1, prior to infection, the normal $CD4^+$ T cell count is between 500 and 1500 cells/µl of blood. In the early stages of infection, plasma viremia increases and $CD4^+$ T cell count in the blood decreases. The subsequent acute phase (weeks 2-9) is therefore characterized by high levels of viral RNA in the blood ($>10^7$ copies of viral RNA/ml) and spreading of infection to susceptible tissues and organs. In this phase, the adaptive immune response induces the production of antibodies against HIV proteins (Cohen et al. 2011, Tomaras and Haynes 2009) and the $CD8^+$ cytotoxic T lymphocytes attach to productively infected $CD4^+$ T lymphocytes contributing to the CD4 count decrease (Jones and Walker 2016). Typically, people show flu-like symptoms, such as fever, headache, and rash. The following phase corresponds to the clinical latency that can last 2-12 years (Lemp et al. 1990, Moss and Bacchetti 1989), but in cART virally suppressed individuals, this period can be extended for years (Nakagawa et al. 2013). During this phase, plasma viremia is low or undetectable due to cART (~50 copies of HIV RNA/ml plasma) but $CD4^+$ T lymphocytes progressively decline due to chronic immune activation exhaustion and inflammation (Coffin and Swanstrom 2013). The last phase, that does not directly involve infected individuals under effective cART, is defined by $CD4^+$ T lymphocytes decline (<350 $CD4^+$ T cells/µl of blood) and

high viremia levels (>10^6 copies of viral RNA/ml plasma) causing the loss of the immune control and leading to opportunistic infections and cancers (Cribbs et al. 2019, McNally 2019, Shi et al. 2019). Therefore, the death of the HIV-infected population is mainly due to immunological disorders, opportunistic infections and aging related issues (Coffin and Swanstrom 2013).

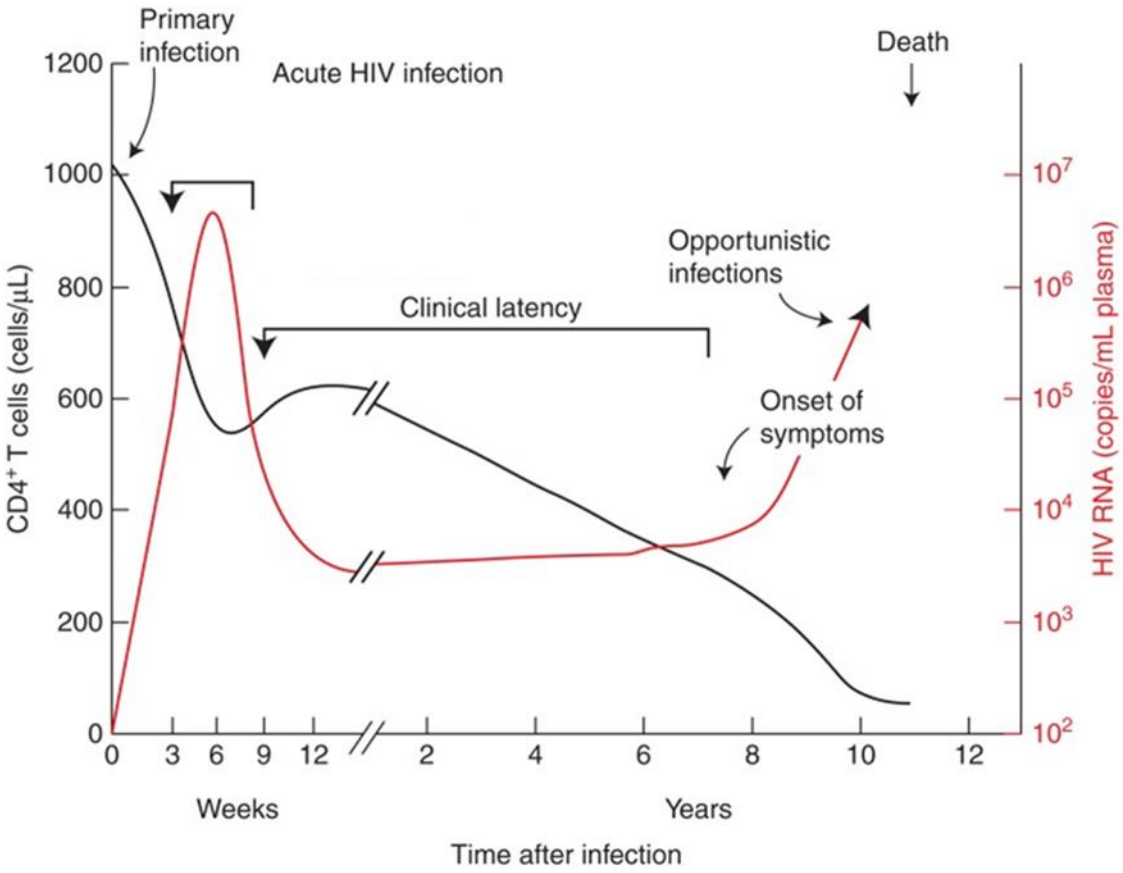

Figure 1.1. Clinic time-line of HIV-infection, replication, and CD4 counts in humans, adapted from (Fauci and Desrosiers 1997)

The black line represents the amount of $CD4^+$ cells in the blood, the red line shows the amount of HIV RNA copies in the plasma of HIV-infected individuals. Early after primary infection, viral replication increases and CD4 count decreases. These parameters also characterize the acute phase of infection with high levels of viral RNA in the plasma (>10^7 copies of viral RNA/ml) and decreased $CD4^+$ T cells, but with spreading of infection in the tissues. On another hand, the long clinical latency phase is characterized by low or undetectable plasma viremia and by a progressive reduction of $CD4^+$ T lymphocytes. In the last phase, $CD4^+$ T lymphocytes continue to decline, and plasma viremia rapidly increases causing opportunistic infections and cancers, leading to death.

HIV life cycle

HIV is a positive-sense single-stranded enveloped RNA virus. HIV is classified as a retrovirus and its RNA genome is structured in nine-open reding frames (ORF) (German Advisory Committee Blood 2016). Three major ORFs are retrovirus common: gag, pol and env; which encode for the polyprotein precursors of structural proteins. Specifically, gag encodes for a polyprotein cleaved to form 6 structural proteins: matrix protein p17, capsid proteins p24, p7 and p6, and two spacer peptides. The matrix protein p17 ensures capsid integrity, while p24, p7, p6 and the spacer peptides are essential for capsid assembly (Freed 1998). The pol ORF encodes for reverse transcriptase, integrase, and protease, which provide critical enzymatic functions. Reverse transcriptase transcribes viral RNA into double stranded cDNA, integrase modulates the insertion of viral cDNA into the host cell genome, instead, HIV protease is involved in the final maturation of the released virions after budding (Tekeste et al. 2015). The env gene encodes for the envelop protein gp160 which is proteolytical cleaved by furin to form gp120 and gp41, which are involved in the initial viral binding entry (Checkley et al. 2011). The other six ORFs of the HIV genome encode for regulatory and accessory proteins such as trans-activator of transcription protein (tat), regulator of expression of viral protein (rev), negative factor (nef), virion infectivity factor (vif), viral protein r (vpr) and viral protein u (vpu) (Karn and Stoltzfus 2012). Tat facilitates activation of viral transcription after integration, stabilizing the interaction between the RNA polymerase II and the viral integrated DNA, and phosphorylating the RNA polymerase II C-terminal domain inducing the elongation process. Rev and vpr regulate the transport. Nef, vif and vpu manipulate the host cell signaling and the immunity to attenuate immune surveillance (Freed and Mouland 2006, Turner and Summers 1999).

The HIV infection is initiated by the Env-mediated adhesion viral particles binding to host attachment factors present on the surface of targeted cells (heparan sulfate proteoglycans for macrophages, α4β7 integrin for T cells, and dendritic cell-specific intercellular adhesion molecule-3-grabbing non-integrin for dendritic cells), as well as by HIV envelop protein gp120 interacting with the CD4 receptor. Binding to CD4 induces a conformational change in gp120 that facilitates binding to co-receptor C-X-C chemokine receptor type 4 (CXCR4) or C-C chemokine receptor 5 (CCR5) (Kwong et al. 1998). After gp120 binding to CD4 and co-receptor, the envelop protein gp41 is exposed into the host lymphocytes

membrane and inserts into the outer leaflet to facilitate the fusion process between the host cell and virus (Freed et al. 1992, Shugars et al. 1996).

Once viral fusion with the host cell is completed, the HIV capsid containing two strands of viral RNA is deposited into the host cytoplasm to begin the process of reverse transcription (Campbell and Hope 2015). Reverse transcription is performed by reverse transcriptase that has two enzymatic activities, the DNA polymerase activity to copy either RNA or DNA template, and the RNase H that degrades RNA of the RNA–DNA duplex (Hu and Hughes 2012). Reverse transcription process induces the formation of double stranded DNA (dsDNA) with long terminal repeats (LTRs) sequences at the 5' and 3' ends. These repeats contain all the useful elements for gene expression (enhancer, promoter, transcription terminator, and polyadenylation signal), and they are also used as a substrate for HIV protein integrase which allow the HIV DNA insertion into the host cell genome (Klaver and Berkhout 1994). Specifically, the viral DNA made by reverse transcription within the cytoplasm is part of a large nucleoprotein complex, the pre-integration complex (PIC) (Bowerman et al. 1989), which allows crossing of the nuclear membrane through the nuclear pore complexes (NPCs). The nuclear import process is a crucial process in the establishment of infection and several viral proteins such as integrase, Vpr, Matrix, capsid, HIV-1 central DNA flap, and host importin proteins with host tRNAs are involved (Jayappa et al. 2012). In the nucleus, integrase catalyzes the reaction generating a hydroxyl nucleophile for DNA strand insertion in an LTR region adjacent to a cytosine-adenine (CA) dinucleotide sequence of the host genome (Roth et al. 1989). Later, the hydroxyl group cleaves the host cell DNA and become integrated following strand transfer and DNA repair (Engelman et al. 1991). The integration of HIV DNA into the host cell genome does not guarantee viral production. HIV integration is not random and preferentially occurs in host DNA areas with actively transcribed genes, gene-rich regions, intronic regions, and largely avoids promoter regions (Anderson E. M. and Maldarelli 2018). Therefore, the nuclear topography of HIV integration may impact HIV replication (Lusic et al. 2013). For instance, HIV pre-integrated complex preferentially targets those areas of open chromatin that are proximal to the nuclear pore, excluding the internal regions in the nucleus as well as the peripheral regions associated with the nuclear lamina. When HIV genome is transcribed by the host RNA polymerase II, the full-length (unspliced), singly spliced, and

multiply spliced RNAs are recognized by rev and transported to the cytoplasm by host exportin 1 (XPO1)-RanGTP nuclear export pathway (Dayton 2004, Mahboobi et al. 2015), where they can be translated in polyprotein precursors, regulatory and accessory proteins. Nevertheless, Gag and gag-pol polyproteins become localized to the cell membrane and the immature virion begins to bud from the cell surface to infect other cells (Sundquist and Krausslich 2012). This classical process of infection mediated by the virions is called "cell-free spread" (Figure 1.2). Recent studies recognized a more efficient and predominant spreading process called "cell-to-cell spread" (Martin et al. 2010), in which intercellular structures such as gap junctions (GJs) and tunneling nanotubes (TNTs) transfer ions, small molecules, organelles, as well as pathogens, between the connected cells (Ariazi et al. 2017, Bracq et al. 2018, Eugenin et al. 2009, Okafo et al. 2017). Part of this thesis also involved a detailed description of these communication systems in the contest of HIV spread (see Part II of General introduction).

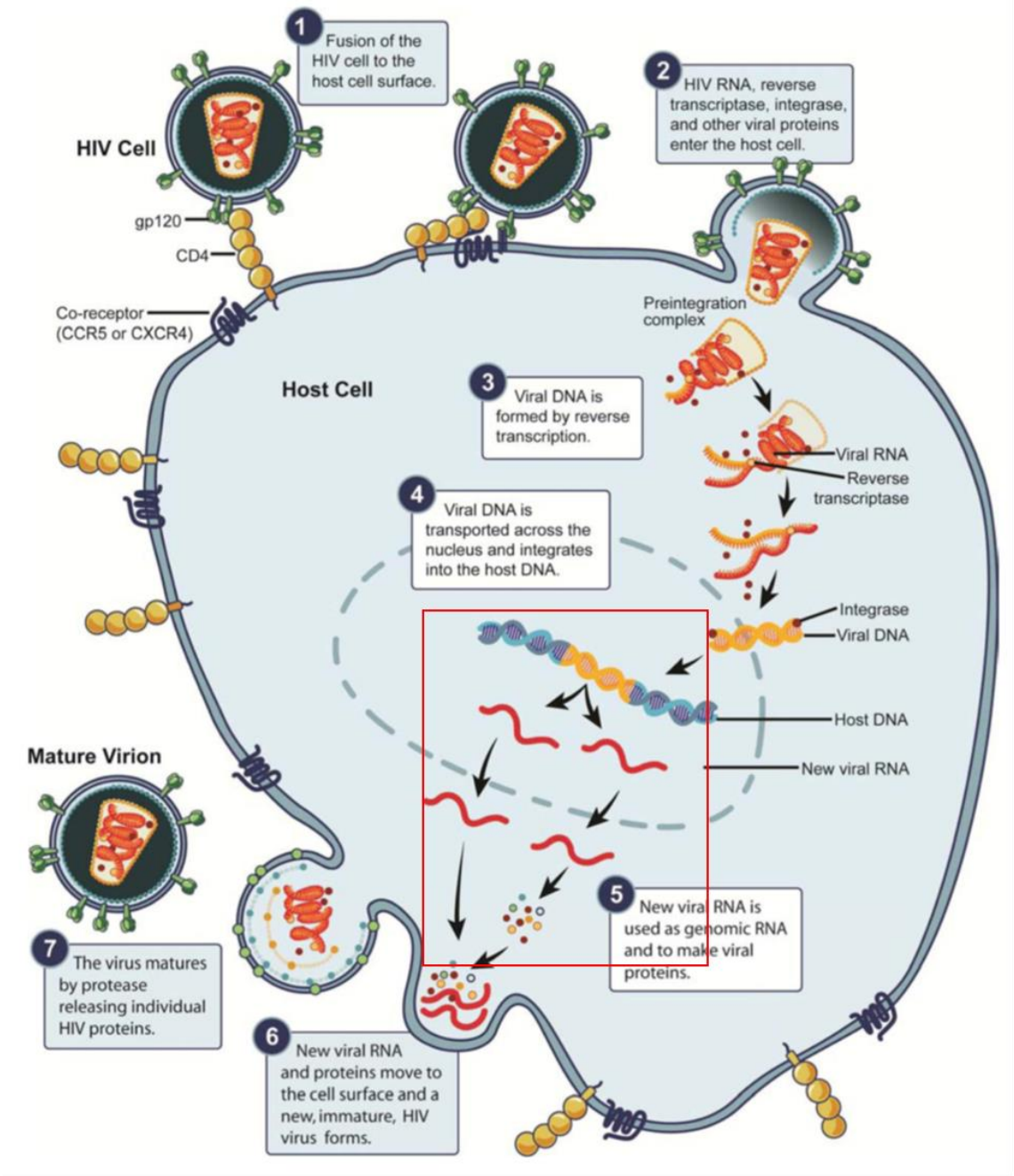

Figure 1.2. HIV life cycle adapted from (Pau and George 2014)

(1) Attachment. The HIV infection starts with the Env-mediated adhesion viral particles binding to host attachment factors present on the surface of targeted cells, as well as by HIV envelop protein gp120 interacting with the CD4 receptor and co-receptor (CXCR4 or CCR5), later gp41 inserts into the outer leaflet to facilitate the fusion between the HIV

envelop and the host plasma membranes. **(2) Fusion.** The viral genome, the pre-integration complex, and proteins from capsid such as p24 are released in the cytoplasm of the host cells. **(3) Reverse transcription.** It is performed by reverse transcriptase to convert HIV RNA into HIV dsDNA. **(4) Integration.** It is conducted by an intermediate PIC which includes reverse transcriptase and integrase to transport the HIV dsDNA into the nucleus to be integrated into the host genome. HIV begins to use the cell machinery to transcribe HIV mRNAs that are transported to the cytoplasm. **(5) HIV protein production.** This occurs in the cytoplasm, where HIV proteins are synthetized from viral mRNA. **(6) Assembly.** The new synthetized HIV proteins, as well as HIV RNA, accumulate and move to the host plasma membrane to generate immature virions. **(7) Budding.** Newly immature formed virions are released into the extracellular space. Protease induce the maturation of the virions to become infectious.

The red box in the figure indicates the topic of this thesis: HIV-integrated DNA, HIV mRNA production and HIV protein synthesis.

Antiretroviral therapies

The first anti-retroviral agent was introduced in 1987. Although, over 50% of patients treated with singular drug longer than 6 months develop the drug resistance (Larder et al. 1989). Currently, HIV-infected individuals use combined antiretroviral therapy (cART), which transformed HIV from a deadly to a chronic disease. The first combined treatment, which block the virus replication at the multiple stages of the HIV life cycle, was introduced in 1996 (https://www.niaid.nih.gov/diseases-conditions/antiretroviral-drug-development). Combined ART treatment consists in a combination of anti-retroviral drugs with the purpose of reducing the viral load, delaying disease progression and prolonging patient survival. The first therapy combinations commonly prescribed include a "backbone" of 2 inhibitors of the HIV reverse transcriptase (nucleoside reverse transcriptase inhibitor NRTI) plus a non-nucleoside reverse transcriptase inhibitor (NNRTI), an integrase strand transfer inhibitors (INSTI) or a protease inhibitor (PI) boosted with cobicistat or ritonavir (https://aidsinfo.nih.gov/understanding-hiv-aids/fact-sheets/21/53/what-to-start-choosing-an-hiv-regimen). Other new generated drugs include CCR5 antagonist, fusion inhibitor, and post-attachment inhibitor. The NRTIs are prodrugs that need to be activated into diphosphate or triphosphate metabolites. They inhibit the reverse transcriptase enzyme for the insertion of nucleotide analogue. NNRTs inactivate the reverse transcriptase enzyme inducing conformational change and they do not need intracellular phosphorylation to be active. The PIs block proteolytic activities necessary for the formation of mature infectious virions. The INSTIs work by preventing the integration of viral DNA into the host genome. In addition, the CCR5 antagonist and the fusion inhibitor obstruct the fusion process blocking the interaction of the HIV gp120 and the CCR5 receptor and avoiding conformational changes of gp41, respectively. The last class of drug is the post-attachment inhibitor or entry inhibitor that is a competitive inhibitor for the CD4 receptor. Together these drugs conform the cART targeting different steps of the viral replication, with the purpose of improving the $CD4^+$ T cell count, prolonging patient survival, and reducing the risk of transmission. However, cART is not able to eradicate HIV. Moreover, cART need to be administrated regularly and constantly because viral rebound occurs rapidly after treatment discontinuation (https://aidsinfo.nih.gov/guidelin, https://aidsinfo.nih.gov/understanding-hiv-aids/fact-sheets/21/58/fda-approved-hiv-

medicines). Even though cART blocks peripheral viral replication, cART does not prevent viral mRNA and protein expression. Thus, damage in the absence of viral production, is dependent on viral proteins.

HIV latency

Stable and productive HIV DNA integration is the most important aspect of HIV latency (Lafeuillade and Stevenson 2011). Thus, productively infected cells can become latently infected through viral silencing mechanisms that are still under investigation (Kim M. et al. 2014, Mok and Lever 2007). Several transcriptional and post-transcriptional molecular mechanisms have been proposed (Bruner et al. 2016, Hiener et al. 2017). Post-integration latency can be dependent on histone deacetylases (HDACs) (Margolis 2011) and methyl-CpG-binding proteins which form complexes with HDACs (Bednarik et al. 1990) promoting chromatin condensation and HIV silencing. Other mechanisms involve the regulation of the essential Tat-cofactor P-TEFb (Kim Y. K. et al. 2011), NF-κB (nuclear factor κB) and NFAT (nuclear factor of activated T-cells) (Mbonye and Karn 2014) characterized by occlusion of transcription initiation or elongation complexes. For example, the elongation process requires P-TEFb that is recruited by Tat (Mbonye and Karn 2014). On another hand, a post-transcriptional mechanism involves microRNAs that regulate the levels of cyclin T1 protein, which is essential for T cell activation and viral replication (Chiang et al. 2012).

Recent studies have proposed a new therapeutic approach based on the reactivation of latently-infected reservoirs by small molecules, called latency reversing agents (LRAs) that reactivate the virus stimulating the immune system with the goal of killing the viral reservoirs. This is called “shock and kill” strategy (Petravic et al. 2017, Schwartz et al. 2017). The several LRAs proposed include drugs that induce NF-κB pathway activation, extra-terminal domain inhibitors enhancing the binding of the viral Tat protein to the HIV TAR element, and histone deacetylase inhibitors (HDACi-SAHA) that work as epigenetic modifiers, or a combination of them (Sadowski and Hashemi 2019). Moreover, current detection methods for viral reservoirs also use viral reactivators such as Phytohaemagglutinin (PHA) and phorbol myristate acetate (PMA) that block the binding of IκBα to NF-κB that can translocate to the nucleus and activate transcription (Chauhan

2015). Although several groups focus primarily on LRAs or several stimulators to induce HIV reactivation, they are unable to reactivate all the integrated viruses, suggesting that there is a gap between the signals required for reactivation of some viruses, depending on where they are integrated, degree of epigenetic modulation and specific respond to different stimuli to induce reactivation.

Viral reservoirs

As discussed above, HIV remains incurable due to the early viral seeding and generation of latent-infected cells. Viral reservoirs are defined as a cell type in which a replication-competent form of HIV persists. HIV reservoirs are long-lived infected cells due to their slow decay rate ($t_{1/2}$=3.7 years) (Siliciano et al. 2003). Thus, the virus remains integrated in the host genome and it can be reactivated. The transient increase in plasma HIV RNA called blips, which are common in HIV patients under cART and there are typically related to viral rebound (Grennan et al. 2012). This stochastic reactivation of viral reservoirs is probably due to gaps in circulating concentration, toxicity or discontinuation of cART regimen.

Currently, the best described viral reservoirs are resting $CD4^+$ T lymphocytes including central memory T cells, transitional T cells, effector T cells, and naïve T cells (Stein et al. 2016). However, other viral reservoirs are also described in circulation and in tissues such as peripheral blood monocytes, dendritic cells, macrophages (such as microglial), astrocytes and other myeloid cells (Castellano et al. 2017, Eugenin et al. 2011, Ganor et al. 2019, Mitchell et al. 2019). The mechanism by which T cells survive and become latent has been investigated by the Siliciano group, creating a CD4 cell line transduced with the B cell Lymphoma 2 gene (Bcl-2) (Yang et al. 2009). Bcl-2 are pro-apoptotic members that regulate the mitochondrial outer membrane pore formation inducing apoptosis. Siliciano group showed that the Bcl-2 cell line survive infection and later are able to revert to the latent state, suggesting that Bcl-2 pathway can explain the survival mechanism of these viral reservoirs (Kim M. et al. 2014). However, there is no evidence that Bcl-2 can contribute to the latent stage since distinct cell types react differently after infection with HIV. Other mechanisms of cell survival are associated with other upregulated anti-apoptotic proteins such as cFLIP and Mcl-1 or downregulated pro-apoptotic proteins such

as BAX and FADD (Timilsina and Gaur 2016), suggesting that blocking apoptosis contributes to viral reservoir survival.

On another hand, data in our laboratory demonstrated that macrophage survival in response to HIV infection has a metabolic and an anti-apoptotic component. Latent macrophages show mitochondrial fusion, lipid accumulation, and reduced mitochondrial ATP production and use glutamine/glutamate as a primary energy source (Castellano et al. 2019). Therefore, it's necessary to enlighten on the importance of myeloid cells as viral reservoirs. Two critical cases are the "Berlin Patient" and the "Mississippi baby", which can demonstrate the effective role of the myeloid cells in HIV infection. The first one achieved viral remission after a bone marrow transplant with stem cells from a donor who was homozygous for CCR5 delta32 used to cure acute myeloid leukemia (AML) (Hutter et al. 2009). In the case of the "Mississippi baby" after an early administration of ART (30 hours after birth), plasma viremia was undetectable without cART, suggesting a crucial role of the myeloid reservoirs to viral persistence in the earliest stage of infection (Persaud et al. 2013). Several strategies have been proposed to study and target myeloid reservoirs, using the shock and kill mechanism with HDACi or protein kinase C activator, or using cell transplant and gene therapy to modify CCR5 in myeloid compartments (Mitchell et al. 2019).

Current methods to detect viral reservoirs

The current methods to detect viral reservoirs are not able to precisely measure their size and the cell type involved. Currently, most viral reservoirs are detected in blood, but they are a poor representation of viral reservoirs in tissues. Quantitative Viral Outgrowth Assay (QVOA), Tat/rev Induced Limiting Dilution Assay (TILDA) and other Quantitative PCR assays for total HIV RNA or HIV DNA are frequently used to detect viral reservoirs. QVOA is a cultured based assay that identifies reservoir in circulating cells (Finzi et al. 1997). TILDA is a PCR-based assay that measure the frequency of cells harboring HIV-integrated genomes. Other PCR-based methods can also measure the frequency of cells harboring HIV-integrated and unintegrated DNA. QVOA is performed in the blood $CD4^+$ T lymphocytes which are stimulated with phytohemagglutinin (PHA) in the presence of irradiated allogeneic peripheral blood mononuclear cells (PBMCs) that induces global T

cell activation of HIV-integrated genomes. The replication of the virus is detected by HIV-p24 ELISA on the media of 2-3 week cultures combined with $CD4^+$ lymphoblasts from HIV-negative donors (Finzi et al. 1997). Instead, TILDA measures the frequency of cells harboring viral genomes that produce tat/rev multiply-spliced HIV RNA upon maximal stimulation. It also needs isolation of the total $CD4^+$ T lymphocytes that are stimulated with PMA and ionomycin for 12 hours to induce the maximal production of tat/rev RNA and later the qRT-PCR is used to quantify tat/rev transcripts. TILDA requires 10 ml of blood and can be completed in 2-3 days (Procopio et al. 2015). Other PCR-based techniques PCR assays such as digital droplet PCR for total HIV DNA/RNA or integrated HIV sequences (Alu or 2LTR) can be used to quantify HIV DNA or RNA in PBMCs, in purified $CD4^+$ T cells or in plasma. They are expensive, use a large amount of starting materials and time consuming, as well as overestimate the size of the latent reservoirs (Eriksson et al. 2013).
Overall, QVOA, TILDA, and other PCR-based techniques have enormous limitations such as timing, cost, accuracy, precision, sensitivity and use of a large volume of blood. Additionally, they detect just one component of viral cell cycle and are limited to only circulating viral reservoirs. Generally, they can misinterpret the data and incorrectly estimate the replication-competent viruses within the circulating and tissue reservoirs (Churchill et al. 2016).

Recently, Dr. Eugenin's laboratory generated a highly sensitive and innovative protocol that is specific for viral DNA, viral RNA, several viral proteins and characterizes circulating and tissue-associated viral reservoirs in HIV-infected individuals (Prevedel et al. 2019). This technique is based on improved staining and confocal microscopy analysis. It determines the stage of the viral life cycle detecting, quantifying, and localizing concurrently HIV DNA, HIV mRNA, HIV proteins and host cell markers *in vitro* and *in vivo* (Prevedel et al. 2019). HIV reservoir identification and localization are necessary to study the mechanism of bystander damage and to find new molecular targets for HIV efficacious treatments. Our laboratory has developed techniques to identify viral reservoirs in urethral tissue (Ganor et al. 2019) and in other human tissues such as bone marrow (Real F. et al. in press). In this thesis, we present data about localization, identification, and quantification of viral reservoirs in brain and lymph nodes in Chapter 2.

Part II – HIV in CNS

HIV CNS infection

HIV-infection of the Central Nervous System (CNS) arises very early after primary infection (15 days). It is accepted that HIV transmigration into the brain occurs by the "Trojan Horse" mechanism (Hazleton et al. 2010). Briefly, circulating HIV-infected monocytes, specifically $CD14^{+}CD16^{+}$ intermediate monocytes, cross the Blood Brain Barrier (BBB) in response to chemotactic signals as such CCL2 and CXCL12 (Eugenin et al. 2006, Williams et al. 2012). The high sensitivity of HIV-infected cells to sense these chemokines is due to enhanced capacity of HIV-infected cells to sense physiological chemokine gradients such as CCL2 (Eugenin et al. 2006). During the process of transmigration of HIV-infected cells in response to CCL2, the BBB become compromised further contributing to local inflammation. In the CNS, migrated HIV-infected monocytes infect local resident cells such as microglia, perivascular macrophages and a small population of astrocytes (Williams et al. 2014). In particular, microglial cells and perivascular macrophages are the major productively infected cells by HIV (Cosenza et al. 2002). On the contrary, astrocytes support a low viral replication. Astrocytes are CD4 negative cells and they are infected by HIV using a mannose receptor that mediates vesicle endocytosis from the membrane that have to also avoid endolysosomal destruction, or via viral synapses using cell-to-cell contacts with infected lymphocytes (Do et al. 2014, Galloway et al. 2015, Liu Y. et al. 2004).

During active CNS infection, formation of multinucleated giant cells and neuronal and glial cell death were common in infected individuals in the pre-ART-era. However, upon cART introduction, damage still occurs but is more controlled.

Viral reservoirs within the CNS

During the acute phase of HIV, infection of human microglia/macrophages and astrocytes results in inflammation due to the release of cytokines and chemokines, finishing in a massive apoptosis (Castellano et al. 2017). However, a small population of HIV-infected cells survive and become latently infected (Castellano et al. 2017, Eugenin and Berman 2007, 2013, Eugenin et al. 2011, Orellana et al. 2014). Macrophages/microglia are the

primary CNS target of HIV (Wong and Yukl 2016). It was shown that uninfected macrophages derived from recently transmigrated monocytes die in few days (Bellingan et al. 1996), whereas microglia, perivascular, and alveolar macrophages have an long half-life (months-years) (Lassmann and Hickey 1993). Latently HIV-infected macrophages are terminally differentiated and non-dividing cells that derive from circulating monocytes residing in all tissues. They are able to survive HIV infection principally due to metabolic alterations and apoptosis inhibition (Castellano et al. 2017, Castellano et al. 2019). In latently HIV-infected microglia/macrophages the pro- and anti-apoptotic pathways are blocked and Bim that is a highly pro-apoptotic negative regulator of Bcl-2 is upregulated and recruited into the mitochondria preventing apoptosis (Castellano et al. 2017). Thus, the mechanism of survival is different than $CD4^+$ T cells mediated by Bcl-2 (Kim M. et al. 2014).

In macroglia/macrophage reservoirs, the mitochondria become larger and show lipid accumulation and produce less ATP for the compromised metabolic steps in the tricarboxylic acid (TCA) cycle preceding oxidative phosphorylation (OXPHOS). While HIV-infected macrophages use fatty acids and glucose as primary sources of energy as well as the uninfected cells, they also use glutamine/glutamate and alpha-ketoglutarate (αKG) as an alternative energy supply (Castellano et al. 2019). Otherwise, latently HIV-infected astrocytes survival is principally due to cytochrome C mislocalization from the mitochondria to the cytoplasm and for the following alterations in inositol triphosphate (IP_3), IP_3 receptors and calcium that block the formation of the apoptosome (Figure 1.3) (Eugenin and Berman 2013). Despite the fact that only a small fraction of astrocytes become infected, they induce bystander apoptosis of neighboring cells through cell-to-cell mechanism (Eugenin and Berman 2007, Eugenin et al. 2011). Thus, macrophages and astrocytes have different survival mechanisms than $CD4^+$ T cells. Moreover, HIV envelope sequencing studies from blood, brain and other non-brain tissues such as bone marrow, colon, lung and liver showed an HIV macrophage tropism with a different HIV compartmentalization and evolution within the blood and the tissues (Holman et al. 2010), suggesting that viral reservoirs are different in each compartment.

Data showed in this thesis demonstrate the adaptation of glial networks to limited HIV infection. Briefly, we have shown that HIV-infected astrocytes prefer an alternative source

of energy independent from mitochondria such as pentose phosphate (see details in Chapter 6).

Novel mechanism of bystander CNS damage in the current cART-era

HIV-associated neurocognitive disorders (HAND) are present in around 50% of HIV-infected individuals of the post cART-era. CNS damage was identified in 90% of autopsied brains from HIV-infected patients displaying chronic neuroinflammation and neurocognitive impairment even after they received cART for many years (Lamers et al. 2016). Moreover, HAND can be exacerbated by HIV-related infections, cART-related toxicities, cART discontinuation and comorbidities (alcohol and substance of abuse) (Byrd et al. 2011, Justice et al. 2010, Tedaldi et al. 2015). According to the severity of the clinical manifestations, HAND are divided in asymptomatic neurocognitive impairment (ANI), mild neurocognitive disorder (MND), and HIV-associated dementia (HAD) (Antinori et al. 2007). In the post-cART era, the proportion of HIV-infected individuals with neurocognitive symptoms is the same of the pre-cART era, but the percentage of infected patients with HAD has decreased in favor of ANI and MND (Heaton et al. 2010, Saylor et al. 2016). The symptoms displayed in the milder forms of HAND include memory loss, problems in concentration, difficulty learning new tasks, diminished reflexes, personality changes, and mood swing. Instead, people diagnosed with HAD have severe memory and concentration problems, wild mood swings, symptoms of psychosis and loss of physical coordination (Eggers et al. 2017).

Nowadays, the diagnosis and the monitoring of HAND is based on neuropsychometric performance tests, blood tests, CSF analysis, and neuroimaging (Clifford and Ances 2013). These techniques may provide metabolic and structural alteration in the blood and in the brain. However, techniques to identify viral reservoirs are lacking. In Chapter 2, we will describe a novel method to identify, localize, and quantify viral reservoirs in circulation and in tissues. In addition, in Chapter 4, we will show new potential biomarkers of HAND. Later, we will discuss the bystander effect of viral proteins and lipids.

Our laboratory identified that viral reservoirs can promote a bystander damage into neighboring cells *via* GJs mediated mechanism. Gap junctions are expressed in most cell types of the nervous system, including astrocytes, neurons, oligodendrocytes, neuronal

stem cells, endothelial cells, and under inflammatory conditions in microglia/macrophages (Eugenin et al. 2012, Kielian 2008, Palacios-Prado et al. 2013, Vejar et al. 2019). Gap junctions are low-resistance bridges that perform electrical and metabolic functions, connecting the cytoplasm of adjacent cells and allowing the exchange of electrical signals and intracellular messengers, such as IP_3, calcium, cyclic nucleotides, metabolites, neurotransmitters, and viral peptides (Yeager and Nicholson 1996). Gap junctions consist in connexin (Cx) dodecamer channels formed of two hexameric unopposed hemichannels (uHCs), one from each of the coupled cells (Harris A. L. 2001). Connexin-containing uHCs are defined homomeric when 6 monomers of Cx that compose it are the same, or heteromeric when the Cxs are different. Gap junctions can be docked by two identical (homotypic) or different (heterotypic) subunits of HCs. Homo- and hetero-combinations generate channels with different biophysical properties and permeability (Harris A. L. 2007). Hemichannels and GJ channels have an internal pore of approximately 12 A° enabling the diffusion of molecules up of 1.2 kDa (Villanelo et al. 2017). The role of HCs and GJs in HIV infection has acquired an increased interest. Although uHCs exist physiologically in a closed state, HIV infection is one of the few cases where uHCs become opened enabling the release of pro-apoptotic and pro-inflammatory factors such as prostaglandin E_2 (PGE_2) and adenosine-triphosphate (ATP) in the extracellular space (Eugenin 2014). For instance, in HIV-infected astrocytes the opened Cx43 containing uHCs led the secretion of dickkopf-1 protein (DKK1) that is a soluble Wnt pathway inhibitor. It has been shown in neuron and astrocyte mixed cultures treated with DKK1 resulted in a significant collapse of neuronal processes (Orellana et al. 2014). Thus, it can explain the synaptic compromise observed in HIV-infected individuals. On another hand, GJs that are regulated in order to control synaptic function, after HIV infection they are permanently open and used by the virus to spread and maintain infection in the CNS. Specifically HIV reservoirs mediate bystander damage into the neighboring cells *via* Connexin-43 (Cx43) containing GJs and uHCs (Malik et al. 2017). To prove GJs crucial role in CNS damage, the Cx43-GJ blockers 18-α-glycerritenic acid (AGA) or octanol were used to treat HIV-infected astrocyte cultures resulting in decreased level of apoptosis in the neighboring HIV-uninfected cells (Eugenin and Berman 2007). In addition, bystander apoptosis was related to inositol trisphosphate and intracellular calcium (Figure 1.3) and to

endothelial apoptosis, dysregulation of lipoxygenase/cyclooxygenase, BK calcium channels, and ATP receptor activation within astrocytes (Eugenin and Berman 2013). Recently it was demonstrated that HIV Tat protein enhances Cx43 expression in primary human astrocytes to maintain communication between the few HIV-infected cells and surrounding uninfected cells suggesting a critical link between HIV proteins, commonly present in the brain of virally-suppressed infected individuals, and cell-to-cell communication (Malik et al. 2017). To conclude, we can remark that HIV reservoirs used a different way to survive to infection and to generate bystander effect on the neighboring uninfected cells. Several of these communication systems will be discussed in Chapter 6.

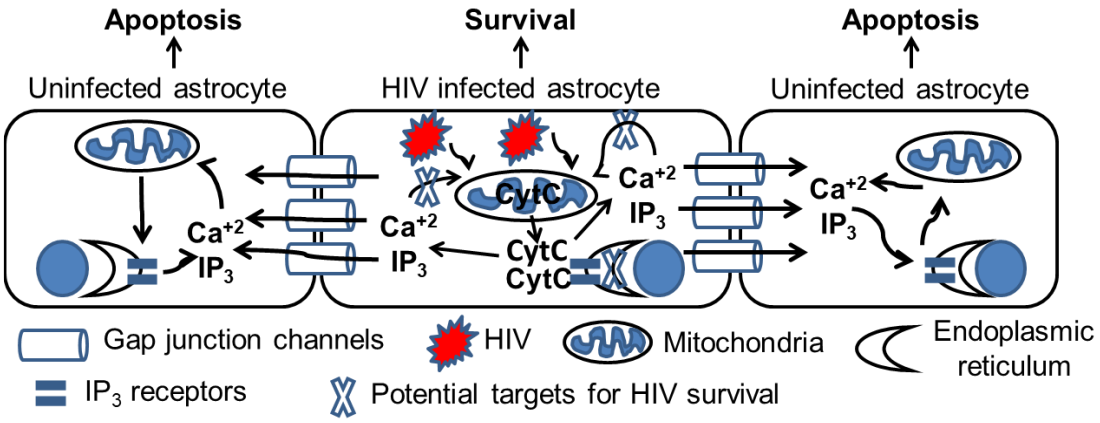

Figure 1.3. Proposed model of HIV-infected astrocytes for survival and bystander damage mediated by Cx43 containing GJs, from (Eugenin and Berman 2013)

HIV-infected astrocyte survives to apoptosis for cytochrome c secretion in the cytoplasm that blocks the apoptosome formation and increases IP_3 and intracellular calcium concentration. IP_3 and calcium can diffuse into the neighboring cells through Cx43 containing GJs and induce apoptosis.

Neuroimaging used to diagnose and monitor HAND in the current cART-era

Neuroimaging includes the use of different techniques that directly or indirectly image metabolic, structural, and functional changes of the brain. They can be partially useful to generate a diagnosis and to monitor the clinical course of HAND (Clifford and Ances 2013). The more common techniques for metabolic imaging are proton-magnetic resonance spectroscopy (H-MRS or MRS), positron emission tomography (PET), and single photon emission computer tomography (SPECT). H-MRS is a non-invasive technique that gives information on brain pathophysiology measuring signals from hydrogen atoms of specific brain metabolites, such as N-acetylaspartate (NAA), myoinositol (MI), choline (CHO), and glutamate-glutamine (GLX) (Van Zijl and Barker 1997). N-acetylaspartate is a neuronal functional marker and it is synthesized as a result of the reaction between aspartate and acetyl coenzyme A (Baslow 2003). Myoinositol is an astrocyte marker associated with inflammation, astrocytosis and gliosis (Harris J. L. et al. 2015). Choline is a cell membrane marker that specifically represents the membrane lipid turnover and reflects macrophage infiltration and inflammation (Lin et al. 2005). Glutamate (Glu) is the major excitatory neurotransmitter in the brain, stored as glutamine (Gln) in glial cells. Glutamate-glutamine balance cycling is essential for normal functioning of brain cells. Astrocytes are responsible for uptake of most extracellular glutamate *via* glutamate transporters GLT1 (or EAAT1) and GLAST (or EAAT2), in order to maintain Glu extracellular concentration and avoid excitotoxicity (Schousboe and Waagepetersen 2005). In MRS the magnet strength is not always sufficient to resolve Glu from Gln and in some cases they are combined as GLX (Ramadan et al. 2013). Moreover, some MRS data are expressed as a ratio of the specific metabolites compared to creatine (Cr) that is a reference marker (Vigneswaran et al. 2015). The most common MRS features in HIV seropositive population are increased levels of CHO and MI that suggest inflammation and microglial proliferation, and decreased levels of NAA and GLX that are related to neuronal-axonal injury or dysfunction (Mohamed M. A. et al. 2010). During HIV infection, MRS is also used to monitor changes in brain inflammation and neuronal integrity associated with cART effects. The biggest limit of MRS is that the results of the analysis are restricted to certain brain regions. During acute HIV infection, brain

metabolites have been measured in frontal grey and white matter, in the occipital grey matter, and in basal ganglia. Elevated levels of CHO/CR in the basal ganglia and in the occipital grey matter of acute HIV cases (14 days after HIV infection) were detected compared to uninfected controls, as well as chronic HIV subjects. These values became normal after 6 months of cART (Sailasuta et al. 2012). Moreover, the levels of Cho/Cr, NAA/Cr, Glu/Cr and MI/Cr have been shown to be increased in frontal white matter, in parietal grey matter and in basal ganglia, but after cART initiation their excitotoxicity and neuronal injury effect were attenuated (Young et al. 2014). In addition, the relationship between HIV-cognitive impairment and brain metabolism was investigated in older HIV-infected individuals under cART and it was shown that NAA and Glu were lower and correlated with worse performance on neuropsychological tests in MND or HAD individuals (Mohamed M. et al. 2018). Although, MRS can detect several brain metabolites only one study mentions the possibility to detect lipid molecules (Bairwa et al. 2016), without identifying either the class or their specific alteration.

Other techniques that can be applied for metabolic investigation in HIV pathology are PET and SPECT. Positron emission tomography (PET) and single photon emission computed tomography (SPECT) were used to study HIV patients with or without HAND. PET and SPECT are used to evaluate glucose metabolism or cerebral perfusion applying nuclear medicine tracers (^{18}F-deoxyglucose - ^{99}Tc-HMPAO) that specifically bind to a positron-emitting radioisotope, such as 18fluorine (^{18}F) or 11carbon (^{11}C) (Sathekge et al. 2014). Decreased glucose metabolism in the frontal cortex detected by PET in HIV seropositive patients may reflect neuronal injury or dysfunction (Andersen et al. 2010). PET imaging is also used to assess dopamine (DA) function in HIV-infected patients, because HIV-infected patients with HAND often present psychomotor slowing and parkinsonian symptoms. For this particular technique, (^{11}C)-cocaine and (^{11}C)-raclopride are used to measure presynaptic dopaminergic transporter and postsynaptic D2 dopaminergic receptor, respectively. These tracers demonstrated lower levels of dopamine transporters (DAT) that are associated with dopaminergic neuronal injury especially in HIV-positive patients with HAD (Wang et al. 2004) and worst neurocognitive performance (Chang et al. 2008). Likewise, SPECT is utilized to put in evidence the central dysfunction of the dopaminergic pathways in HIV infection and ^{123}I-FP-CIT and ^{123}I-IBZM are the trackers used for these

analyses (Scheller et al. 2010). Current studies are focusing on the development of radiotracers ((^{11}C)PK11195, (^{11}C)PBR18, (^{11}C)DPA-713, and (^{11}C)PBR28) specific for microglia in order to quantify and localize brain inflammation in HIV-infected patients (Chang and Shukla 2018, Hammoud et al. 2005).

For the structural neuroimaging, two techniques have been applied to HAND investigation: volumetric analysis and diffusion tensor imaging. Structural neuroimaging involves brain tissue contrast that is based on differences in proton density and relaxation times amongst brain structures (Ashburner and Friston 2000, Good et al. 2001, Sanford et al. 2017). The measurement of cortical and subcortical grey matter and total and abnormal white matter (aWM) volumes showed that HAD and MND patients had smaller grey and white matter volumes and more aWM than neurocognitively unpaired patients (Alakkas et al. 2019). On the other hand, diffusion tensor imaging is an MRI-based neuroimaging technique used for the detection of microarchitectural changes. Using this technique, microstructural disruptions were localized especially in the frontal and motor white-matter regions of the HIV-infected individuals (Wright et al. 2012).

Currently, functional neuroimaging techniques include magnetic resonance imaging (MRI) for blood oxygen level dependent imaging (BOLD) and perfusion. BOLD fMRI signal investigates the ratio of oxygenated to deoxygenated hemoglobin in the microvasculature. Although, HIV regional injury can be associated with a partial dysfunction of the brain networks, BOLD task-activated fMRI and resting-state fMRI (rsfMRI) are used to evaluate functional networks (Fox and Raichle 2007). For instance, HIV seropositive patients showed a selective activation for networks involving attention, working memory, and hippocampal function (Chang et al. 2001), as well as risky choices (Connolly et al. 2014). On another hand, rsfMRI showed lesser connectivity within frontostriatal, salience, frontal, motor, and executive networks and within precuneus seed and prefrontal cortex in HAND population, suggesting a compromised brain activity (Ann et al. 2016, Chaganti et al. 2017). Perfusion MRI is another functional method using arterial spin labeling (ASL) technique to measure the proton spins associated to endogenous oxyhemoglobin and deoxyhemoglobin for calculating the arterial function. Using ASL low levels of cerebral blood flow were demonstrated in HIV seropositive population that can be partially restored after cART (Ances et al. 2009).

Together all these neuroimaging techniques are useful to assess HAND onset and progression, but better markers in term of prediction and selectivity are required. Several of these neuroimaging techniques can also measure different species of lipids, but most of these data has been ignored. In this thesis, we study lipid metabolic alteration in the brain of HIV-infected patients and correlate them with neurocognitive impairments in order to find a specific biomarker that can be predictive of the risk to develop HAND.

Brain volume changes and localized damage in HAND in the current cART-era

Neuroimaging data have shown that volumetric changes involve the brain of HIV-infected patients virally suppressed with cART (Alakkas et al. 2019). By diffusion tensor imaging it was demonstrated that white matter deficits comprise dramatic thinning of the corpus callosum, reduction in blood flow to white matter, loss of structural integrity and volume in white matter structures such as the superior longitudinal fasciculus, superior corona radiata, and the internal capsule (Correa et al. 2015, Leite et al. 2013). A recent CHARTER study used structural MRI to determine reduced white matter volume in HIV-infected individuals with HAD and MND compared with HIV-infected patients who were neurocognitively normal, all of them were virally suppressed with cART (Alakkas et al. 2019). Higher levels of abnormal white matter were associated with higher risk of HAND. Specifically, HIV-infected individuals of the post-cART era displayed synapto-dendritic damage (Ellis et al. 2007) with prominent atrophy in subcortical structures, such as caudate, putamen, amygdala, hippocampus, and thalamus, instead of neuronal loss often observed in pre-cART era (Ances et al. 2012, Harezlak et al. 2011). In addition, cortical thinning or regional volume loss affect parietal white matter, orbitofrontal cortex, cingulate cortex, primary motor and sensory cortices, frontal and temporal lobes suggesting worst cognitive performance (Sanford et al. 2017). One cross-sectional study performed using a volumetric analysis compared HIV-infected patients virally unsuppressed and suppressed to uninfected individuals showing that reduced brain volumes in the corpus callosum, amygdala, caudate, thalamus, and putamen volumes is independent of cART because both HIV positive groups displayed similar changes. As discussed before, volumetric reductions of subcortical regions happen despite cART, suggesting a faster morphometry change after seroconversion that is persistent also in the virologically suppressed cohorts (Ances et al.

2012). Thus, cART has no significant effects on these volume changes (Brier et al. 2015), and we propose it cannot prevent lipid dysregulation. Our idea for this thesis is to study lipid dysregulation and the future direction aim to better characterize the pathway involved for obtaining target molecules for a specific therapeutic approach.

Potential biomarkers of HAND in the HIV-infected population

Several blood and CSF biomarkers for HAND are under investigation in order to determine the risk of HIV-infected patients developing neurocognitive impairment. However, it is difficult to assess their unequivocal role because most of the performed studies are cross-sectional or do not consider the evolution of cognitive impairment that in NeuroHIV is not linear (Bandera et al. 2019). The CSF/blood biomarkers for HAND may be divided into markers for neuronal injury, inflammation, and immune activation. Markers of neuronal injury previously investigated include β-Amyloid 1-42 (Petersen et al. 2016), the light subunit of the neurofilament protein (Yilmaz et al. 2017), calcium binding protein B (S100B) (Du Pasquier et al. 2013, Guha et al. 2019), extracellular vesicles (Urbanelli et al. 2019), and the Wnt pathway (Al-Harthi 2012), but none of these studies clearly explain the reason why they can be used as a biomarkers, especially in the virally suppressed patients with neurocognitive disorders. Although neuronal injury biomarkers have been long investigated, interest in inflammatory biomarkers has exponentially grown due to the persistent neuro inflammatory feature in cART suppressed individuals (Suh et al. 2014). Included among these biomarkers are: Monocyte Chemoattractant Protein-1 (CCL2) (Kamat et al. 2012), Tumor Necrosis Factor Alpha (TNF-α) (Oliveira et al. 2017), Interleukin-6 (IL-6) (Cassol et al. 2013), Interferon-γ-Inducible Protein (IP-10 or CXCL-10) (Yuan et al. 2015), Interleukin-8 (IL-8 or CXCL-8) (Kamat et al. 2012, Yuan et al. 2015), Interferon Alpha (IFN-α) (Anderson A. M. et al. 2017), Intercellular adhesion molecule-5 (ICAM5) (Yuan et al. 2017), Lipopolysaccharide (LPS) (Ancuta et al. 2008, Vassallo et al. 2013) and Growth Factors (Kallianpur et al. 2019, Yuan et al. 2015). Recently, our laboratory has identified ATP as a potential biomarker for HAND, affecting BBB function, stability, and neuroinflammation (Velasquez et al. 2019). Although several of these inflammatory factors may be directly or indirectly involved in HAND and increased in the blood and/or CSF of infected patients virally suppressed with cART and

with cognitive impairment, none of them explore the neuronal damage progression in HAND.

To conclude, recent research focus in HAND biomarkers include immune activators such as neopterin (Valcour et al. 2013), soluble CD163 (Burdo et al. 2013), soluble CD14 (Burdo et al. 2011) and Cathepsin B (Cantres-Rosario et al. 2013).

Still, although all these markers are increased in HAND condition, their role in HAND pathophysiology is often ambiguous and still under investigation. Moreover, the large range of variabilities in infected and neurocognitive impaired populations obstruct the absolute validation of blood/CSF biomarkers. Additionally, all these biomarkers are late indicators of the CNS damage that need a total disruption of neurons to be released in the circulation and be detected, so they are not predictive.

We demonstrated that sulfatide distributions in brain are perturbed in HIV-infected patients. Here, we explore the possibility that lipids, such as sulfatide, are potential biomarkers of HIV cognitive impairment.

Part III – Lipids in HAND

General introduction of lipids

Lipids are amphipathic biomolecules (Fahy et al. 2011). Lipids assist several important cellular functions, they are structural elements of the lipid bilayers, are sources of chemical energy, and are precursors for several second messengers (Glatz 2015). Lipids are classified into eight categories based on the ketoacyl groups and the isoprene groups: glycerophospholipids, fatty acyls, glycerolipids, sphingolipids, sterol lipids, prenol lipids, saccharolipids, and polyketides (Fahy et al. 2005). In order to simplify their metabolic characterization, we divided them in phospholipids, neutral lipids, and glycolipids.

Phospholipids are the major class of lipids present in all cells and they can be divided into glycerophospholipids and sphingomyelins. Glycerophospholipids include phosphatidylcholine, phosphatidylethanolamine, phosphatidylserine, phosphatidylinositol, phosphatidic acid, phosphatidylglycerol, and cardiolipin. All of them have a structural function in the cellular membranes in which are asymmetrically distributed in the bilayer (Fadeel and Xue 2009). The major phospholipid component present in cell membranes is phosphatidylcholine, which represents the 40-50% of the total phospholipid pool. Moreover, phosphatidylcholine is a precursor of several signaling molecules such as phosphatidic acid, diacylglycerol, lysophosphatidylcholine, platelet-activating factor, and arachidonic acid (Billah and Anthes 1990). Phosphatidylethanolamine is the second most abundant phospholipid in the membrane representing the 20-30% of the total cell phospholipid. Its function is to stabilize the membrane proteins in the bilayer. Phosphatidylserine is a minor membrane phospholipid and it is involved in the early phases of apoptosis and in the production of anti-inflammatory mediators (Bratton and Henson 2008, Vance and Steenbergen 2005). Phosphatidylinositol is also a minor lipid in mammalian cells, but it is involved in several signaling processes. It is the precursor of polyphosphoinositol lipids (PIP, PIP_2, and PIP_3) which regulate intracellular calcium signaling, gene transcription, RNA editing, nuclear export, and protein phosphorylation (Di Paolo and De Camilli 2006). Other classes of glycerophospholipids such as phosphatidic acid, phosphatidylglycerol, and cardiolipin are lower in abundance compared to phosphatidylcholine, phosphatidylethanolamine, phosphatidylinositol, and

phosphatidylserine. Specifically, phosphatidic acid is less than 1% abundant in the membrane but is a very important intermediate for the synthesis of membrane phospholipids and an important regulator of signal transduction, membrane trafficking, secretion, and cytoskeletal rearrangement (Jenkins and Frohman 2005). Phosphatidylglycerol is more express in the mitochondrial membranes and it is the precursor of cardiolipin which is necessary for normal electron transport and oxidative phosphorylation (Claypool 2009).

Sphingomyelins are also important components of cell membranes and they amount at 10% of the total phospholipids. Specific sphingomyelin metabolites such as ceramide (Cer), sphingosine (Sph), sphingosine-1-phosphate (S1P), diacylglycerol (DAG) and gangliosides (GMs), are also involved in cell signaling (Merrill et al. 1997). Ceramide is a crucial metabolite for sphingolipid metabolism. It is involved in cellular apoptosis (Hannun and Obeid 1995), cell differentiation (Okazaki et al. 1990), and inflammatory responses (Masini et al. 2008). Sphingosine and S1P are cofactors of inflammatory signaling, SPH inhibits proliferation and promotes apoptosis, S1P mediates cell growth arrest and apoptosis inhibition (Hannun and Obeid 2008). DAG is a second messenger that supports the biosynthesis (and degradation) of glycerolipids regulating protein kinase C (PKC) activity (Bishop and Bell 1988). Gangliosides are predominantly localized in the outer leaflets of neuronal plasma membranes where they contribute to cell-cell recognition, adhesion, and signal transduction (Kolter 2012, Yu et al. 2011).

Neutral lipids are comprised of sterols and glycerolipids. Sterols play a key role in the membrane integrity maintaining its microfluid state. The most abundant sterol in the cellular membranes is cholesterol (Dufourc 2008). Glycerolipids include triacylglycerols and steryl esters, and they are typically used as energy store (Athenstaedt and Daum 2006).

Glycolipids are glycans with a lipidic portion that bind to monosaccharide or polysaccharide chains that is extended into the extracellular space. Glycolipids include glyceroglycolipids, lipopolysaccharides, glycosphingolipids, and glycosylphosphatidyl-inositols. They have structural role for the cellular membrane and participate in immune responses to bacterial infections and cell-to-cell communication (Paulick and Bertozzi 2008, Stoffel and Bosio 1997, Zajonc and Kronenberg 2009).

Lipids within the CNS

Lipids such as cholesterol, fatty acids, sphingolipids, and glycerophospholipids are important structural components of the neuronal cells (Cermenati et al. 2015).

Within CNS, cholesterol facilitates the extension of axons, promotes the neurons survival and the myelin formation (Bruce et al. 2017). On another hand, fatty acids determine membrane fluidity and plasticity of neuronal membranes, serving also as signaling molecules. They are classified in saturated fatty acids that are made by single bonds between neighbor carbons and unsaturated fatty acids that present one or more carbon–carbon double-bonds. The neuronal membranes are mostly composed by polyunsaturated fatty acids (PUFAs), which are very abundant in the myelin sheath (Hooijmans and Kiliaan 2008). Instead, glycerophospholipids and sphingolipids maintain structural integrity in neuronal membrane (Olsen and Faergeman 2017). Sphingolipids are also involved in synaptic transmission and neuronal differentiation.

Altered lipid metabolism and changes in lipids concentration were presented in several neurodegenerative disorders, such as Alzheimer's (AD) and Parkinson's diseases (PD) (Hussain et al. 2013). The main changes in the brain of Parkinson's and Alzheimer's individuals were described in the altered levels of cholesterol and sphingolipids (Hussain et al. 2019), but also fatty acids and glycerophospholipid alterations contribute to the CNS structural compromise. For example, the high cholesterol in membrane causes incorporation of amyloid-β (Aβ) into the membrane in AD and accumulation of α-synuclein in PD leading to neuronal death (Abramov et al. 2011, Galvagnion et al. 2015). On another hand, fatty acids accelerates AD progression by enhancing the production of amyloid beta (Aβ) (Amtul et al. 2011). It has also been demonstrated that in patients with AD, the expression of Cer, the precursor of sphingolipids, in membrane was increased, whereas the level of sphingomyelin was reduced as a result of sphingomyelinase activation (He et al. 2010) inducing synaptic loss and neuronal cell death in response to amyloid accumulation (Couttas et al. 2014). Altered levels of sphingolipids were also observed in the brains of Parkinson's patients. Interestingly, oxidative stress results in the activation of neutral sphingomyelinase enzyme resulting in increased levels of Cer, leading to apoptosis in the substantia nigra (Posse de Chaves and Sipione 2010).

Moreover, glycerophospholipids, especially phosphatidylethanolamines, phosphatidylinositols, and phosphatidylcholines are significantly reduced in the neural membrane during the progression of AD (Gonzalez-Dominguez et al. 2014, Kosicek and Hecimovic 2013). This excessive degradation of glycerophospholipids may be due to stimulation of phospholipase A2 producing arachidonic acid (AA) that induces the release of inflammatory cytokines (Frisardi et al. 2011)

Arachidonic Acid and Ceramide synthesis pathways

Lipids are active compounds involved in important physiological and pathological processes. Disruption or imbalance in lipid composition or metabolism lead to various metabolic disorders including infections and neurodegenerative diseases (Lee et al. 2003). Although, any investigated biomarker will represent HAND onset and progression, few studies have investigated lipids as possible indicator of neurocognitive impairment in HAND. The dysregulation in lipid metabolism that occurs in the CNS and in the CSF/blood of HIV-infected population (Farooqui et al. 2007, Haughey et al. 2004) has never been considered as a direct or indirect cause of HAND.

As previously discussed, phospholipids are the most abundant structural elements of the lipid bilayers, they support chemical energy and are precursors for inflammatory messengers such as AA and ceramides (van Meer et al. 2008). Arachidonic acid is an omega-6 (n-6) polyunsaturated fatty acid, esterified on the sn-2 acyl position of phospholipids such as phosphatidylethanolamine, phosphatidylcholine, and phosphatidylinositol (Yin et al. 2013). During CNS injury, microglial cells release cytokines/chemokines that activate the cytosolic calcium-dependent phospholipases A2 ($cPLA_2$) that catalyzes the hydrolytic release of AA from membrane phospholipids. Oxidation of AA produces pro-inflammatory eicosanoids, which are local hormones that can be further subdivided into prostaglandins, leukotrienes, prostacyclins, and thromboxanes (Figure 1.4) (Farooqui et al. 2007). Eicosanoids in the brain can be secreted by several classes of cells such as microglia, astrocytes, oligodendrocytes, neurons and endothelial cells (Bendani et al. 1995). They are proinflammatory lipid mediators with autocrine and paracrine activities. From AA, the cyclooxygenase (COX) pathway gives

rise to prostaglandins, prostacyclines and thromboxanes; alternatively, the lipoxygenase pathway generates leukotrienes and lipoxins (Figure 1.4) (Radmark and Samuelsson 2009). Another dysregulated lipidic pathway observed in the CNS of HIV-infected patients is the ceramide pathway. Ceramide is a crucial mediator of cell differentiation, proliferation, survival, and apoptosis (Andrieu-Abadie et al. 2001). It is a metabolic and structural precursor for many sphingolipids, such as sphingomyelin (SM), ceramide-1 phosphate (Cer1-P) and glucosylceramide. The *de novo* synthesis of ceramide originates in the endoplasmic reticulum (ER) through a series of condensation and reduction reactions. Specifically, serine palmitoyltransferase (SPT) catalyzes the initial step of the pathway converting the L-serine (L-ser) and the palmityl coenzyme A (PalmitylCoA) in 3-keto-dihydrosphingosine (3KdhSph) that is translated in dihydrosphingosine (dhSph) by 3-keto-dihydrosphingosine reductase (3KSR). (Dihydro)ceramide synthase (dihydroCS) removes sphingoid bases and produces dihydroceramide (dhCer), which is converted into Cer by dihydroceramide desaturase (DES). Next, Cer is transported *via* non-vesicular transport by ceramide transfer protein (CERT) and *via* vesicular transport by four-phosphate adaptor protein 2 (FAPP2) to the Golgi apparatus. There, Cer is modified to form SM, Cer1-P and glucosylceramide (GluCer). The latter is the precursor for complex glycosphingolipids (GSL). After Cer synthesis in the Golgi apparatus, SM and complex GSL are delivered to the plasma membrane by vesicular transport. Several sphingolipid metabolic enzymes are present at the plasma membrane to regulate the levels of SM, Cer, Sph and sphingosine-1-phosphate (S1P). The latter is produced from Sph by sphingosine kinase (SK) and may also take part in the salvage pathway for generation of Cer. Coordination between S1P and Cer1-P is crucial for eicosanoid inflammatory mediator production such as prostaglandins (Hannun and Obeid 2008). During endocytosis, membrane sphingolipids are internalized and transported to the lysosome *via* endocytic vesicles, where acid sphingomyelinase (aSMase), acid ceramidase (aCDase), and glycosidase catalyze the hydrolysis (Figure 1.5) (Bartke and Hannun 2009).

An important Cer related metabolite is sulfatide because it is the major lipidic component of the myelin sheet (~4%). It is synthetized in the Golgi apparatus of oligodendrocytes and Schwann cells. Sulfatide is a class of anionic sulfoglycolipids mainly found in the outer leaflet of the plasma membranes of cells (Honke 2013). Its presence is not exclusive to

oligodendrocytes and Schwann cells, where is located to the plasma membrane, it is also produced in neurons and astrocytes, where is located in intracellular compartments (Ishizuka 1997). The precursor of sulfatide is galactosylceramide, which undergoes 3-O-sulfation of the galactose residue by the enzyme 3′-phosphoadenosine-5′-phosphosulfate: cerebroside sulfotransferase (CST). Galactosylceramide is synthesized in the ER from ceramides and UDP-galactose by the enzyme UDP-galactose: ceramide galactosyltransferase (CGT) and is then transported to the Golgi apparatus prior to sulfation to sulfatide. Sulfatide is specifically degraded by a sulfatase (arylsulfatase A) in the lysosome (Figure 1.5) (Eckhardt 2008).

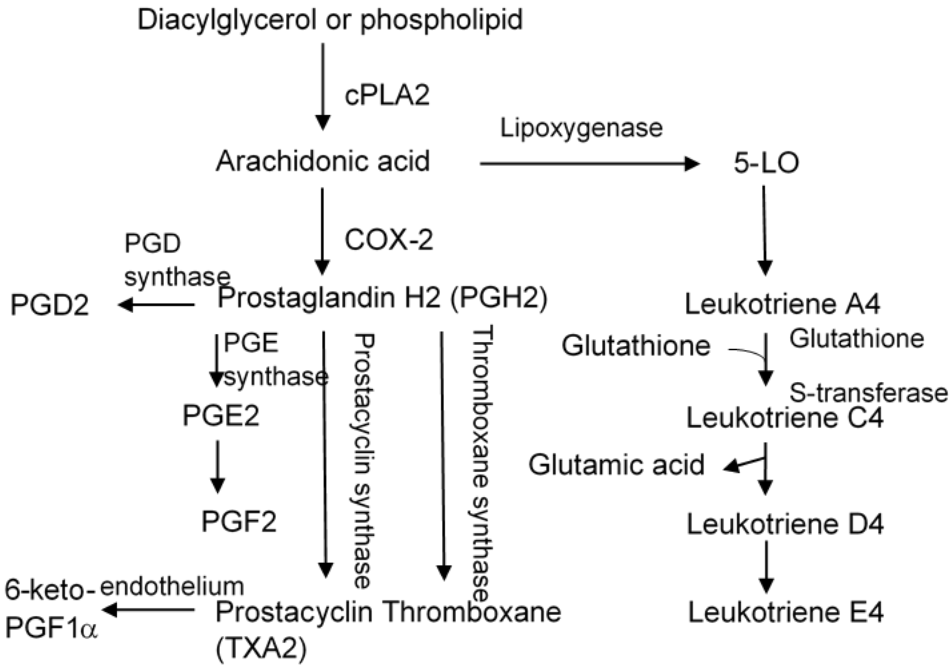

Figure 1.4. Metabolic pathway of Arachidonic acid (AA) transformation into eicosanoid products

After proinflammatory stimulus, AA can be cleaved by cytosolic phospholipase A2 (cPLA2) from diacylglycerol or phospholipids that compose cellular membranes. Free AA can take part in the Cyclooxygenase (COX) and Leukotriene (LO) pathways. For the cyclooxygenase pathway, AA is converted into prostaglandin H2 (PGH2), which generates prostacyclin (TXA2) by prostacyclin synthase and thromboxane by thromboxane synthase. In addition, PGH2 is converted in prostaglandin D2 (PGD2) and prostaglandin F2 (PGF2) by PGD and PGE synthetases. On another hand, AA can be transformed in Arachidonate 5-lipoxygenase (5-LO) by lipoxygenase. The same enzyme catalyzes the conversion of 5-LO to leukotriene A4, which is conjugated with reduced glutathione to be transformed into leukotriene C4. Next, leukotriene C4 is converted into leukotriene D4 and leukotriene E4 with subsequent production of glutamic acid.

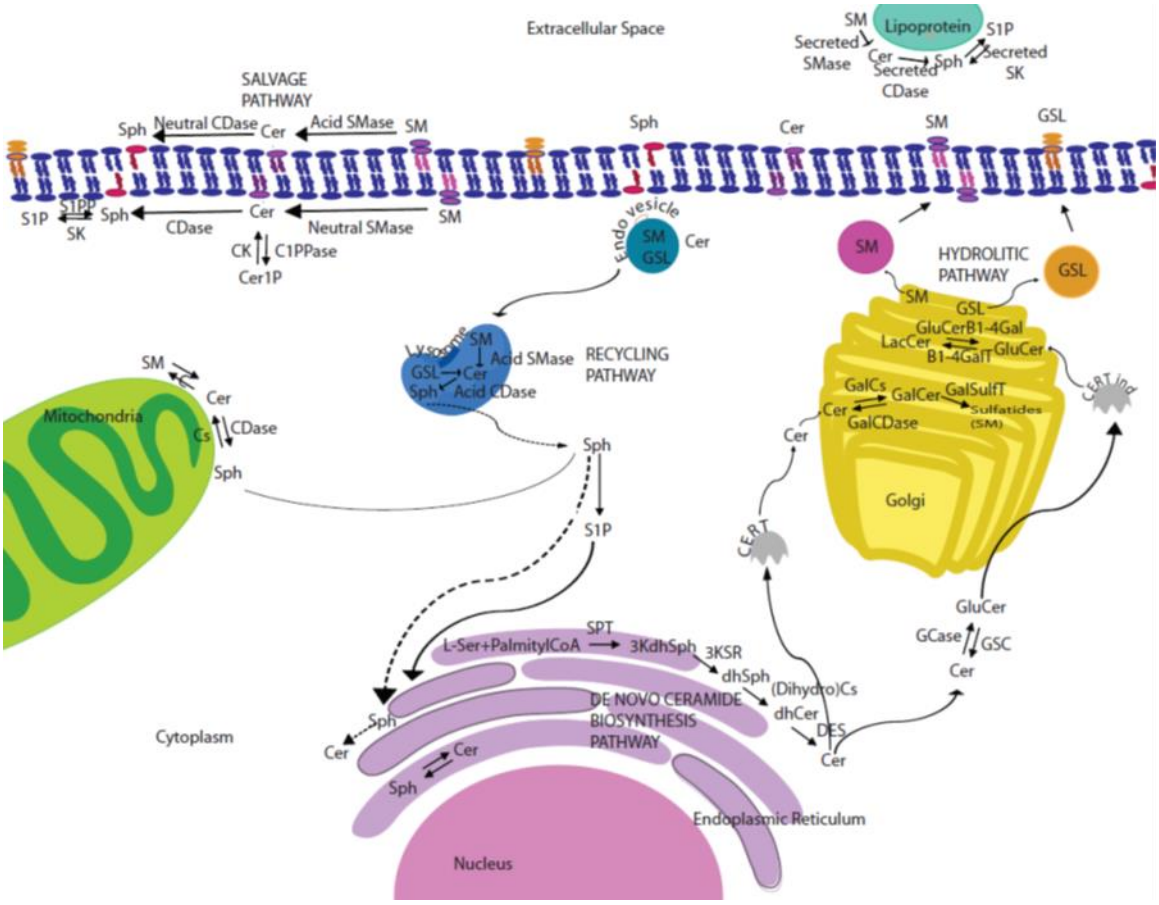

Figure 1.5. Localization and metabolism of Ceramide

Ceramide is generated either by hydrolysis of SM through SM-specific Phospholipase-C (PLC) termed Sphingomyelinases (SMases), by de novo synthesis through the enzyme ceramide synthase (CerS) in the endoplasmic reticulum (ER), through the acylation of sphingosine in the salvage pathway, by dephosphorylation of Cer1-P, and catabolism of glycosphingolipids**.**

Arachidonic Acid and Ceramide related metabolites as possible HAND indicators

HIV-infection and subsequent treatment with cART is often associated with perturbations in lipid profiles (Archibald et al. 2014, Griffin et al. 1994, Padmapriyadarsini et al. 2017), but any studies have investigated their altered metabolism in the brain. For instance, HIV-infected population show decreased levels of high density lipoprotein (HDL) cholesterol and increased levels of low density lipoprotein (LDL) cholesterol, total cholesterol (TC) and triglycerides in the blood (Archibald et al. 2014, Padmapriyadarsini et al. 2017). Interesting AA and Cer pathways have foreshadowed their direct or the indirect function in HAND but limited data are present in the literature. Some AA metabolites are upregulated in the HIV-infected CNS, which may be correlated with cognitive impairment. Prostaglandin E2 elevated levels in the CSF of HIV-positive individuals correlates with dementia (Griffin et al. 1994). However, the direct role of these inflammatory lipid mediators in the development and progression of HAND is still not completely understood. Relatively more investigations have been performed for Cer metabolites in the brain of HIV-infected patients. Levels of Cer and SM are significantly increased in brain tissues and CSF of HIV-infected patients with dementia compared to mild demented and HIV-infected without cognitive disorder individuals (Haughey et al. 2004). The same group demonstrated elevated level of Cer and SM in hippocampal neuronal cultures after stimulation with Tat or gp120 which induces apoptosis (Haughey et al. 2004). This suggest a possible correlation between lipid secretion and HIV proteins. In conclusion, our studies aim to demonstrate that lipid biomarkers associated with the cART can fill an important gap in the field of NeuroHIV. The screening of these structural and inflammatory lipids may have a potential use for diagnosis and follow-up of HIV aviremic population affected by HAND. Only a recent study by MRS showed increased lipids in HIV patients with CNS lesion versus asymptomatic HIV individuals and healthy controls (Bairwa et al. 2016). Whilst, they demonstrated increased lipid levels in HIV patients with CNS lesion suggesting a critical role of inflammatory lipid in HAND pathophysiology, the lipid species involved were not elucidated. To fully understand lipidomic and metabolic changes occurring due to advancing disease state, lipid classes and species need to be fully identified at the molecular level. Mass spectrometry has emerged as the leading technique for accurate, sensitive and detailed lipid analysis (Han and Gross 2003). Advanced mass

spectrometry technologies such as matrix-assisted laser desorption/ionization (MALDI) are very useful tools for making available lipidic signature in several disease conditions including HAND.

Mass Spectrometry Imaging

Mass spectrometry imaging (MSI) is a powerful tool allowing molecule investigations without extraction, purification, separation, or labeling of biological samples (Chughtai and Heeren 2010). MSI was introduced in 1994 by Spengler B., Hubert M. and Kaufmann R. at the 42nd Annual Conference on Mass Spectrometry and continue to be used to examine numerous analytes such as lipids (Jackson et al. 2014), proteins (Seeley and Caprioli 2008), peptides (Schober et al. 2012), metabolites (Bhandari et al. 2015), drugs (Mdanda et al. 2019) in different samples including mammalian tissues, plant tissues (Li B. et al. 2018), insects (Ly et al. 2019) and microbial cultures (Hoffmann and Dorrestein 2015). Mass spectrometry imaging determines the molecule distribution present in biological samples by direct ionization from the tissue surface and without the requirement for chromatographic separation. The mass spectrometer ionizes and analyzes the molecules on the surface of the sample and generates a mass spectrum at each acquisition point (pixel in the resulting image) of the tissue section surface. Every mass spectrum is analyzed by computational software selecting individual mass-to-charge (m/z) values and calculating the intensity from each pixel. Signal intensities are later plotted to generate a heat map image showing the relative distribution of every molecule with specific m/z values (Buchberger et al. 2018). Matrix-assisted laser desorption/ionization (MALDI) is the most sensitive and used ionization technique for MSI (Leopold et al. 2018). For MALDI-MSI, fresh frozen samples are used, which are later sectioned (~12 μm thickness), thaw-mounted onto the microscope slides (e.g., indium tin oxide coated glass slides for MALDI-MSI lipidomics) and placed into a desiccator to dry in order to not compromise molecules distribution and structures. MALDI requires matrix or nanoparticles application to facilitate the production of charged ions. Commonly used matrices for lipids and small molecules include: 2,5-dihydroxybenzoic acid (DHB), 9-aminoacridine (9-AA), 1,5-Diaminonaphthalene (DAN), and norharmane (NRM) (Goto-Inoue et al. 2011). The matrix is typically applied to the tissue by spraying method (Agar et al. 2007). The matrix absorbs

the energy of the UV laser resulting in thermal desorption and ionization of the co-crystal analytes in the gas phase where they are measured using by a mass analyzer (Karas and Kruger 2003). The tissue remains intact and the same section can be washed with methanol and used for histological examinations (Schwamborn and Caprioli 2010). The use of high-mass resolution and high mass accuracy analyzers (such as the Orbitrap) provides specific and unequivocal information about the elemental composition of the desorbed ion from the tissue (Landgraf et al. 2009).

Although MALDI-MS is used in lipidomics, proteomics, metabolomics, and glycomics, several reasons have encouraged the use of MSI for lipids. As discussed before, lipids are abundant molecules in the cells, especially in the membranes, and they can be easily ionized in order to generate abundant positive or negative ions during the MALDI process. Moreover, many (but not all) lipids have molecular weights below 1,000 Daltons, that is an optimal mass range for their diffusion into the matrix crystals and for sensitive operation of MALDI (Berry et al. 2011). Whether lipids can be detected in positive mode or negative mode depends upon the charge of the head group. Several types of lipids, such as phospholipids (Zaima et al. 2009), neutral lipids (Hayasaka et al. 2009), glycolipids (Goto-Inoue et al. 2010), and fatty acids (Hayasaka et al. 2010) have been investigated by MSI. Multiple lipid species have been identified as potential markers for diseases including cancer (Paine et al. 2019), cardiovascular infarction (Menger et al. 2012), Alzheimer's (Hong et al. 2016), and hepatitis B (Park E. S. et al. 2014).

For example, MALDI-MSI was applied to investigate specific host lipidic distribution as well as for accurate localization of Mycobacterium Tuberculosis in pulmonary granulomas. Using serial sections to perform MALDI-MSI assessed the spatial distribution of drugs for tuberculosis and mycobacterial glycolipids in lesion sections detected by acid-fast staining and microscopy. Thus, they obtained a perfect map of drugs colocalizing with specific metabolites and bacterial target populations (Blanc et al. 2018, Prideaux et al. 2015a, Prideaux et al. 2015b, Zimmerman et al. 2018). Using a similar approach, we have applied MALDI-MSI lipidomic analysis to investigate lipidic dysregulations that are very common in pathological conditions such as HAND. We identified in post-mortem brain tissues multiple structural lipids that maintain their distribution and abundance under HIV condition indicating little to no structural damage is occurring in these tissues. However,

we detected significant changes in sulfatide brain distribution and abundance compared to the control condition. Thus, we proposed sulfatide as a potential indicator of neurocognitive impairment. In the future, we want to expand our research to detect this specific lipid in the blood or in the CSF of HIV-infected patients and predict CNS damage.

Part IV - Aims of the study

This Ph.D. thesis aims to test the hypothesis that "neurocognitive decline in HIV-infected population is mediated through CNS viral reservoirs by local lipid dysregulation". To address this hypothesis, we generated a protocol to identify, localize, and quantify viral reservoirs in HIV-infected brain and lymph node tissues. We identified that the cells with HIV-integrated DNA are not totally silent and still producing viral proteins even in patients under efficient cART. In addition, viral proteins diffused to the neighboring uninfected cells. Therefore, viral reservoirs were shown to generate CNS damage using a bystander mechanism. Using MALDI-MSI, we aimed to identify whether altered lipid distribution in both grey and white matter could be involved in bystander damage. We identified sulfatide as a potential indicator for HAND pathogenesis. We also determined that HIV proteins can induce the secretion of sulfatide. Subsequently, we examined sulfatide effects by detecting key molecules involved in cell-to-cell communication such as Connexin43, Connexin36 and Zonula Occludens-1. Additionally, we investigated the extracellular effects of sulfatide on cellular metabolism by performing proteomics analysis and cell mito stress Seahorse.

Through the following aims, we intend to provide evidence for a new mechanism that can justify CNS viral reservoirs and lipid alternation connection with HAND.

For the future, we will complete and expand our data to identify whether sulfatide and its biosynthetic pathways can be potential pharmaceutical targets to cure or prevent neurocognitive impairment in HIV-infected population that under cART show an undetectable viral replication.

Chapter 2: Identification, localization, and quantification of HIV viral reservoirs using improved staining and microscopy technique in human tissues

Donoso Maribel[1]; D'Amico Daniela[1,2]; Prideaux Brendan[1]; Eugenin Eliseo A.[1]

[1]University of Texas Medical Branch (UTMB), Department of Neuroscience, Cell Biology and Anatomy, Galveston, TX, USA

[2]University of Palermo (UniPa), Department of Biomedicine, Neuroscience and Advanced Diagnostics, Palermo, Italy

The National NeuroAIDS Tissue Consortium (NNTC) provided all human samples. The NNTC is made possible through funding from the NIMH and NINDS by the following grants: Manhattan HIV Brain Bank (MHBB): U24MH100931; Texas NeuroAIDS Research Center (TNRC): U24MH100930; National Neurological AIDS Bank (NNAB); U24MH100292; California NeuroAIDS tissue Network (CNTN): U24MH100928; and Data Coordinating Center (DCC): U24MH100925. This work was funded by The National Institute of Mental Health grant, MH096625, the National Institute of Neurological Disorders and Stroke, NS105584, and UTMB internal funding (to E.A.E).

Associated paper: Donoso M., D'Amico D., Prevedel L., Prideaux B. and Eugenin E.A. "Localization, quantification, and characterization of HIV reservoirs in the current cART era: focus on the brain and lymph nodes". In preparation.

Introduction

HIV persists in the body of infected individuals despite effective c-ART due to the presence of viral reservoirs in different tissues (Balcom et al. 2019, Blankson et al. 2002). Viral reservoirs are characterized as a small population of cells with integrated HIV DNA into the host DNA that does not produce or produce low levels of virus. This process is called latency (Dahabieh et al. 2015). Upon cART interruption, virus rebounds and repopulates the body in few weeks (Sengupta and Siliciano 2018). Currently, most viral reservoir studies are performed in blood due to the easy access. The current clinical limit of viral detection is 20-50 HIV RNA copies (Tan et al. 2018). However, recent advances in the field indicate that most viral reservoirs are present in different tissue compartments (Lamers et al. 2016). Several tissues have been proposed as anatomical compartments for viral reservoirs including gastrointestinal mucosa, the liver, the brain, the lymph nodes and the associated lymphatic tissues, and the genital tract (Svicher et al. 2014). Currently, there are two schools of thought about viral reservoir compartmentalization; one describes that there is no difference between viral strains and evolution in tissues versus the blood (Bozzi et al. 2019) and a second one that indicates that virus and viral reservoirs in different tissues can evolve in a different way than blood strains (De Scheerder et al. 2019). Most of these views are based on sequencing of HIV strains because there are no available techniques to detect viral reservoirs in tissues in a reliable manner. Also, all the techniques that detect and quantify viral reservoirs are based on the detection of only one component of the virus such as viral DNA, mRNA or proteins. These techniques to detect viral reservoirs are described in Table 1, overall, they involve the particular amplification of the viral reservoir population or viral component by inducing proliferation and selection by viral reactivation with phytohaemagglutinin (PHA) and phorbol myristate acetate (PMA). However, it is unclear whether these amplification systems overrepresent or only detect a partial size of the total viral reservoirs poll (Finzi et al. 1997, Massanella et al. 2018).

Viral reservoirs are characterized by having a potentially productive HIV DNA integrated into the host DNA (Pinzone and O'Doherty 2018). Moreover, HIV DNA integration cannot assure viral replication because there are several mechanisms that could compromise HIV replication including mutations, wrong site or direction of integration, and epigenetic regulation (Abbas and Herbein 2012, Cary et al. 2016). If the HIV DNA

enables viral production, viral mRNA will be produced upon infection or reactivation. Viral mRNA expression results in viral protein production and subsequent viral particle assembly and release of mature virions. However, the ratio of HIV integration, viral RNA and protein production, are totally unknown in viral reservoirs. Several laboratories indicate that during effective cART, several HIV proteins are produced and several animal models overexpress them (Nesbit and Schwartz 2002). Furthermore, these viral proteins are secreted as soluble proteins and the proteins, not the virus, induce inflammation and bystander damage into the neighboring cells. However, there are no data *in vivo* that show this mechanism in latently HIV-infected individuals. Most of these models are accepted mechanisms but not based on strong data. The main problem to demonstrate that these models and bystander mechanisms of damage are present is due to the inability to correctly identify, localize, and quantify latent HIV reservoirs within infected individuals in the circulation and in the tissues.

One of the major objectives of this thesis was to design, test, and validate a method to detect, localize, and quantify viral reservoirs in tissues and in circulation using a multi-probe and antibody-based system visualized using microscopy. Our method enables the identification of HIV integrated DNA, HIV mRNA, and several viral proteins in a single test.

Materials and Methods

Sample Preparation

Human brain and lymph node tissue blocks were obtained from the National NeuroAIDS Tissue Consortium (NNTC). The patient information are indicated in Table 2. Fixed and unfixed tissue blocks were cut in seven µm thick tissue serial sections using a Leica RM2235 microtome or Leica CM1850 cryostat (Buffalo Grove, IL) and thaw-mounted onto frosted glass microscope slides. After sectioning, unfixed tissues were fixed with PFA 4% (15710-S, Electron Microscopy Science, Hatfield, PA) for 20 minutes and stored at 4 ^{o}C.

For blood, an entire Leukopak was used to isolate PMBC using Ficoll-Paque (GE17-1440, GE Healthcare, Chicago, IL). Centrifugation of 30 minutes at 400 x g was required to obtain a clean buffy coat and an additional centrifugation of 10 minutes at ≥450 x g was

necessary for removing the ficoll from the white cells. The PMBC pellet obtained was sliced and fixed with PFA 4%.

For all these analyses serial sections were essential to perform 3D reconstructions of large pieces of tissues with the main objective to quantify thousand-millions of cells in the 3D reconstructed samples.

Protocol for Detecting Viral Reservoirs (fixed and fresh tissue blocks)

Rehydration:

1. Immerse slides into two separate xylene solutions, 5 minutes each.
2. Immerse slides into two separate solutions containing 100% ethanol, 3 minutes each.
3. Immerse slides into a solution containing 96% ethanol dissolved in ddH_2O, 3 minutes.
4. Immerse slides into a solution containing 90% ethanol dissolved in ddH_2O, 3 minutes.
5. Immerse slides into a solution containing 70% ethanol dissolved in ddH_2O, 3 minutes.
6. Immerse slides into a solution containing 60% ethanol dissolved in ddH_2O, 3 minutes.
7. Immerse slides into a solution containing 50% ethanol dissolved in ddH_2O, 3 minutes.
8. Immerse slides into pure water for at least 3 minutes.
5. Encircle the specimen with Dako Pen (cat # 52002).
6. Immerse slides into a solution of pure water for 3 minutes.

Pre-treatment:

7. Place slides in humidity chamber.
8. Dilute the needed amount of Proteinase K (0.01 mol/ml, K5201, Dako products-Agilent Technologies, Santa Clara, CA),1:10 in TBS.
9. Add 150 µl of diluted Proteinase K to each section and incubate for 10 minutes at room temperature.

11. Immerse slides into pure water for 3 minutes.
12. Immerse slides in 96% ethanol for 20 seconds and air-dry the slides for 5 minutes.

DNA probe Hybridization:

13. Dilute probe stocks to 10 µM in TBS and add to the specific sections Nef-PNA Alexa 488 (Alexa488-GCAGCTTCCTCATTGATGG) and Alu-PNA Cy5 (Cy5-GCCTCCCAAAGTCGTGGGATTACAG) (PNA Bio, Thousand Oaks, CA).
14. Place slides in a pre-warm humidity chamber.
15. Incubate slides at 42 ºC for 30 minutes then at 55 ºC for 1 hour.

Note: from this point try to work in the dark.

DNA Probe Stringent wash:

16. Preheat stringent wash working solution (PNA ISH kit, K520111-2, Dako products-Agilent Technologies, Santa Clara, CA) diluted 1:60 to 55 ºC in a water-bath.
17. Place slides in stringent wash solution for 25 minutes in an orbital shaker at 55 ºC.
18. Equilibrate the slides to room temperature by immersion in TBS for 20 seconds.

Note: Probe will be detected in the subsequent steps.

Viral RNA Probe detection:

21. Place slides in humidity chamber.
22. Apply RNAscope probe (HIV RNAscope 2.5 HD Detection Reagent–RED Kit, 322360, ACD).
23. Incubate slides at 42 ºC for 30 minutes then at 55 ºC for 50 minutes.

Note: the autofluorescence of the probe is used for accurate measure.

RNA Probe Stringent wash:

24. Preheat stringent wash working solution (PNA ISH kit, K520111-2, Dako products-Agilent Technologies, Santa Clara, CA) diluted 1:60 to 55 ºC in a water-bath.
25. Place slides in stringent wash solution for 15 minutes in an orbital shaker at 55 ºC.
26. Equilibrate the slides to room temperature by immersion in TBS for 20 seconds.

Hybridize RNA (RNAscope 2.5 HD Detection Reagent–RED kit, 322360, ACD):

26. Add three drops of tube 1 and incubate for 30 minutes at 40 ºC.
27. Immerse slides in TBS for 5 minutes.
28. Add three drops of tube 2 and incubate for 15 minutes at 40 ºC.
29. Immerse slides in TBS for 5 minutes.
30. Add three drops of tube 3 and incubate for 30 minutes at 40 ºC.
31. Immerse slides in TBS for 5 minutes.
32. Add three drops of tube 4 and incubate for 15 minutes at 40 ºC.
33. Immerse slides in TBS for 5 minutes.
34. Add three drops of tube 5 and incubate for 30 minutes at room temperature.
35. Immerse slides in TBS for 5 minutes.
36. Add three drops of tube 6 and incubate for 15 minutes at room temperature.
37. Immerse slides in TBS for 5 minutes.
36. Add three drops of tube RED and incubate for 10 minutes at room temperature.
37. Immerse slides in TBS for 5 minutes.

Immunofluorescence:

38. Perform antigen retrieval incubating the section in antigen retrieval solution (S1700, Dako products-Agilent Technologies, Santa Clara, CA) at 80 ºC in water-bath for 30 minutes.
39. Permeabilize with Triton X-100 (X-100, Sigma-Aldrich, St. Luis, MO) 0.1% in TBS for 2 minutes.
40. Block unspecific binding sites of presence of Fc receptors using the blocking solution (1 ml 0.5 M EDTA pH 8.0 (15575-038, Thermo Fisher Scientific, Waltham, MA), 100 µl gelatin from cold-water fish skin (G7765, Sigma-Aldrich, St. Luis, MO), 0.1 g bovine serum albumin (BSA immunoglobulin-free, A2058, Sigma-Aldrich, St. Luis, MO; or BSA fraction V, BP1605, Thermo Fisher Scientific, Waltham, MA), 100 µl horse serum (H1138, Sigma-Aldrich, St. Luis, MO), 5% human serum (Corning, New York), and 9 ml ddH_2O) to incubate the sections for at least 1 hour at room temperature or overnight at 4 ºC.

41. Applied biotinylated primary antibodies for viral proteins (p24 GXT40774, Irvine, CA; integrase NIH 7374; Gp120 NIH 1476; tat NIH 705; Nef NIH 2949; Vpr NIH 3951) and cellular markers (Iba-1, anti-goat, dilution 1:200, ab5076, Cambridge, UK; and GFAP, anti-mouse, dilution 1:100, G3893, Sigma-Aldrich, St. Luis, MO) and incubate overnight at 4 ºC.

42. Wash 3 times with TBS every 5 minute to eliminate the unbound antibodies.

43. Add the secondary antibodies at the right dilution and incubate for at least 2 hours.

44. Wash 3 times with TBS every 5 minute to eliminate the unbound antibodies.

45. Mount slides with Prolong Diamond Antifade Mount Medium containing DAPI (P36930, Thermo Fisher Scientific, Waltham, MA).

Analysis:

To identify the probes and the antibodies a Nikon A1 confocal microscopy with spectral detection was used. Absorption and emission of each fluorophore were examined using spectral detection to narrow the wavelengths into 20-40 nm. These analyses were also performed using RNAscope due to the significant amount of red color present in uninfected samples. The fluorescent detection of RNAscope precipitate was only found in HIV infected samples. For further analysis, NIS Elements (Japan) and other proprietary software were used.

Statistical Analysis

All data were expressed as mean ± standard deviation (STD). Differences among groups were analyzed by the one-way analysis of variance (ANOVA test), using Bonferroni's multiple comparison test for post-hoc analysis. The level of significance was accepted at $p<0.05$. Origin v9.0 software was used for all statistical analyses performed.

Results

Identification of viral reservoirs by staining and microscopy method. As described in Table 1, the current techniques to detect viral reservoirs are limited to circulating cells. Specifically, quantitative viral outgrowth assay (QVOA), Tat/rev induced limiting dilution assay (TILDA), and PCR based methods use large amount of blood and require

proliferation and reactivation by PHA and PMA, resulting in overestimation of the viral reservoirs. Using these techniques, the sensitivity is 0.02 copies per million cells (see details in Table 1). Moreover, all these methods detected only one component of the viral cell cycle (e.g. viral DNA, viral mRNA or viral proteins). Thus, the size of HIV reservoirs within infected individuals virally suppressed with cART is not well defined.

To develop a better system, we generated new methodologies for multi probe and antigen detection to identify, localize and quantify viral reservoirs as described in Figure 2.1. Briefly, to detect multiple HIV and host markers, we sectioned large pieces of tissues (cm or inches) to detect a sufficient number of total cells, due to the presence of only one viral reservoir into millions of uninfected cells. In addition, to the large pieces, we also prepared serial sections to create a sufficient volume to perform 3D reconstructions if required.

The main premise and specificity of our method is based on a redundant system of control probes and staining to assure proper viral reservoir detection. Briefly, for the HIV-DNA probe to be considered as a positive signal it needs to colocalize with Alu-repeats probe. Alu repeats are abundant repetitive DNA sequences dispersed throughout the human genome (Batzer and Deininger 2002). Also, both HIV DNA and Alu repeats need to colocalize with DAPI. Any inconsistence of these colocalizations indicates un-specificity. However, minor inconsistences were observed (data not presented). For viral mRNA, signal does not colocalize with DAPI and Alu-repeats due to the different subcellular distribution. A similar selection for specificity was used for HIV viral proteins. An example of staining protocol is presented in Figure 2.1. Serial sections were used to perform the staining for HIV-integrated DNA (DNA Nef probe), HIV mRNA (RNA scope), Alu repeats (DNA probes), DAPI (nuclear staining), HIV proteins (p24, integrase, Gp120, Tat, Nef, or Vpr) and cellular markers (Iba-1 and GFAP). In addition, H&E and trichrome staining were also performed and repeated between the staining to evaluate the changes in morphology of serial tissue sections used to identify the viral reservoirs. So far, we have identified myeloid and lymphoid viral reservoirs in bone marrow (Real F. et al. in press), vaginal, and urethral tissues (Ganor et al. 2019). Currently, we are expanding our identification of viral reservoirs into other human tissues and HIV/SIV animal models.

Identification, localization, and quantification of HIV reservoirs within the brain of HIV-infected individuals. Based on the literature, two populations of CNS cells have been identified in the pre-cART to be HIV infected *in vitro* and *in vivo*, they are microglia/macrophages and a small population of astrocytes (Clayton et al. 2017, Li G. H. et al. 2016). Nevertheless, their contribution to CNS damage and to the pool of viral reservoirs is still controversial due to the lack of reliable data in the current cART era. Thus, we applied our protocol to large pieces of brain and lymph node tissue sections to detect viral components (HIV DNA, mRNA and viral proteins) in combination with staining for microglia/macrophages and astrocytes (positive cells for Iba-I and GFAP, respectively).

Using cortical brain tissue sections obtained from uninfected and HIV-infected individuals under cART (see patient information in Table 2), we stained the tissues as described in Figure 2.1. In the patient samples analyzed we detected few cells with HIV-Nef DNA colocalizing with DAPI and Alu-repeats. Our analysis identified that most of the HIV-integrated DNA (colocalizing with DAPI and Alu-repeats) was in Iba-1 and in a small percentage of GFAP positive cells. A representative example was given in Figure 2.2, where it is shown that one section of an image 6x6 covers approximately 1500 μm^2. This area was multiplied by 6 fields to either side. Furthermore, this figure represents only 1 tissue section of 12 serially analyzed (84 to 144 µm combined thickness, depending on the protocol). Thus, the analyzed area was large enough to detect the few infected cells in a pool of million uninfected cells.

Interestingly, positive cells for HIV-DNA were always in clusters of 3-10 cells containing virus, suggesting a cooperative niche generated by HIV-infected cells within the brain. Most of these clusters were closely associated with blood vessels and areas rich in neuronal bodies. Unequivocally, HIV-integrated DNA had never been detected in Iba-1 and GFAP negative cells such as endothelial cells or neurons. Thus, our results confirmed that our innovative strategies to detect viral reservoirs is extremely specific and demonstrates that the virus infects microglia/macrophages and a small population of astrocytes in the CNS. In conclusion, our data *in vivo* determines that HIV-reservoirs are present in a small population of CNS resident cells such as microglia/macrophages but also in a smaller population of astrocytes (see quantification in Figure 2.5).

The same specificity that we detected for HIV-integrated DNA was obtained for HIV mRNA (data not shown). Overall, minimal colocalization with DAPI and Alu-repeats was found because HIV mRNA is mainly localized in the cytoplasm. Moreover, HIV mRNA staining was detected only in cells containing HIV-integrated DNA (see quantifications in Figure 2.5 B). However, only half of the cells having integrated DNA also expressed HIV mRNA. The mechanism of low expression of mRNA in HIV DNA positive cells could be explained by the use of cART that induced an effective viral control, or by the presence of abortive sequences of DNA, as well as by the lack of right reactivation mechanism or latency (Cary et al. 2016, Ishizaka et al. 2016, Kaiser et al. 2017, Pasternak and Berkhout 2018, van den Dries et al. 2017). Again, mRNA was only detected in cells that could support viral replication such as microglia/macrophages and a small population of astrocytes. No unspecific staining for HIV mRNA was observed in other cell types or uninfected tissues. An important note is the specificity of the spectral detection system to detect viral mRNA over traditional colorimetric systems promoted by several companies (RNAscope). Several laboratories reported unspecific HIV mRNA staining due to aging samples or precipitates related to salts or crystals. None of these artifacts were observed if the tissues were analyzed by fluorescence. A critical limitation of our approach is that currently we can only determine HIV mRNA for Nef. Therefore, it is unknown whether other viral mRNAs are produced. Future experiments will focus on developing probes and approaches to analyze additional viral mRNAs to complete these studies.

A small population of the viral reservoirs express viral proteins in the current cART-era. Using the same human tissue samples described above, we quantified the number of positive cells for Nef, Gp120, Integrase, Vpr, and Tat protein. As an example of the analysis, we focus this discussion on the data acquired for HIV Nef protein, but the results need to be expanded for all the proteins indicated (Figure 2.5 C). In cells containing HIV integrated DNA and expressing HIV Nef mRNA, only 2% of these cells expressed HIV-Nef protein in tissues obtained from HIV infected individuals under cART (Figure. 2.5 B). As a positive control, HIV encephalitic (HIVE) brain tissue was used. In HIVE conditions HIV-integrated DNA, perfectly correlated with expression of HIV Nef mRNA and Nef

protein expression as expected due to the high HIV replication rates observed in the brain of HIV-infected individuals without cART (Figure 2.5 B).

However, HIV Nef protein did not fully colocalized with cells containing HIV-integrated DNA, suggesting that viral proteins, including Nef, gp120, Integrase, Vpr, and Tat, diffuse or are secreted into neighboring uninfected cells (Fig. 2.5 B and C). The most abundant viral proteins secreted into neighboring uninfected cells were Nef, Gp120, Vpr and Tat (Figure 2.5 C). Secretion of Integrase protein was less than other proteins analyzed, but still significant as compared to cells containing HIV-integrated DNA (Figure 2.5 C). In contrast, in HIVE tissues a perfect correlation was observed between Nef, Gp120, Integrase, Vpr and Tat protein expression in cells containing HIV-integrated DNA and uninfected surrounding cells (Figure 2.5 C).

Figure 2.3 and 2.4 show representative examples of human brain tissue sections stained for DAPI, Gp120 protein, HIV-Nef DNA and Iba-1. In Figure 2.3, we showed the staining for human brain tissue from a HIV-infected patient under cART, with a normal CD4 count and without systemic viral replication, where it was possible to observe that cells positive for HIV-Nef DNA (in green), for Alu repeats (data not shown) and Gp120 protein (in red) corresponded to macroglia/macrophages (Iba-1 positive in white). However, most of the Gp120 signals did not colocalize with HIV-Nef DNA in microglia/macrophages, suggesting that Gp120 diffused from the HIV-integrated positive cells into the neighboring cells. No unspecific staining was detected in human brain tissue sections from uninfected individuals (Figure 2.4).

Quantification and extrapolation of our results into the size of the viral reservoirs within the brain. In the field of viral reservoirs, several questions need to be addressed for the brain. 1) Are there infected cells within the brain in the current cART era? 2) Are there viral reservoirs within the brain? 3) Which are the cell types infected *in vivo*? And 4) Is the brain a significant anatomical compartment for viral reservoirs compared to other tissues? To address these questions, we extrapolated our data into the entire brain (Table 3) as compared to our data in lymph nodes (Table 4). Our data, described above, can give an answer for the first three questions. To address the last question, we calculated the volume of tissue analyzed versus the entire volume of the human brain (Figure 2.6). We repeated

the same analysis for the total human lymph nodes. Two important caviars of these extrapolation are present. First, cortex tissue was used, other brain structures (such as basal ganglia) have higher levels of HIV-infected cells, this means that the total number of viral reservoirs may be bigger. Second, we quantified the total number of reservoirs including all lobes of the cerebrum, the basal ganglia, the thalamus, the ventricles and the hippocampi, excluding the cerebellum and peripheral areas.

Our analysis for brain used 8 serial sections of large brain areas obtained from uninfected and HIV infected individuals with different sizes as indicated in Figure 2.6 A. Overall, we estimated that the volume analyzed was 0.005152 cm^3 (Figure 2.6 B). The numbers of total Iba-1 positive cells (microglia/macrophages) containing HIV DNA was 5170 ± 6689 cells in the volume analyzed. Also, the total number of GFAP positive cells (astrocytes) containing HIV DNA corresponded to 1645 ± 2128 cells in the volume analyzed; thus, combining the numbers of both populations, the total numbers of cells containing HIV DNA was 6580 ± 8514 in the volume analyzed (Figure 2.6 D).

If we consider that the total volume of the human brain in males is 1135 cm^3 and female is 1003 cm^3 including all lobes of the cerebrum, the basal ganglia, the thalamus, the ventricles and the hippocampi (Allen et al. 2002). Thus, the mean volume of the brain is 1069.1 cm^3 (Figure 2.6 D). Furthermore, overall quantifications of the numbers of cells in the entire brain indicate that the human brain contains approximately 1.1 trillion cells between neurons and glia (von Bartheld et al. 2016).

To extrapolate our data into the entire brain several assumptions were used: first, a mean brain volume between male and female; second, a uniform distribution of viral reservoirs even that dopaminergic areas, not quantified in our analysis, that in general have higher numbers of HIV infected cells (Gaskill et al. 2014, Purohit et al. 2011); third, a constant ratio between glia/neurons/and other cell types to maintain similar percentages. Overall, the ratio between total brain volume and volume of the sample analyzed corresponded to 207511.6 fold. Thus, the total numbers of cells with HIV-integrated DNA, expressing viral mRNA and viral proteins can be calculated as described in Table 3.

Analyzing the lymph nodes, we considered that the human body contains ~500 lymph nodes and one lymph node, oval in shape, has a mean volume of 1.6 cm^3 (https://opentextbc.ca/anatomyandphysiology/chapter/21-1-anatomy-of-the-lymphatic-

and-immune-systems/). Thus, the mean volume of the total lymph nodes in the human body is 785.4 cm^3 and the ratio between total volume of all the lymph nodes and volume of the sample analyzed corresponded to 457692.3 fold. In addition, we evaluated that the lymphocytes in the total lymph nodes are approximately 0.5 trillion (https://assets.thermofisher.com/TFS-Assets/LSG/brochures/I_WEB.pdf). Thus, we extrapolated the numbers of lymphocytes with HIV-integrated DNA, expressing viral mRNA and Gp120 proteins for the total lymph nodes of the human body (Table 4). We calculated that the 7.8% of lymphocytes of the total cells in all the human lymph nodes presented HIV-integrated DNA, 4.6% presented HIV-integrated DNA and HIV mRNA, and the 0.6% were in addition positive for Gp120 (Table 4). Consistent with the brain quantification of viral reservoirs (Table 3), lymphocytes negative for HIV-integrated DNA and presenting Gp120 protein were higher (2%) compared to the lymphocytes positive for HIV-integrated DNA and Gp120 protein, confirming the bystander effect of HIV proteins also in lymph nodes. Comparing the brain with the 500 lymph nodes of the human body, the total number of microglia/macrophages and astrocytes with HIV-integrated DNA is 1/62 of the total lymphocyte reservoirs with HIV-integrated DNA in the lymph nodes. However, lymph nodes may present higher levels of viral reservoirs compared to brain, as for this reason used as a control, it is necessary to consider that the lymphoid tissues are important sites of viral replication during active infection and are numerous (Huot et al. 2018, Wong and Yukl 2016). Nevertheless, we showed that brain is a valid anatomic niche for viral reservoirs.

In conclusion, our data demonstrated several points. First, our methodology cannot only detect viral reservoirs, but can identify cells with active replication and viral protein synthesis. Second, our method enables us to detect bystander protein secretion or diffusion into uninfected cells. Third, certainly, the brain contains HIV reservoirs. Fourth, these viral reservoirs are mostly microglia/macrophages and a small population of astrocytes. Fifth, the brain is a considerable viral reservoir compartment, compared to the lymph tissues.

Discussion

HIV, as well as other viruses, has evolved to persist within the host. HIV persistence involves the generation of viral reservoirs that remain undetectable in cellular and

anatomical sites (Denton et al. 2019). As discussed in the general introduction, most of the current techniques to detect viral reservoirs only detect one component of the viral cell cycle and require amplification or cell proliferation for efficient detection. Our method is extremely sensitive, reliable and specific for all the components analyzed. We did not detect any signal in uninfected tissues and the negative and positive controls included in the methodology were reliable.

Overall, the numbers of detected viral reservoirs were lower than the described data in isolated microglia/macrophage and astrocytes (Castellano et al. 2017, Churchill et al. 2009, Russell et al. 2017, Thompson et al. 2011). Thus, our data *in vivo* may be representative of the more realistic number of viral reservoirs present in HIV-infected individuals under effective cART, with low numbers of HIV-infected cells, with minimal viral mRNA and protein synthesis. Also, in the current cART era, not all the microglia/macrophages and astrocytes contain HIV. Thus, there is a selection mechanism that is not full known.

An important point to discuss is that for the first time, we can detect basal synthesis and release of several HIV proteins in tissue samples from HIV-infected individuals under effective cART, with normal CD4 counts and undetectable systemic replication. This result is unique and validates the multiple papers describing the toxic and inflammatory effects of viral proteins in tissue cultures and animal models without active HIV replication (Jaeger and Nath 2012, Kanmogne et al. 2002, Kovalevich and Langford 2012, Nath 2002).

The clustering of the cells between microglia/macrophages and astrocytes denote a unique symbiosis between both cell types to keep viral reservoirs within the brain. Viral reservoirs in the brain, but not in the lymph nodes, aggregate into cellular clusters. In the brain most clusters were close to the blood vessels. Contrary to the belief that viral reservoirs are only present in different kinds of $CD4^+$ T cells, the identification of infected microglia/macrophages and astrocytes indicate that several cells may be infected with HIV. Recent data from our laboratory showing that specific macrophages of the urethral tissue and megakaryocytes can be infected with HIV (Ganor et al. 2019). Furthermore, data of human macrophages identified several mechanisms of survival that are not present in $CD4^+$ T cells and require urgent examination to eliminate these cells.

Our data provides a unique demonstration of the presence of viral reservoirs within the brain and their contribution to chronic inflammation and bystander damage is mediated by several HIV proteins. Our accurate process of localization and quantification is essential for the development of therapeutic strategies targeting specific areas of viral reservoirs and to treat HIV comorbidities such as the neurocognitive manifestations seen in HAND.

Assay	Sample size	Assay input	Amplification required	Limit of detection	References
QVOA	500 ml blood	Purified resting CD4+ T cells	Yes	0.02 infectious units per million resting CD4+ cells	Finzi et al., 1997
TILDA	10-240 ml of blood	Purified resting CD4+ cells	Yes	Copies per million cells	Procopio et al., 2015
Other PCR-based methods	Variable amount of blood	PBMCs, Purified resting CD4+ cells, Plasma	Yes	Copies per million cells	Eriksson et al., 2013

Table 1. Summary of the current techniques used to identify circulating associated viral reservoirs. Sample size indicates the amount of blood required; assay input reveals the cells used; amplification required means the necessity of clones to proliferate or sequences to be amplified before the assay; limits of detection indicates the lowest number of cells detectable.

Sample	HIV Status	Age	Gender	cART	CD4 Counts (cell/mm)	Viral Load (copies/ml)	Years with HIV
1	+	64	M	Yes	801	<50	14
2	+	49	F	Yes	759	231	14
3	+	43	M	Yes	584	65	13
4	+	40	F	No	5	69	1
5	+	43	M	Temporary	77	4238	13
6	-	49	F	No	NP	-	-
7	-	64	F	No	NP	-	-
8	-	64	F	No	NP	-	-

Table 2. **Clinical data of HIV-infected and uninfected patients.** Tissues of the patients, provided by NNTC, used for this thesis. Data show the status of infection, the gender, the age, the possible cART administration during life, the last CD4 count (NP means not provided) and viral load of the patients analyzed plus the years following HIV diagnosis. Specifically, patients 1 to 5 were HIV-infected, instead, patients 6, 7, and 8 were HIV-uninfected and used as controls.

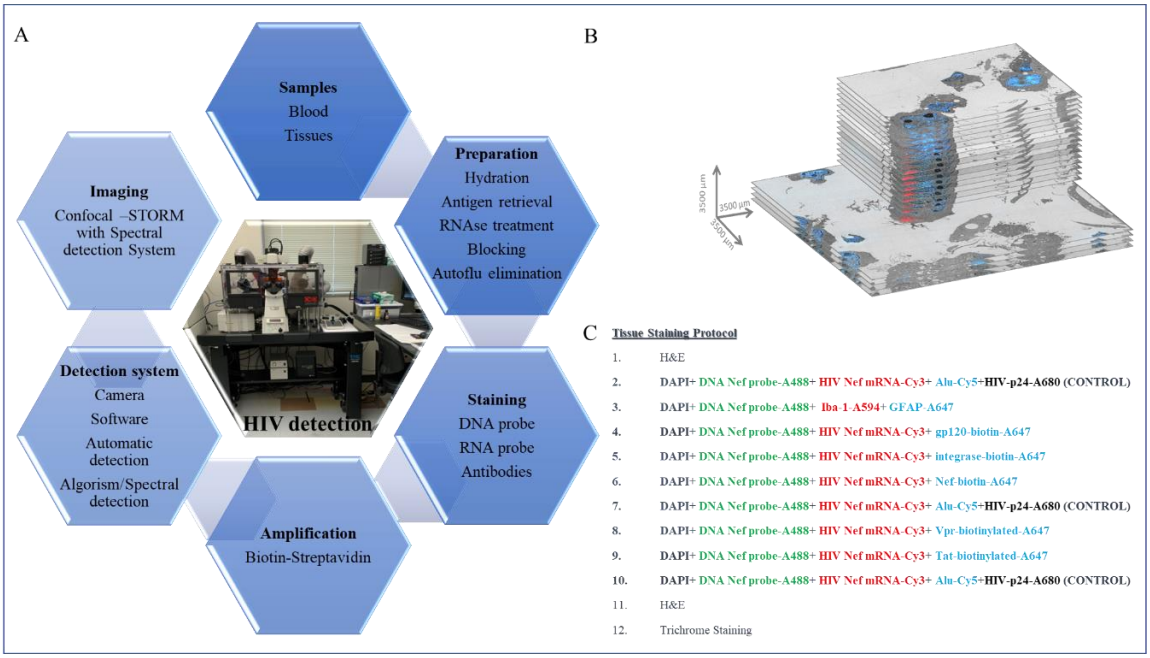

Figure 2.1. Summary of the microscopy and staining protocols used to detect viral reservoirs. (A) Detection method. For our methodologies, blood or tissues can be used to detect circulating or tissue-associated viral reservoirs. Blood was prepared as described in the materials and methods section. Tissue sections can be unfixed or fixed with PFA 4% as explained in materials and methods section. The improved methods to detect viral reservoirs included hydration, antigen retrieval, RNA treatment, blocking and autofluorescence elimination that are well explained in the materials and methods section. The staining involved the use of 2 DNA probes, one for HIV DNA and one for Alu repeats; an RNA probe for HIV Nef mRNA; DAPI for the nuclear staining; and several antibodies for HIV and host cellular proteins. To amplify the small signals present in viral reservoirs, we take advantage of the biotin-streptavidin amplification system. The detection system required camera, software, automatic detection and algorism/spectral detection. This protocol was analyzed using Confocal-Stochastic Optical Resolution microscopy (STORM) with spectral detection capabilities. **(B)** Representative picture of 12 stained serial sections, reconstructed to generate a 3D map of the viral reservoirs. **(C)** Representative example of the protocol used to detect viral reservoirs. Serial sections were generated for a large piece of tissue and sections 1,11 and 12 were used to perform H&E and trichrome staining to assess histology and volume changes (62 µm of distance between

section 1 and 11). Serial sections 2, 7 and 10 were used to stain DAPI, HIV-integrated DNA, HIV mRNA, Alu repeats, and p24 protein to evaluate the correct 3D reconstruction of the tissue considering that the size of the cells is ~40 µm. Serial section 3 was stained for DAPI, HIV-integrated DNA, Iba-1 (microglia/macrophages marker), and GFAP (astrocytes marker). The other serial sections were stained for DAPI, HIV-integrated DNA, HIV mRNA, and HIV proteins such as Gp120, Integrase, Nef, Vpr, and Tat. Overall this experiment investigated 84 µm (in thickness) of tissue.

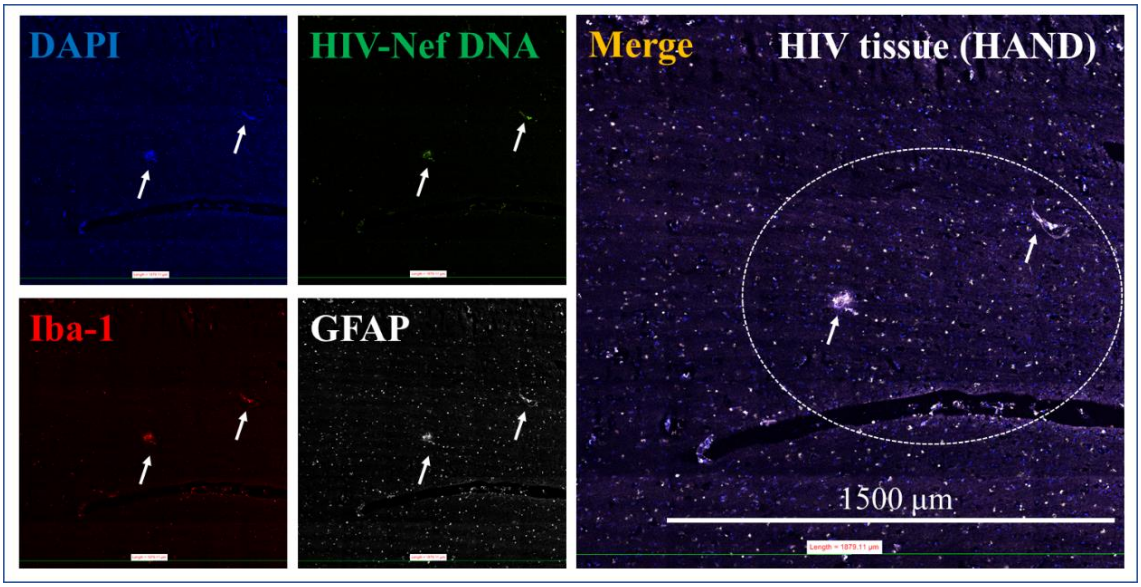

Figure 2.2. Representative example of staining for DAPI, HIV-Nef DNA, Iba-1 and GFAP in human brain tissue of HIV-infected patient under cART, with a normal CD4 count and without systemic viral replication. Shown is a positive field of 1500 μm^2 from a 6 by 6 picture, where it is possible to observe cells positive for HIV-Nef DNA (in green) and for Alu repeats (data not shown). These HIV-integrated DNA cells correspond to macroglia/macrophages (Iba-1 positive in red) and astrocytes (GFPA positive in white) that generate clusters as indicated by the arrows. Clusters are made by 3 to 10 cells located in the sample place.

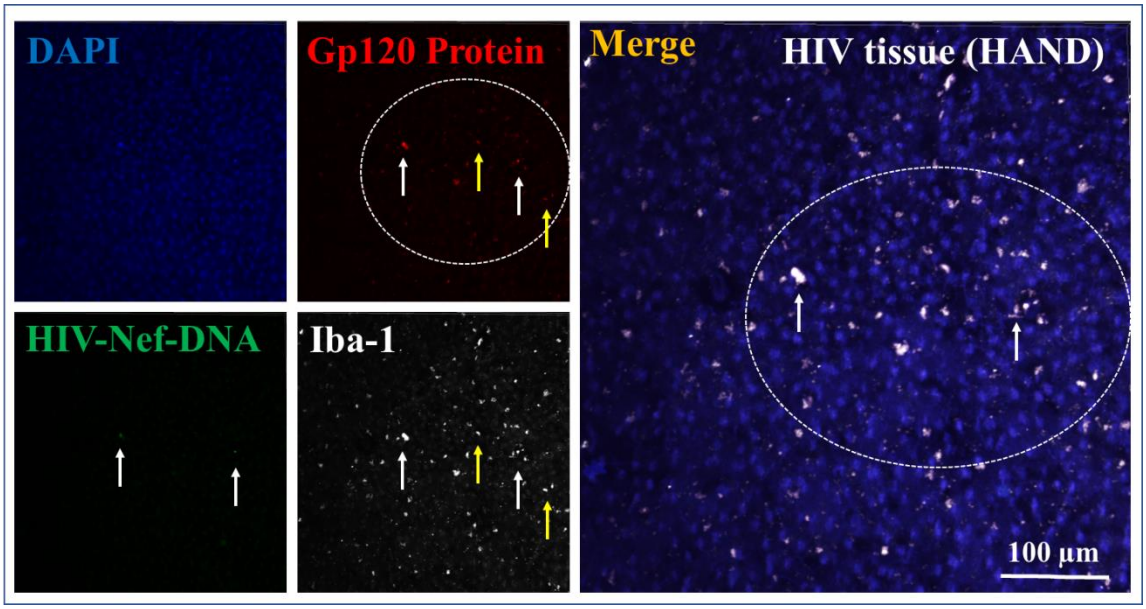

Figure 2.3. Representative example of staining for DAPI, Gp120 protein, HIV-Nef DNA and Iba-1 in human brain tissue of HIV-infected patient under cART, with a normal CD4 count and without systemic viral replication. Shown is a positive field from a 6 by 6 picture, where it is possible to observe cells positive for HIV-Nef DNA (in green), for Alu repeats (data not shown) and Gp120 protein (in red). These HIV-integrated DNA and Gp120 protein positive cells correspond to macroglia/macrophages (Iba-1 positive in white), as indicated by the white arrows. But most of the Gp120 signals do not colocalize with HIV-Nef DNA in microglia/macrophages, as indicated by the yellow arrows, suggesting that Gp120 can diffuse into the neighboring cells negative for HIV-integrated DNA.

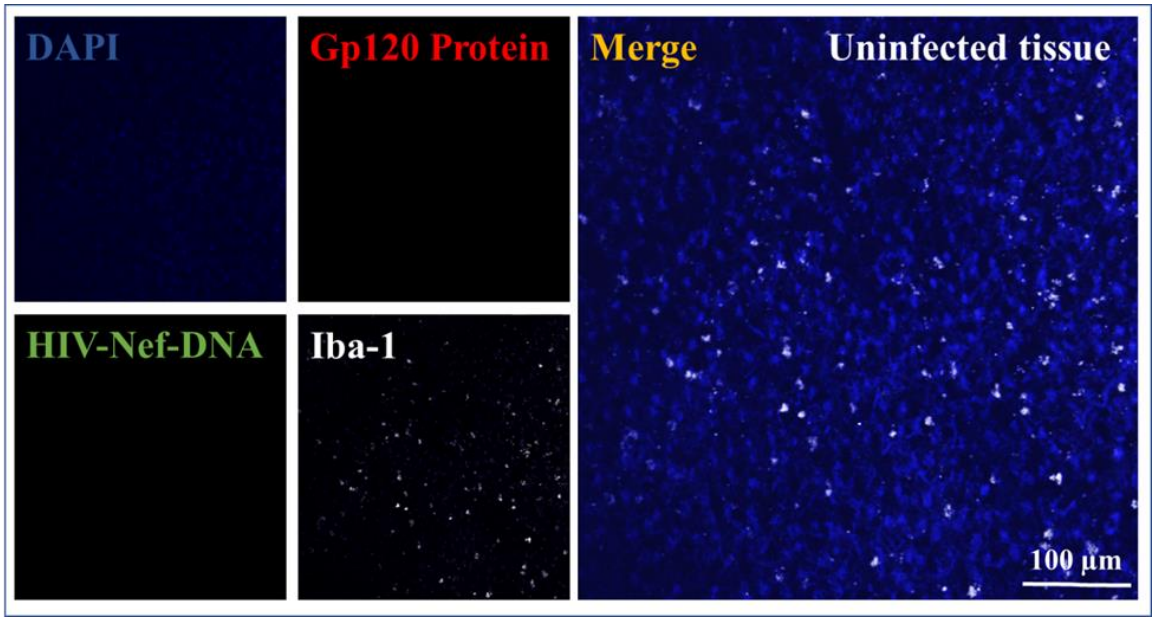

Figure 2.4. Human brain uninfected tissue showing no staining for HIV-Nef DNA and Gp120 protein. The staining is only positive for DAPI showing nuclear localization and Iba-1 indicating microglia/macrophages in the tissue.

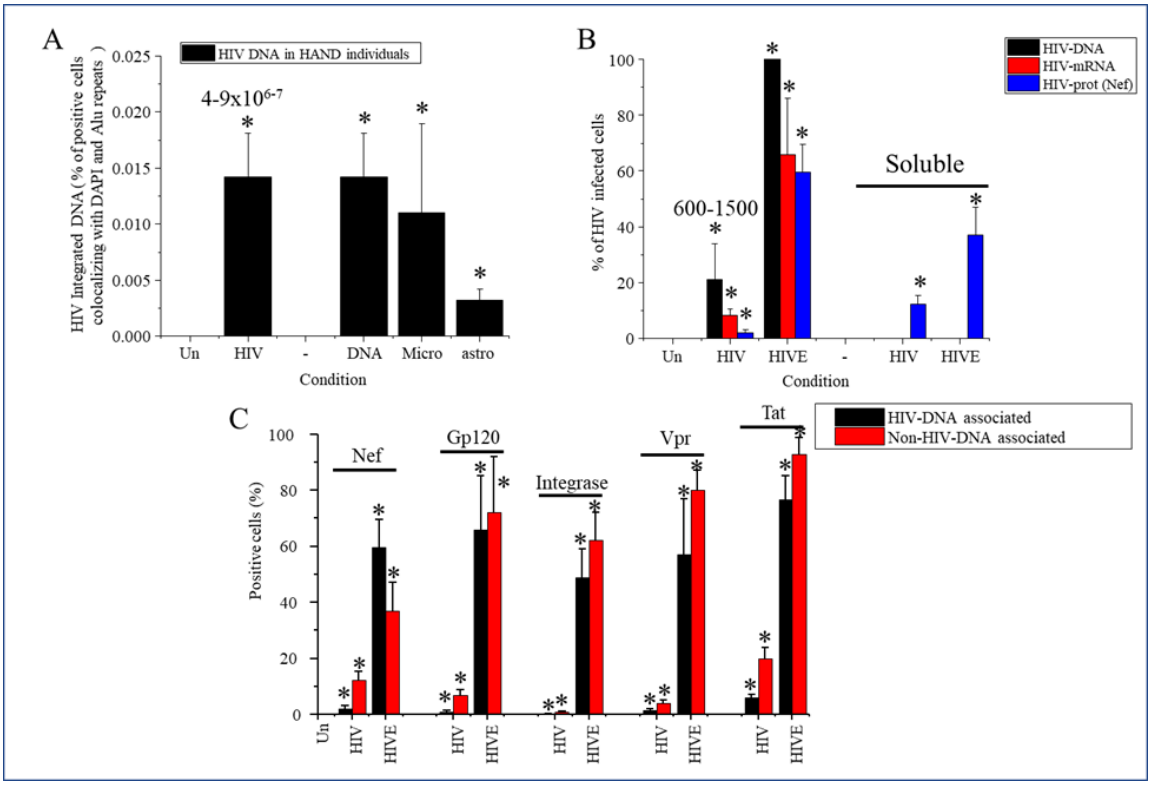

Figure 2.5. Quantification of the viral reservoirs in brain tissue. (A) Identification of cell containing HIV-integrated DNA in human brain tissue sections. HIV-integrated DNA was not detected in any of the uninfected tissues analyzed. Between the HIV-infected brain tissue sections, we counted a total amount of 4-9x10$^{6-7}$ cells. From them, the HIV-integrated DNA positive cells represented 0.014% of the total volume analyzed. 0.011% of these cells were Iba-1 positive identifying microglia/macrophages and 0.003% were GFAP positive identifying them as astrocytes (* p<0.0001). **(B)** Identification of localized HIV-integrated Nef DNA, HIV Nef mRNA and Nef protein in uninfected, HIV-infected and HIV-encephalitis conditions. HIV-integrated DNA, HIV-mRNA, and Nef protein were not detected in any of the uninfected tissues analyzed. Between the HIV-infected brain tissue sections we counted 600-1500 of HIV-integrated DNA positive cells that represent the 20% of the total cells, 8% of them were HIV mRNA positive and 2% were Nef protein positive. These small percentages are due to administration of cART during the life of the patients considered. HIV-encephalitis was used as a positive control for its correlation between HIV-integrated DNA, HIV mRNA and viral proteins. Moreover, Nef proteins were also located in the neighboring HIV-associated DNA negative cells, suggesting HIV protein

diffusion in both HIV and encephalitis conditions (* $p<0.0001$). **(C)** Identification of HIV proteins (Nef, Gp120, Integrase, Vpr, Tat) in HIV-integrated DNA positive and negative cells within uninfected, HIV-infected and HIV-encephalitis human brain sections. No viral proteins were detected in uninfected tissues. HIV-encephalitis human brain tissue sections indicated a good correlation for all the HIV proteins in HIV-integrated DNA positive and negative cells. On the contrary, HIV-infected human brain tissue sections showed a major localization of the viral protein in HIV-integrated DNA negative cells than the positive one (* $p<0.0001$).

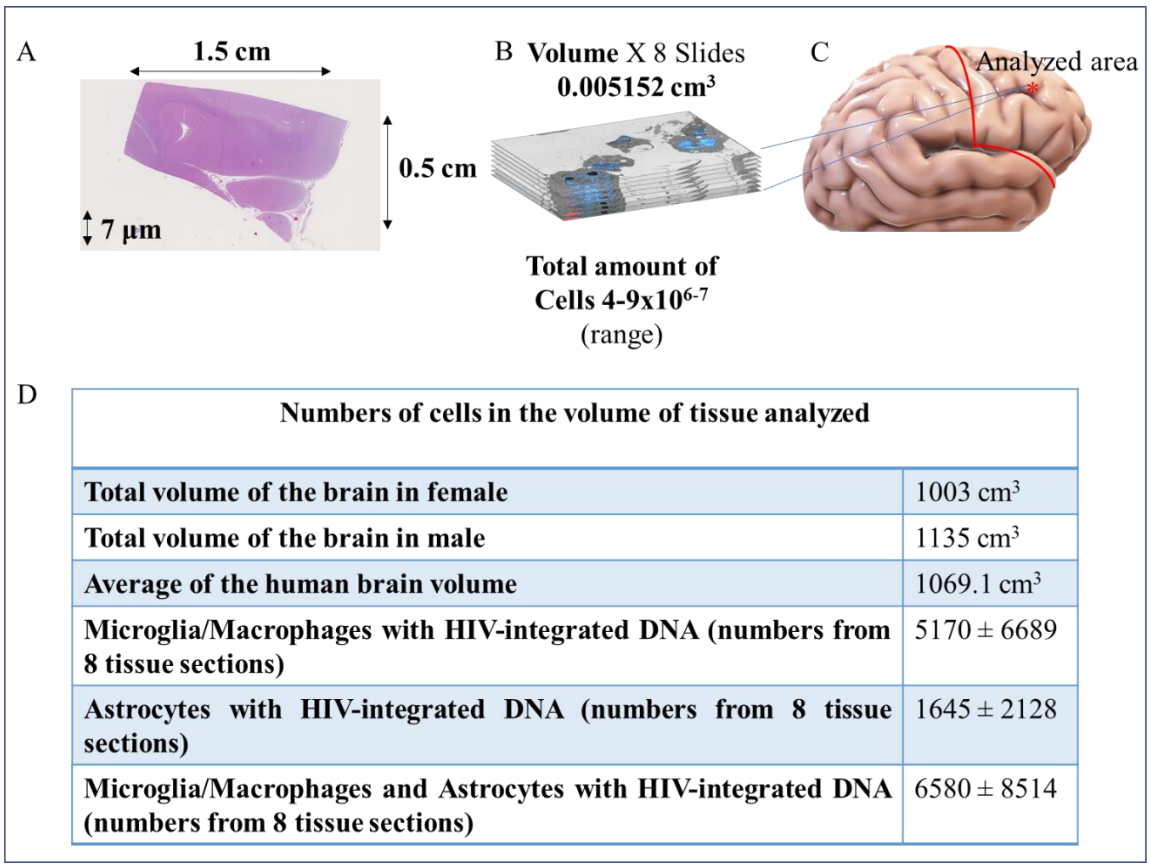

D

Numbers of cells in the volume of tissue analyzed	
Total volume of the brain in female	1003 cm^3
Total volume of the brain in male	1135 cm^3
Average of the human brain volume	1069.1 cm^3
Microglia/Macrophages with HIV-integrated DNA (numbers from 8 tissue sections)	5170 ± 6689
Astrocytes with HIV-integrated DNA (numbers from 8 tissue sections)	1645 ± 2128
Microglia/Macrophages and Astrocytes with HIV-integrated DNA (numbers from 8 tissue sections)	6580 ± 8514

Figure 2.6. Explanation of the quantification of HIV reservoirs in human brain tissues: rationale for approach. (A) H&E staining section used for calculating the volume of the tissue. **(B)** Quantification of the total brain volume analyzed of 8 human occipital cortex slides used to investigate HIV reservoirs, 0.005152 cm^3. The number of 4-9x10^{6-7} cells corresponds to the total cells in one slide. **(C)** Representation of the analyzed area. For the large-scale quantification brain included all lobes of the cerebrum, the basal ganglia, the thalamus, the ventricles and the hippocampi. **(D)** Table showing the numbers of cells in the total volume of tissue analyzed, including the total volume of the brain in female and male, the average of the human brain volume that we used to quantify viral reservoirs in the total brain, and quantification of microglia/macrophages and astrocytes with HIV-integrated from the 8 tissue sections analyzed.

Viral reservoirs in the total human brain	
Microglia/Macrophages with HIV-integrated DNA in the total human brain	1072835210 ± 1388093159 (0.09765 ± 0.136 % of the total cells in the human brain)
Astrocytes with HIV-integrated DNA in the total human brain	341357157.7 ± 441666712 (0.03102 ± 0.040 % of the total cells in the human brain)
Microglia/Macrophages and Astrocytes with HIV-integrated in the entire human brain	1140426631 ± 1448465969 (0.1245 ± 0.161 % of the total cells in the human brain)
Microglia/Macrophages and Astrocytes with HIV-integrated DNA and HIV mRNA in the total human brain	87154891.3 ± 52823841.1 (0.00792 ± 0.005 % of the total cells in the human brain)
Microglia/Macrophages and Astrocytes with HIV-integrated DNA and Nef protein in the total human brain	21788722.8 ± 13205960.3 (0.00196 ± 0.001 % the total cells in the human brain)
Microglia/Macrophages and Astrocytes without HIV-integrated DNA and with Nef protein in the total human brain	108943614.2 ± 66029801.4 (0.00988 ± 0.005 % of the total cells in the human brain)
Microglia/Macrophages and Astrocytes with HIV-integrated DNA and Gp120 protein in the total human brain	312045637.7 ± 439098179.5 (0.00010 ± 0.0001 % of the total cells in the human brain)
Microglia/Macrophages and Astrocytes without HIV-integrated DNA and with Gp120 in the total human brain	8715489.1 ± 5282384.1 (0.00079 ± 0.0005 % of the total cells in the human brain)
Microglia/Macrophages and Astrocytes with HIV-integrated DNA and Integrase protein in the total human brain	544718.1 ± 330149 (0.00005 ± 0.00003 % of the total cells in the human brain)
Microglia/Macrophages and Astrocytes without HIV-integrated DNA and with Integrase protein in the total human brain	807077.1 ± 509365.6 (0.00007 ± 0.00004 % of the total cells in the human brain)
Microglia/Macrophages and Astrocytes with HIV-integrated DNA and Vpr protein in the total human brain	1634153.8 ± 990447.6 (0.00015 ± 0.00009 % of the total cells in the human brain)
Microglia/Macrophages and Astrocytes without HIV-integrated DNA and with Vpr protein in the total human brain	4357744.6 ± 2641192.1 (0.000396 ± 0.00024 % of the total cells in the human brain)
Microglia/Macrophages and Astrocytes with HIV-integrated DNA and Tat protein positive cells in the total human brain	6536616.8 ± 3961788.1 (0.00060 ± 0.00036 % of the total cells in the human brain)
Microglia/Macrophages and Astrocytes without HIV-integrated DNA and with Tat protein in the total human brain	21788722.8 ± 13205960.3 (0.00198 ± 0.00120 % of the total cells in the human brain)

Table 3. Quantification of HIV reservoirs in the entire human brain.

Viral reservoirs in the total human lymph nodes	
Lymphocytes with HIV-integrated DNA in the total human lymph nodes	38877757693 ± 53051279141 (7.77555 ± 10.610 % of the total cells in the human lymph nodes)
Lymphocytes with HIV-integrated DNA and HIV mRNA in the total human lymph nodes	12151730769 ± 15320991414 (4.59706 ± 0.264 % of the total cells in the human lymph nodes)
Lymphocytes with HIV-integrated DNA and Gp120 protein in the total lymph nodes	2739517266 ± 2344752452 (0.547903 ± 0.469 % of the total cells in the human lymph nodes)
Lymphocytes without HIV-integrated DNA and with Gp120 protein in the total lymph nodes	9874482192 ± 13446159628 (1.97489 ± 2.689 % of the total cells in the human lymph nodes)

Table 4. Quantification of HIV reservoirs in the total human lymph nodes.

Chapter 3: Characterization of astrocyte metabolism in HIV-infected condition

D'Amico Daniela[1,2]; Prideaux Brendan [1]; Eugenin Eliseo A.[1]

[1]University of Texas Medical Branch (UTMB), Department of Neuroscience, Cell Biology and Anatomy, Galveston, TX, USA

[2]University of Palermo (UniPa), Department of Biomedicine, Neuroscience and Advanced Diagnostics, Palermo, Italy

This work was funded by The National Institute of Mental Health grant, MH096625, the National Institute of Neurological Disorders and Stroke grant, NS105584, and UTMB internal funding (to E.A.E).

Associated paper: D'Amico D., Gorska A.M., Prideaux B., and Eugenin E.A. "Characterization of mitochondrial-associated metabolism in HIV-infected astrocytes". In preparation.

Introduction

As described in Chapter 2, our data generated *in vivo* demonstrated that microglia/macrophages and a small population of astrocytes are infected with HIV and survive infection for extended periods of time, even in the presence of cART. In agreement, our data *in vitro* using human primary astrocyte cultures demonstrated that only 5% of cells are infected with HIV (Eugenin and Berman, 2007). However, despite the low number, HIV-infected astrocytes can trigger bystander cellular dysfunction compromising neighboring uninfected endothelial cells, neurons and astrocytes by a gap junction-dependent mechanism (Eugenin and Berman 2007, Eugenin et al. 2011, Malik et al. 2017). Also, our laboratory demonstrated that the bystander mechanism of toxicity was mediated by the Cytochrome C, inositol triphosphate, and calcium dependent mechanism (Eugenin and Berman 2013). Electron microscopy analysis of HIV-infected astrocytes indicated that mitochondria were enlarged and membrane contacts with other organelles were compromised (data in process of publication). This phenotype was similar to that data obtained in latently HIV macrophage reservoirs described by us (Castellano et al. 2019). Briefly, we demonstrated that latent HIV-infected macrophages have a specific metabolic signature characterized by the use of unusual sources of energy such as glutamine/glutamate (Castellano et al. 2019). Uninfected macrophages use fatty acid and glucose as a major source of energy and upon blocking a particular metabolic pathway they can switch to alternative sources of carbon. In contrast, HIV-infected macrophages use fatty acid and glucose but also glutamine/glutamate as a major source of energy. More importantly, they cannot shift between different carbon sources to produce energy (Castellano et al. 2019). However, whether this metabolic signature was present in HIV-infected astrocytes is unknown.

In contrast, the metabolism of latent HIV-infected T cells has been correlated with enhanced glycolysis and OXPHOS. Glucose metabolism rather than fatty acid oxidation characterized the primary sources of energy for the latent $CD4^+$ T cells (Valle-Casuso et al. 2019). Glucose transporter-1 (Glut1), which is a marker for glycolysis, is up-regulated in $CD4^+$ T cells of HIV-infected patients compared with uninfected controls (Palmer et al. 2014). Glut1 mediates the glucose metabolic pathways by the homeostatic cytokine IL-7

(Loisel-Meyer et al. 2012). However, it is unknown whether a similar pathway is present in HIV-infected astrocytes.

Overall, the investigated latently HIV-infected cells have different metabolic signatures, but all of them have a common feature, they are not able to shift from one source of energy to another by shifting away from OXPHOS towards glycolysis that is useful to support the rapid cell progression and proliferation (as demonstrated in glioblastoma cells) (Guda et al. 2019). This finding is unique and enables us to target this "weak" mechanism present in HIV reservoirs. Therefore, we examined OXPHOS in HIV-infected astrocyte cultures using the Seahorse Biosystems platform (Agilent Technologies, Santa Clara, CA) by testing different sources of carbon related to the tricarboxylic acid cycle (TCA) as we previously described for macrophages (Castellano et al. 2019).

Materials and Methods

Cell Culture Methods

Human primary astrocytes were cultured using high glucose Dulbecco's modified Eagle's medium (DMEM, 11995-065, Thermo Fisher Scientific, Waltham, MA) supplemented with 10% fetal bovine serum (FBS, S12450H, Atlanta Biologicals, Flowery Branch, GA), penicillin, and streptomycin (15070063, Thermo Fisher Scientific, Waltham, MA) and grown at 37 °C in a humidified atmosphere with 5% CO_2.

HIV-infection of astrocyte cultures

Confluent cultures of human astrocytes were infected by incubation with HIV_{ADA} (20–50 ng p24/ml), using a previously described protocol (Eugenin et al. 2011). Briefly, astrocytes were exposed to the HIV_{ADA} for 24 hours. Later HIV-infected astrocytes were washed extensively to eliminate the unbound virus before addition of fresh medium supplemented with 5% fetal bovine serum (FBS, S12450H, Atlanta Biologicals, Flowery Branch, GA) and leaved for 6 days.

Metabolic assessment through extracellular flux analysis

Analysis of the oxygen consumption rate (OCR) were measured using an XFp Analyzer (Agilent Seahorse Technologies, Santa Clara, CA). XFp Seahorse plates were seeded with

10,000 human primary astrocytes per well. Cells were infected with HIV_{ADA} for 7 days. Culture medium was replaced by XF base medium (102353-100, Agilent Seahorse Technologies, Santa Clara, CA) supplemented with 2 mM Glutamine (25030081, Thermo Fisher Scientific, Waltham, MA), 1 mM Pyruvate (P5280, Sigma-Aldrich, St. Luis, MO) and 10 mM Glucose (47829, Sigma-Aldrich, St. Luis, MO) according to the manufacturer's instructions (https://www.agilent.com/cs/usermanuals/public/XFCellMitoStressTest). For testing single source of carbon for the TCA cycle, culture medium was replaced by XF base medium with Glutamine only, Pyruvate only, Glucose only, 2 mM Glutamate (1446600, Sigma-Aldrich, St. Luis, MO), or 50 µM Fumarate (242926, Sigma-Aldrich, St. Luis, MO) (Kornberg et al. 2018) with an adjusted pH of 7.4. Cells were then incubated at 37°C without CO_2 for 45 minutes. Four compounds from the XFp cell mito stress test kit (103010-100, Agilent Seahorse Technologies, Santa Clara, CA) were injected during the assay at the following final concentrations: oligomycin (2 µM), p-trifluoremethoxyphenylhydrazone (FCCP, 0.8 µM), and a mixture of antimycin A (0.5 µM) and rotenone (0.5 µM). Agilent Seahorse software Wave 2.3 was used for data analysis. The mitochondrial basal respiration, the maximal respiration, the proton leak, the ATP production, the spare respiratory capacity and the non-mitochondrial respiration were used to compare metabolic activities of the HIV-infected astrocyte cultures with the uninfected controls.

Statistical Analysis

All data were expressed as mean ± standard error of the mean (SEM). Differences among groups were analyzed by t-test and one-way analyses of variance (ANOVA test), using Bonferroni's multiple comparison test for post-hoc analysis. The level of significance was accepted at $p<0.05$. Prism8.0 software was used to perform statistical analyses.

Results

Analysis of the mitochondrial metabolic profile of human astrocytes by the Seahorse system. The Seahorse systems enables us to measure electron transport chain (ETC) (Figure 3.2 A) and the OXPHOS function in the mitochondria. As indicated in the Figure 3.2 A, the ETC mechanism occurs in the inner mitochondrial membrane and the five

protein complexes that compose it transfer electrons and pump protons into the inter membrane space. Protons in the mitochondrial inter membrane space generate a high proton gradient that enable the complex V to convert ADP into ATP and produce energy. Rotenone, Antimycin A and Oligomycin are used for the seahorse analysis to specifically inhibits complex I, IV and V, respectively and evaluate oxygen consumption rate (Figure 3.2 A).

OXPHOS is the main source of oxygen consumption in the mitochondria and OCR is used to assess mitochondrial integrity and performance (Figure 3.2 B). Through the Seahorse analysis, it is possible to evaluate the mitochondrial basal respiration, the ATP production, the proton leak, the maximal respiration, the spare respiratory capacity, the non-mitochondrial respiration, and the coupling efficiency (Figures 3.2 B and 3.3). The mitochondrial basal respiration (Figure 3.2 A, blue box) represents the energetic demand of the cell under baseline conditions. The ATP production (Figure 3.2 B, pink box), evaluated after the inhibition of complex V by oligomycin, shows the ATP molecules produced by the mitochondria. The proton leak (Figure 3.2 A, violet box) characterizes the remaining basal respiration not coupled to ATP production. The maximal respiration (Figure 3.2 A, green box) calculated after the FCCP injection shows the maximum rate of respiration that the cells can accomplish. The spare respiratory capacity (Figure 3.2 B, dark green box) indicates the capability of the cell to respond to an energetic demand. The non-mitochondrial respiration (Figure 3.2, red box) reveals the consume of oxygen after the addition of rotenone and antimycin A and it is driven by processes outside the mitochondria. The coupling efficiency represents the relationship between the ATP production rate and the basal respiration rate. Thus, we used this assay to provide insight about mitochondrial function to understand the metabolic profile of HIV-infected astrocytes compared to the uninfected astrocytes using different sources of carbons (Figure 3.1), as we recently described for HIV-infected macrophages (Castellano et al. 2019).

Human astrocytes can use different sources of carbon to produce energy. As indicated in the Figure 3.1, glucose, pyruvate, glutamine, glutamate, and fumarate can be metabolic sources for the TCA cycle in the mitochondria (Figure 3.1) and used by viral reservoirs to produce energy and survive (Castellano et al. 2019). Thus, we determined how these

alternative sources of carbon for the TCA cycle can affect mitochondria metabolism in uninfected and HIV-infected astrocytes cultures. We treated uninfected and HIV-infected astrocyte cultures with media supplemented with 10 mM Glucose, 1 mM Pyruvate and 2 mM Glutamine as a mix reference media, with 10 mM Glucose, 1 mM Pyruvate, 2 mM Glutamine, 2 mM Glutamate, or 50 μM Fumarate containing media to perform the Seahorse analysis. As control, uninfected astrocytes were used and we showed that basal respiration (Figure 3.3 B), maximal respiration (Figure 3.3 C), proton leak (Figure 3.3 D), ATP production (Figure 3.3 E), spare respiratory capacity (Figure 3.3 F), coupling efficiency (Figure 3.3 G) and non-mitochondrial oxygen consumption (Figure 3.3 H) in mix control uninfected condition were induced by the ETC inhibitors using the same timecourse showed in Figure 3.3 A, as well as other cell types (Pence and Yarbro 2018, van der Windt et al. 2016). When we replaced the mix media with the media containing only glucose, we observed decrease in basal respiration (Figure 3.3 B, ! p=0.0215), maximal respiration (Figure 3.3 C, ! p=0.0069) and spare respiratory capacity (Figure 3.3 F, ! p=0.0068). In contrast to what we noticed for glucose, when the mix media was replaced with media containing only pyruvate or glutamine, we did not observed differences in basal respiration, maximal respiration, proton leak, ATP production, spare respiratory capacity, coupling efficiency and non-mitochondrial oxygen consumption. Remarkably, even that glutamate is a sub-product of glutamine, we observed a significant decrease in basal respiration (Figure 3.3 B, ^ p<0.0001), maximal respiration (Figure 3.3 C, ^ p<0.0001), proton leak (Figure 3.3 D, ^ p=0.0012), ATP production (Figure 3.3 E, ^ p=0.0067), spare respiratory capacity (Figure 3.3 F, ^ p<0.0001), and coupling efficiency (Figure 3.3 G, ^ p=0.0038) compared to the mix media condition, the media containing only glucose, glutamate or glutamate conditions. This may suggest impairment in glutamine synthetase or glutaminase enzymes in the HIV-infected cultures (Figure 3.1). Normally, the reaction between glutamine and glutamate is reservable. Thus, a gradient problem may be present and will be explored in future studies. When we replaced the media mix with the media containing only fumarate, the differences observed were for maximal respiration (Figure 3.3 C, ~ p=0.0312) and spare respiratory capacity (Figure 3.3 F, ~ p=0.0212) that decreased, and for non-mitochondrial oxygen consumption (Figure 3.3 H, ~ p=0.0446)

which increased. These data suggest that OXPHOS is not compromised and that uninfected astrocytes can use different sources of carbon to produce energy.

HIV-infected astrocytes can use different sources of carbon to produce energy in a similar manner to uninfected astrocytes. Our Seahorse analysis comparing uninfected and HIV-infected astrocyte cultures treated with media supplemented with glucose, pyruvate and glutamine as a mix reference media, with glucose, pyruvate, glutamine, glutamate, or fumarate containing media did not show any significative changes in basal respiration (Figure 3.3 B), maximal respiration (Figure 3.3 C), proton leak (Figure 3.3 D), ATP production (Figure 3.3 E), spare respiratory capacity (Figure 3.3 F), coupling efficiency (Figure 3.3 G) and non-mitochondrial oxygen consumption (Figure 3.3 H). This may be explained by the low numbers of HIV-infected cells in cultures. Nevertheless, when we compared the HIV-infected astrocytes cultures treated with the mix media to HIV-infected astrocytes cultures treated with glucose, pyruvate, glutamine, glutamate, or fumarate containing media, we detected differences. Replacing the mix media with glucose containing media, we only observed decreasing levels of maximal respiration (Figure 3.3 C, !! p=0.0032) and spare respiratory capacity (Figure 3.3 F, !! p=0.0009), but no significant differences were detected between HIV-infected astrocytes and uninfected astrocytes treated with glucose. Moreover, when we replaced mix media in HIV-infected astrocytes with medium containing only pyruvate we did not detect any changes in basal respiration (Figure 3.3 B), maximal respiration (Figure 3.3 C), proton leak (Figure 3.3 D), ATP production (Figure 3.3 E), spare respiratory capacity (Figure 3.3 F), and coupling efficiency (Figure 3.3 G). Instead, the media containing only glutamine in HIV-infected astrocytes cultures induced decrease of spare respiratory capacity (Figure 3.3 F, ** p=0.0368) compared to the HIV-infected astrocyte cultures treated with media mix. In agreement with the control uninfected condition, media containing only glutamate also generated several changes compared to the mix media in HIV-conditions. In fact, the media containing only glutamate in HIV-infected astrocyte cultures decreased basal respiration (Figure 3.3 B, ^^p=0.0026), maximal respiration (Figure 3.3 C, ^^ p<0.0001), proton leak (Figure 3.3 D, ^^ p=0.0180), ATP production (Figure 3.3 E, ^^ p=0.0171), and spare respiratory capacity (Figure 3.3 F, ^^ p<0.0001) compared to HIV-infected astrocytes

treated with media mix, glucose, pyruvate, and glutamine containing media. Again, when we replaced the media mix with the media containing only fumarate in HIV-infected astrocyte cultures, the maximal respiration (Figure 3.3 C, ~~ p=0.0342) and the spare respiratory capacity (Figure 3.3 F, ~~ p=0.0368) decreased, but were maintained at the same levels as the uninfected astrocyte cultures treated with the media containing only fumarate. These results suggest that also in HIV conditions OXPHOS is not fully compromised, thus uninfected and HIV-infected astrocytes can use different sources of carbon to produce energy.

HIV infection changes the non-mitochondrial oxygen consumption in astrocytes. As indicated above, Seahorse analysis comparing uninfected and HIV-infected astrocyte cultures treated with media supplemented with glucose, pyruvate and glutamine as a mix reference media, with glucose, pyruvate, glutamine, glutamate, or fumarate containing media did not show any significative changes in basal respiration (Figure 3.3 B), maximal respiration (Figure 3.3 C), proton leak (Figure 3.3 D), ATP production (Figure 3.3 E), spare respiratory capacity (Figure 3.3 F), coupling efficiency (Figure 3.3 G) and this was valid also for the non-mitochondrial oxygen consumption (Figure 3.3 H). In addition, when we replaced the media mix in HIV-infected astrocyte cultures with media containing only glucose or pyruvate, any differences were detected for the non-mitochondrial oxygen consumption. Noteworthy, only glutamine (Figure 3.3 H, ** p=0.0308) and glutamate (Figure 3.3 H, ^^ p=0.0449) treated HIV-infected astrocyte cultures showed decreased levels of non-mitochondrial oxygen consumption compared to the HIV-infected astrocytes treated with mix media and media containing only glucose, pyruvate or fumarate. This data suggests that HIV-infected astrocytes can use alternative sources of energy that are completely independent from mitochondria, such as the pentose phosphate pathway (Loreck et al. 1987).

Discussion

Measurement of cellular respiration can be used to assess cellular energy metabolism for the oxygen consumption during oxidative phosphorylation (Divakaruni et al. 2014). For our analysis, we used glucose, pyruvate, glutamine, glutamate and fumarate as respiratory

substrates from which electrons are transported through the electron transport chain to measure oxygen consumption and evaluate if HIV infection can alter mitochondrial metabolism in astrocytes.

Metabolic analyses for latently HIV-infected macrophages and $CD4^+$ T cells have shown that they use glutamine/glutamate and glucose, respectively, as primary sources of energy. Therefore, we demonstrated that HIV-infected astrocytes compared with uninfected astrocytes did not show compromised metabolic steps in the tricarboxylic acid cycle preceding oxidative phosphorylation, even in the presence of different carbon sources. This may be due to the culture's composition of around 95% of uninfected astrocytes and only 5% of HIV-infected astrocytes. Nevertheless, the non-mitochondrial oxygen consumption rate decreased for glutamine and glutamate in HIV-infected astrocytes suggesting that glutaminase (GLS) and/or glutamine synthase (GS) enzymes do not work properly and that HIV-infected astrocytes need to be partially supported by a non-mitochondrial source of energy such as pentose phosphate pathway. The pentose phosphate pathway can metabolize glucose in the cytoplasm, parallelly to glycolysis (Loreck et al. 1987). Its activity has been investigated in astrocytes (Brekke et al. 2012, Sickmann et al. 2005), where it covers approximately 5% of the glucose metabolism, but can be upregulated to in response to pathological conditions (Allaman et al. 2010, Dusick et al. 2007). Therefore, for future experiments we intend to investigate GLS and GS activity in HIV-infected astrocytes. In parallel, we plan to examine the glucose-6-phosphate dehydrogenase (G6PDH) activity because it catalyzes the conversion of glucose-6-phosphate to 6-phosphoglucono-δ-lactone that is the first and rate-limiting step of the pentose phosphate pathway (PPP) testing its role in HIV-infected astrocytes.

Thus, if our analysis cannot draw a specific metabolic profile for HIV-infected astrocytes due to their low number in culture, we can assess that they use glucose as a major energy source as well as that they can be partially dependent on non-mitochondrial energy sources such as the pentose phosphate pathway.

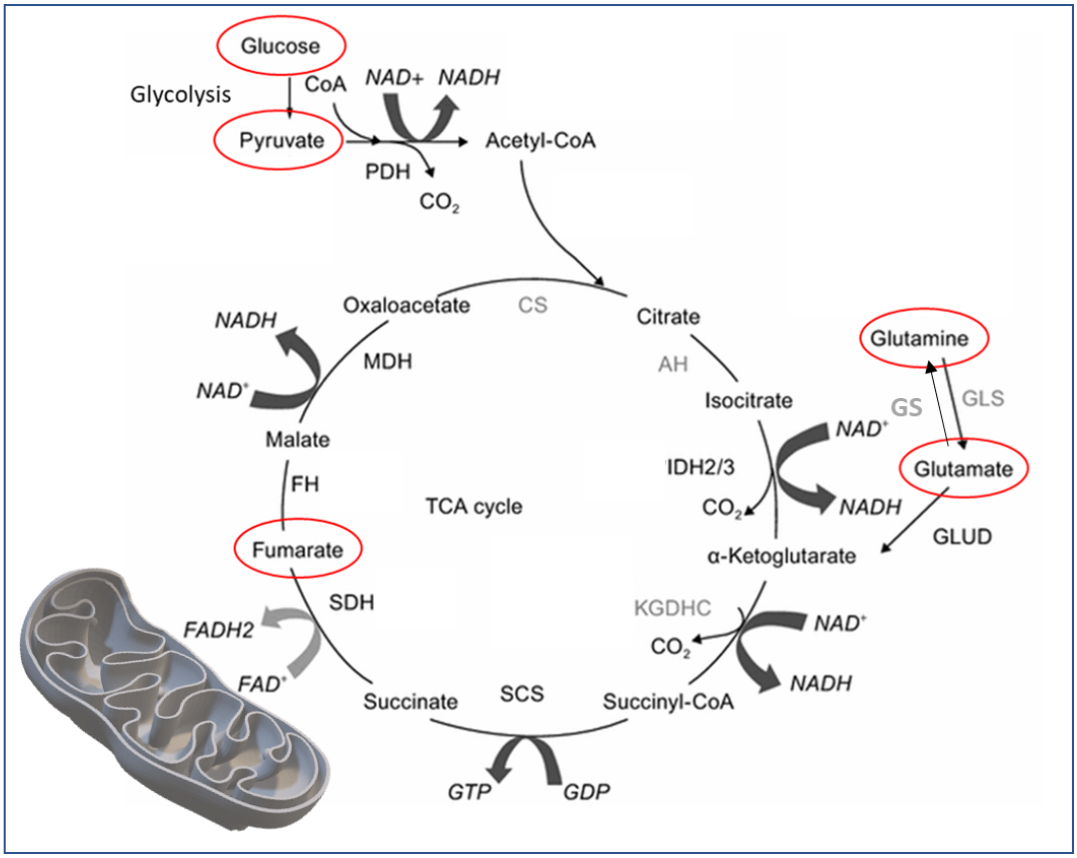

Figure 3.1. Biochemical reactions driving the TCA cycle, adapted from (Anderson N. M. et al. 2018). Glucose represents the major source of energy for the cells. Glucose is transported into the cell by glucose transporters and delivered to the TCA cycle in the form of pyruvate. The starting metabolite for the TCA cycle is acetyl-CoA, deriving from pyruvate. Specifically, the pyruvate dehydrogenase (PDH) enzyme transforms pyruvate, nicotinamide adenine dinucleotide (NAD+), coenzyme A into acetyl-CoA, CO_2, and NADH. Several redox reactions allow acetyl-CoA to produce high-energy electrons, which are carried to the electron transport chain by nicotinamide adenine dinucleotide (NAD^+) and flavin adenine dinucleotide (FAD). Thus, oxidative phosphorylation produces adenosine triphosphate (ATP). Since NAD^+ and FAD require oxygen, the TCA cycle works in aerobic environments. Eight steps characterize the TCA cycle. Three of them are irreversible: the generation of citrate from oxaloacetate and acetyl-CoA by citrate synthase (CS); the conversion of isocitrate to α-ketoglutarate (α-KG) by isocitrate dehydrogenase

(IDH2/3); and the formation of succinyl-CoA from α-KG by α-ketoglutarate dehydrogenase complex (KGDHC). The other steps include the conversion of citrate into isocitrate by aconitase (AH), the formation of the succinate from succinyl CoA by succinyl-CoA synthase (SCS) generating guanosine triphosphate (GTP), the oxidization of succinate by succinate dehydrogenase (SDH) to have fumarate and transfer two hydrogen atoms to the FAD^+ to obtain $FADH_2$, the conversion of fumarate in malate by fumarate hydratase (FH), and the oxidation of malate in oxaloacetate by malate dehydrogenase (MDH) and generation to a molecule of NAD^+.

In addition to glucose, amino acids can also participate to the TCA cycle. Glutamine, which is the most abundant amino acid in the human body, enters the TCA cycle in the form of α-KG. Glutamine is first hydrolyzed by glutaminase (GLS) into glutamate (which can be converted into glutamine again by glutamine synthase, GS), which subsequently is dehydrogenated by glutamate dehydrogenase (GLUD) to form α-KG that continues the TCA cycle. The sources of carbon for the TCA cycle used in our experiment are highlighted in red.

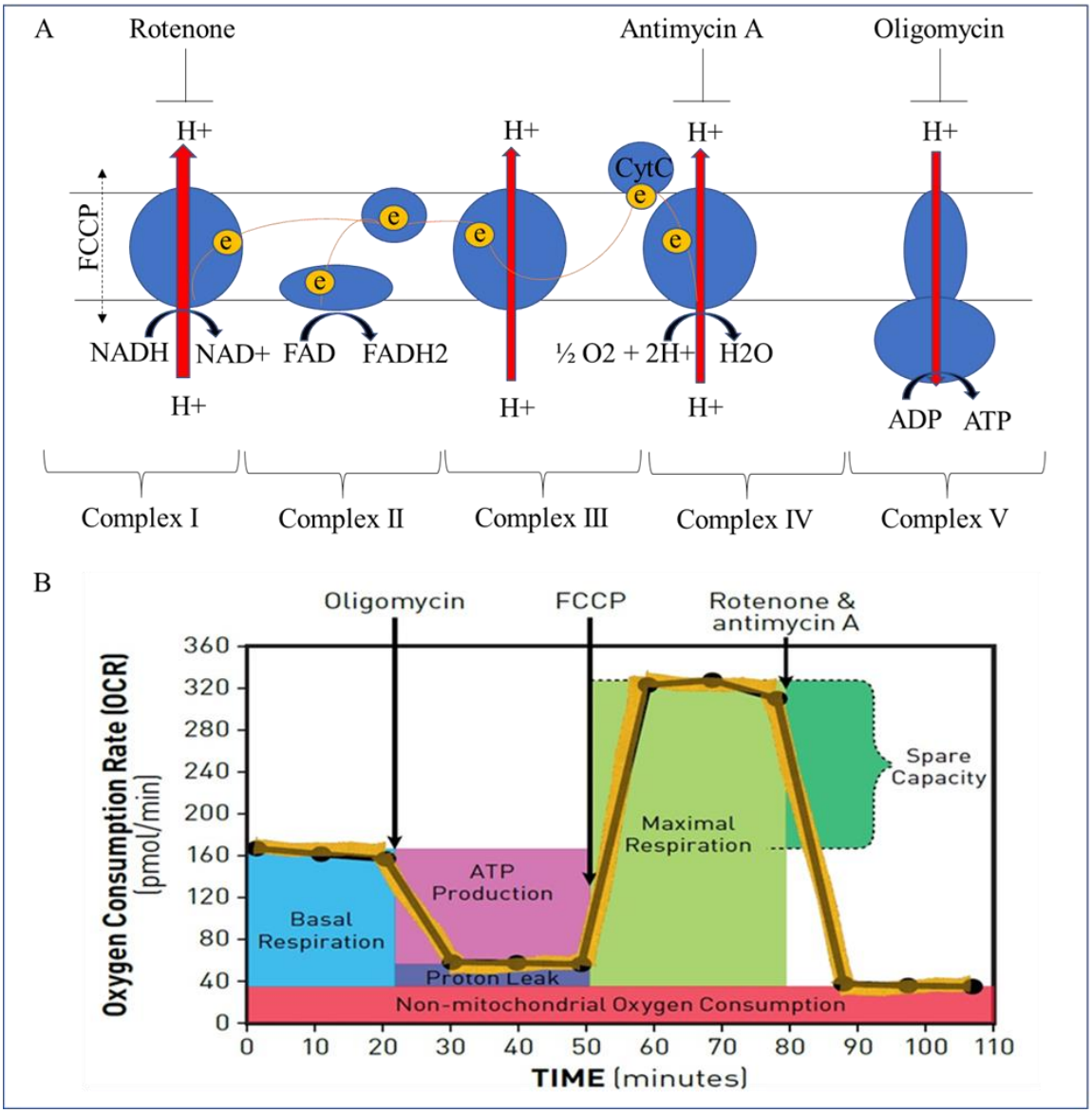

Figure 3.2. Mitochondrial metabolic profile by Seahorse system: rationale for approach. (A) Electron transport chain mechanism. Electron transport chain mechanism occurs in the inner mitochondrial membrane and is composed of five protein complexes that transfer electrons and pump protons from the matrix to the inter membrane space, generating a high proton gradient within the inter membrane space that is used to pump protons through complex V to convert ADP into ATP. Briefly, complex I receives two electrons from NADH and facilitates the transport of four hydrogen ions from the matrix to the inter membrane space. Complex II, which receives two electrons from complex I, converts succinate to fumarate to produce the hydrogen ions needed to convert FAD to

$FADH_2$. $FADH_2$ transfers electrons to the complex III, which gives them to the Cytochrome C (CytC) and pumps four hydrogens into the inter membrane space. CytC is a mobile electron carrier that shuttles electrons from complex II to complex IV, which transfers two protons to the intermembrane space. Complex IV also mediates the conversion of oxygen into water using two protons removed from the matrix. In conclusion, the transport of two electrons trough the ETC enables hydrogens to be pumped into the intermediate space generating a chemical potential gradient necessary for complex V to convert ADP into ATP. Rotenone, Antimycin A and Oligomycin are inhibitors of complex I, IV and V, respectively, used to evaluate oxygen consumption rate. **(B)** Oxygen consumption rate examined by Seahorse analyzer. After the measurement of basal OCR (blue box), oligomycin is injected to inhibit complex V and shut down ATP production. Therefore, oligomycin is used to indirectly assess the amount of ATP produced by OXPHOS (pink box) and the remaining basal respiration not coupled to ATP production generates proton leak (violet box). The second injection is characterized by FCCP that determines the maximal OCR (green box), which dissipates the membrane potential between the intermembrane space inducing an increase of electron transport chain to compensate the chemical gradient. The difference between maximal respiration and the basal respiration represents the spare respiratory capacity (dark green box) that is a measure of the ability of the cell to respond to increased energy demand or stress. The final injection with rotenone and antimycin A completely shuts down electron transport, inhibiting complex I and complex II. This combination collapses mitochondrial respiration and enables the calculation of non-mitochondrial respiration (red box) driven by processes outside the mitochondria.

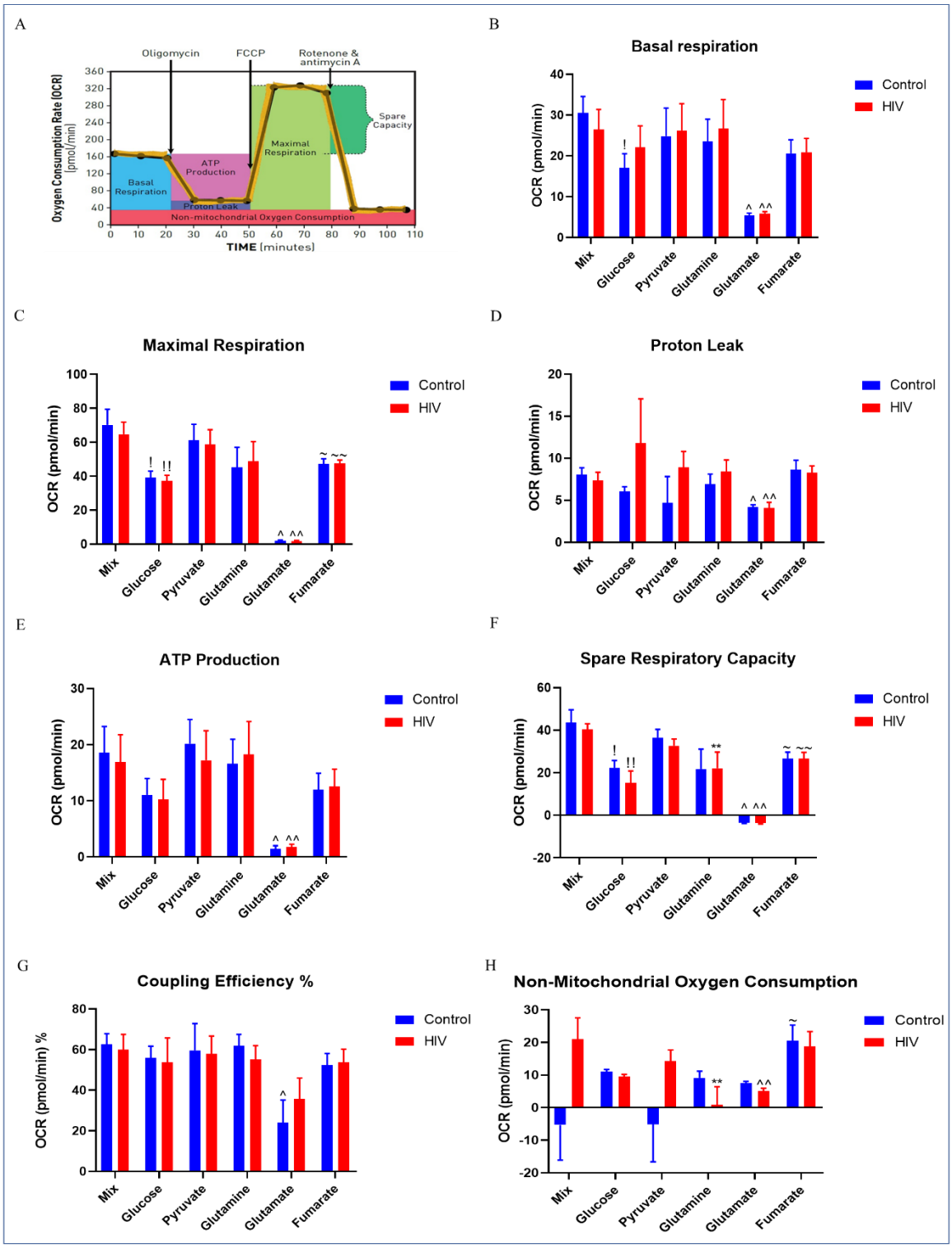

Figure 3.3. HIV-infection of astrocytes decreases the non-mitochondrial oxygen consumption after treatment with media containing only glutamine and glutamate as major carbon sources. (A) Schematic representation of oxygen consumption rate by the

Seahorse analyzer. OCR measurements were performed in human primary astrocytes (both HIV-infected and uninfected) treated with media supplemented with 10 mM Glucose, 1 mM Pyruvate and 2 mM Glutamine as mix, with 10 mM Glucose, 1 mM Pyruvate, 2 mM Glutamine, 50 μM Fumarate, and 2 mM Glutamate, separately. **(B)** Basal respiration measurement. Basal respiration did not change between control uninfected and HIV-infected astrocytes treated with mix media, media containing only glucose, pyruvate, glutamine, glutamate media, or fumarate, as well as the other measurements. Decreased levels of basal respiration were detected in glucose control uninfected condition (! as compared to the mix control uninfected condition, p=0.0215, n=9), in glutamate control uninfected condition (^ as compared to the mix control uninfected condition, p<0.0001, n=9), in glutamate HIV-infected conditions (^^ as compared to the mix HIV-infected condition, p=0.0026, n=9), and was unchanged for the other conditions respectively compared with the control uninfected and the HIV-infected mix. **(C)** Maximal respiration measurement. The maximal respiration decreased only in glucose uninfected control condition (! as compared to the mix control uninfected condition, p=0.0069, n=9), in glucose HIV-infected condition (!! as compared to the mix HIV-infected condition, p=0.0032, n=9), in fumarate control uninfected condition (~ as compared to the mix control uninfected condition, p=0.0312, n=9), in fumarate HIV-infected condition (~~ as compared to the mix HIV-infected condition, p=0.0342, n=9), in the glutamate uninfected control (^ as compared to the mix control uninfected condition, p<0.0001, n=9) and HIV-infected conditions (^^ as compared to the mix HIV-infected condition, p<0.0001, n=9). **(D)** Proton leak measurement. The proton leak was only reduced in the glutamate conditions (^as compared to the mix control uninfected condition, p=0.0012; ^^ as compared to the mix HIV-infected condition, p=0.0180, n=9). **(E)** ATP production measurements. Consistent with D, ATP production was reduced in glutamate conditions (^ as compared to the mix control uninfected condition, p=0.0067; ^^ as compared to the mix HIV-infected condition, p=0.0171, n=9). **(F)** Spare respiratory capacity measurement. In agreement with the other measurements, the spare respiratory capacity was reduced in glutamate conditions (^ as compared to the mix uninfected control condition, p<0.0001; ^^ as compared to the mix HIV-infected condition, p<0.0001, n=9) but also in glucose conditions (! as compared to the mix control uninfected condition, p=0.0068; !! as compared to the mix HIV-infected

condition, p=0.0009, n=9), in glutamine HIV condition (** as compared to the mix HIV-infected condition, p=0.0368, n=9), and in fumarate conditions (~ as compared to the mix control uninfected condition, p=0.0212; ~~ as compared to the mix HIV-infected condition, p=0.0368, n=9). **(G)** Coupling efficiency measurement. The coupling efficiency, ratio between ATP production rate basal respiration rate, was only reduced for glutamate uninfected control (^ as compared to the mix control uninfected condition, p=0.0038, n=9). **(H)** Non-mitochondrial oxygen measurement. The non-mitochondrial oxygen consumption was increased in fumarate uninfected control condition (~ as compared to the mix control uninfected condition, p=0.0446, n=9) and decreased in glutamine and glutamate HIV conditions (** as compared to the mix HIV-infected condition, p=0.0308; ^^ as compared to the mix control HIV-infected condition, p=0.0449, n=9).

Our results indicate that HIV-infected astrocytes compared with the uninfected astrocytes do not show compromised metabolic steps in the tricarboxylic acid cycle in the presence of glucose, pyruvate, glutamine, glutamate or fumarate as sources of carbon. In addition, glutamine and glutamate in HIV-infected astrocytes decrease non-mitochondrial oxygen indicating that HIV-infected astrocytes are partially supported by a non-mitochondrial source of energy.

Chapter 4: Lipid dysregulation in the brain of HIV-infected patients

D'Amico Daniela[1,2]; Prideaux Brendan[1]; Holzlechner Matthias[1]; Eugenin Eliseo A.[1]

[1]University of Texas Medical Branch (UTMB), Department of Neuroscience, Cell Biology and Anatomy, Galveston, TX, USA

[2]University of Palermo (UniPa), Department of Biomedicine, Neuroscience and Advanced Diagnostics, Palermo, Italy

The National NeuroAIDS Tissue Consortium (NNTC) provided all human samples. The NNTC is made possible through funding from the NIMH and NINDS by the following grants: Manhattan HIV Brain Bank (MHBB): U24MH100931; Texas NeuroAIDS Research Center (TNRC): U24MH100930; National Neurological AIDS Bank (NNAB); U24MH100292; California NeuroAIDS tissue Network (CNTN): U24MH100928; and Data Coordinating Center (DCC): U24MH100925. This work was funded by The National Institute of Mental Health grant, MH096625, the National Institute of Neurological Disorders and Stroke, NS105584, and UTMB internal funding (to E.A.E).

Associated paper: D'Amico D., Prideaux B. and Eugenin E.A. "Sulfatide, a novel biomarker for HIV-associated neurocognitive disorders". In preparation.

Introduction

Lipids are highly abundant in the brain (Hancock et al. 2017), where they perform several functions as vital components of membranes structure, metabolism, cell proliferation, survival, apoptosis, and signaling (Cermenati et al. 2015). Disruption or imbalance in lipid composition or metabolism has been associated with several neurodegenerative diseases (Mesa-Herrera et al. 2019). In Chapter 2, we demonstrated that the failure in eradicate HIV is due to the presence of latently viral reservoirs located in different anatomical compartments including the brain. Thus, we propose that HAND is dependent on the viral reservoirs present within the brain and one of the mechanisms of damage amplification is mediated by lipids.

In a similar manner to other neurocognitive diseases (Adibhatla and Hatcher 2007, Xicota et al. 2019), HAND has been linked to lipid dysregulation including structural, signaling and circulating lipids (Bandaru et al. 2013, Kearns et al. 2017, Kelesidis and Currier 2014). Our interest in structural/signaling lipids was also supported by data from our laboratory showed peripheral lipid dysregulation in HIV-infected patients. The levels of PGE_2 (a bioactive eicosanoid lipid) in the sera of HIV-infected individuals virally suppressed with cART were elevated compared to the uninfected individuals (Velasquez et al. 2019). In addition, PGE_2 secretion in the media of the peripheral blood mononuclear cells (PBMCs) isolated from HIV-infected individuals or isolated from uninfected individuals and stimulated with Gp120 was higher compared to the secretion obtained in PBMCs isolated from uninfected individuals (Velasquez et al. 2019). PGE_2 is an eicosanoid synthetized from arachidonic acid (AA) *via* cyclooxygenase 2 and prostaglandin E synthase. It is a potent inflammatory lipid mediator (Park J. Y. et al. 2006) that according to our laboratory data, can be secreted *via* pannexin 1 (Panx-1) channels into the extracellular space (Velasquez et al. 2019), where it binds to E-prostanoid (EP) receptors to trigger toxic signaling pathways into the neighboring cells (Andreasson 2010).

Thus, we used MALDI-MSI with a high spatial resolution and high mass accuracy, to investigate altered structural/signaling lipid distribution in HIV-infected brain tissues compared to uninfected controls. We used an untargeted lipidomics approach to identify the major lipids spectral peaks corresponding to phospholipids highly abundant in the brain. Phospholipids are essential membrane lipids, they are comprised of a glycerol

molecule, two hydrophobic fatty acids chains, and a hydrophilic phosphate head group. They can be classified in several molecular species based on the fatty acid tail groups, who have a standard nomenclature constructed with the number of carbon atoms in the fatty acid chain and the number of double bonds, thereby providing information on the saturation of the chain. Phospholipids containing very long chain fatty acids (fatty acids with more than 22 carbons) are known to be predominantly located within the grey matter (Kihara 2012). Additionally, phospholipids containing polyunsaturated fatty acids (PUFAs - fatty acids containing 2 or more double bonds) are mostly localized into the grey matter (Soderberg et al. 1991). Conversely, white matter is enriched in saturated and monounsaturated fatty acids (Lopez et al. 1995). Furthermore, monounsaturated fatty acids, particularly oleic acid, are known to be predominantly localized into myelin (Guest et al. 2013).

Thus, we applied MALDI-MSI analysis to HIV-infected human brain tissue samples to identify potential lipid biomarkers of HAND and to verify the link between altered lipid distribution in the brains obtained from individuals with minimal to undetectable viral replication, few viral reservoirs, but with cognitive impairment. Our data demonstrate that despite all previous points, we identified a significant lipidic dysregulation in vast areas of the CNS, supporting our hypothesis that lipids "help" HIV reservoirs to spread damage within the CNS.

Materials and Methods

Human brain tissue sections

Unfixed human brain tissue blocks of HIV-infected and uninfected patients were obtained from NNTC (Table 2 in Chapter 2). Unfixed human brain tissues were cut in 12 µm thick tissue serial sections using a Leica CM1850 cryostat (Buffalo Grove, IL) and thaw-mounted onto stainless steel slides. After sectioning, tissues were placed in a dessicator for 15 minutes and then transferred to a -80 °C freezer for storage and for preventing lipid degradation. All these tissues come from postmortem donations (2 hours after death), where blood was eliminated by PBS perfusion to prevent any lipid accumulation within the blood vessels.

Matrix application to tissue sections

Prior to MALDI-MSI analysis, the thaw-mounted tissue sections were removed from the -80 °C freezer and allowed to reach room temperature for 15 minutes. α-Cyano-4-hydroxycinnamic acid (C2020, Sigma-Aldrich, St. Luis, MO) and 1,5-Diaminonaphthalene (D21200, Sigma-Aldrich, St. Luis, MO) matrices were evaluated for positive and negative lipid imaging, respectively. 5 mg/ml of α-Cyano-4-hydroxycinnamic acid was dissolved in 70% Acetone (34850, Sigma-Aldrich, St. Luis, MO) and 5 mg/ml of α-Cyano-4-hydroxycinnamic acid was dissolved in 70% Acetonitrile (34851, Sigma-Aldrich, St. Luis, MO) and 0.1% Trifluoroacetic acid (91707, Sigma-Aldrich, St. Luis, MO). All matrices were applied to the tissue by airspray deposition using the TM-sprayer (HTX Technologies LLC, Chapel Hill, NC). The nozzle temperature was set to 60 °C, flow rate was 50 μL/min and 20 passes over the tissue were performed.

MALDI-MSI Analysis

MALDI-MSI analysis was performed using Q Exactive HF Hybrid Quadrupole-Orbitrap Mass Spectrometer (Thermo Fisher Scientific, Waltham, MA) equipped with an Elevated Pressure Matrix Assisted Laser/Desorption Ionization (EP MALDI) source integrating an Nd:YAG laser (Spectroglyph LLC). Data were acquired at 40 μm^2 lateral resolution in negative and positive ion mode. External mass calibration was performed using calibration solutions (A39239, Thermo Fisher Scientific, Waltham, MA). Accurate mass measured lipid peaks were identified by matching to reference lipids in the LIPID MAPS and Human Metabolome Database within a ±0.002 Da mass tolerance window. Data visualization was performed using Thermo ImageQuest software. Ion images were plotted within a ±0.002 m/z mass tolerance window and all lipid images were normalized to the total ion current (TIC) chromatogram. Extracted ion images were interpolated using the linear interpolate function.

Results

MALDI-MSI analysis for lipid markers of the grey and white matter. The workflow for lipidomic profiling of the human brain tissues by MALDI-MSI is shown in Figure 4.1. The human brain tissues were acquired from uninfected and HIV-infected individuals

undergoing cART, with a good CD4 count and with undetectable viral load as indicated in Table 2 of Chapter 2. Initially, the phospholipid profile of the frontal cortex from HIV-infected individuals was compared to uninfected individuals to evaluate alterations in lipid distribution and relative intensity. To guide phospholipid localization in the grey matter and in the white matter, H&E staining (Figures 4.2 A, 4.3 A, and 4.4 A) was performed on adjacent tissue sections to the ones used for MALDI-MSI.

Membrane phospholipids such as phosphatidylethanolamine (PE), phosphatidylinositol (PI), and phosphatidic acid (PA) have previously been demonstrated using MALDI-MSI to show altered abundance and distribution within the brain following damage caused by infection, inflammation, and/or trauma (Adibhatla and Hatcher 2008, Ojo et al. 2018). Our MALDI-MSI results indicated that membrane phospholipids of the grey matter (Figure 4.2 B, C, D) and the white matter (Figure 4.3 B, C, D) did not show significative changes in relative expression and localization in HIV-infected brain tissues when compared to the controls uninfected. In Figure 4.2, we show representative images for membrane phospholipids containing polysaturated fatty acids that are markers of the grey matter such as phosphatidylethanolamine 40:6 (PE 40:6, Figure 4.2 B), phosphatidylinositol 18:0/20:4 (PI 18:0/20:4, Figure 4.2 C) and phosphatidic acid 40:6 (PA 40:6, Figure 4.2 D). Note, the distribution and relative abundance of the lipids do not significantly change between HIV-infected brain tissue and uninfected control. As they are essential structural membrane glycolipids of the grey matter and unaltered in our analysis, we can assess that the grey matter in HIV-infected patients under cART and with undetectable viral load is structurally intact. Next, we repeated the same analysis for the white matter phospholipids, and we did not observe significant dysregulation of the membrane lipids. The short chain and monounsaturated fatty acid membrane phospholipids, phosphatidylethanolamine 36:2 (PE 36:2, Figure 4.3 B), phosphatidylserine 36:1 (PS 36:1, Figure 4.3 C), and phosphatidic acid 36:1 (PA 36:1, Figure 4.3 D) were showed as representation. Even though PA 36:1 relative expression appeared increased in the cell bodies of HIV-infected tissues compared to controls, it is necessary to increase the numbers of the samples to better investigate this variation. Nevertheless, these markers maintained similar relative intensity and localization in the white matter of uninfected and HIV-infected brain tissues. Thus, these results indicated that also the structure of the white

matter is not compromised in HIV conditions even that most HIV-infected individuals had neurocognitive decline.

MALDI-MSI showed sulfatide dysregulation in HIV-infected human brain tissues. Although the gross grey and white matter are not perturbed in HIV-infected brain, through our untargeted MSI analyses, we identified a specific lipid class, sulfatide, that showed a significative change in relative abundance between the uninfected and the HIV-infected brain tissues. Sulfatide, is a glycosphingolipid with a polar galactosyl-3-O-sulfate head group and a lipid core of ceramide made by a fatty acid and a long-chain base. Sulfatide is expressed in both grey and white matter (Takahashi and Suzuki 2012). Literature data indicate that the white matter mostly present long-chain sulfatides with structural roles in the plasma membrane, instead, the grey matter mainly shows short-chain sulfatides typically localized in intracellular vesicles (Isaac et al. 2006). As shown in Figure 4.4, sulfatide relative intensity was much higher in HIV-infected tissues than in uninfected controls, specifically in the white matter where sulfatide is known to be largely located (Han 2007). We analyzed several species of sulfatide, and we demonstrated that sulfatide containing short acid-chain 16:0 (labeled sulfatide 16:0 in Figure 4.4 B) did not show significative increase of relative expression between HIV-infected brain tissue as compared to uninfected control, but it still maintains its location in the white matter. On another hand, sulfatide containing short acid-chain 18:0 (labeled sulfatide 18:0 in Figure 4.4 C) and particularly sulfatide containing long acid-chains 24:1 (labeled sulfatide 24:1 in Figure 4.4 D) and 25:1 (labeled sulfatide 25:1 in Figure 4.4 E) significantly increased their relative expression in the white matter of HIV-infected brain tissues. This result is highly important because it is the first data identifying and visualizing potential lipid markers in HIV-infected patients with neurocognitive disorders.

Discussion

Lipidomics by MALDI-MSI is a young discipline with enabling high spatial resolution, highly specific imaging of lipids in tissue without the requirement for additional labeling steps (Luberto et al. 2019). Although, MALDI-MSI was previously applied to investigate cART distribution and efficacy in HIV-infected individuals or animal models

of HIV infection (Ntshangase et al. 2019, Seneviratne et al. 2018), this potent tool has not been used to explore lipids alteration in HIV-infected tissues, especially in the brain. Therefore, we proposed to investigate lipid alteration by MALDI-MSI in human brain tissues from HIV-infected individuals undergoing cART, with normal CD4 count and without detectable viral replication but developing asymptomatic or mild neurocognitive disorders.

Although, HIV persists in the brain of HIV-infected individuals in few viral reservoirs and introduces changes in neuronal branching (Kovalevich and Langford 2012) generating a change in volume of the infected brain (Ances et al. 2012), the neurons do not die. Thus, our results showing no significative changes in relative expression and distribution for the essential membrane phospholipids in grey and white matter confirmed that the brain structures of the HIV-infected individuals undergoing cART and without viral replication are not compromised.

Thereafter, analyzing ceramide related metabolites, we found that sulfatide increased in relative expression in the white matter of HIV-infected tissues, especially sulfatides containing long acid-chain. Sulfatide increase in intensity cannot be due to the diffusion or release from damaged brain structures because the grey and the white matter resulted structurally intact. Hence, we propose it is due to an increased synthesis in white matter or the inability of the arylsulfatase A enzyme to degrade sulfatide in the lysosome of the white matter. Thus, our future experiments will focus on investigating sulfatide synthesis pathway in HIV-infected brain tissues.

Sulfatide has been shown to be dysregulated in several neurodegenerative diseases. A substantial reduction in sulfatide levels has been observed in the brain and the CSF of Alzheimer's disease subjects, in which the low levels of sulfatide is accompanied with a significant increase in ceramide, possibly caused by increased sulfatide degradation (Han et al. 2002). On the contrary, elevated levels of sulfatide was detected in the superior frontal and cerebellar grey matter of Parkinson's disease subjects (Cheng et al. 2003). Thus, literature data and our results suggest that sulfatide has a strong potential for being considered a biomarker for neurocognitive impairment and a potential target for therapeutic molecules that can prevent or cure HAND.

In addition, antiretroviral drugs, particularly protease inhibitor drugs, has been demonstrated to directly cause lipid dysregulation and all the HIV-infected tissues in our study came from patients on cART. However, current evidence supports that HAART-induced lipid dysregulation primarily affects triglyceride and cholesterol metabolism (Lo 2011). For HIV-infected individuals, white matter thinning with loss of volume and structural integrity of myelin were reported by immunohistochemical staining in postmortem tissues (Langford et al. 2003) or by diffusion tensor imaging (Correa et al. 2015) analyses suggesting a possible relation with the antiretroviral compounds used to treat HIV individuals (Jensen et al. 2019). Our analysis did not detect significant structural damage in the white matter of HIV-infected patients under cART but we intend to expand our analysis. Moreover, there are no current reports of direct drug-induced sulfatide dysregulation. Thus, the observed changes in sulfatide distribution are unlikely to be due to the drug therapy.

In summary, the key points of this chapter are: 1) grey and white matters of the brain of HIV-infected individuals under cART and with undetectable viral replication are not structurally compromised; 2) sulfatide is a potential biomarker for HAND that increase in the white matter of HIV-infected individuals. Thus, MALDI-MSI was essential for identifying sulfatide, whose role will be investigated *in vitro* in the following chapters.

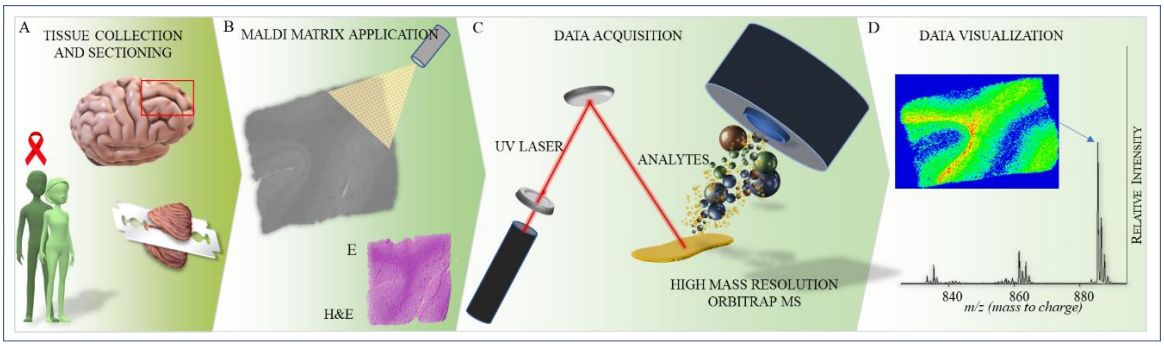

Figure 4.1. Lipidomic profile by MALDI-MSI: rationale for approach. (A) Tissue collection and sectioning. Post-mortem frontal lobe brain tissues from uninfected and HIV-infected individuals virally suppressed with cART, with a normal CD4 count and undetectable viral load were obtained from the NNTC and cryo-sectioned at 12 µm. **(B)** MALDI matrix application. Matrix was sprayed matrix using a TM-sprayer. **(C)** Data acquisition. MSI data were acquired at 40 μm^2 lateral resolution in negative and positive ion mode using a Q Exactive HF Hybrid Quadrupole-Orbitrap Mass Spectrometer (Thermo Scientific) equipped with an Elevated Pressure Matrix Assisted Laser/Desorption Ionization (EP MALDI) source integrating an Nd:YAG laser (Spectroglyph LLC). **(D)** Data visualization. It was performed using Thermo ImageQuest software by plotting ion intensity versus relative position of the data from the sample. **(E)** H&E staining. Adjacent brain tissue sections were stained with H&E to visualize brain morphology.

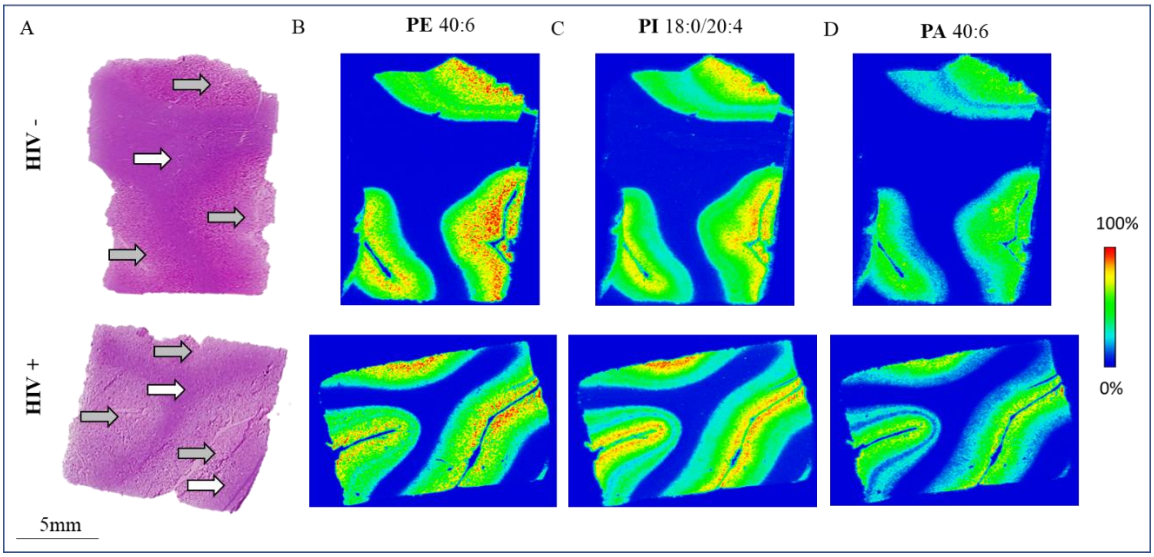

Figure 4.2. Representative distribution of phospholipids in the grey matter of uninfected and HIV-infected brain tissues. The top and the lower panels present brain sections of uninfected and HIV-infected individuals, respectively. **(A)** H&E-stained reference sections for the grey matter (indicated with grey arrows) and the white matter (indicated with white arrows). MALDI-MSI images for **(B)** phosphatidylethanolamine (PE) 40:6, **(C)** phosphatidylinositol (PI) 18:0/20:4, **(D)** phosphatidic acid **(**PA) 40:6. Intensity is expressed by the gradient intensity scale. Scale bar=5mm.

Our results indicate that the relative intensity and the localization of the phospholipids characteristic for the grey matter do not significantly change under HIV condition.

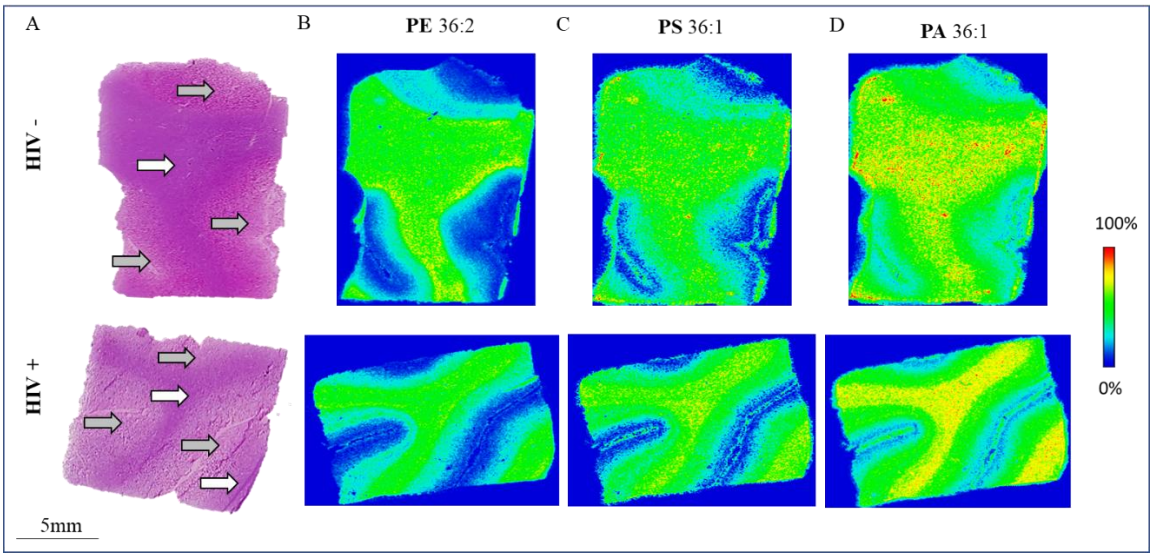

Figure 4.3. Representative distribution of phospholipids in the white matter of uninfected and HIV-infected brain tissues. The top and the lower panels present brain sections of uninfected and HIV-infected individuals, respectively. **(A)** H&E-stained reference sections for the white matter (indicated with white arrows) and the grey matter (indicated with grey arrows). MALDI-MSI images for **(B)** phosphatidylethanolamine (PE) 36:2, **(C)** phosphatidylserine (PS) 36:1, **(D)** phosphatidic acid (PA) 36:1. Intensity is expressed by the gradient intensity scale. Scale bar=5mm.

Our results indicate that the relative intensity and the localization of the phospholipids characteristic for white matter do not significantly change under HIV condition.

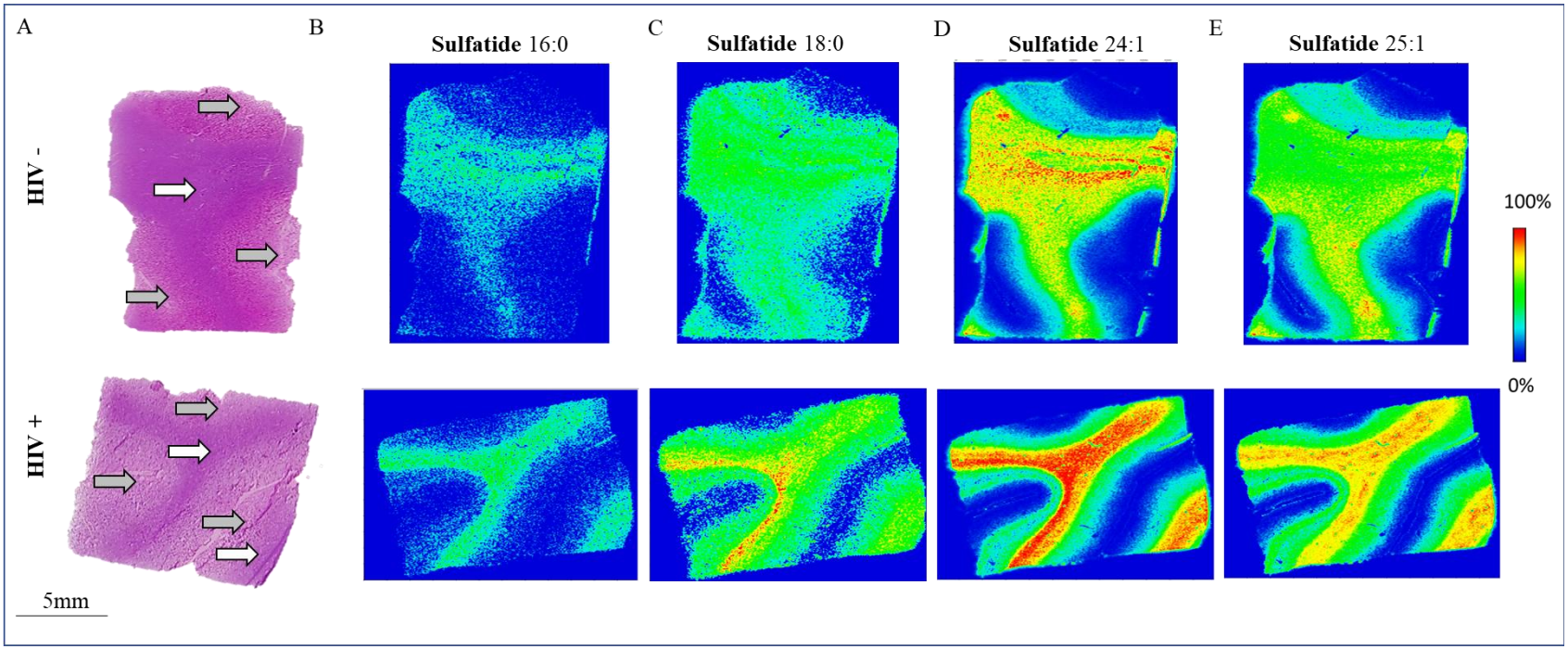
A
B
C
D
E
Sulfatide 16:0
Sulfatide 18:0
Sulfatide 24:1
Sulfatide 25:1
HIV -
HIV +
100%
0%
5mm

Figure 4.4. Representative distribution of sulfatide in uninfected and HIV-infected brain tissues. The top and the lower panels present brain sections of uninfected and HIV-infected individuals, respectively. **(A)** H&E-stained reference sections for the grey matter (indicated with grey arrows) and the white matter (indicated with white arrows). MALDI-MSI images for **(B)** sulfatide 16:0, **(C)** sulfatide 18:0, **(D)** sulfatide 24:1, and **(E)** sulfatide 25:1. Intensity is expressed by the gradient intensity scale. Scale bar=5mm.

Our results indicate that sulfatide containing short acid-chain 18:0 and long acid-chains increase in relative expression in white matter under HIV condition.

Chapter 5: Sulfatide secretion is regulated by HIV proteins *in vitro*

D'Amico Daniela[1,2]; Prideaux Brendan[1]; Eugenin Eliseo A.[1]

[1]University of Texas Medical Branch (UTMB), Department of Neuroscience, Cell Biology and Anatomy, Galveston, TX, USA

[2]University of Palermo (UniPa), Department of Biomedicine, Neuroscience and Advanced Diagnostics, Palermo, Italy

This work was funded by The National Institute of Mental Health grant, MH096625, the National Institute of Neurological Disorders and Stroke grant, NS105584, and UTMB internal funding (to E.A.E).

Associated paper: D'Amico D., Prideaux B. and Eugenin E.A. "Sulfatide, a novel biomarker for HIV-associated neurocognitive disorders". In preparation.

Introduction

As described in Chapter 4, we identified that sulfatide increases its relative expression in the white matter of HIV-infected individuals without any sign of structural membrane phospholipid dysregulation. Thus, sulfatide change in relative concentration was associated with HIV infection and cognitive disease. As described in Table 2, the brain tissue sections investigated were obtained from individuals with minimal to undetectable HIV replication, normal CD4 count, and asymptomatic neurocognitive impairment. Despite these minimal neurocognitive alterations, sulfatide changes were significant. Also, we described in Chapter 2 that the brain tissues analyzed only showed minimal numbers of viral reservoirs with perivascular localization comprised microglia/macrophages and a small population of astrocytes. Surprisingly, we detected that several proteins diffused to the neighboring areas of the brain from areas containing HIV-integrated DNA. Thus, we propose that HIV proteins dysregulate sulfatide release and we focused our investigation on Gp120, Tat_{1-72}, Nef, Vif and Vpr. All the selected proteins have already been identified to have significant toxicity within the brain.

For example, the soluble viral envelope protein Gp120 has neurotoxic effect that induces axonal degeneration *via* activation of several neurotoxic pathways including dysregulated calcium homeostasis, activation of oxidative stress, induction of the proapoptotic transcription factor p53, mitochondrial fission/fusion, and impaired mitochondrial dynamics (Avdoshina et al. 2016).

The viral transactivator protein, Tat, induces neuronal apoptosis through the formation of a macromolecular complex composed by the low-density lipoprotein receptor-related protein (LRP), postsynaptic density protein-95 (PSD-95), N-methyl-d-aspartic acid (NMDA) receptors, and neuronal nitric oxide synthase (nNOS) in the neuronal plasma membrane (Eugenin et al. 2007). Moreover, Tat upregulates Cx43 gene and protein expression binding Cx43 promoter and supporting gap junctional communication in human primary astrocytes (Berman et al. 2016), which is the topic of the following chapter. The viral transactivator is a 101-residue protein encoded by two exons. We decided to use Tat_{1-72} that defines the first exon and that activates transcription with the same proficiency of the full-length protein.

The negative factor, Nef, is a small protein expressed abundantly in astrocytes of HIV-infected brains. It induces axonal and neurite degeneration of neurons through oxidative stress (Sami Saribas et al. 2017). Nef also contributes to inflammation inducing the production of pro-inflammatory cytokines such as CCL5 by the Akt, p38MAPK, NF-κB, CEBP, and AP-1 pathways (Liu X. et al. 2014).

The viral initial factor, Vif, shows its neurotoxic properties by inhibiting proteasomal degradation of ubiquitinated proteins (Royal et al. 2012).

Instead, Vpr induces neuronal apoptosis altering the mitochondrial transition pore formation, inducing cytochrome c release, and increasing the activation of caspase-8 (Jacotot et al. 2000, Pomerantz 2004).

In our analysis, we choose all these HIV proteins for their full blow neurotoxic effects and because some of them were directly detected as soluble proteins diffusing into the non-HIV-associated DNA cells of the HIV-infected brain tissues. However, it was unknown whether HIV proteins compromised sulfatide release.

Materials and Methods

Cell Culture Methods

Human primary astrocytes and SH-SY5Y human neuroblastoma cells were separately maintained in culture. High glucose Dulbecco's modified Eagle's medium (DMEM, 11995-065, Thermo Fisher Scientific, Waltham, MA) supplemented with 10% fetal bovine serum (FBS, S12450H, Atlanta Biologicals, Flowery Branch, GA), penicillin, and streptomycin (15070063, Thermo Fisher Scientific, Waltham, MA) was used to grow the human primary astrocytes at 37 °C in a humidified atmosphere with 5% CO_2. SH-SY5Y human neuroblastoma cells were grown in gelatin coated coverslips using the same medium of astrocytes supplemented with 2 mM L-glutamine (25030081, Thermo Fisher Scientific, Waltham, MA), 2% B27 (17504044, Thermo Fisher Scientific, Waltham, MA) and 2 mM Glutamax (35050-061, Thermo Fisher Scientific, Waltham, MA). Before to obtain co-cultures, SH-SY5Y human neuroblastoma cells were differentiated with 10 µM Retinoic Acid (R2625, Sigma-Aldrich, St. Luis, MO-Aldrich, St. Luis, MO) for 7 days. Differentiated SH-SY5Y human neuroblastoma cells were flipped on the human primary astrocytes to obtain co-cultures that were maintained for 12 hours in the media of

differentiated SH-SY5Y human neuroblastoma cells before to be treated with HIV proteins. This is a similar protocol described for hippocampal neurons to enable proper differentiation and synaptic development (Kaneko et al. 2014).

ELISA for sulfatide and PGE_2

Co-cultures of human primary astrocytes and differentiated neurons were treated with HIV recombinant proteins Gp120 (HIV-1 BaL; 50 and 100 nM; 4961, NIH AIDS Reagent Program, Germantown, MD), Tat_{1-72} (HIV-1;100, and 300 nM), Nef (HIV-1 HXB2; 100 and 250 nM; 13134, NIH AIDS Reagent Program, Germantown, MD), Vif (HIV-1 HXB2; 100 and 300 nM; 11050, NIH AIDS Reagent Program, Germantown, MD) or Vrp (HIV-1; 100 and 300 nM; 6447, NIH AIDS Reagent Program, Germantown, MD), for 6, 12, 24, and 48 hours. Sulfatide concentration was evaluated in the co-culture media using Human sulfatide ELISA kit (MBS7242142, MyoBioSource, San Diego, CA), and PGE_2 concentration with human PGE_2 ELISA kit (ab133021, Abcam, Cambridge, UK) according to the manufacturer's instructions. Human sulfatide ELISA kit had a sensitivity of 1 ng/ml, human PGE_2 ELISA kit had a sensitivity of 13.4 pg/ml. Sulfatide and PGE_2 concentrations were quantified by bioluminescence (Optical Density 450/415 nm) using a Perkin Elmer envision system (2102 Multilabel Reader, Perkin Elmer, Waltham, MA).

Statistical Analysis

All data were expressed as mean ± standard error of the mean (SEM). Differences among groups were analyzed by a one-way analysis of variance (ANOVA test), using Bonferroni's multiple comparison test for post-hoc analysis. The level of significance was accepted at $p<0.05$. Prism8.0 software was used for the statistical analyses performed.

Results

Evaluation of sulfatide secretion in mixed co-cultures of differentiated neurons and human primary astrocytes. Although, magnetic resonance spectroscopy and magnetic resonance imaging can provide elucidation about lipid distribution and characterization, they have never been applied to assess lipid alteration in HIV condition, especially for sulfatide, due to lack of specificity. Sulfatide, is a sulfoglycolipid synthetized by

oligodendrocytes, Schwan cells, astrocytes and neurons (Takahashi and Suzuki 2012). Our MALDI-MSI results for HIV-infected brain tissues showed higher sulfatide relative intensity in the white matter. On the contrary, elevated levels of sulfatide were detected in the grey matter of Parkinson's disease subjects (Fabelo et al. 2011) and decreased level were identified in the grey and in white matters of Alzheimer's disease subjects (Cheng et al. 2003). These pathologies show significant brain destruction and their progression is irreversible, critical difference with the milder forms of HAND. However, in HIV condition cognitive disorders can be reversible and even fluctuating. We detected that brain structural damage was minimal. Thus, we propose that sulfatide may be used as a marker of brain compromise and can provide signs of early CNS damage.

In control untreated condition, analysis of our co-cultures of differentiated neurons and human primary astrocytes indicated that sulfatide was released into the media in a stable manner during the time course analyzed (6, 12, 24 and 48 hours) with a concentration of 2.331 mg/ml.

Gp120 increases sulfatide secretion in mixed co-cultures of differentiated neurons and human primary astrocytes. Treatment of mixed cultures of differentiated neurons and human primary astrocytes with Gp120 50 nM for 6, 12, 24 and 48 hours and subsequent ELISA for sulfatide demonstrated that Gp120 50 nM transiently increased sulfatide secretion. Specifically, sulfatide secretion was only increased after 24 hours (Figure 5.1 A, * p=0.0040) to be reduced at 48 hours (Figure 5.1 A, # p=0.0040). In addition, increasing Gp120 concentration at 100 nM did not change the transient increase in sulfatide secretion at 24 hours (Figure 5.1 B, * p=0.0257) that was again decreased at 48 hours (Figure 5.1 B, # p=0.0012). Thus, Gp120 data indicates that some HIV proteins at specific concentrations and time points can increase sulfatide secretion, even transiently.

Tat prevents sulfatide secretion in mixed co-cultures of differentiated neurons and human primary astrocytes. In contrast to the Gp120 data upregulating sulfatide secretion at 24 hours at different concentrations, we identify that HIV-1 Tat_{1-72} 100 ng/ml reduced sulfatide secretion at 48 hours (Figure 5.2 A, # p=0.0457). Although at 6 hours sulfatide secretion was also reduced, it was not statistically significant. On another hand, Tat_{1-72} at

increased concentration of 300 ng/ml did not reduce sulfatide secretion at 48 hours (Figure 5.2 B) and any significative differences compared to control were detected at 6,12, and 24 hours. Thus, Tat_{1-72} data indicate that some HIV proteins at specific concentrations can reduce sulfatide secretion.

Nef and Vif increase sulfatide secretion in mixed co-cultures of differentiated neurons and human primary astrocytes. Treatment of mixed cultures of differentiated neurons and human primary astrocytes with Nef or Vif for 6, 12, 24 and 48 hours and subsequently analyzed by ELISA for sulfatide demonstrated that Nef 100 ng/ml and Vif 100 ng/ml, in the same manner, increased sulfatide secretion at 48 hours (Figure 5.3 A, * p=0.0148; Figure 5.4 A, * p=0.0005). Increasing Nef concentration to 250 nM and Vif to 300 ng/ml did not further increase sulfatide secretion at 48 hours (Figure 5.3 B, * p=0.0002; Figure 5.4 B, p=0.0157) and any significative differences compared to control were detected at 6, 12, and 24 hours, as observed at the lower concentration. Thus, Nef and Vif data indicate that several HIV proteins at specific time points can increase sulfatide secretion.

Vpr increases sulfatide secretion in mixed co-cultures of differentiated neurons and human primary astrocytes. In agreement with Gp120 data showing upregulating sulfatide secretion, we identified that Vpr 100 ng/ml transiently increased sulfatide secretion at 24 hours (Figure 5.5 A, * p=0.0094). Partially consistent with this observation, treatment with a higher concentration of Vpr (300 ng/ml) induced an earlier increase in sulfatide secretion at 12 hours (Figure 5.5 B, * p=0.0439) compared to control condition. Thus, Vpr data confirm that several HIV proteins at specific concentrations and time points can increase sulfatide secretion, even transiently.

HIV proteins do not change PGE_2 secretion *in vitro*. PGE_2, an AA-related metabolite that stimulates inflammation, was used as control (Figures 5.6 to 5.10). Our previous laboratory data showed that it is altered in the sera of all the HIV individuals. Thus, we evaluated whether viral proteins can regulate PGE_2 release *in vitro*. Analysis of our mixed co-culture of differentiated neurons and human primary astrocytes indicated that PGE_2 was released into the media in a stable manner at 6, 12, 24 and 48 hours with a concentration of 30 pg/ml

(Figures 5.5 to 5.10). Treatment of the mixed cultures of differentiated neurons and human primary astrocytes with Gp120 (50 nM, Figure 5.6 A; 100 nM, Figure 5.6 B), Tat_{1-72} (100 ng/ml, Figure 5.7 A; 300 ng/ml, Figure 5.7 B), Nef (100 ng/ml, Figure 5.8 A; 250 ng/ml, Figure 5.8 B), Vif (100 ng/ml, Figure 5.9 A; 300 ng/ml, Figure 5.9 B) or Vpr (100 ng/ml, Figure 5.10 A; 300 ng/ml, Figure 5.10 B) for 6, 12, 24 and 48 hours and subsequent ELISA for PGE_2 did not demonstrate difference in PGE_2 secretion compared to the control. These results indicate that PGE_2 secretion is not dependent on HIV protein stimulations.

Discussion

In this chapter, we identified that Gp120, Tat, Nef, Vif and Vpr HIV proteins are able to dysregulate sulfatide secretion in the co-cultures of human primary astrocytes and SH-SY5Y neuroblastoma cells, but the mechanism of sulfatide release is still under investigation.

As described in Chapter 2, HIV protein secretion or diffusion can compromise large regions of tissue in close contact with viral reservoirs. This is supported by the fact that HIV proteins have previously been shown to be a source of neuronal damage (Kaul and Lipton 2006, Nath 2002). Neuronal damage occurs in the absence of neuronal infection and exposure of the neurons to the HIV proteins is able to trigger neuronal damage cascades. However, neurons in HIV-infected individuals do not necessary die but can show dendritic simplification and synaptic pruning, decreasing the synaptodendritic connectivity (Kovalevich and Langford 2012, Ru and Tang 2017). However, it still controversial whether *in vivo* HIV proteins are released into the neurons and glia cells. We demonstrated that this mechanism occurs in HIV-infected individuals without sign of viral replication (see Table 2, Chapter 2) and our research prove that the current cART blocks peripheral viral replication but does not prevent HIV protein synthesis.

As described in Figure 1.5, sulfatide is concentrated in the cellular membrane including Golgi apparatus and lysosome. Although we demonstrated that sulfatide secretion can be regulated by several HIV proteins, the source of sulfatide release in response to HIV proteins is unknown. We cannot discard that viral proteins induce sulfatide secretion *via* gap junctions, exoxomes or other extracellular vesicles.

Sulfatide was released in control conditions, however, Gp120, Nef, Vif and Vpr were shown to increase its secretion and potentially increase apoptosis too. The concentration of sulfatide released as described in the subsequent chapters was not associated with apoptosis but toxicity cannot be excluded.

Sulfatide may also contribute to synaptic pruning and for this reason our future experiments aim to analyze synaptic proteins in SH-HY5Y neuroblastoma cells stimulated with viral proteins to investigate synaptic stability and signaling.

Moreover, our results for PGE_2 secretion in the human primary astrocyte-SH-SY5Y neuroblastoma cell co-cultures did not show any significant changes in the presence of all the viral proteins used in this study. PGE_2 secretion has been detected in PBMC isolated from HIV-infected individuals using a Panx-1 dependent mechanism (Velasquez et al. 2019). To further elucidate the role of sulfatide in neuroHIV, future studies will focus on assessing the mechanism of sulfatide release.

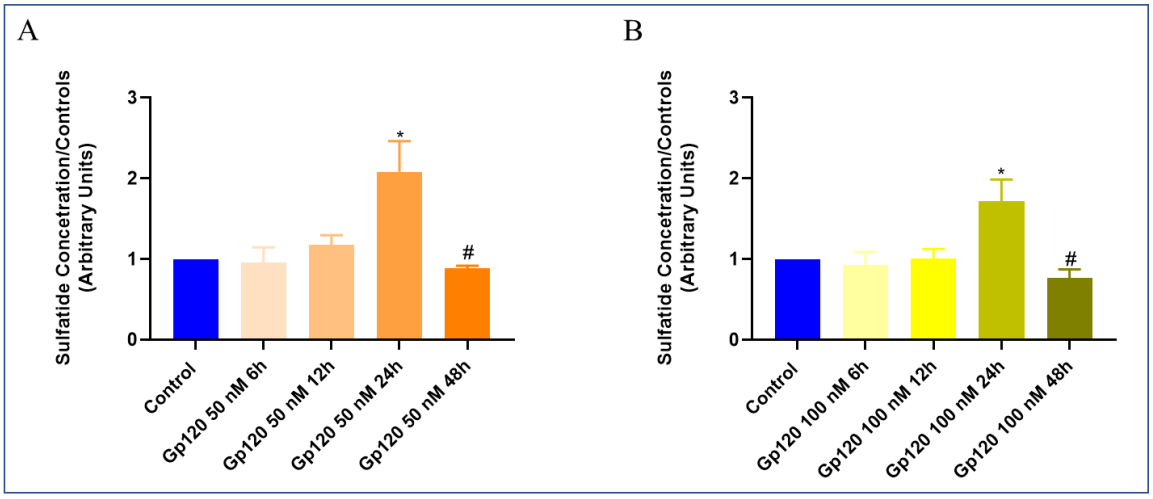

Figure 5.1. Gp120 treatment of mixed cultures of human primary astrocytes and differentiated neurons increases sulfatide secretion. Media collected from co-cultures of human primary astrocytes and differentiated SH-SY5Y human neuroblastoma cells at different time points were assessed for sulfatide by ELISA. Sulfatide secretion did not significantly change in control cultures at different time points (control equal to 2.331 mg/ml). Due to the minimal variations, we set the control sulfatide secretion at 1. **(A)** Quantification of extracellular release of sulfatide in the media of co-cultures of human primary astrocytes and differentiated SH-SY5Y human neuroblastoma cells treated with HIV-1 BaL Gp120 50 nM for 6, 12, 24 and 48 hours. Sulfatide secretion increased at 24 hours (* as compared to Control condition, p=0.0040, n=3) and decreased at 48 hours (# as compared to Gp120 50 nM 24h condition, p=0.0040, n=3), showing a transient secretion; **(B)** the same conditions used in A were repeated with a higher concentration of HIV-1 BaL Gp120 (100 nM). Consistent with A, the higher concentration resulted in increased sulfatide secretion at 24 hours (* as compared to Control condition, p=0.0257, n=3), which was then reduced at 48 hours (# as compared to Gp120 100 nM 24h condition, p=0.0012, n=3).

Our results indicate that independently of the different concentrations of Gp120, sulfatide release increases transiently at 24 hours.

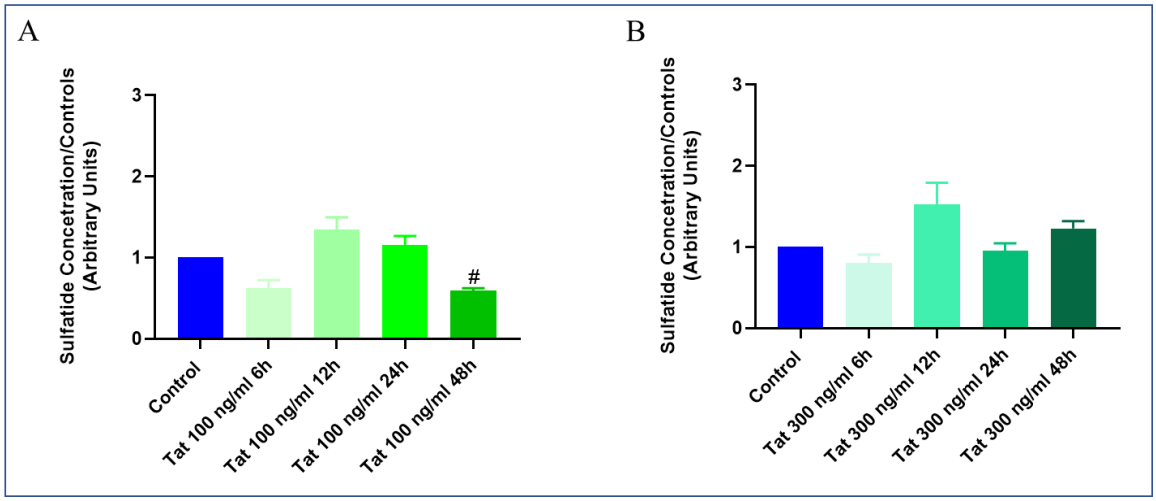

Figure 5.2. Tat treatment of mixed cultures of human primary astrocytes and differentiated neurons prevents sulfatide secretion. Media collected from co-cultures of human primary astrocytes and differentiated SH-SY5Y human neuroblastoma cells at different time points were assessed for sulfatide by ELISA. Control cultures at different time points did not significantly change (control equal to 2.331 mg/ml) in sulfatide secretion. Due to the minimal variations, we set the control sulfatide secretion at 1. **(A)** Quantification of the extracellular release of sulfatide in the media of co-cultures of human primary astrocytes and differentiated SH-SY5Y human neuroblastoma cells treated with HIV-1 Tat_{1-72} 100 ng/ml for 6, 12, 24 and 48 hours. Sulfatide secretion appeared to be reduced at 6 hours, however the change was not significant. In addition, sulfatide secretion did not change at 6, 12 and 24 hours compared to the control, except at 48 hours when it was reduced (# compared to Control condition, p=0.0457, n=3); **(B)** the same conditions used in A were repeated with HIV-1 Tat_{1-72} at 300 ng/ml showing that no significant changes in sulfatide secretion were observed during the time course analyzed compared to the control.

Our results indicate that sulfatide secretion can be reduced after treatment with Tat_{1-72}.

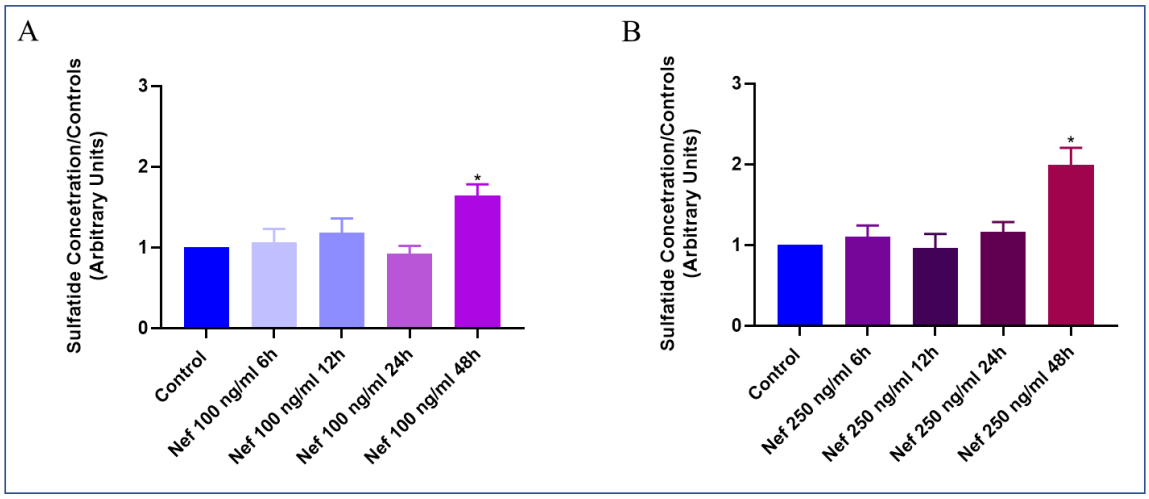

Figure 5.3. Nef treatment of mixed cultures of human primary astrocytes and differentiated neurons increases sulfatide secretion. Media collected from co-cultures of human primary astrocytes and differentiated SH-SY5Y human neuroblastoma cells at different time points were assessed for sulfatide by ELISA. Control cultures at different time points did not significantly change (control equal to 2.331 mg/ml) in sulfatide secretion. Due to the minimal variations, we set the control sulfatide secretion at 1. **(A)** Quantification of the extracellular release of sulfatide in the media of co-cultures of co-cultures of human primary astrocytes and differentiated SH-SY5Y human neuroblastoma cells treated with HIV-1 HXB2 Nef 100 ng/ml for 6, 12, 24 and 48 hours. Sulfatide secretion increased at 48 hours (* as compared to Control condition, p=0.0148, n=3); **(B)** the same conditions used in A were repeated with HIV-1 HXB2 Nef 250 ng/ml. Consistent with A, sulfatide secretion was higher at 48 hours after administration of higher concentration of Nef (* as compared to Control condition, p=0.0002, n=3).

Our results indicate that sulfatide release is increased 48 hours after treatment with Nef.

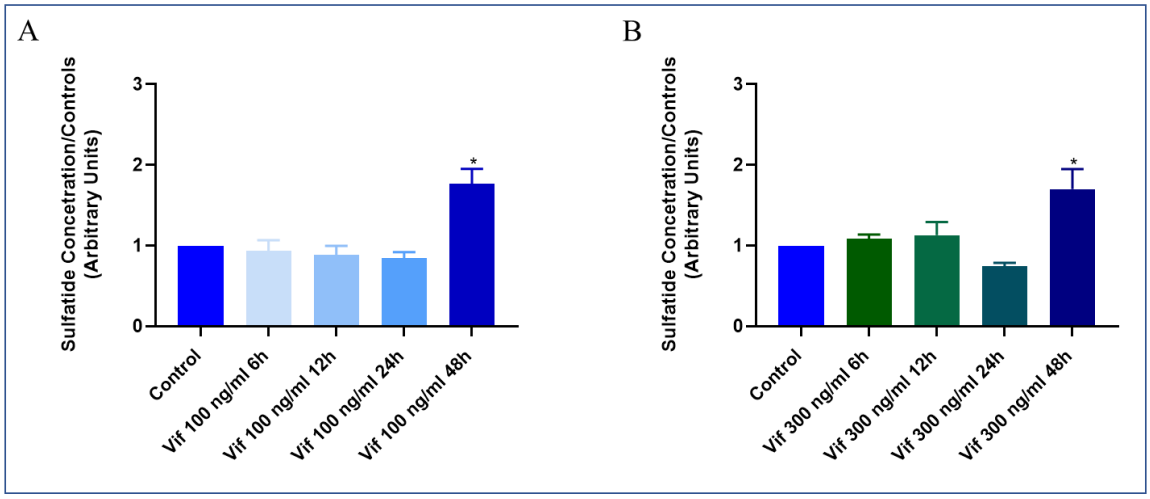

Figure 5.4. Vif treatment of mixed cultures of human primary astrocytes and differentiated neurons increases sulfatide secretion. Media collected from co-cultures of human primary astrocytes and differentiated SH-SY5Y human neuroblastoma cells at different time points were assessed for sulfatide by ELISA. Control cultures at different time points did not significantly change (control equal to 2.331 mg/ml) in sulfatide secretion. Due to the minimal variations, we set the control sulfatide secretion at 1. **(A)** Quantification of the extracellular release of sulfatide in the media of co-cultures of co-cultures of human primary astrocytes and differentiated SH-SY5Y human neuroblastoma cells treated with HIV-1 HXB2 Vif 100 ng/ml for 6, 12, 24 and 48 hours. Sulfatide secretion increased at 48 hours (* as compared to Control condition, p=0.0005, n=3); **(B)** the same conditions used in A were repeated with HIV-1 HXB2 Vif 300 ng/ml. Consistent with A, sulfatide secretion was increased at 48 hours (* as compared to Control condition, p=0.0157, n=3).

Our results indicate that Vif can increase sulfatide release at 48 hours.

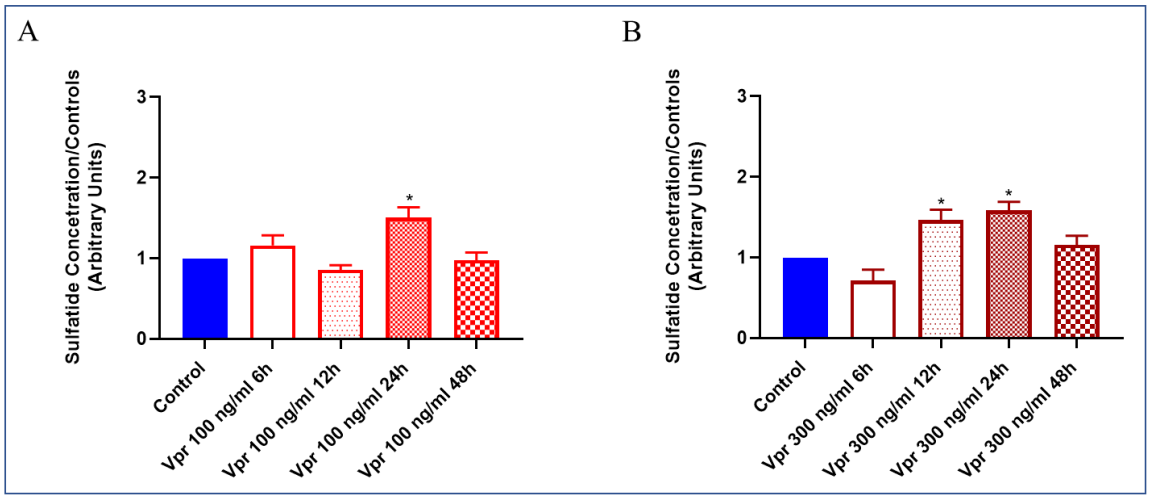

Figure 5.5. Vpr treatment of mixed cultures of human primary astrocytes and differentiated neurons increases sulfatide secretion. Media collected from co-cultures of human primary astrocytes and differentiated SH-SY5Y human neuroblastoma cells at different time points were assessed for sulfatide by ELISA. Control cultures at different time points did not significantly change (control equal to 2.331 mg/ml) in sulfatide secretion. Due to the minimal variations, we set the control sulfatide secretion at 1. **(A)** Quantification of the extracellular release of sulfatide in the media of co-cultures of co-cultures of human primary astrocytes and differentiated SH-SY5Y human neuroblastoma cells treated with HIV-1 Vpr 100 ng/ml for 6, 12, 24 and 48 hours. Sulfatide secretion increased at 24 hours (* as compared to Control condition, p=0.0094, n=3). The release of sulfatide returned to control levels at 48 hours, showing a transient secretion; **(B)** the same conditions used in A were repeated with HIV-1 Vpr 300 ng/ml. Consistent with A, also at higher concentration, sulfatide secretion resulted increased at 12 and 24 hours (* as compared to Control condition, p=0.0439, n=3). The release returned to control levels at 48 hours, indicating a transient secretion similar to the time course observed in A.

Our results indicate that sulfatide release is increased at 12 and 24 hours after treatment with Vpr.

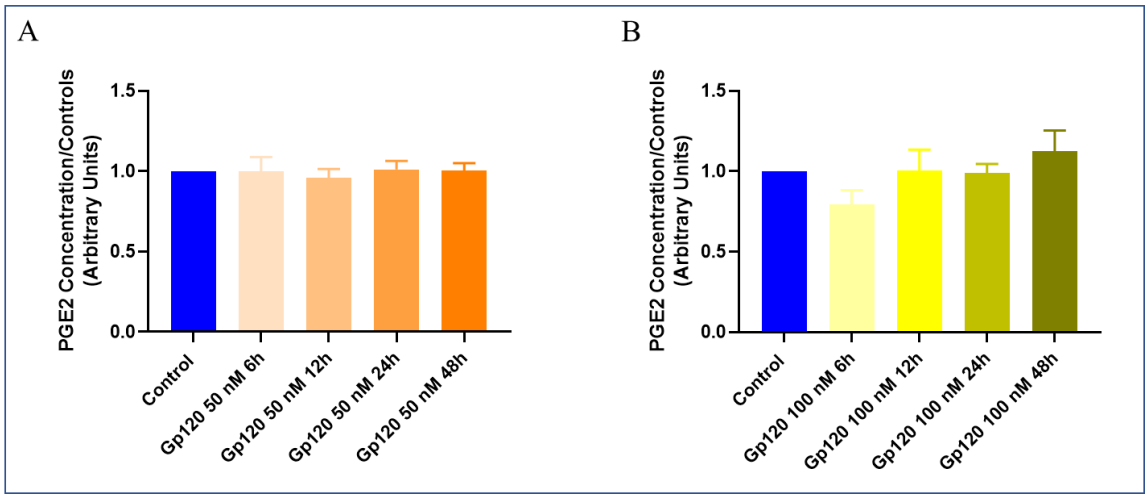

Figure 5.6. Gp120 treatment of mixed cultures of human primary astrocytes and differentiated neurons does not change PGE_2 secretion. Media collected from co-cultures of human primary astrocytes and differentiated SH-SY5Y human neuroblastoma cells at different time points were assessed for PGE_2 by ELISA. Control cultures at different time points did not significantly change (control equal to 30 pg/ml) in PGE_2 secretion. Due to the minimal variations, we set the control PGE_2 secretion at 1. **(A)** Quantification of the extracellular release of PGE_2 in the media of co-cultures of human primary astrocytes and differentiated SH-SY5Y human neuroblastoma cells treated with HIV-1 Bal Gp120 50 nM for 6, 12, 24 and 48 hours. PGE_2 secretion did not change during the analyzed time course; **(B)** the same conditions used in A were repeated with HIV-1 Bal Gp120 100 nM. Consistent with A, secretion of PGE_2 did not change compared to the control.

Our results indicate that independent of time points and concentrations, PGE_2 secretion does not change after treatment with Gp120.

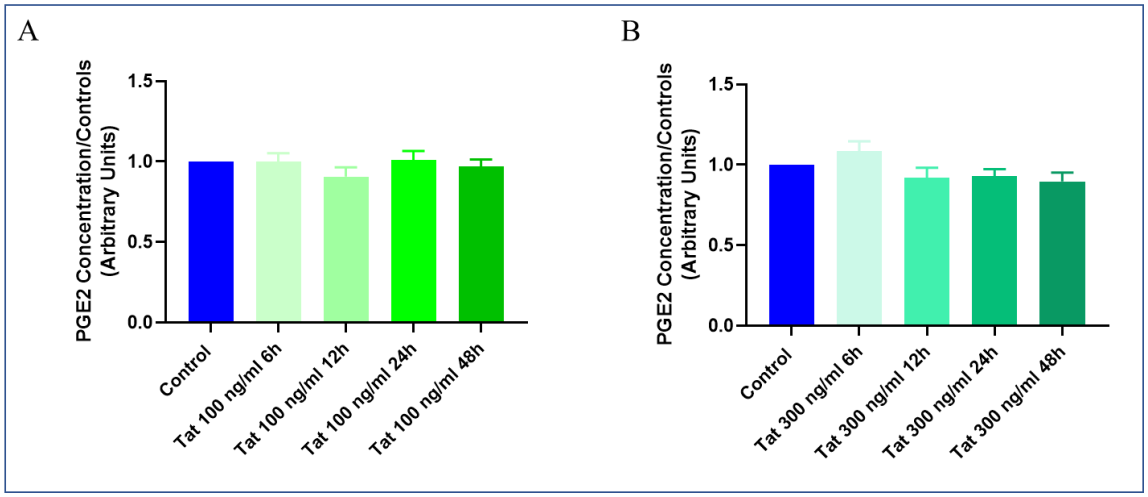

Figure 5.7. Tat treatment of mixed cultures of human primary astrocytes and differentiated neurons does not change PGE_2 secretion. Media collected from co-cultures of human primary astrocytes and differentiated SH-SY5Y human neuroblastoma cells at different time points were assessed for PGE_2 by ELISA. Control cultures at different time points did not significantly change (control equal to 30 pg/ml) in PGE_2 secretion. Due to the minimal variations, we set the control PGE_2 secretion at 1. **(A)** Quantification of the extracellular release of PGE_2 in the media of co-cultures of human primary astrocytes and differentiated SH-SY5Y human neuroblastoma cells treated with HIV-1 Tat_{1-72} 100 ng/ml for 6, 12, 24 and 48 hours. PGE_2 secretion did not change during the time course analyzed; **(B)** the same conditions used in A were repeated with HIV-1 Tat_{1-72} 300 ng/ml. Consistent with A, secretion of PGE_2 did not change compared to the control. Our results indicate that independently of time points and concentrations, PGE_2 secretion does not change after treatment with Tat.

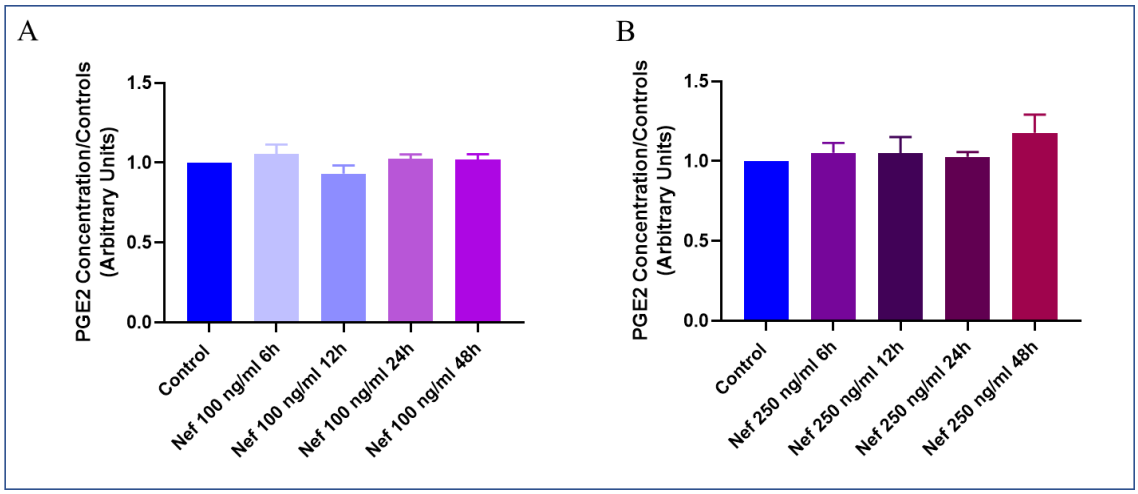

Figure 5.8. Nef treatment of mixed cultures of human primary astrocytes and differentiated neurons do not change PGE_2 secretion. Media collected from co-cultures of human primary astrocytes and differentiated SH-SY5Y human neuroblastoma cells at different time points were assessed for PGE_2 by ELISA. Control cultures at different time points did not significantly change (control equal to 30 pg/ml) in PGE_2 secretion. Due to the minimal variations, we set the control PGE_2 secretion at 1. **(A)** Quantification of the extracellular release of PGE_2 in the media of co-cultures of human primary astrocytes and differentiated SH-SY5Y human neuroblastoma cells treated with HIV-1 HXB2 Nef 100 ng/ml for 6, 12, 24 and 48 hours. PGE_2 secretion did not change during the time course analyzed; **(B)** the same conditions used in A were repeated with HIV-1 HXB2 Nef 250 ng/ml. Consistent with A, secretion of PGE_2 did not change compared to the control.
Our results indicate that PGE_2 secretion after treatment does not change with Nef.

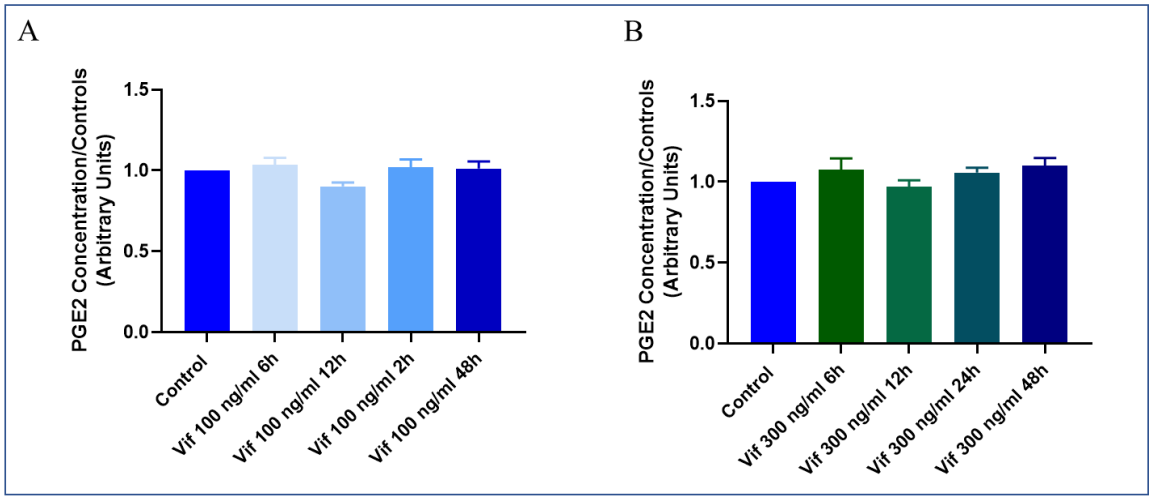

Figure 5.9. Vif treatment of mixed cultures of human primary astrocytes and differentiated neurons does not change PGE_2 secretion. Media collected from co-cultures of human primary astrocytes and differentiated SH-SY5Y human neuroblastoma cells at different time points were assessed for PGE_2 by ELISA. Control cultures at different time points did not significantly change (control equal to 30 pg/ml) in PGE_2 secretion. Due to the minimal variations, we set the control PGE_2 secretion at 1. **(A)** Quantification of the extracellular release of PGE_2 in the media of co-cultures of human primary astrocytes and differentiated SH-SY5Y human neuroblastoma cells treated with HIV-1 HXB2 Vif 100 ng/ml for 6, 12, 24 and 48 hours. PGE_2 secretion did not change at all the time points; **(B)** the same conditions used in A were repeated with HIV-1 HXB2 Vif 300 ng/ml. Consistent with A, secretion of PGE_2 did not change compared to the control. Our results indicate that PGE_2 secretion does not change after treatment with Vif.

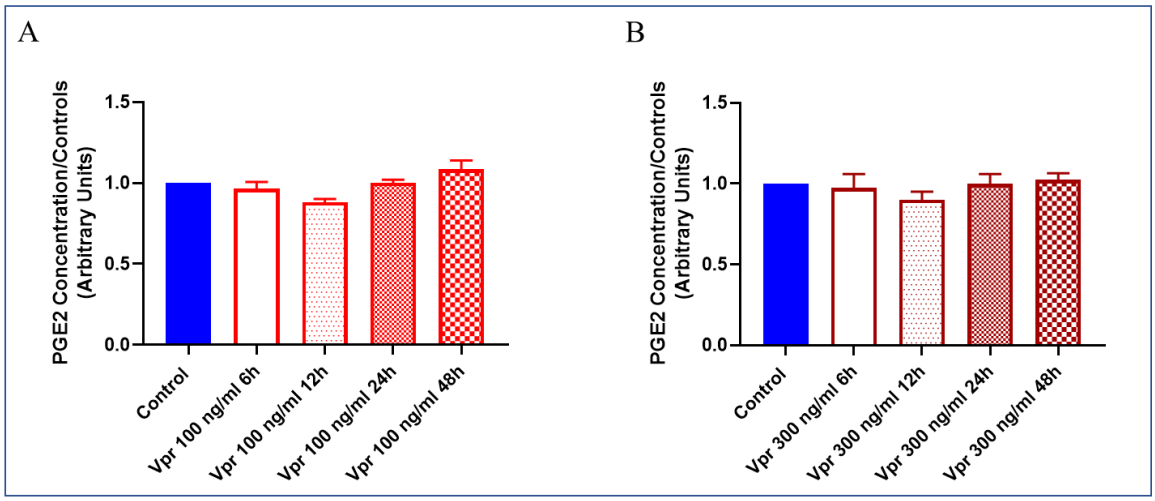

Figure 5.10. Vpr treatment of mixed cultures of human primary astrocytes and differentiated neurons does not change PGE_2 secretion. Media collected from co-cultures of human primary astrocytes and differentiated SH-SY5Y human neuroblastoma cells at different time points were assessed for PGE_2 by ELISA. Control cultures at different time points did not significantly change (control equal to 30 pg/ml) in PGE_2 secretion. Due to the minimal variations, we set the control PGE_2 secretion at 1. **(A)** Quantification of the extracellular release of PGE_2 in the media of co-cultures of human primary astrocytes and differentiated SH-SY5Y human neuroblastoma cells treated with HIV-1 Vpr 100 ng/ml for 6, 12, 24 and 48 hours. PGE_2 secretion did not change at all the time points; **(B)** the same conditions used in A were repeated with HIV-1 Vpr 300 ng/ml. Consistent with A, secretion of PGE_2 did not change compared to the control.

Our results indicate that PGE_2 secretion does not change after treatment with Vpr.

Chapter 6: Extracellular sulfatide regulates cell-to-cell communication mediated by Cx43 containing channels

D'Amico Daniela[1,2]; Prideaux Brendan [1]; Eugenin Eliseo A.[1]

[1]University of Texas Medical Branch (UTMB), Department of Neuroscience, Cell Biology and Anatomy, Galveston, TX, USA

[2]University of Palermo (UniPa), Department of Biomedicine, Neuroscience and Advanced Diagnostics, Palermo, Italy

This work was funded by The National Institute of Mental Health grant, MH096625, the National Institute of Neurological Disorders and Stroke grant, NS105584, and UTMB internal funding (to E.A.E).

Associated paper: D'Amico D., Prideaux B. and Eugenin E.A. "Sulfatide dysregulates Cx43 containing channels: role in neuroHIV". In preparation.

Introduction

A critical mechanism discovered in our laboratory is that HIV, even in the absence of viral replication, uses gap junctional communication to spread toxicity and inflammation from HIV-infected into uninfected cells. We identified that Tat is a key viral protein to maintain Cx43 expression and functional gap junction channels (Berman et al. 2016). Our data described in Chapter 2 further reinforce our previous results. Thus, we examined whether extracellular sulfatide regulates Connexin 43 (Cx43), Zonula-Occludens 1 (ZO-1), and Connexin 36 (Cx36) expression using human primary astrocytes and SH-SY5Y neuroblastoma cells.

We propose that sulfatide helps to maintain Cx43 expression in neurons and glia cells. We specifically analyzed whether sulfatide changes Cx43 mRNA and protein expression.

Cx43 is the major expressed connexin in astrocytes and Cx36 is exclusively expressed in neurons (Rash et al. 2001). In addition, we investigated the tight-junction protein ZO-1. ZO-1 binds to both connexins, Cx43 and Cx36, in order to stabilize them on the plasma membrane (Thevenin et al. 2013). Although, ZO-1 binds to the extreme carboxyl terminus of Cx43 with the second PDZ domain (Giepmans and Moolenaar 1998), it interacts with the C-terminal tail of Cx36 using the first PDZ domain (Li X. et al. 2004) while performing a scaffold role for the GJs in the plasma membrane. Notably, ZO-1 interaction regulates GJs dynamic turnover maintaining GJ channels in an open and functional state. On the contrary, when ZO-1 separates from Cxs, it induces GJs closure and transitioning for endocytosis (Thevenin et al. 2017). This dynamic turnover of GJs determines a relative short half-life (1–5 hours) of Cxs and GJs, regulating the physiological presence of GJs into the plasma membrane and resulting in GJs recycling or the triggering of apoptosis in pathological conditions. In particular, the dynamic turnover of Cx43 is mediated by an organized process of phosphorylation/dephosphorylation in specific serine (S) residues of the Cx43 C-term (Thevenin et al. 2017). When Cx43 is phosphorylated in the S373, Cx43 does not interact with ZO-1, but forward trafficking towards the plasma membrane occurs. The S373 phosphorylation step explains the unphosphorylated isoform (NP) detected in our western blotting experiment that specifically indicates Cx43 non-phosphorylated in S365. Once S373 is dephosphorylated, ZO-1 can bind to Cx43 and S365 is phosphorylated (P1 isoform of our western blotting) allowing the GJs to be open and functional. Another

important step includes the phosphorylation of S262 by ERK1/2 that allows Cx43 inclusion into the plaque (Solan and Lampe 2007), it explains the P2 isoform detected in our western blotting. After that, S365 and S262 become dephosphorylated, and S368 can be phosphorylated causing the closure of GJs and release of ZO-1. The phosphorylation on S368, S255, S279, and S282 cause Cx43 GJs internalization by endocytosis *via* clathrin system. Overall, we evaluate whether extracellular sulfatide compromise cell-to-cell communication *in vitro*.

Materials and Methods

Cell Culture Methods

Human primary astrocytes, SH-SY5Y human neuroblastoma cells, and Hela cells stably transfected with Cx43-CFP were used. High glucose Dulbecco's modified Eagle's medium (DMEM, 11995-065, Thermo Fisher Scientific, Waltham, MA) supplemented with 10% fetal bovine serum (FBS, S12450H, Atlanta Biologicals, Flowery Branch, GA), penicillin, and streptomycin (15070063, Thermo Fisher Scientific, Waltham, MA) was used to grow all the cells at 37 °C in a humidified atmosphere with 5% CO_2.

SH-SY5Y human neuroblastoma cells were differentiated with 2 mM L-glutamine (25030081, Thermo Fisher Scientific, Waltham, MA), 2% B27 supplement (17504044, Thermo Fisher Scientific, Waltham, MA), 2 mM Glutamax (35050-061, Thermo Fisher Scientific, Waltham, MA) and 10 µM Retinoic Acid (R2625, Sigma-Aldrich, St. Luis, MO-Aldrich, St. Luis, MO) for 7 days.

Media for Hela cells stably transfected with Cx43-CFP was supplemented with 2 mM Geneticin (10131-027, Thermo Fisher Scientific, Waltham, MA).

Total mRNA isolation

Human primary astrocytes and SH-SY5Y cultures were treated with Sulfatide (10 ng/ml) for 6, 12 and 24 hours. Arachidonic acid (AA) (100 µM) was used as a control due to its effects in astrocytes (Martinez A. D. and Saez 1999). These concentrations were chosen according to lower pathological levels detected in non-myelinated areas (for sulfatide) and in the sera (for AA) of virologically suppressed HIV-infected individuals. Untreated and treated cells were harvested in TRI REAGENT (93289, Sigma-Aldrich, St. Luis, MO)

according to the manufacturer's instructions. Cells were scratched in TRI REAGENT (1ml for 60 mm well plate) and 0.2 ml of chloroform (288306, Sigma-Aldrich, St. Luis, MO) were then added to the samples. After 3 minutes, the mixtures were transferred to 1 ml Eppendorf containing 0.5 ml pf phase lock gel (2302830, QuantaBio, Beverly, MA) and centrifuged at 12000 x g for 15 minutes at 4°C, to separate the RNA (aqueous phase) from proteins (red organic phase) and DNA (interphase). The aqueous phase was transferred to a fresh tube in which 0.5 ml of isopropanol (278475, Sigma-Aldrich, St. Luis, MO) was added. After 10 minutes, the samples were centrifuged at 12000 x g at 4°C for 15 minutes. The supernatant was removed and 1 ml of 75% ethanol (51976, Sigma-Aldrich, St. Luis, MO) was added to the RNA pellet at the bottom of the tube. The mixture was centrifuged at 7500 x g at 4°C for 5 minutes. The RNA was eluted from the filter in 100µl of DEPC-treated water (AM9938, Invitrogen, Carlsbad, CA) and warmed for 10-15 minutes at 60 ºC to be fully dissolved. The RNA extract obtained was stored at -20 °C until use. The concentration of each sample was calculated by spectrophotometric analysis (OD 260/280) using NanoDrop 2000 UV-Vis Spectrophotometer (Thermo Fisher Scientific, Waltham, MA).

Reverse Transcription PCR

Reverse transcription for first-strand cDNA synthesis was performed using the SuperScript III First-Strand (18080-051, Invitrogen, Carlsbad, CA) according to the manufacturer's instructions. 50 µM oligo (dT) was complexed with 300 ng of extracted RNA, in a final volume of 10 µl. Samples were incubated at 65 °C for 5 minutes and then placed on ice for at least 1 minute. 10 µl of cDNA synthesis mix (containing 10x RT buffer, 2 mM MgCl2, 0.1 M DTT, 40 U/ µl RNaseOUT, 200 U/ µl SuperScript III RT) was added prior to use of the Thermocycler (50°C for 50 minutes, 85°C 60' for 5 minutes) (170-9703, BioRad, Hercules, CA). The cDNA obtained was stored at -20 °C until use.

Quantitative real-time PCR (qRT-PCR)

Human Cx43, ZO-1, Cx36 and Glyceraldehyde 3-phosphate dehydrogenase (GAPDH) expression in untreated and treated astrocytes and SH-SY5Y neuroblastoma cell line were analyzed by qRT-PCR using a StepOnePlus Real Time PCR system (4376600, Thermo

Fisher Scientific, Waltham, MA) (Table 5), absolute blue QPCR SYBR low Rox Mix (AB4323A, Thermo Fisher Scientific, Waltham, MA), and the primers in Table 6. Single product amplification was confirmed by melting curve analysis, and primer efficacy was near or close to 100% in all experiments.

Table 5. qRT-PCR parameters.

Temperature	Time	Process	Number of Cycles
95 ºC	15’	Enzyme Activation	1 cycle
95 ºC	30’’	Denaturation	40 cycles
Tº annealing primers (~56 ºC)	30’’	Annealing	
72 ºC	30’’	Extension	
95 ºC	15’’	Denaturation	1 cycle
60 ºC	1’	Starting Temperature	
95 ºC	15’	Melting Step	

Table 6. Human reverse and forward primer sequences for Cx43, ZO-1, Cx36 and GAPDH.

Gene	Reverse Primer	Forward Primer
Cx43	5′-GGGTTAAGGGAAAGAGCGACC -3′	5′-CCCCATTCGATTTTGTTCTGC-3’
ZO-1	5′-CGCCTTTGGACAAAGAGAAG-3′	5′-TTTTAGGATCACCCGACGAC-3’
Cx36	5′-TTCCTAGCCCTGGACAGAGA-3′	5′-GATGCAGTGCGTAGACCTGA-3’

GAPDH	5′-AACGGATTTGGTCGTATTGGGC-3′	5′-CTTGACGGTGCCATGGAATTTG-3’

Western blotting

Human primary astrocytes and SH-SY5Y neuroblastoma cultures were treated with sulfatide (10 ng/ml, 24323, Cayman Chemical, Ann Arbor, MI) and AA (100 µM, 2756, Tocris, Bristol, UK) for 6, 12 and 24 hours and harvested in RIPA buffer (9806, Cell Signaling, Danvers, MA) containing protease and phosphatase inhibitors (20 mM; pyrophosphate, 20 mM; NaF, 100 mM; NaVO3, 200 µM; leupeptin, 500 µg/ml; aprotinin, 40 µg/ml; soybean trypsin inhibitor, 2 mg/ml; benzamidine, 1 mg/ml; ω-amino caproic acid, 1 mg/ml; PMSF, 3 mM; and EDTA, 20 mM). Untreated and treated cells were lysed, and the protein content of each cell lysate was determined using Bradford’s method (Bio-Rad labs, Hercules, CA). Samples containing 50 µg of proteins were used to analyze Cx43, ZO-1, Cx36 and GAPDH. Proteins were separated in 7.5 % SDS-PAGE and electrophoretically transferred to nitrocellulose membrane, which was incubated sequentially with blocking solution (5 % non-fat milk in Tris-buffered saline); anti-Cx43 (dilution 1:1000, anti-rabbit, C6219, Sigma-Aldrich, St. Luis, MO), anti-ZO-1 (dilution 1:1000, anti-rabbit, 402200, Thermo Fisher Scientific, Waltham, MA), anti-Cx36 (dilution 1:1000, anti-mouse, 37-4600, Thermo Fisher Scientific, Waltham, MA), and anti-GAPDH (dilution 1:1000, anti-rabbit, 14C10, Cell Signaling, Danvers, MA); and anti-rabbit/mouse IgG conjugated to HRP (dilution 1:1000, 7074S/7076S, Cell Signaling, Danvers, MA). Antigen-antibody complexes were detected by ECL (NEL103E001EA, Perkin Elmer, Boston, MA). The resulting immunoblot signals were scanned and densitometric analysis was performed using ImageJ NIH-image software. All results were normalized to the values obtained for control conditions.

Immunofluorescence

Human primary astrocytes and Hela cells stably transfected with Cx43-CFP were grown on coverslips and were treated with sulfatide and AA (resulting in a final concentration of 10 ng/ml and 100 µM, respectively) for 6, 12 and 24 hours. Later, untreated and treated

cells were fixed with 4% PFA (15710-S, Electron Microscopy Science, Hatfield, PA) and permeabilized in 0.1% Triton (X-100, Sigma-Aldrich, St. Luis, MO) for 2 min at room temperature. Cells were incubated in blocking solution (0.5 M EDTA pH 8.0 (15575-038, Thermo Fisher Scientific, Waltham, MA), 1% Fish gelatin from cold water (G7765, Sigma-Aldrich, St. Luis, MO), 0.1 g Albumine from bovine serum fraction V (BP1605, Thermo Fisher Scientific, Waltham, MA), 1% Horse serum (H1138, Sigma-Aldrich, St. Luis, MO), 5% human serum (31876, Thermo Fisher Scientific, Waltham, MA), 9 ml ddH_20) overnight at 4 °C and then in diluted primary antibodies (anti-Cx43, dilution 1:1000, anti-rabbit, C6219, Sigma-Aldrich, St. Luis, MO; anti-ZO-1, dilution 1:200, anti-mouse, MABT339, Millipore, Burlington, MA) overnight at 4 °C. Cells were washed several times with PBS (BP665-1, Thermo Fisher Scientific, Waltham, MA) at room temperature and incubated with the appropriate secondary antibodies (plus Phalloidin 680 or Texas Red, dilution 1:250, A22286/T7471, Thermo Fisher Scientific, Waltham, MA) for at least 2 hours at room temperature followed by several washes in PBS. Cells were then mounted using Prolong Gold anti-fade reagent (P36930, Thermo Fisher Scientific, Waltham, MA) and examined using an A1 confocal microscope (Nikon, Japan). Specificity was confirmed by replacing the primary antibodies with the appropriate isotype matched control reagent, anti-IgG_2A, or the IgG fraction of normal mouse/rabbit serum (A-2179/A-0418, Sigma-Aldrich, St. Luis, MO).

Statistical Analysis

All data were expressed as mean ± standard error of the mean (SEM). Differences among groups were analyzed by a one-way analysis of variance (ANOVA test), using Bonferroni's multiple comparison test for post-hoc analysis. The level of significance was accepted at $p<0.05$. Prism8.0 software was used for the statistical analyses performed.

Results

Extracellular sulfatide increases cell-to-cell communication in human primary astrocytes. Considering that HIV-infected astrocytes use GJs and uHCs to spread inflammatory and pro-apoptotic molecules into the neighboring uninfected cells (Eugenin and Berman 2007) and that HIV proteins induce the secretion of sulfatide (see Chapter 5),

we mimicked these pathological conditions *in vitro*. We evaluated mRNA and protein expression by carrying out qRT-PCR, western blotting, and immunofluorescence in human primary astrocytes treated with 10 ng/ml sulfatide for 6, 12 and 24 hours. We showed that sulfatide upregulates Cx43 mRNA expression at 24 hours (Figure 6.1 A, * p=0.0425). Furthermore, sulfatide increased Cx43 P1 and P2 isoforms after 24 hours (Figure 6.2 C, * p<0.0001; Figure 6.2 D, * p=0.0092). This means that sulfatide induced S365 and S262 phosphorylation in the C-term of Cx43 to make GJs open, functional, and well incorporated in the plaque between the cells. In addition, immunofluorescence analysis for Cx43, ZO-1, actin and DAPI in human primary astrocytes treated with sulfatide showed an increase in Cx43 intensity (Figure 6.3 B, * p=0.0099), and Cx43-ZO-1 colocalization (Figure 6.3 D, * p=0.0117; Figure 6.2 E, * p=0.0006), based on the maximum peak from all the groups treated. Thus, it suggests that Cx43 can be regulated by sulfatide in the forward trafficking towards the plasma membrane and in the stabilization into the plasma membrane.

Although, sulfatide did not change ZO-1 mRNA compared to the control conditions (Figure 6.1 B), it increased ZO-1 protein level after 12 (Figure 6.2 F, * p=0.0006) and 24 hours (Figure 6.2 F, * p=0.0006). Any significative changes were detected for ZO-1 maximal peak intensity compared to the controls in the immunofluorescence analysis (Figure 6.3 C). This indicates that sulfatide upregulates astrocyte cell communication systems, especially working on the protagonist of the channels, Cx43.

Likewise, we performed the same experiments in human astrocytes using AA, because several previous unpublished data in our laboratory and data from the literature (Martinez A. D. and Saez 1999, Puebla et al. 2017) showed that AA either decreased or did not change junctional communication. We showed that AA, as well as other inflammatory molecules, decreased cell-to-cell communication systems in human primary astrocytes. Specifically, AA transiently reduced Cx43 mRNA expression after 12 hours (Figure 6.4 A, * p=0.0414), as well as decreased all the protein isoforms of Cx43 after 24 hours compared to the control conditions (Figure 6.5 B, * p=0.0007; C, * p=0.0074; D * p=0.0034), suggesting that AA supports the close status of GJs. On another hand, AA did not change ZO-1 mRNA (Figure 6.4 B) but drastically decreased ZO-1 proteins at all timepoints compared to the control conditions (Figure 6.5 F, * p<0.0001), confirming that AA destabilizes Cx43 in the plaque and obstructed cellular communication. In addition, immunofluorescence for Cx43, ZO-1,

actin and DAPI in human primary astrocytes treated with AA demonstrated that Cx43 trafficking was not affected due to any significative changes in Cx43 and ZO-1 intensities (Figure 6.6 B and C) and colocalization (Figure 6.6 D and E), considering the maximum peak from all the treated groups. So, AA perfectly reproduced inflammatory conditions enhancing GJ closure.

Extracellular sulfatide downregulates mRNA and proteins involved in cell-to-cell communication in differentiated SH-SY5Y neuroblastoma cell line. Neurons are not directly infected by HIV, but they are targets of HIV proteins. As sulfatide secretion is regulated by HIV proteins, we assessed sulfatide effect on cell-to-ell communication using qRT-PCR and western blotting on SH-SY5Y neuroblastoma cells differentiated for 1 week with retinoic acid and treated with sulfatide for 6, 12 and 24 hours. We analyzed the level of Cx43, ZO-1 and Cx36 (which allow neuron cellular communication and maintain electrical connectivity between different populations of neurons). Our results showed that sulfatide downregulated Cx43 mRNA expression after 24 hours compared to the control conditions (Figure 6.7 A, * p=0.002), downregulated ZO-1 mRNA expression at all the time points compared to control conditions (Figure 6.7 B, * p<0.0001), but did not affect Cx36 mRNA expression (Figure 6.7 C). Nevertheless, only ZO-1 protein underwent a significant reduction after sulfatide treatment all the time points (Figure 6.8 E, * p<0.0001), suggesting that sulfatide decrease expression of mRNA and proteins involved in cellular communication in neurons by reducing ZO-1, whose interaction with Cxs is necessary to establish cellular communication. Although, sulfatide decreased Cx43 mRNA, the two isoforms of proteins detected in neurons were repristinated. Moreover, Cx36 protein, as well as Cx36 mRNA, did not undergo significantly changes.

Using the same approach as applied to astrocytes, SH-SY5Y cells were treated with AA as a positive control. In differentiated neurons, AA transiently decreased Cx43 mRNA after 6 hours (Figure 6.9 A, * p<0.0001) and 24 hours (Figure 6.9 A, * p<0.0001), but did not change Cx43 protein expressions (Figure 6.10 B and C). Moreover, AA increased ZO-1 mRNA level after 12 (Figure 6.9 B, * p<0.0001) and 24 hours (Figure 6.9 B, * p<0.0001), but any change was detected at the protein level (Figure 6.10 E). In addition, neither Cx36

mRNA (Figure 6.9 C) or Cx36 protein (Figure 6.10 G) significantly changed. Thus, we can assess that AA does not change the cellular communication system between neurons.

Extracellular sulfatide induces Cx43 internalization in Hela cells. Although, sulfatide can differentially regulate cellular communication in astrocytes and neurons, we investigated Cx43 trafficking using Hela cells stably transfected with Cx43-CFP. We also treated these cells with 10 ng/ml sulfatide for 6, 12 and 24 hours and we stained them for phalloidin Texas Red to visualize the cellular membrane (Figure 6.11 A). Thus, we identified that in all the control conditions and at 0 hour sulfatide, Cx43 was mostly localized in the plasma membrane to generate plaques (Figures 6.11 A as indicated by the yellow arrows). On the contrary, in sulfatide conditions Cx43 had a cytoplasmatic localization (Figures 6.11 A, as indicated by the white arrows), suggesting that sulfatide induces Cx43 internalization, moving Cx43 from the plaques (Figures 6.11 A, as indicated by the yellow arrows, and Figure 6.11 B, ** p<0.0001) in the cellular membrane to the intracellular vesicles (Figures 6.11 A, as indicated by the white arrows, and Figure 6.11 B, ** p<0.0001) into the cytoplasm. This demonstrates that, sulfatide can modulate Cx43 trafficking towards the cytoplasm.

Hela cells stably transfected with Cx43-CFP were treated with AA for 6, 12 and 24 hours. Our results showed that AA did not induce Cx43 internalization. Internalized vesicles were also present in 6, 12 and 24 hours control conditions (Figure 6.12 A, as indicated by white arrows, and Figure 6.12 B, ** p<0.0001). This Cx43 internalization may be due to the soya oil/water solvent (Tocrisolve) used to dissolve AA and that we also used to treat 6, 12 and 24 hours control conditions. This consideration is supported by Cx43 localization in the plaques at no treatment (0 hour control and 0 hour sulfatide) conditions (meaning no treatment with Tocrisolve and AA, respectively) (Figure 6.12 A, as indicated by yellow arrows, and Figure 6.12 B), when the cells never came in contact with Tocrisolve. Thus, we cannot assess that AA regulates Cx43 trafficking.

Discussion

As we explained in the general introduction and in this chapter's introduction, cell-to-cell communication is a common physiological and pathological system used by cells to share

signaling as well as toxic molecules. Although, several pathological conditions showed a decreased level of GJs and uHC (Rouach et al. 2002), HIV is the only case that showed the opposite. In fact, HIV-infected astrocytes use GJs and uHCs to communicate with and induce apoptosis to the neighboring neurons, the other nearby astrocytes and the adjacent endothelial cells. Therefore, we investigated whether our potential lipid biomarker of the HIV CNS disease, sulfatide, could be involved in the regulation of cellular communication. Our data from human primary astrocytes showed that sulfatide upregulated Cx43. These results support our proposed mechanism of bystander damage and can be related to the common feature of GJs and uHCs being opened and functional in HIV-infected astrocytes. On the contrary, in differentiated SH-SY5Y neuroblastoma cells, sulfatide downregulates ZO-1, but it did not regulate Cx43 and Cx36. Thus, in neurons sulfatide displayed a different effect decreasing cell-to-cell communication. Sulfatide decreased ZO-1 destabilizing Cxs in the plaques.

In addition, in Hela cells stably transfected with Cx43-CFP, we demonstrated that sulfatide induced internalization of the plaques, regulating Cx43 trafficking from the plasma membrane to the cytoplasm. Although, this result seems to show an opposite mechanism from that one proposed for astrocytes, it is necessary to consider that the systems used are different. However, both in astrocytes and in Hela cells transfected with Cx43-CFP, sulfatide modulated Cx43 trafficking. Future experiments will further evaluate changes in cell-to-cell communication by using die coupling or electrophysiology.

In conclusion, sulfatide may directly and indirectly contributes to the expansion of neuronal damage and neurocognitive disorders observed in the numerous cases of HIV-infected individuals under cART and with undetectable viral replication.

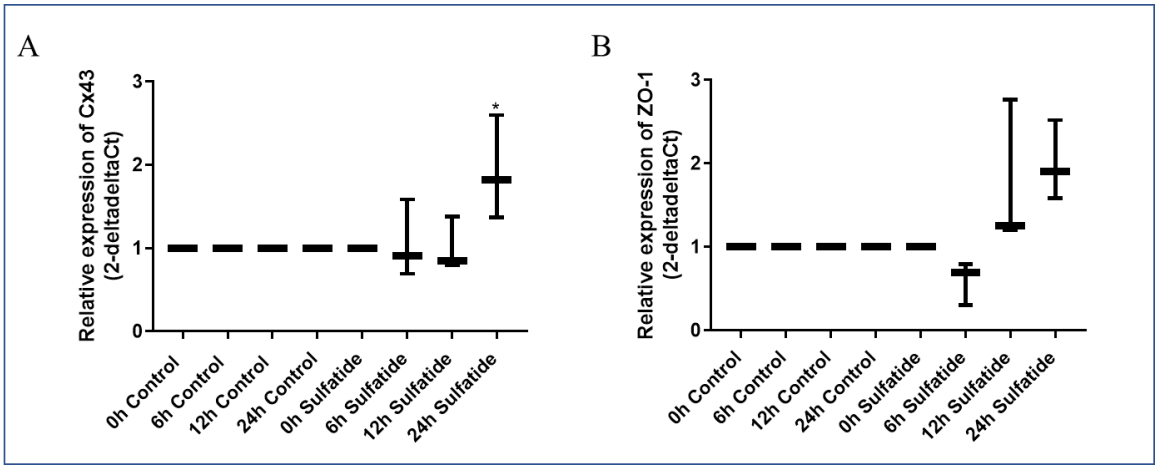

Figure 6.1. Extracellular sulfatide upregulates Cx43 mRNA in human primary astrocytes. Treatment of human primary astrocytes with sulfatide resulted in increased level of Cx43 mRNA. mRNA was isolated from human primary astrocytes and were assessed for Cx43 and ZO-1 using RT-PCR. **(A)** Quantification of Cx43 mRNA in human primary astrocytes treated with 10 ng/ml sulfatide for 6, 12 and 24 hours. Controls at different time points did not significantly change (controls equal to 1.8 $2^{-\Delta\Delta Ct}$, was set to 1). Cx43 mRNA increased at 24 hours (* as compared to controls and 0h Sulfatide conditions, p=0.0425, n=3). **(B)** The same conditions used in A were repeated for ZO-1 mRNA level (controls equal to 2.9 $2^{-\Delta\Delta Ct}$, was set to 1). In contrast with A, sulfatide did not significantly upregulate ZO-1 mRNA.

Our results indicate that sulfatide treatment upregulates Cx43 mRNA level after 24 hours.

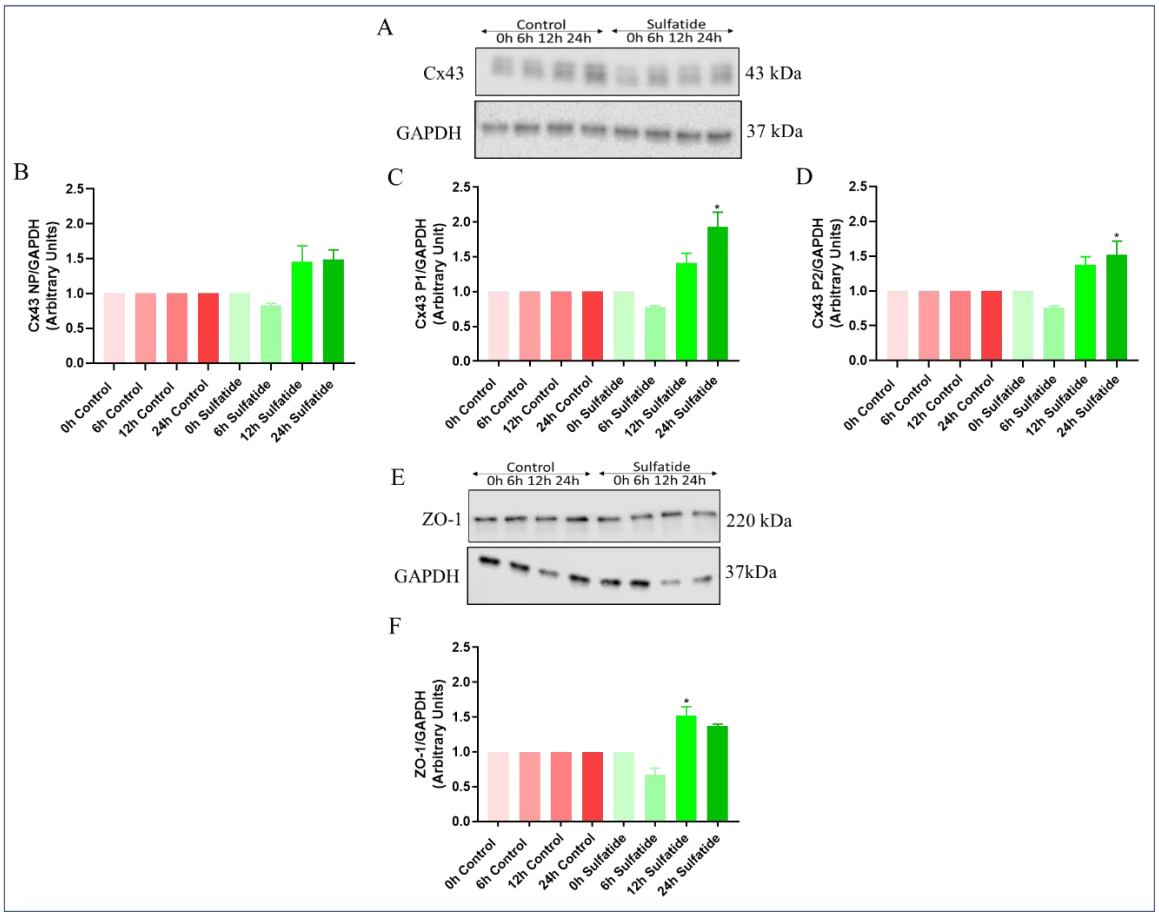

Figure 6.2. Extracellular sulfatide upregulates Cx43 and ZO-1 proteins in human primary astrocytes. Treatment of human primary astrocytes with sulfatide resulted in increased level of Cx43 and ZO-1 proteins. Proteins were extracted from human primary astrocytes and were assessed for Cx43 and ZO-1 using wester blotting. **(A)** Detection of Cx43 resulted in several bands representing different isoforms of around 43 kDa, according to the literature (Thevenin et al. 2017). GAPDH was used as control loading. **(B)** Quantification of Cx43 non-phosphorylated (NP) isoform in human primary astrocytes treated with 10 ng/ml sulfatide for 6, 12 and 24 hours. Controls at different time points did not significantly change (controls equal to 0.5 arbitrary units, was set to 1). **(C)** The same conditions used in A were repeated for Cx43 phosphorylated isoform (P1) (controls equal to 0.3 arbitrary units, was set to 1). Sulfatide increased Cx43 P1 protein level after 24 hours (* as compared to controls and 0h Sulfatide conditions, $p<0.0001$, n=3). **(D)** The same conditions used in A and in B were repeated for Cx43 phosphorylated isoform (P2)

(controls equal to 0.4 arbitrary units, was set to 1). Sulfatide increased Cx43 P2 protein level after 24 hours (* as compared to controls and 0h Sulfatide conditions, p=0.0092, n=3). **(E)** Detection of ZO-1 resulted in a single band of 220 kDa, GAPDH was used as loading control. **(F)** Quantification of ZO-1 protein in human primary astrocytes treated with 10 ng/ml sulfatide for 6, 12 and 24 hours. Controls at different time points did not significantly change (controls equal to 0.5 arbitrary units, was set to 1). Sulfatide increased ZO-1 protein level after 12 hours (* as compared to controls and 0h Sulfatide conditions, p=0.0006, n=3), suggesting a transient increase that came back to the control levels at 24 hours.

Our results indicate that sulfatide treatment upregulates Cx43 P1 and P2 isoforms protein level at 24 hours and transiently ZO-1 protein level at 12 hours.

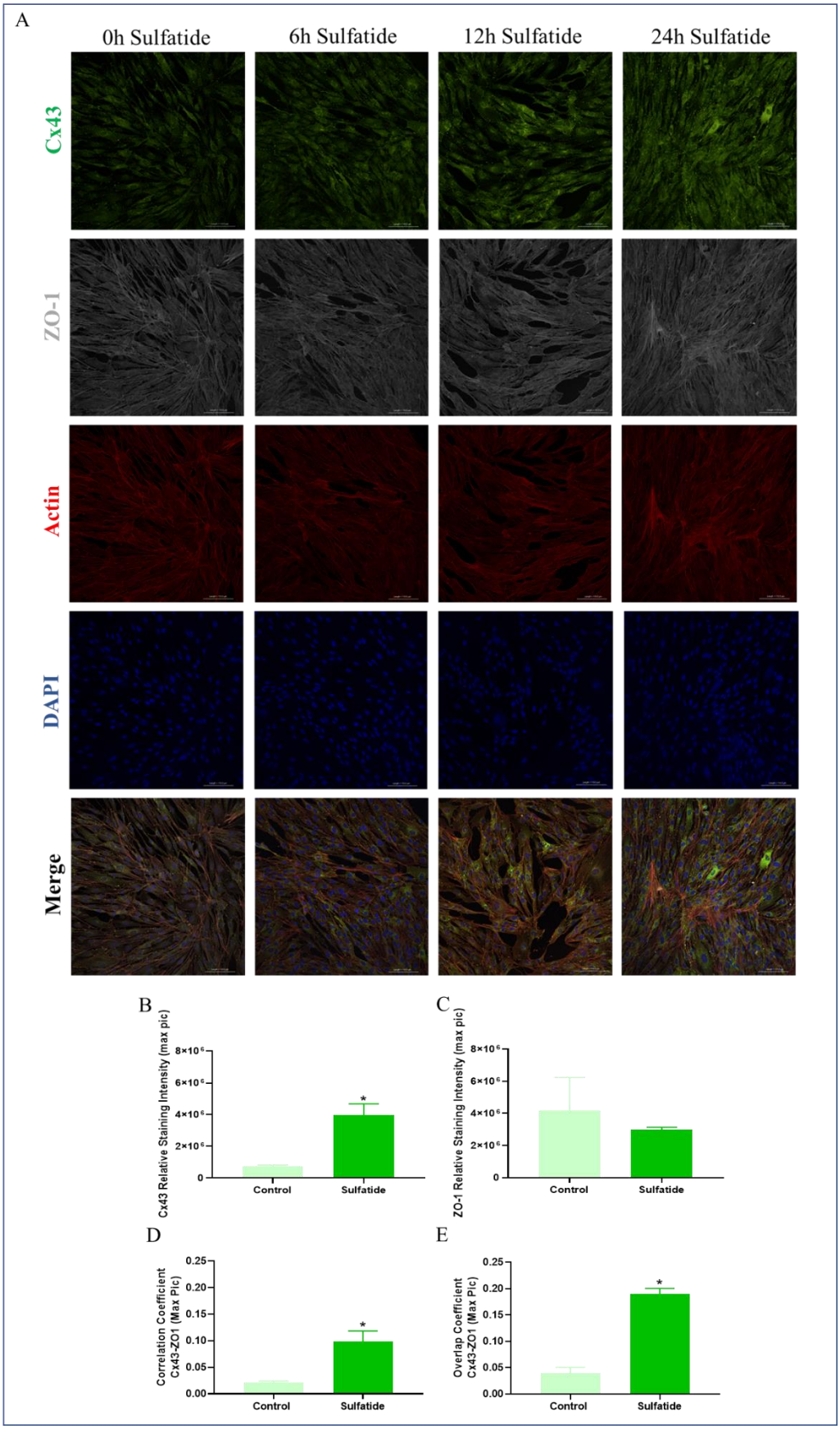
A
0h Sulfatide
6h Sulfatide
12h Sulfatide
24h Sulfatide
Cx43
ZO-1
Actin
DAPI
Merge
B
Cx43 Relative Staining Intensity (max pic)
8×10⁶
6×10⁶
4×10⁶
2×10⁶
0
Control
Sulfatide
*
C
ZO-1 Relative Staining Intensity (max pic)
8×10⁶
6×10⁶
4×10⁶
2×10⁶
0
Control
Sulfatide
D
Correlation Coefficient Cx43-ZO1 (Max Pic)
0.25
0.20
0.15
0.10
0.05
0.00
Control
Sulfatide
*
E
Overlap Coefficient Cx43-ZO1 (Max Pic)
0.25
0.20
0.15
0.10
0.05
0.00
Control
Sulfatide
*

Figure 6.3. Extracellular sulfatide upregulates Cx43-ZO-1 colocalization in human primary astrocytes. Treatment of human primary astrocytes with sulfatide resulted in increased Cx43 and ZO-1 colocalization as well as stabilizing Cx43 plaques at the plasma membrane. Immunofluorescence staining for Cx43, ZO-1, actin and DAPI was performed in human primary astrocytes in control and sulfatide treated conditions after 6, 12 and 24 hours. **(A)** Representative staining for Cx43 in green, ZO-1 in white, actin in red and DAPI in blue (20X). Quantification for 5 pictures per condition representing the total number of the pixels was performed considering the relative staining intensity from the maximal peak of all the treated groups **(B)** for Cx43 that was upregulated in sulfatide conditions (* as compared to control conditions, p=0.0099, n=3) and **(C)** for ZO-1 that did not show any difference in intensity for the controls and the treated groups (n=3). Co-localization for Cx43 and ZO-1 was measured by **(D)** correlation coefficient between Cx43 and ZO-1 (* as compared to control condition p=0.0117, n=3) and **(E)** overlap coefficient between Cx43 and ZO-1 (* as compared to control conditions, p=0.0006, n=3;) considering the maximal peak of all the control and treated groups. Both analyses used to calculate Cx43 and ZO-1 colocalization showed upregulation for the sulfatide treated groups.

Our results indicate that sulfatide treatment upregulates Cx43 intensity and Cx43-ZO-1 colocalization in human primary astrocytes.

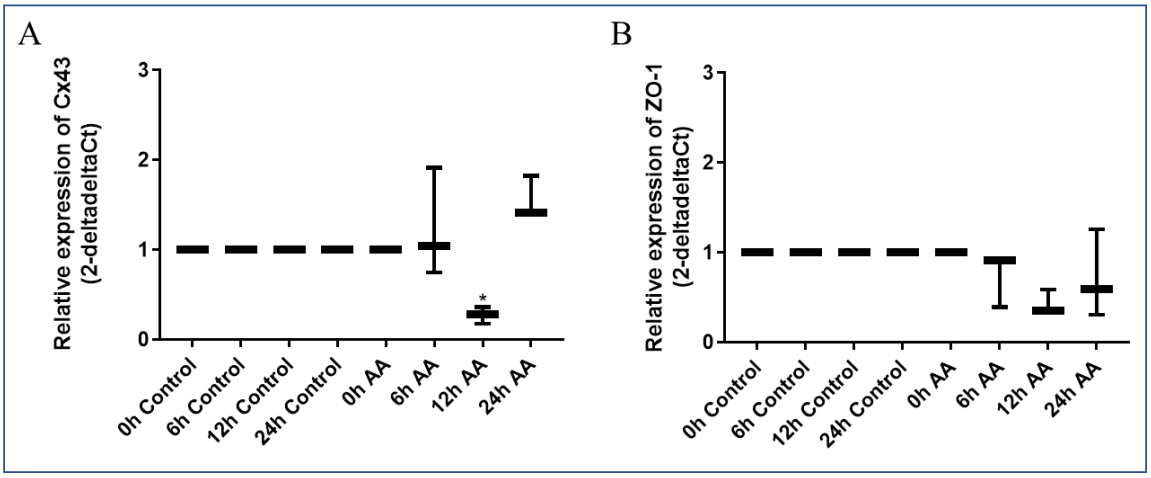

Figure 6.4. Arachidonic acid (AA) downregulates Cx43 mRNA in human primary astrocytes. Treatment of human primary astrocytes with AA resulted in decreased level of Cx43 mRNA. mRNA was isolated from human primary astrocytes were assessed for Cx43 and ZO-1 using RT-PCR. **(A)** Quantification of Cx43 mRNA in human primary astrocytes treated with 100 µM AA for 6, 12 and 24 hours. Controls at different time points did not significantly change (controls equal to 2.7 $2^{-\Delta\Delta Ct}$, was set to 1). Cx43 mRNA decreased at 12 hours (* as compared to controls and 0h Sulfatide conditions, p=0.0414, n=3), supporting a transient downregulation. **(B)** The same conditions used in A were repeated for ZO-1 mRNA level (controls equal to 2.5 $2^{-\Delta\Delta Ct}$, was set to 1). In contrast with A, sulfatide did not change ZO-1 mRNA.

Our results indicate that sulfatide treatment transiently downregulates Cx43 mRNA level at 12 hours.

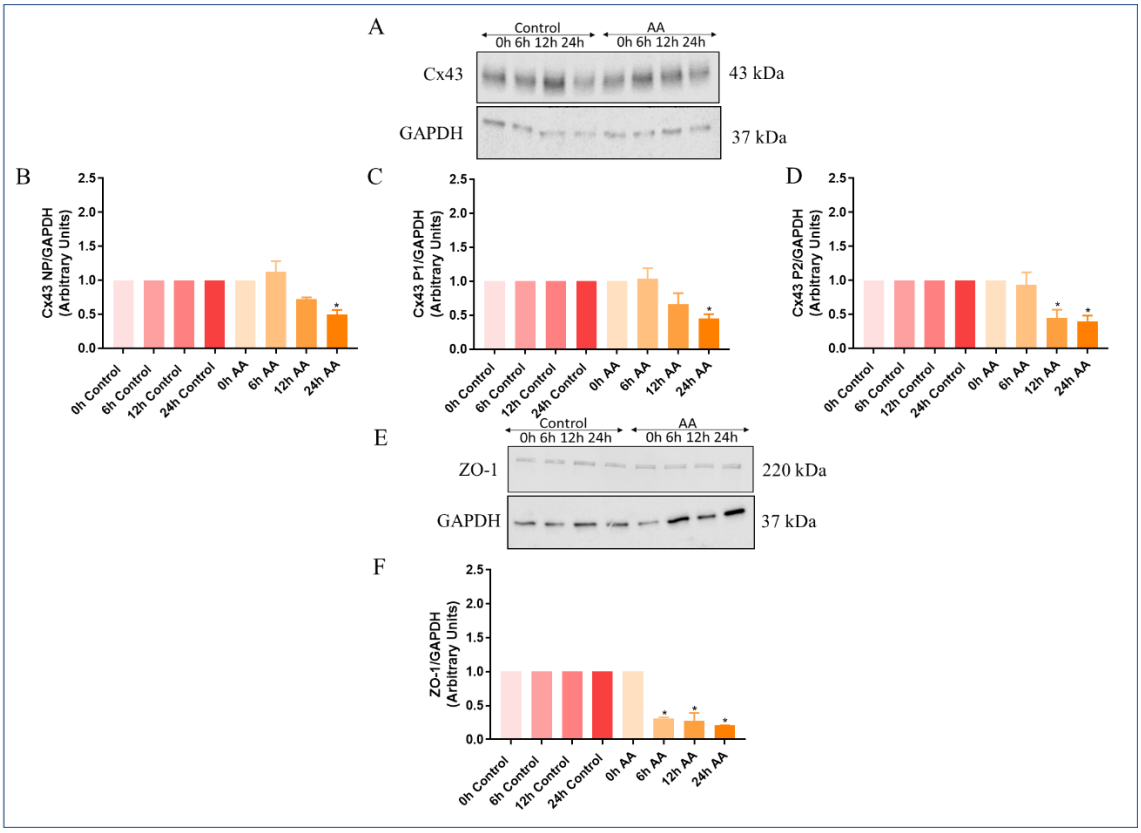

Figure 6.5. Arachidonic acid (AA) downregulates Cx43 and ZO-1 proteins in human primary astrocytes. Treatment of human primary astrocytes with AA resulted in decreased level of Cx43 and ZO-1 proteins. Proteins were extracted from human primary astrocytes and were assessed for Cx43 and ZO-1 using wester blotting. **(A)** Detection of Cx43 resulted in several bands representing different isoforms of around 43 kDa, according to the literature (Thevenin et al. 2017). GAPDH was used as control loading. **(B)** Quantification of Cx43 non-phosphorylated (NP) isoform in human primary astrocytes treated with 100 µM AA for 6, 12 and 24 hours. Controls at different time points did not significantly change (controls equal to 0.5 arbitrary units, was set to 1). AA decreased Cx43 NP protein level after 24 hours (* as compared to controls and 0h AA conditions, p=0.0007, n=3). **(C)** The same conditions used in B were repeated for Cx43 phosphorylated isoform (P1) (controls equal to 0.7 arbitrary units, was set to 1). Consistent with A, AA decreased Cx43 P1 protein level after 24 hours (* as compared to controls and 0 hour AA conditions, p=0.0074, n=3). **(D)** The same conditions used in B and C were repeated for Cx43

phosphorylated isoform (P2) (controls equal to 0.5 arbitrary units, was set to 1). AA decreased Cx43 P2 protein level after 12 and 24 hours (* as compared to controls and 0h AA conditions, p=0.0034 and p=0.0067, n=3). **(E)** Detection of ZO-1 resulted in a single band of 220 kDa, GAPDH was used as loading control. **(F)** Quantification of ZO-1 protein in human primary astrocytes treated with 100 µM AA for 6, 12 and 24 hours. Controls at different time points did not significantly change (controls equal to 3.5 arbitrary units, was set to 1). AA decreased ZO-1 protein level after 6, 12 and 24 hours (* as compared to controls and 0h AA conditions, p<0.0001, n=3).

Our results indicate that AA treatment downregulates Cx43 and ZO-1 protein levels.

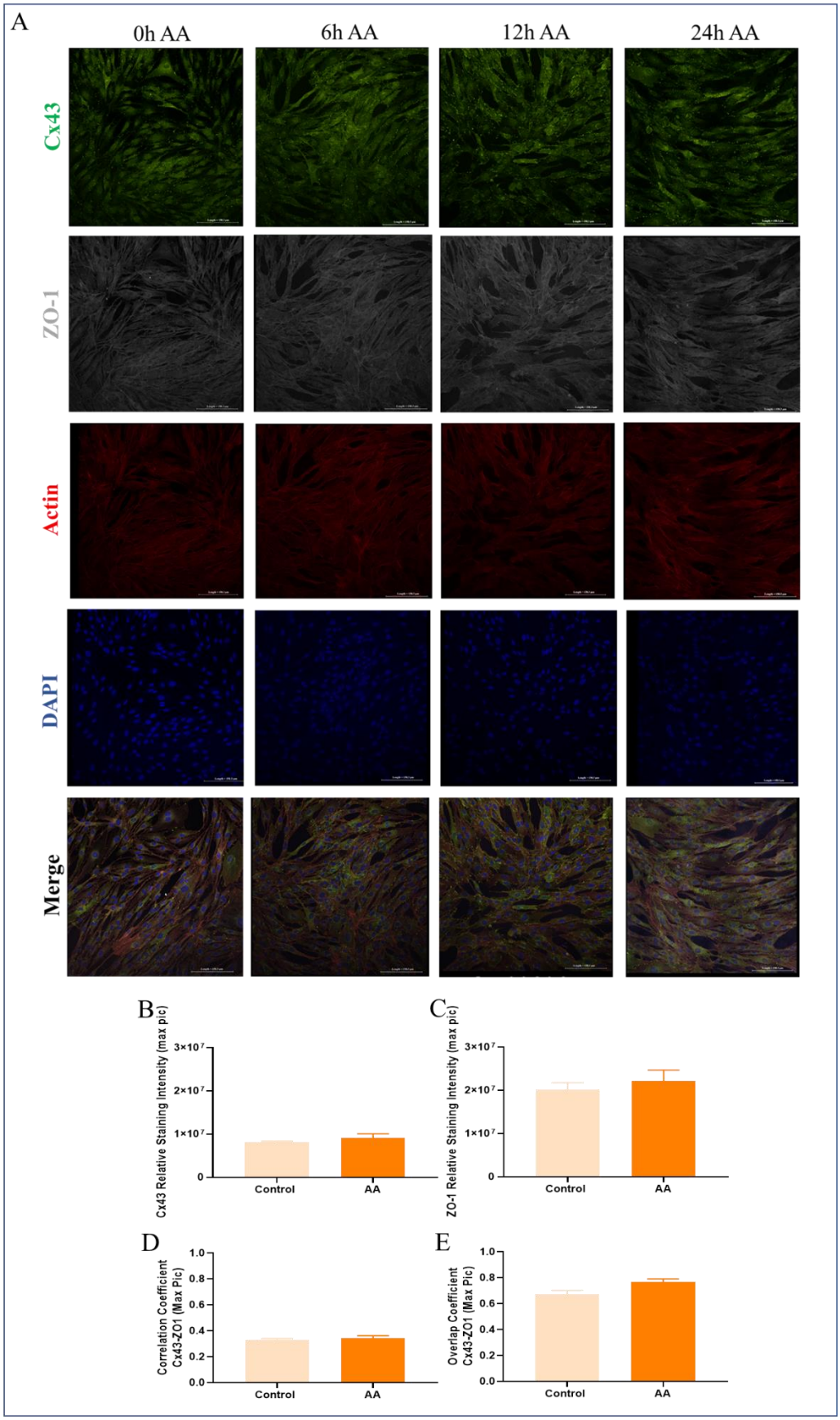
A
0h AA
6h AA
12h AA
24h AA
Cx43
ZO-1
Actin
DAPI
Merge
B
Cx43 Relative Staining Intensity (max pic)
3×10⁷
2×10⁷
1×10⁷
0
Control
AA
C
ZO-1 Relative Staining Intensity (max pic)
3×10⁷
2×10⁷
1×10⁷
0
Control
AA
D
Correlation Coefficient Cx43-ZO1 (Max Pic)
1.0
0.8
0.6
0.4
0.2
0.0
Control
AA
E
Overlap Coefficient Cx43-ZO1 (Max Pic)
1.0
0.8
0.6
0.4
0.2
0.0
Control
AA

Figure 6.6. Arachidonic acid (AA) does not change Cx43-ZO-1 colocalization in human primary astrocytes. Treatment of human primary astrocytes with AA does not upregulate Cx43 and ZO-1 colocalization. Immunofluorescence staining for Cx43, ZO-1, actin and DAPI was performed in human primary astrocytes in control and AA treated conditions after 6, 12 and 24 hours. **(A)** Representative staining for Cx43 in green, ZO-1 in white, actin in red and DAPI in blue (20X). Quantification for 5 pictures per condition representing the total number of the pixels was performed considering the relative staining intensity from the maximal peak of all the treated groups **(B)** for Cx43 that did not show any difference in intensity (n=3) and **(C)** for ZO-1, that consistent with B did not show any difference in intensity for the controls and the treated groups (n=3). Co-localization for Cx43 and ZO-1 was measured by **(D)** correlation coefficient between Cx43 and ZO-1 (n=3) and **(E)** overlap coefficient between Cx43 and ZO-1 (n=3) considering the maximal peak of all the control and treated groups. Both analyses used to calculate Cx43 and ZO-1 colocalization do not show significant changes for the AA treated groups compared to controls.

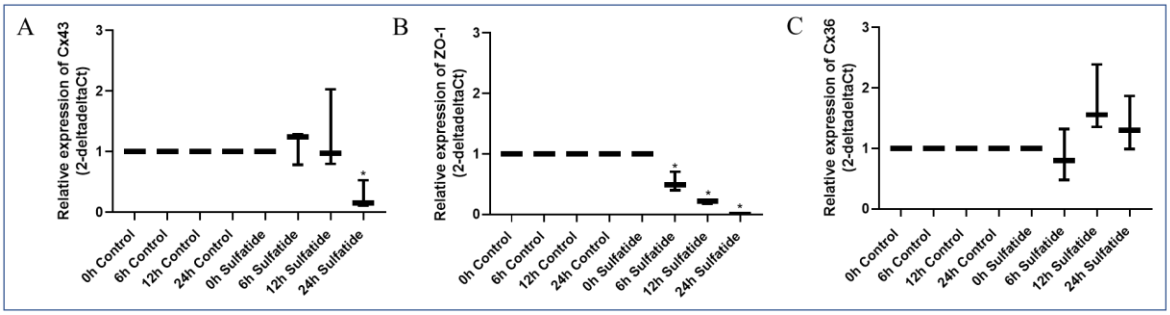

Figure 6.7. Extracellular sulfatide downregulates Cx43 and ZO-1 but not Cx36 mRNA in SH-SY5Y neuroblastoma cells. Treatment of in SH-SY5Y neuroblastoma cells with sulfatide resulted in decreased level of Cx43 and ZO-1 mRNA. mRNA was isolated from SH-SY5Y neuroblastoma cells and was assessed for Cx43, ZO-1, Cx36 using RT-PCR. **(A)** Quantification of Cx43 mRNA in SH-SY5Y neuroblastoma cells treated with 10 ng/ml sulfatide for 6, 12 and 24 hours. Controls at different time points did not significantly change (controls equal to 5 $2^{-\Delta\Delta Ct}$, was set to 1). Cx43 mRNA decreased at 24 hours (* as compared to controls and 0h Sulfatide conditions, p=0.0002, n=3). **(B)** The same conditions used in A were repeated for ZO-1 mRNA level (controls equal to 1.2 $2^{-\Delta\Delta Ct}$, was set to 1). ZO-1 mRNA decreased at 6, 12 and 24 hours (* as compared to controls and 0h Sulfatide conditions, p<0.0001, n=3). **(C)** The same conditions used in A and B were repeated for Cx36 mRNA level (controls equal to 1 $2^{-\Delta\Delta Ct}$, was set to 1). Sulfatide treatment did not change Cx36 mRNA level.

Our results indicate that sulfatide treatment downregulates Cx43 mRNA level at 24 hours and ZO-1 at all the time points considered.

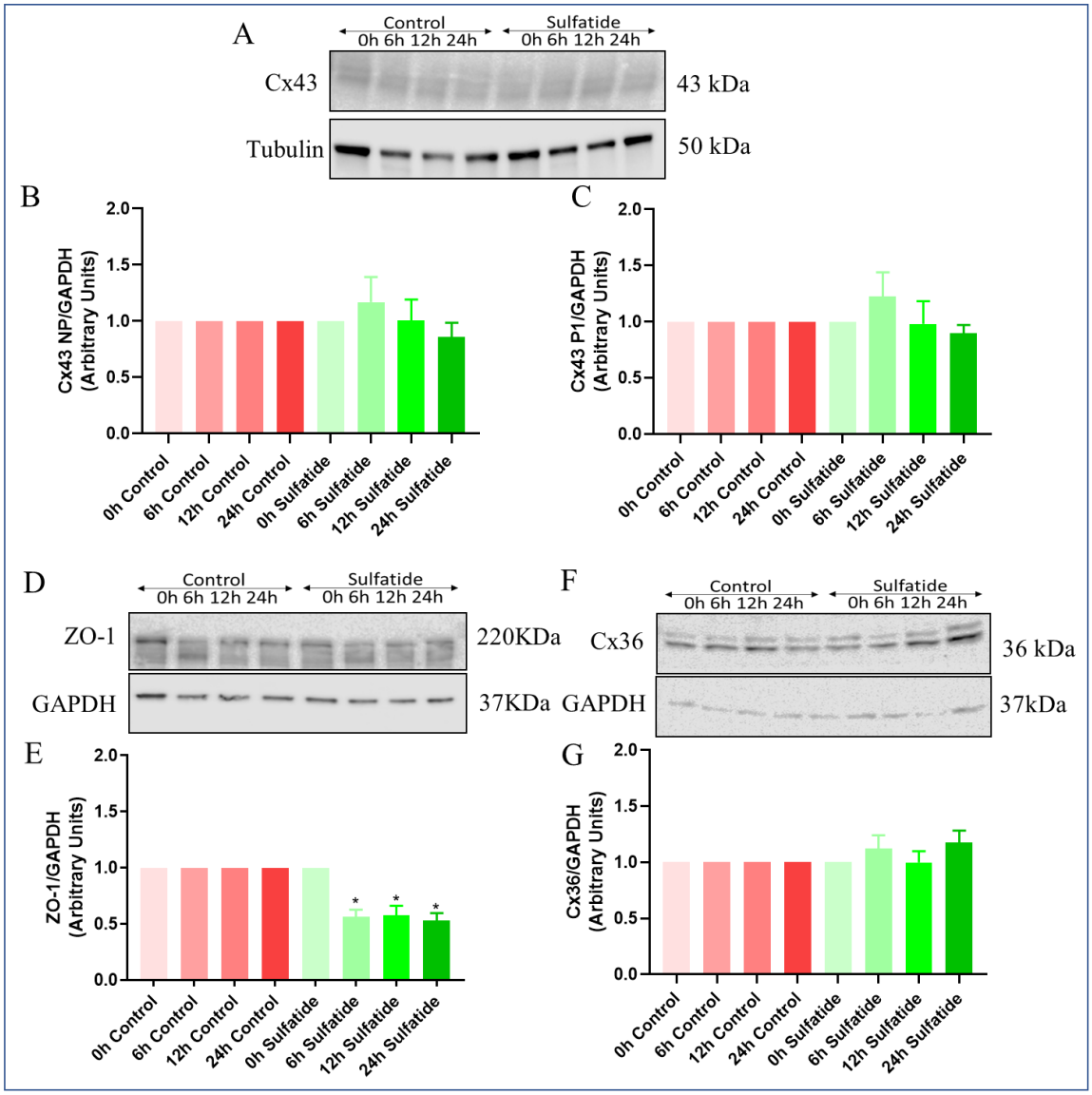

Figure 6.8. Extracellular sulfatide downregulates ZO-1 protein in SH-SY5Y neuroblastoma cells. Treatment of in SH-SY5Y neuroblastoma cells with sulfatide resulted in decreased level ZO-1 protein. Proteins were extracted from in SH-SY5Y neuroblastoma cells and were assessed for Cx43, ZO-1 and Cx36 using wester blotting. **(A)** Detection of Cx43 resulted in two bands representing different isoforms of around 43 kDa, according to the literature (Thevenin et al. 2017). Tubulin was used as control loading. **(B)** Quantification of Cx43 non-phosphorylated (NP) isoform in SH-SY5Y neuroblastoma cells treated with 10 ng/ml sulfatide for 6, 12 and 24 hours. Cx43 at different time points did not significantly change (controls equal to 0.3 arbitrary units, was set to 1). **(C)** The

same conditions used in B were repeated for Cx43 phosphorylated isoform (P1) (controls equal to 0.3 arbitrary units, was set to 1). Consistent with B, Cx43 at different time points did not significantly change **(D)** Detection of ZO-1 resulted in two bands of around 220 kDa that were analyzed as sum. GAPDH was used as loading control. **(E)** Quantification of ZO-1 protein in SH-SY5Y neuroblastoma cells treated with 10 ng/ml sulfatide for 6, 12 and 24 hours. Controls at different time points did not significantly change (controls equal to 1.1 arbitrary units, was set to 1). In contrast with B and C, Sulfatide decreased ZO-1 protein level after 6,12 and 24 hours (* as compared to controls and 0h Sulfatide condition, $p<0.0001$, n=3). **(F)** Detection of Cx36 resulted in two bands of around 36 kDa that were analyzed as sum. GAPDH was used as loading control. **(G)** Quantification of Cx36 protein in SH-SY5Y neuroblastoma cells treated with 10 ng/ml sulfatide for 6, 12 and 24 hours. Consistent with B and C, sulfatide did not significantly change Cx36 protein level (controls equal to 1 arbitrary unit, was set to 1).

Our results indicate that sulfatide treatment downregulates ZO-1 protein level at all the time points considered.

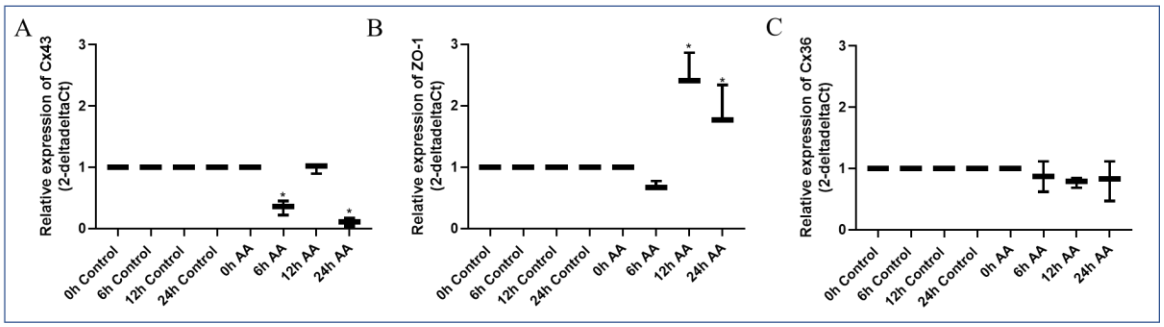

Figure 6.9. Arachidonic acid (AA) downregulates Cx43 but not Cx36 mRNA and upregulates ZO-1 mRNA in SH-SY5Y neuroblastoma cells. Treatment of SH-SY5Y neuroblastoma cells with AA resulted in transient decreased level of Cx43 mRNA. mRNA was isolated from SH-SY5Y neuroblastoma cells and was assessed for Cx43, ZO-1 and Cx36 using RT-PCR. **(A)** Quantification of Cx43 mRNA in SH-SY5Y neuroblastoma cells treated with 100 µM AA for 6, 12 and 24 hours. Controls at different time points did not significantly change (controls equal to 1.7 $2^{-\Delta\Delta Ct}$, was set to 1). Cx43 mRNA decreased transiently at 6 hours (* as compared to controls and 0h AA conditions, $p<0.0001$, n=3) and again at 24 hours (* as compared to controls and 0h AA conditions, $p<0.0001$, n=3), supporting transient downregulation. **(B)** The same conditions used in A were repeated for ZO-1 mRNA level (controls equal to 1.7 $2^{-\Delta\Delta Ct}$, was set to 1). In contrast with A, AA upregulated ZO-1 mRNA at 12 and 24 hours (* as compared to controls and 0h AA conditions, $p<0.0001$, n=3). **(C)** The same conditions used in A and B were repeated for Cx36 mRNA level (controls equal to 1 $2^{-\Delta\Delta Ct}$, was set to 1).

Our results indicate that AA treatment transiently downregulates Cx43 mRNA level at 6 and 24 hours, in contrast to ZO-1 that is upregulated.

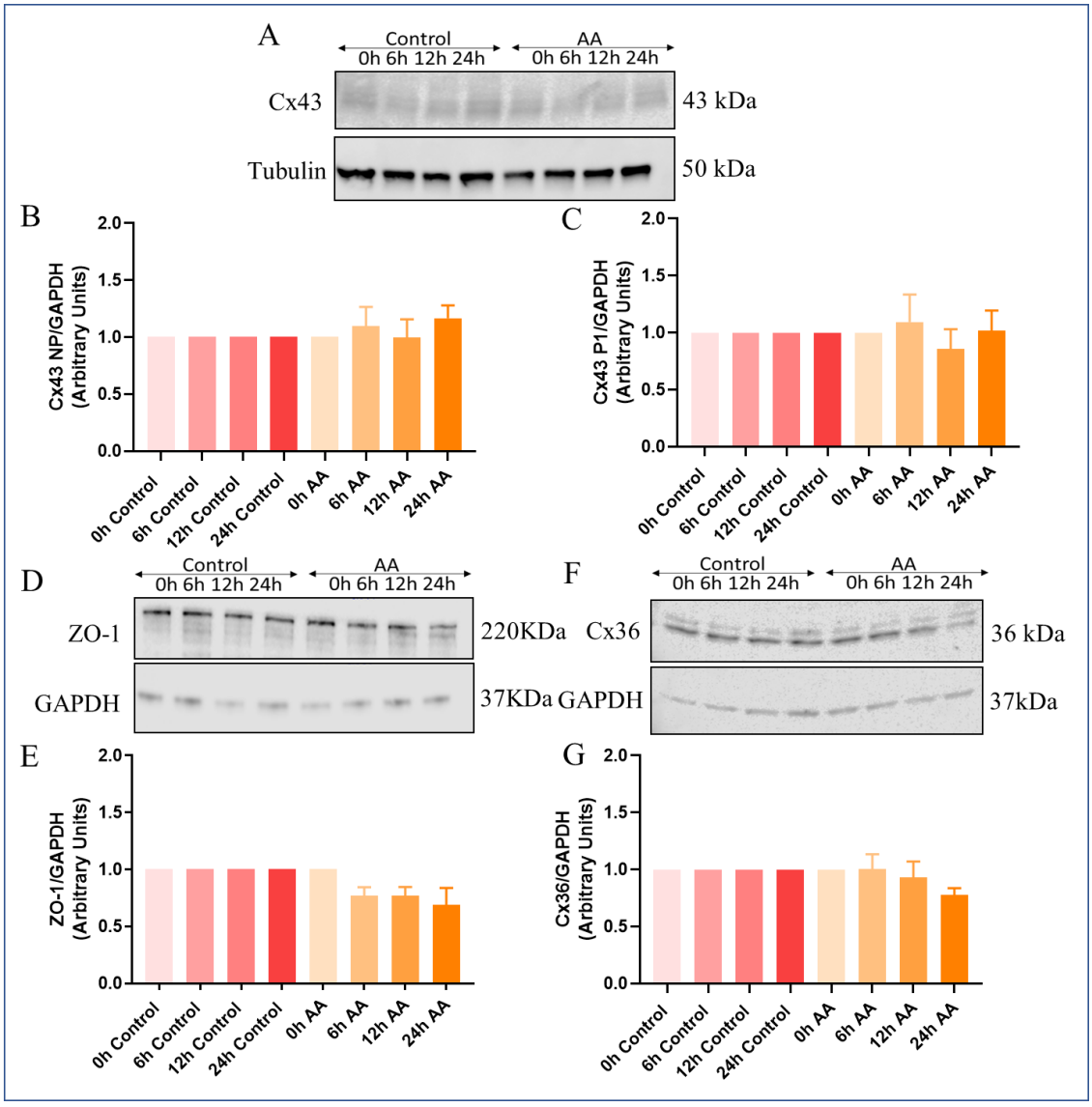

Figure 6.10. Arachidonic acid (AA) does not change Cx43, ZO-1 and Cx36 proteins in SH-SY5Y neuroblastoma cells. Treatment of SH-SY5Y neuroblastoma cells with AA resulted in any changes. Proteins were extracted from SH-SY5Y neuroblastoma cells and were assessed for Cx43, ZO-1 and Cx36 using wester blotting. **(A)** Detection of Cx43 resulted in two bands representing different isoforms of around 43 kDa, according to the literature, Tubulin was used as control loading. **(B)** Quantification of Cx43 non-phosphorylated (NP) isoform in human primary astrocytes treated with 100 µM AA for 6, 12 and 24 hours. AA did not significantly change Cx43 NP (controls equal to 0.4 arbitrary units, was set to 1). **(C)** The same conditions used in B were repeated for Cx43

phosphorylated isoform (P1) (controls equal to 0.3 arbitrary units, was set to 1). Consistent with B, AA did not significantly change Cx43 P1. **(D)** Detection of ZO-1 resulted in two bands of around 220 kDa that were calculated as sum. GAPDH was used as loading control. **(E)** Quantification of ZO-1 protein in SH-SY5Y neuroblastoma cells treated with 100 µM AA for 6, 12 and 24 hours (controls equal to 1.1 arbitrary units, was set to 1). Again, AA did not significantly change ZO-1 expression. **(F)** Detection of Cx36 resulted in two bands of around 36 kDa that were calculated as sum. GAPDH was used as loading control. **(G)** Quantification of Cx36 protein in SH-SY5Y neuroblastoma cells treated with 100 µM AA for 6, 12 and 24 hours. Consistent with Cx43 and ZO-1 results, AA did not significantly change Cx36 expression. (controls equal to 0.8 arbitrary units, was set to 1).

Our results indicate that AA, independently of the time points, does not change cellular communication system in neurons.

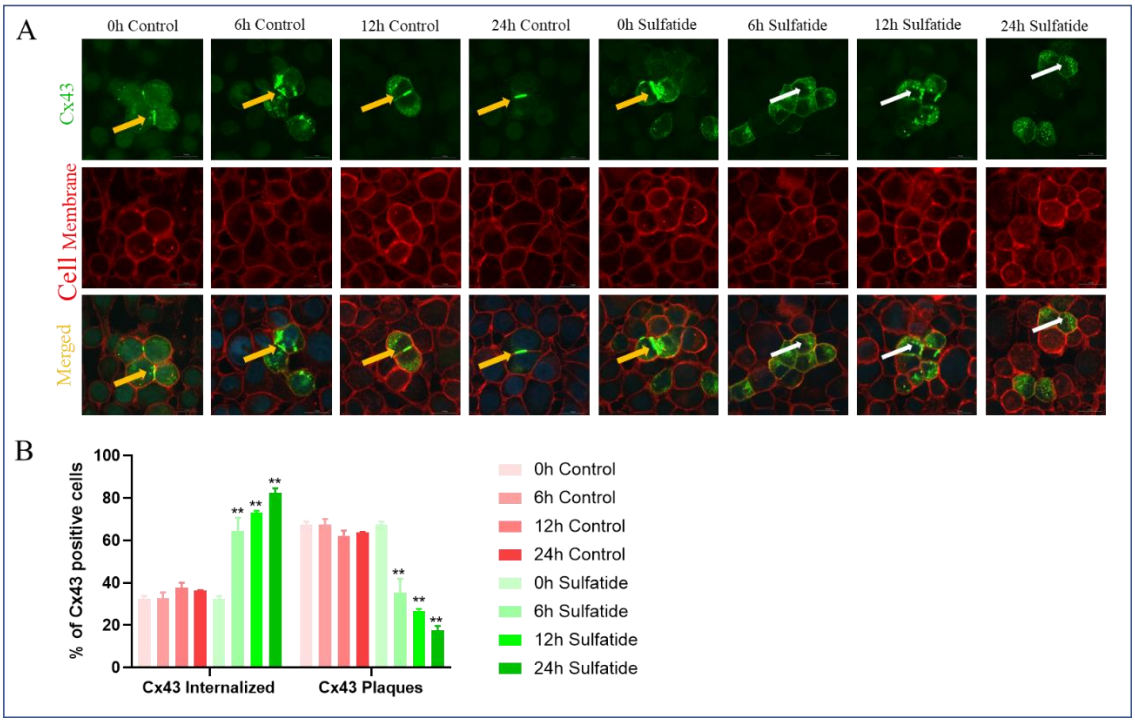

Figure 6.11. Extracellular sulfatide induces internalization of Cx43-CFP in Hela cells. Treatment with sulfatide of Hela cells stably transfected with Cx43-CFP resulted in internalization of Cx43-CFP. **(A)** Representative staining for actin (red) in Hela cells stably transfected with Cx43-CFP (green) for controls and sulfatide groups at 6, 12 and 24 hours (40X). Plaques and internalized vesicles are indicated by yellow and white arrows, respectively. **(B)** Quantification for 5 pictures per condition representing the total number of the pixels was performed considering the percentage of Cx43 positive cells. Cx43 in the control conditions is mostly localized in the plasma membrane creating the plaques (yellow arrows, ** as compared to controls and 0h Sulfatide conditions, $p<0.0001$), instead, in sulfatide conditions Cx43 localized in the cytoplasm (white arrows, ** as compared to controls and 0h Sulfatide conditions, $p<0.0001$).

Our results indicate that sulfatide increases the trafficking of Cx43 in Hela cells stably transfected with Cx43-CFP.

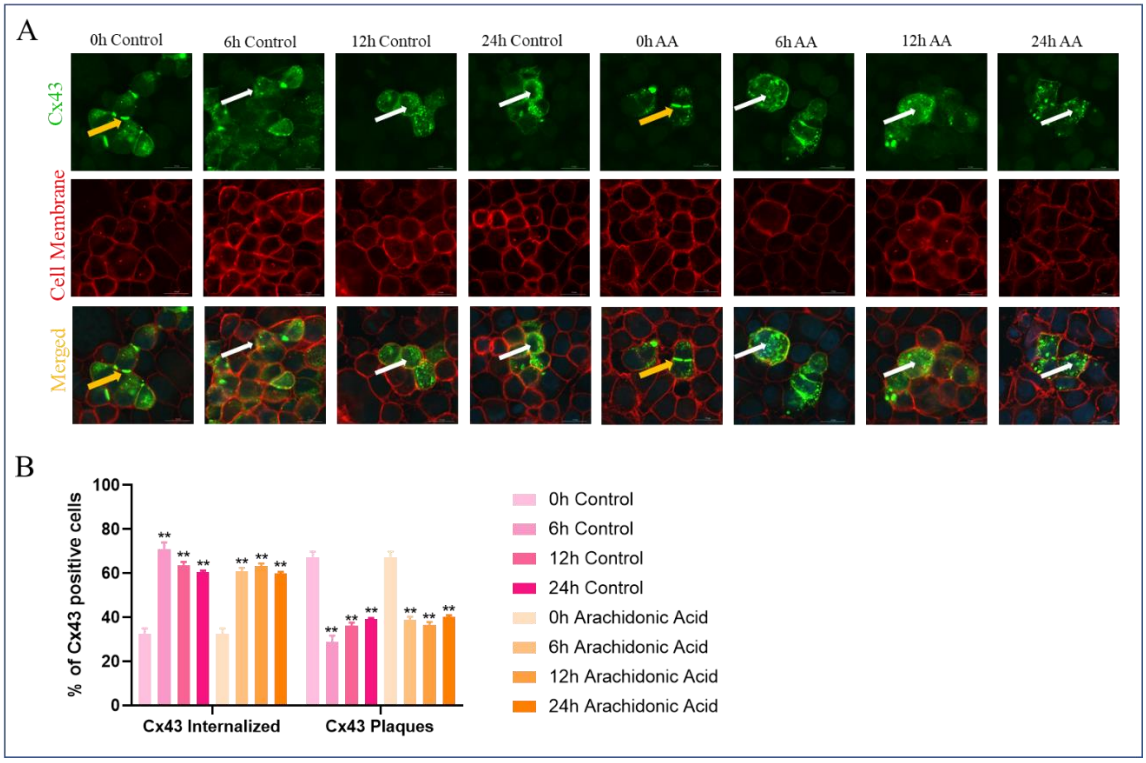

Figure 6.12. Internalization of Cx43-CFP is not observed in AA treated Hela cells versus controls Hela cells. Treatment with AA of Hela cells stably transfected with Cx43-CFP did not affect Cx43-CFP trafficking. **(A)** Representative staining for actin (red) in Hela cells stably transfected with Cx43-CFP (green) for controls and AA groups at 6, 12 and 24 hours (40X). Plaques and internalized vesicles are indicated by yellow and white arrows, respectively. **(B)** Quantification for 5 images per condition representing the total number of the pixels was performed considering the percentage of Cx43 positive cells. Cx43 in control and AA conditions at 6, 12, 24 hours were localized in intracellular vesicles (** as compared to 0h control and 0h AA conditions, $p<0.0001$). The 6, 12 and 24 hours control conditions were treated with the vehicle (Tocrisolve) which may induce the observed changes.

Results suggest that AA does not change Cx43 trafficking in Hela cells stably transfected with Cx43-CFP, Cx43 internalization is due to the soya oil/water solvent used to dissolve AA, and that was used to treat 6, 12 and 24 hours control conditions.

Chapter 7: Characterization of protein-protein interaction between Cx43 and associated binding proteins: a search for Cx43 partners

D'Amico Daniela[1,2]; Prideaux Brendan[1]; Eugenin Eliseo A.[1]

[1]University of Texas Medical Branch (UTMB), Department of Neuroscience, Cell Biology and Anatomy, Galveston, TX, USA

[2]University of Palermo (UniPa), Department of Biomedicine, Neuroscience and Advanced Diagnostics, Palermo, Italy

This work was funded by The National Institute of Mental Health grant, MH096625, the National Institute of Neurological Disorders and Stroke grant, NS105584, and UTMB internal funding (to E.A.E).

Associated paper: D'Amico D., Prideaux B. and Eugenin E.A. "Sulfatide dysregulates Cx43 containing channels: role in neuroHIV". In preparation.

Introduction

Proteomics is defined as a large-scale study for the identification and the quantification of proteomes, which includes a set of proteins synthetized in a specific biological context. Proteomics can expand genomic and transcriptomics data to directly identify the proteins that are up- or down-regulated in specific conditions, and to investigate the related pathways (Aslam et al. 2017).

Previous transcriptomics and proteomics results from our laboratory (data not shown) supported lipid alteration in HIV-infected astrocytes, mostly related to the up-regulation of ceramide related enzymes. In particular, transcriptomic analysis of 7 days HIV-infected astrocytes showed that HIV infection increased levels of glucosylceramidase, galactosyltransferase, and ceramide synthase that are enzymes critically involved in ceramide and sulfatide synthesis. In addition, proteomics data from 21 days HIV-infected astrocytes confirmed glucosylceramidase and galactosyltransferase up-regulation, suggesting sulfatide accumulation. This result correlates with our MSI data presented in Chapter 4 showing higher sulfatide relative abundance in the brain, specifically in the white matter of HIV-infected individuals under cART and without viral replication (see Table 2, Chapter 2).

Since we have proposed sulfatide as a potential biomarker of neurocognitive disorders in HIV-infected individuals virally suppressed with cART and without detectable viral load, our interest was to investigate whether sulfatide altered cell-to-cell communication (see Chapter 6). Moreover, we demonstrated that sulfatide secretion can be regulated by several HIV proteins and it can modulate cell-to-cell communication, especially Cx43 trafficking in Hela cells stably transfected with Cx43-CFP.

Although, we have not yet determined the molecular pathways that connect sulfatide with Cx43, we decided to identify the Cx43 partners in Hela cells stably transfected with Cx43-CFP under sulfatide and AA conditions. Thus, coimmunoprecipitation for Cx43 was performed to identify potential Cx43 binding proteins.

Materials and Methods

Cell Culture Methods

Hela cells stably transfected with Cx43-CFP were grown with high glucose Dulbecco's modified Eagle's medium (DMEM, 11995-065, Thermo Fisher Scientific, Waltham, MA) supplemented with 10% fetal bovine serum (FBS, S12450H, Atlanta Biologicals, Flowery Branch, GA), 2 mM Geneticin (10131-027, Thermo Fisher Scientific, Waltham, MA), penicillin, and streptomycin (15070063, Thermo Fisher Scientific, Waltham, MA) at 37 °C in a humidified atmosphere with 5% CO_2.

Cx43 immunoprecipitation

Immunoprecipitation analysis was performed for Cx43 as described in Figure 7.1. Hela cells stably transfected with Cx43-CFP were treated with sulfatide (10 ng/ml) or with AA (100 μM) for 24 hours. Cells were homogenized with RIPA buffer containing protease and phosphatase inhibitors and sonicated using 5 pulses of 30 seconds on and 30 seconds off in a Microtip (Misonix, Inc, Microson XL-2000). Samples were pre-cleared with protein G plus agarose (sc-2002, Santa Cruz Biotechnology, Dallas, TX) and immunoprecipitated using Cx43 antibody (C6219, Sigma-Aldrich, St. Luis, MO). These samples were sent to Creative Proteomics (Shirley, NY) to be analyzed and quantified on a high-resolution mass spectrometry platform coupled with nanoflow UPLC to select proteins with a fold-change cutoff above 1.5 or below 1/1.5.

Proteomics for proteins associated with Cx43

The beads samples from untreated and sulfatide/AA treated cultures of Hela cells stably transfected with Cx43-CFP were resuspended in 40 μL of 1× electrophoresis sample buffer, boiled for 15 minutes and run on 12% separating gel for 20 minutes at 80 kV and for 30 minutes at 120 kV. The SDS-PAGE gel was stained with Coomassie Brilliant Blue and each gel band was cut to be subjected to protein precipitation using cold acetone and centrifuged at 12000 rpm. Later, 50 mM ammonium bicarbonate was added, and the protein solution was transferred into Microcon devices YM-10 (Millipore). The device was centrifuged at 12000 rpm at 4°C for 10 min. Subsequently, 200 μL of 50 mM ammonium bicarbonate was added to the concentrate followed by centrifugation and repeated once.

After being reduced by 10 mM DL-dithiothreitol at 56°C for 1 hour and alkylated by 20 mM odoacetamide at room temperature in dark for 1hour, the device was centrifuged at 12000 rpm at 4°C for 10 minutes and washed once with 50 mM ammonium bicarbonate. 100 μL of 50 mM ammonium bicarbonate and free trypsin were added into the protein solution at a ratio of 1:50, and the obtained solution was incubated at 37°C overnight. Finally, the device was centrifuged at 12000 rpm at 4°C for 10 minutes. 100 μL of 50 mM ammonium bicarbonate was added into the device and centrifuged, and then repeated once. The extracted peptides were lyophilized to near dryness and resuspended in 2-20 μL of 0.1% formic acid before LC-MS/MS analysis. These samples were analyzed and quantified on Obitrap Q Exactive HF mass spectrometer coupled with Ultimate 3000 nano UHPLC system. The detected peptides were analyzed and searched against human protein database using Maxquant. The parameters were set as follows: the protein modifications were carbamidomethylation (fixed) and oxidation (variable); the enzyme specificity was set to trypsin; the maximum missed cleavages were set to 2; the precursor ion mass tolerance was set to 10 ppm, and MS/MS tolerance was 0.6 Da.

Pathways analysis

Creative Proteomics identified 455 proteins, 263 and 188 were proteins that bind to Cx43 after sulfatide and AA treatments, respectively. These proteins were classified in 13 families (Tables 7 to 15, Figures 7.2 and 7.3) according to their function and to their location described in GeneCards human gene database. Only the up-regulated recycling-transport (Table 7, in green), mitochondrial (Table 8, in green) and membrane (Table 9, in green) related proteins after sulfatide and AA stimulations were run for the Ingenuity Pathway Analysis (IPA) to build molecular networks of each experimental system (Figures 7.4 and 7.5).

Results

Extracellular sulfatide changes the molecular interactions of Cx43. Although, sulfatide can regulate mRNA and protein expression, we used Hela cells stably transfected with Cx43-CFP treated with 10 ng/ml sulfatide for 24 hours to pull-down Cx43 using G PLUS Agarose beads (Figure 7.1). We repeated the same experiment with Hela cells stably

transfected with Cx43-CFP but treated with AA as control condition, where cell-to-cell communication is not upregulated and Cx43 trafficking does not change. Thus, we confirmed the presence of Cx43 into the beads by SDS-page for both treatments (Figure 7.1). These beads were processed and analyzed by Nano LC-MS/MS for proteomics. Proteomics analysis revealed 455 proteins. Comparing the control sample obtained from the coimmunoprecipitation of Cx43 in Hela cells stably transfected with Cx43-CFP and the sulfatide sample obtained from the same cells treated with sulfatide for 24 hours, 263 proteins that bind to Cx43 were highlighted, 95 were upregulated and 168 downregulated. Comparing the control sample with the AA sample, 188 proteins were identified, 139 were up-regulated and 49 down-regulated. We classified the highlighted proteins of each experimental system into 13 families (nuclear, nuclear membrane, mRNA, ribosomal, metabolic, secreted, Golgi apparatus, endoplasmic reticulum, mitochondrial, recycling-transport, ubiquitin, and membrane related proteins, plus unknown proteins) according to their role and physiological compartments provided by GeneCards information and literature data. We show an illustration that integrates all of them in Figures 7.2 and 7.3. Nuclear, membrane nuclear and mRNA related proteins (in the frame of Figures 7.2 and 7.3) were excluded for the following analysis because they do not bind to Cx43, their detection was an experimental artefact due to the mechanical disruption of the nuclear membrane during processing of the samples. Thus, we focused on plasma membrane, mitochondria (Rodriguez-Sinovas et al. 2018) and transport compartments (Thomas et al. 2005), where Cx43 is predominantly located.

Focusing our analysis in the transport proteins that directly or indirectly bind to Cx43, sulfatide upregulated proteins related to myosin such as Myosin Light Chain 1 (MYOFTA, MYO1B, MYO1C) and proteins involved in vesicular fusion and trafficking like the Rabs membrane-bound proteins (RAB2A, RAB1A) and the N-Ethylmaleimide Sensitive Factor (NSF). Parallelly, tubulin (Tubulin Alpha 1c TUBA1C, Tubulin Beta Class I TUBB, Tubulin Beta 4B Class IVb TUBB4B, Tubulin Folding Cofactor A TFCA) and cytoskeletal organized proteins such as Leucine Rich Pentatricopeptide Repeat Containing (LRPPRC) and Dynein Cytoplasmic 1 Heavy Chain 1 (DYNC1H1) were downregulated (Table 7).

On another hand, AA induced upregulation of actin related proteins (ACTα/ACTβ, ARPC4) and membrane adaptors such as Flotillin 1 (FLOT1) and VAMP Associated Protein B and C (VAPBC), and downregulated Bone Marrow Stromal Cell Antigen 2 (BST2), which blocks the release of nascent virions to the membranes of infected cells (Table 7).

After that, we analyzed the mitochondrial proteins. Coimmunoprecipitation of Cx43 after sulfatide treatment highlighted upregulated proteins related to apoptosis (such as Apoptosis Inducing Factor Mitochondria Associated 1 (AIFM1)), to chaperon (such as Heat Shock Protein Family A Member 9 (HSPA9)), and to the mitochondrial transmembrane electron transport (such as Voltage Dependent Anion Channel 1/2 (VDAC1/2)) (Table 8). At the same time, ATP synthesis (ATP Synthase F1 Subunit Alpha ATP5A, ATP Synthase F1 Subunit Beta ATP5B, ATP Synthase Membrane Subunit G ATP5L, ATP Synthase Subunit O ATP5PO, Carbamoyl-Phosphate Synthase 1 CPS1) and fatty acid metabolism (Hydroxyacyl-CoA Dehydrogenase Trifunctional Multienzyme Complex Subunit Alpha HADHA and Hydroxyacyl-CoA Dehydrogenase Trifunctional Multienzyme Complex Subunit Beta HADHB) related proteins were downregulated in the mitochondria, suggesting that several sources of energy can be used by these cells (Table 8). In contrast, when we analyzed the mitochondrial proteins binding to Cx43 after treatment with AA, the ATP synthase enzymes (ATP Synthase F1 Subunit Alpha ATP5A1, ATP Synthase F1 Subunit Gamma ATP5C1) were upregulated with associated TCA (GOT2) and glycolysis (Lactate Dehydrogenase B LDB) enzymes, suggesting a crucial role of the mitochondrial metabolic pathways for AA (Table 8).

Finally, we analyzed the plasma membrane proteins. In this case, we found a significative difference in proteins that interact with Cx43 following sulfatide and AA treatments. Specifically, sulfatide induced upregulation of proteins that regulate the cellular membrane organization and stability such as actin (ACTN1/4), annexin (ANXA1/5) and spectrin (SPTAN1, SPTBN) (Table 9). In addition, sulfatide upregulated Peptidylprolyl Isomerase A (PPIA), which is necessary for the formation of infectious HIV virions and Protein Phosphatase 1 Catalytic Subunit Alpha (PPP1CA) that is involved in HIV viral transcription, suggesting a mechanistic link between Cx43, sulfatide and HIV-infection. Furthermore, the observed upregulation of thioredoxin (TXN), which plays a key role in

the reversible S-nitrosylation of cysteine residues in target proteins, suggests that TXN may S-nitrosylate Cx43 to maintain open Cx43 hemichannels. Cytoskeleton related proteins (Cytoskeleton Associated Protein 4 CKAP4, Ezrin EZR) were observed to be downregulated in sulfatide condition (Table 9).

AA downregulated Scavenger Receptor Class B Member 2 (SCARB2) and the adhesion molecule Metadherin (MTDH) discouraging cellular communication but upregulated several adaptors and actin related proteins that stabilize the plasma membrane (Table 9).

Subsequently, only the up-regulated recycling-transport (Table 7, in green), mitochondrial (Table 8, in green), and membrane (Table 9, in green) related proteins after sulfatide and AA stimulation were run for the Ingenuity Pathway Analysis (IPA) to build molecular networks of each experimental system (Figures 7.4 and 7.5). Ingenuity pathway analysis for sulfatide provided 4 top canonical pathways including integrin-linked kinase signaling, actin cytoskeleton signaling, remodeling of epithelial adherens junctions and EIF2 signaling. They were represented as network overlapping in the Figure 7.4.

The same analysis was repeated for proteomics data coming from the coimmunoprecipitation of Hela cells stably transfected with Cx43-CFP treated with AA and 5 top canonical pathways were identified including cell cycle G2/M DNA damage checkpoint regulator, Myc mediated apoptotic signaling, extracellular regulated kinase 5 (ERK5) signaling, EIF2 signaling, and remodeling of epithelial adherent junctions (Figure 7.5). Only the EIF2 signaling and remodeling of epithelial adherent junctions' pathways were in common between the two experimental systems.

Discussion

Although, sulfatide can enhance Cx43 expression, we decided to pull-down Cx43 in Hela cells stably transfected with Cx43-CFP treated with sulfatide and perform proteomics analysis to investigate proteins that directly or indirectly bind to Cx43 and related pathways. We also used AA as a control because it reduces Cx43 expression and mediates the rapid channel closure (Martinez A. D. and Saez 1999).

Proteomics analysis provided a contained number of proteins that we divided in 13 families. We focused our attention in the recycling-transport, mitochondria and plasma

membrane compartments to find specific correlations between sulfatide and cell-to-cell communication or sulfatide and mitochondrial metabolism.

Analysis for the transport proteins induced by sulfatide and binding to Cx43 revealed an active vesicular transport that was also observed in the AA experimental condition but triggered by different proteins of the same pathways. Analyzing the mitochondrial proteins, we discovered that sulfatide induces the upregulation of Cx43 binding proteins related to fatty acid, glucose, and glutamate/glutamine synthesis. It is noteworthy that these results correlated to the metabolism of the HIV-infected astrocytes investigated in Chapter 3. In addition, within the plasma membrane proteins that interact with Cx43 in the sulfatide treated cells PPIA and PPP1CA were identified. These proteins play a crucial role in the formation of infectious HIV virions and in the viral transcription, supporting our association between viral reservoirs, bystander damage and lipid dysregulation investigated in Chapter 2 and 4. Sulfatide also upregulated TXN, which may induce S-nitrosylation of Cx43 on cysteine 271 to maintain open and functional Cx43 hemichannels (Retamal et al. 2006, Straub et al. 2011). This result may explain the connection between sulfatide secretion, cellular communication and HIV infection. Thus, future experiments will be performed to confirm this hypothesis. Moreover, the ingenuity pathway analysis for sulfatide highlighted pathways involved in cellular morphology, assembly, organization, and movement that further justify sulfatide contribution to cell-to-cell communication. Although, the same proteomics analysis is required to be repeated in human primary astrocytes treated with sulfatide or in HIV-infected astrocytes, this analysis still identifies proteins that are known in the literature to directly or indirectly bind to Cx43. These proteins include actinin (ACTN1, ACTN4) (Sorgen et al. 2018, Wall et al. 2007), debrin (DBN) (Ambrosi et al. 2016, Butkevich et al. 2004), or ezrin (EZR) (Pidoux et al. 2014) and other new potential partners of Cx43. In summary, the work conducted demonstrates that sulfatide plays an important role in cell metabolism and communication and these findings will form the basis for further studies.

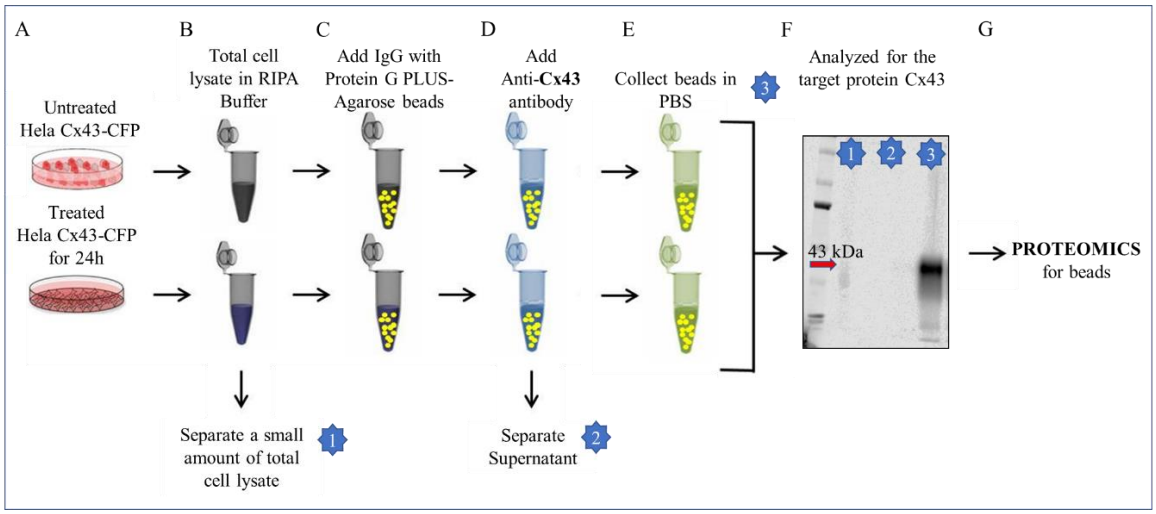

Figure 7.1. Summary of the immunoprecipitation protocol used to pull-down Cx43 for proteomics analysis. **(A)** Hela cells stably transfected with Cx43-CFP were plated and treated with 10 ng/ml sulfatide or with 100 µM AA for 24 hours. **(B)** Untreated and treated cells were scratched with RIPA buffer to obtain the total cell lysates. A small amount of total cell lysate was isolated to be analyzed by SDS-page. **(C**) The total lysates were complemented with IgG and Protein G PLUS-Agarose beads to prevent non-specific binding. **(D)** Antibody against Cx43 was added to pull-down Cx43 and the related binding proteins. **(E)** The beads binding Cx43 and related interacting proteins were collected and dissolved in PBS. **(F)** Total lysate, supernatant and beads were analyzed by SDS-page for Cx43. The band at 43 kDa representing Cx43 was strongly detected in the beads sample (3). **(G)** Beads were analyzed for proteomics.

Cx43 associated proteins involved in Recycling-Transport			
Down-Regulated		Up-Regulated	
Sulfatide	AA	Sulfatide	AA
ACTA 1	AHNAK	B2M	ACTα/ACTβ
ACTB	BST2	CAPZA1	ANXA4
ACTR2B	**CKAP4**	MYH10	ARPC4
ACTR3	**DYNC1H1**	MYL12A	CLTC
ANXA2	FABP5	MYO1B	FLOT1
ANXA4	**GDI2**	MYO1C	HSPB1
ARPC2	NPEPPS	NSF	IghG1
ATP6V1A	RAF1	PPIA	MAP4
CAPZB	SCARB2	RAB1A	MYH9
CKAP4	**TPM4**	RAB2A	RAB7A
CLTC	**TUBA1C**	**S100A11**	RAF
DYNC1H1	**TUBB4B**	SERPINB1	**S100A11**
FLNA	VAT1	TXN	SERPINB6
FLOT1	**YWHAG**	YWHAB	STATHMIN
GDI2	YWHAH	YWHAZ	VAPB
ITGB1			YWHAZ
LRPPRC			YWHAE
MYH9			YWHAQ
PLIN3			
RAB6			
SERPINH1			
SLC3A2			
TBCA			
TPM4			
TFRC			
TUBA1C			
TUBB			
TUBB4B			
VAT1			
YWHAG			
YWHAQ			
YWHAZ			

Table 7. Summary of the recycling-transport related proteins that bind to Cx43 detected after coimmunoprecipitation and subsequent proteomics. List of proteins

involved in the recycling and transport pathways after treatment with sulfatide and AA. Downregulated proteins are shown in red; upregulated proteins are shown in green. The common proteins between sulfatide and AA treatments are marked in bold type.

Cx43 associated proteins involved in Mitochondrial functions			
Down-Regulated		Up-Regulated	
Sulfatide	AA	Sulfatide	AA
ATAD3B	**ATAD3B**	**AIFM1**	**AIFM1**
ATP5PO	**HADHB**	HSPA9	ATP5A1
ATP5A	**TUFM**	**VDAC1**	ATP5C1
ATP5B		VDAC2	DDX5
ATP5L			EIF4A1
CPS1			FH
HADHA			GOT2
HADHB			HMGCL
HMGCL			HSP90
TUFM			LDHB
			MDH2
			PRDX3
			SLC25A5
			VDAC1

Table 8. Summary of the mitochondrial related proteins that bind to Cx43 detected after coimmunoprecipitation and subsequent proteomics. List of proteins involved in the mitochondrial pathways after treatment with sulfatide and AA. Downregulated proteins are shown in red; upregulated proteins are shown in green. The common proteins between sulfatide and AA treatments are marked in bold type.

Cx43 associated proteins involved in Plasma Membrane functions			
Down-Regulated		Up-Regulated	
Sulfatide	AA	Sulfatide	AA
BASP1	AHNAK	ACTN1	ACTA1
CKAP4	MTDH	ACTN4	ACTB
CTTN	NPEPPS	ANXA1	ANXA4
EZR	SCARB2	ANXA5	ATP1A1
IQGAP1	**TLN1**	CFL1	CALM1A
GNB2L1	VAT-1	DBN 1	DBN1
LMNB2		DSG1	DDX5
LMO7		DSP	EZR
MSN		ESYT1	**FLNB**
PHB2		**FLNB**	HSPA1B
SLC3A2		FSCN1	LMO7
STOM		PLEC	MSN
TLN1		PPIA	PLEC
VCL		PPP1CA	PPM1G
		SPTAN1	SLC3A2
		SPTBN 1	SPTAN1
		TXN	SPTBN1
			VAPB
			VCL

Table 9. Summary of the membrane related proteins that bind to Cx43 detected after coimmunoprecipitation and subsequent proteomics. List of proteins involved in the membrane pathways after treatment with sulfatide and AA. Downregulated proteins are shown in red; upregulated proteins are shown in green. The common proteins between sulfatide and AA treatments are marked in bold type.

Cx43 associated proteins involved in Ribosomal functions			
Down-Regulated		Up-Regulated	
Sulfatide	AA	Sulfatide	AA
EEF16	**LARS**	**NACA**	FBL
EEF2	RPS 15		KARS
LARS	**RPS 18**		MARS
NCL	RPS 18A		**NACA**
NPMI	RPS 34		NCL
RPL 13	RPS 5		
RPL 15	RPS 7A		
RPL 18 A	RPS11A		
RPL 26	**RPS7**		
RPL 3			
RPL 34			
RPL 5			
RPS 11			
RPS 13			
RPS 14			
RPS 18			
RPS 19			
RPS 2			
RPS 20			
RPS 23			
RPS 7			
RPS 8			
RPS A			

Table 10. Summary of the ribosomal related proteins that bind to Cx43 detected after coimmunoprecipitation and subsequent proteomics. List of proteins involved in the ribosomal pathways after treatment with sulfatide and AA. Downregulated proteins are shown in red; upregulated proteins are shown in green. The common proteins between sulfatide and AA treatments are marked in bold type.

Cx43 associated proteins induced in Endoplasmic Reticulum			
Down-Regulated		Up-Regulated	
Sulfatide	AA	Sulfatide	AA
CALR	**CCT3**	HS7A9	CCT5
CANX	FKBP4	HSPB1	CCT6A
CCT3	**HSP90 B1**	PDIAG	DDOST
CCT5	HSPA1B	**RPN1**	GANAB
CCT8	SERPINH1	STIP1	HSP90
Ddast			PLIN3
GANAB			PLOD3
HSD90 AB1			POR
HSP90 AA1			PRKCSH
HSP90 B1			**RPNI**
HSPAB			TCP1
HSPD1			
HSPH1			
PRKCSH			
RPN2			
SRP14			

Table 11. Summary of the endoplasmic reticulum related proteins that bind to Cx43 detected after coimmunoprecipitation and subsequent proteomics. List of proteins involved in the endoplasmic reticulum pathways after treatment with sulfatide and AA. Downregulated proteins are shown in red; upregulated proteins are shown in green. The common proteins between sulfatide and AA treatments are marked in bold type.

Cx43 associated proteins induced in Golgi Apparatus			
Down-Regulated		Up-Regulated	
Sulfatide	AA	Sulfatide	AA
	CCT3		CCT5
	FKBP4		CCT6A
	HSP90 B1		PLIN3
	HSPA1B		TCP1

Table 12. Summary of the Golgi apparatus related proteins that bind to Cx43 detected after coimmunoprecipitation and subsequent proteomics. List of proteins involved in the Golgi apparatus pathways after treatment with sulfatide and AA. Downregulated proteins are shown in red; upregulated proteins are shown in green. The common proteins between sulfatide and AA treatments are marked in bold type.

Cx43 associated proteins induced in Secretion System			
Down-Regulated		Up-Regulated	
Sulfatide	AA	Sulfatide	AA
EXOSC4			GRN
PGK1			

Table 13. Summary of the secreted proteins that bind to Cx43 detected after coimmunoprecipitation and subsequent proteomics. List of proteins involved in the pathways of secretion after treatment with sulfatide and AA. Downregulated proteins are shown in red; upregulated proteins are shown in green. The common proteins between sulfatide and AA treatments are marked in bold type.

Cx43 associated proteins induced in Metabolism			
Down-Regulated		Up-Regulated	
Sulfatide	AA	Sulfatide	AA
ALPI		ACLY	AKR1B1
APOA1		AHCY	APOA1
CAD		BSG	APRT
ENO1		GAPDH	CAD
ESYT2		**MAT2A**	CBR1
Fasn		PGAM2	ENO1
GARTS		PGM1	FASN
GOT2		PPP1CA	FH
GPT		SLC25A13	GOT2
IDH1			**MAT2A**
IMPDH2			MDH2
LDHA			
LDHB			
MTHFD1			
PAICS			
PGK1			
PHGDH			
PKM			
UGDH			

Table 14. Summary of the metabolic related proteins that bind to Cx43 detected after coimmunoprecipitation and subsequent proteomics. List of proteins involved in the metabolic pathways after treatment with sulfatide and AA. Downregulated proteins are shown in red; upregulated proteins are shown in green. The common proteins between sulfatide and AA treatments are marked in bold type.

Cx43 associated proteins involved in Ubiquitin-related system			
Down-Regulated		Up-Regulated	
Sulfatide	AA	Sulfatide	AA
UBE2N	**UBE2N**	PSMA1	PSMA4
PSMBG		**PSMA5**	PSMB1
		PSMA6	**PSMB5**
		PSMD2	PSMD3
		RPL11	RDL3
		RPL13A	RDL4
		RPL14	RDLP2
		RPL23	**RPL13A**
		RPL31	**RPL14**
		RPL4	RPL22
		RPL7	**RPL7**
		RPL8	RPL9
		RPS10	RPNI
		RPS12	RPS14
		RPS16	**RPS16**
		RPS25	RPS2
		UBA-1	RPS23
			RPS3
			RPS8

Table 15. Summary of the ubiquitin related proteins that bind to Cx43 detected after coimmunoprecipitation and subsequent proteomics. List of proteins involved in the ubiquitin related pathways after treatment with sulfatide and AA. Downregulated proteins are shown in red; upregulated proteins are shown in green. The common proteins between sulfatide and AA treatments are marked in bold type.

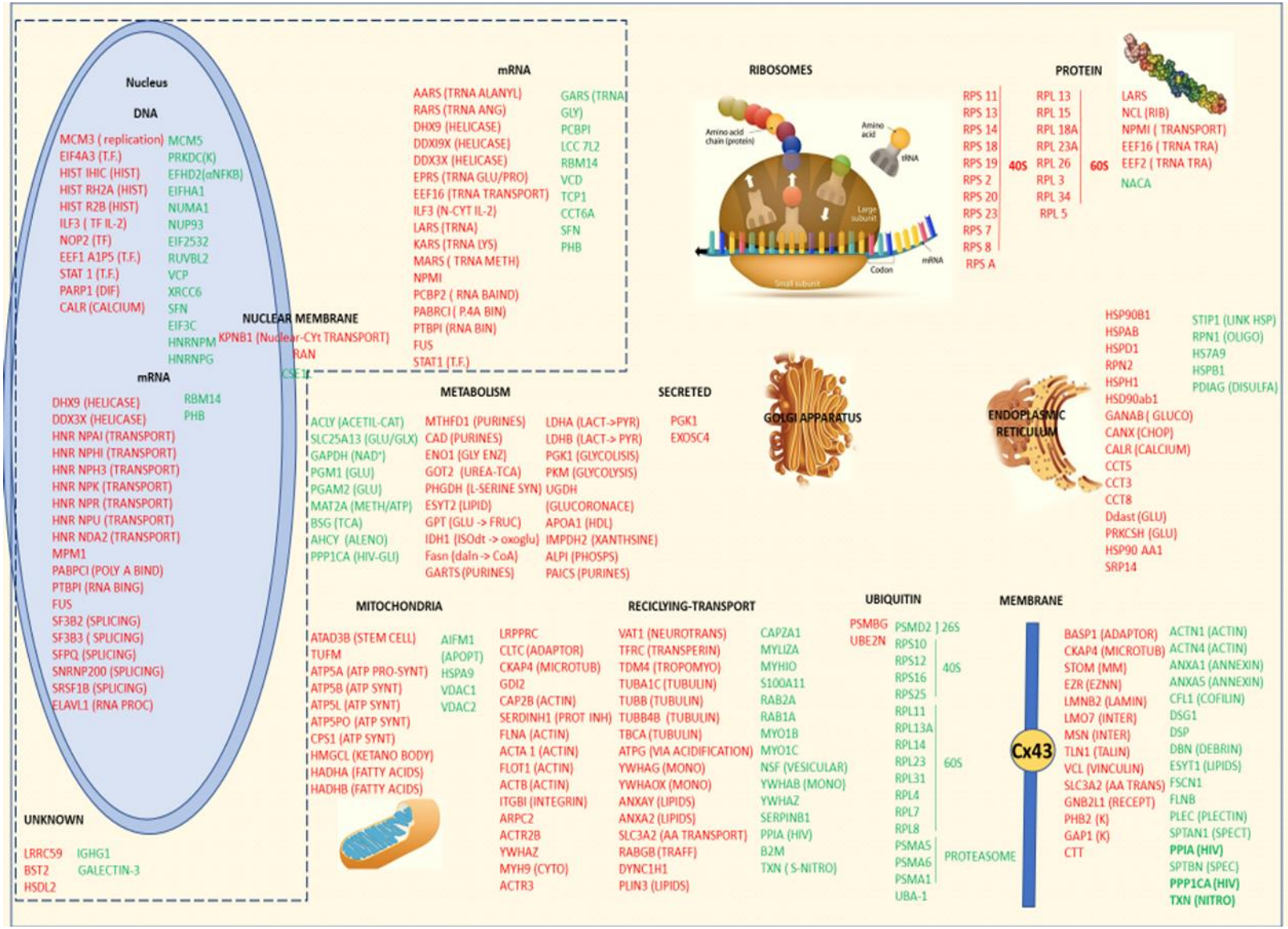
Nucleus
DNA
MCM3 (replication)
EIF4A3 (T.F.)
HIST IHIC (HIST)
HIST RH2A (HIST)
HIST R2B (HIST)
ILF3 (TF IL-2)
NOP2 (TF)
EEF1 A1P5 (T.F.)
STAT 1 (T.F.)
PARP1 (DIF)
CALR (CALCIUM)
MCM5
PRKDC(K)
EFHD2(αNFKB)
EIFHA1
NUMA1
NUP93
EIF2532
RUVBL2
VCP
XRCC6
SFN
EIF3C
HNRNPM
HNRNPG
mRNA
DHX9 (HELICASE)
DDX3X (HELICASE)
HNR NPAI (TRANSPORT)
HNR NPHI (TRANSPORT)
HNR NPH3 (TRANSPORT)
HNR NPK (TRANSPORT)
HNR NPR (TRANSPORT)
HNR NPU (TRANSPORT)
HNR NDA2 (TRANSPORT)
MPM1
PABPCI (POLY A BIND)
PTBPI (RNA BING)
FUS
SF3B2 (SPLICING)
SF3B3 (SPLICING)
SFPQ (SPLICING)
SNRNP200 (SPLICING)
SRSF1B (SPLICING)
ELAVL1 (RNA PROC)
RBM14
PHB
NUCLEAR MEMBRANE
KPNB1 (Nuclear-CYt TRANSPORT)
RAN
CSE1L
UNKNOWN
LRRC59
BST2
HSDL2
IGHG1
GALECTIN-3
mRNA
AARS (TRNA ALANYL)
RARS (TRNA ANG)
DHX9 (HELICASE)
DDXI9X (HELICASE)
DDX3X (HELICASE)
EPRS (TRNA GLU/PRO)
EEF16 (TRNA TRANSPORT)
ILF3 (N-CYT IL-2)
LARS (TRNA)
KARS (TRNA LYS)
MARS (TRNA METH)
NPMI
PCBP2 (RNA BAIND)
PABRCI (P.4A BIN)
PTBPI (RNA BIN)
FUS
STAT1 (T.F.)
GARS (TRNA GLY)
PCBPI
LCC 7L2
RBM14
VCD
TCP1
CCT6A
SFN
PHB
RIBOSOMES
Amino acid chain (protein)
Amino acid
tRNA
Large subunit
mRNA
Codon
Small subunit
RPS 11
RPS 13
RPS 14
RPS 18
RPS 19
RPS 2
RPS 20
RPS 23
RPS 7
RPS 8
RPS A
40S
RPL 13
RPL 15
RPL 18A
RPL 23A
RPL 26
RPL 3
RPL 34
RPL 5
60S
PROTEIN
LARS
NCL (RIB)
NPMI (TRANSPORT)
EEF16 (TRNA TRA)
EEF2 (TRNA TRA)
NACA
METABOLISM
ACLY (ACETIL-CAT)
SLC25A13 (GLU/GLX)
GAPDH (NAD+)
PGM1 (GLU)
PGAM2 (GLU)
MAT2A (METH/ATP)
BSG (TCA)
AHCY (ALENO)
PPP1CA (HIV-GLI)
MTHFD1 (PURINES)
CAD (PURINES)
ENO1 (GLY ENZ)
GOT2 (UREA-TCA)
PHGDH (L-SERINE SYN)
ESYT2 (LIPID)
GPT (GLU -> FRUC)
IDH1 (ISOdt -> oxoglu)
Fasn (daln -> CoA)
GARTS (PURINES)
LDHA (LACT->PYR)
LDHB (LACT-> PYR)
PGK1 (GLYCOLISIS)
PKM (GLYCOLYSIS)
UGDH (GLUCORONACE)
APOA1 (HDL)
IMPDH2 (XANTHSINE)
ALPI (PHOSPS)
PAICS (PURINES)
SECRETED
PGK1
EXOSC4
GOLGI APPARATUS
ENDOPLASMIC RETICULUM
HSP90B1
HSPAB
HSPD1
RPN2
HSPH1
HSD90ab1
GANAB (GLUCO)
CANX (CHOP)
CALR (CALCIUM)
CCT5
CCT3
CCT8
Ddast (GLU)
PRKCSH (GLU)
HSP90 AA1
SRP14
STIP1 (LINK HSP)
RPN1 (OLIGO)
HS7A9
HSPB1
PDIAG (DISULFA)
MITOCHONDRIA
ATAD3B (STEM CELL)
TUFM
ATP5A (ATP PRO-SYNT)
ATP5B (ATP SYNT)
ATP5L (ATP SYNT)
ATP5PO (ATP SYNT)
CPS1 (ATP SYNT)
HMGCL (KETANO BODY)
HADHA (FATTY ACIDS)
HADHB (FATTY ACIDS)
AIFM1 (APOPT)
HSPA9
VDAC1
VDAC2
RECICLYING-TRANSPORT
LRPPRC
CLTC (ADAPTOR)
CKAP4 (MICROTUB)
GDI2
CAP2B (ACTIN)
SERDINH1 (PROT INH)
FLNA (ACTIN)
ACTA 1 (ACTIN)
FLOT1 (ACTIN)
ACTB (ACTIN)
ITGBI (INTEGRIN)
ARPC2
ACTR2B
YWHAZ
MYH9 (CYTO)
ACTR3
VAT1 (NEUROTRANS)
TFRC (TRANSPERIN)
TDM4 (TROPOMYO)
TUBA1C (TUBULIN)
TUBB (TUBULIN)
TUBB4B (TUBULIN)
TBCA (TUBULIN)
ATPG (VIA ACIDIFICATION)
YWHAG (MONO)
YWHAOX (MONO)
ANXAY (LIPIDS)
ANXA2 (LIPIDS)
SLC3A2 (AA TRANSPORT)
RABGB (TRAFF)
DYNC1H1
PLIN3 (LIPIDS)
CAPZA1
MYLIZA
MYHIO
S100A11
RAB2A
RAB1A
MYO1B
MYO1C
NSF (VESICULAR)
YWHAB (MONO)
YWHAZ
SERPINB1
PPIA (HIV)
B2M
TXN (S-NITRO)
UBIQUITIN
PSMBG
UBE2N
PSMD2
RPS10
RPS12
RPS16
RPS25
RPL11
RPL13A
RPL14
RPL23
RPL31
RPL4
RPL7
RPL8
PSMA5
PSMA6
PSMA1
UBA-1
26S
40S
60S
PROTEASOME
MEMBRANE
Cx43
BASP1 (ADAPTOR)
CKAP4 (MICROTUB)
STOM (MM)
EZR (EZNN)
LMNB2 (LAMIN)
LMO7 (INTER)
MSN (INTER)
TLN1 (TALIN)
VCL (VINCULIN)
SLC3A2 (AA TRANS)
GNB2L1 (RECEPT)
PHB2 (K)
GAP1 (K)
CTT
ACTN1 (ACTIN)
ACTN4 (ACTIN)
ANXA1 (ANNEXIN)
ANXA5 (ANNEXIN)
CFL1 (COFILIN)
DSG1
DSP
DBN (DEBRIN)
ESYT1 (LIPIDS)
FSCN1
FLNB
PLEC (PLECTIN)
SPTAN1 (SPECT)
PPIA (HIV)
SPTBN (SPEC)
PPP1CA (HIV)
TXN (NITRO)

Figure 7.2. Schematic representation of all the Cx43 binding proteins detected after sulfatide treatment, coimmunoprecipitation and subsequent proteomics. Proteins binding to Cx43 were immunoprecipitated from Hela stably transfected Cx43-CFP cells treated with sulfatide for 24 hours. Proteins were classified in 13 families (nuclear, nuclear membrane, mRNA, ribosomal, metabolic, secreted, Golgi apparatus, endoplasmic reticulum, mitochondrial, recycling-transport, ubiquitin, and membrane related proteins, plus unknown proteins), according to their functional role and to their location described in GeneCards human gene database and literature data. Nuclear, membrane nuclear and mRNA related proteins (in the frame) were excluded because they do not physiologically bind to Cx43. Their detection was due to the mechanical disruption of the nuclear membrane during the procced of the samples. Downregulated proteins are indicated in red, upregulated in green.

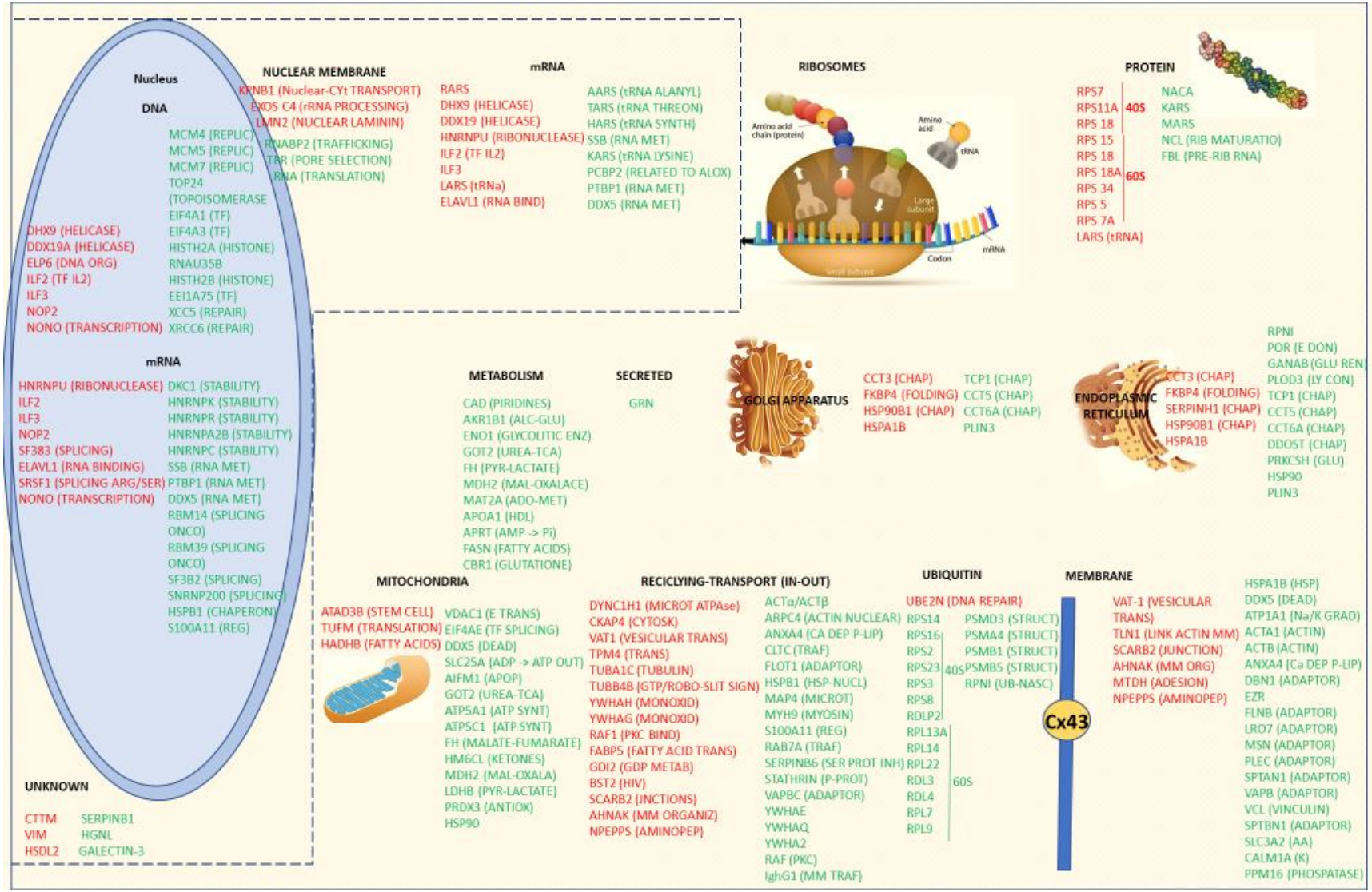
Nucleus
DNA
MCM4 (REPLIC)
MCM5 (REPLIC)
MCM7 (REPLIC)
TOP24 (TOPOISOMERASE
EIF4A1 (TF)
EIF4A3 (TF)
HIST1H2A (HISTONE)
RNAU35B
HIST2B (HISTONE)
EEI1A75 (TF)
XCC5 (REPAIR)
XRCC6 (REPAIR)
DHX9 (HELICASE)
DDX19A (HELICASE)
ELP6 (DNA ORG)
ILF2 (TF IL2)
ILF3
NOP2
NONO (TRANSCRIPTION)
mRNA
HNRNPU (RIBONUCLEASE)
ILF2
ILF3
NOP2
SF3B3 (SPLICING)
ELAVL1 (RNA BINDING)
SRSF1 (SPLICING ARG/SER)
NONO (TRANSCRIPTION)
DKC1 (STABILITY)
HNRNPK (STABILITY)
HNRNPR (STABILITY)
HNRNPA2B (STABILITY)
HNRNPC (STABILITY)
SSB (RNA MET)
PTBP1 (RNA MET)
DDX5 (RNA MET)
RBM14 (SPLICING ONCO)
RBM39 (SPLICING ONCO)
SF3B2 (SPLICING)
SNRNP200 (SPLICING)
HSPB1 (CHAPERON)
S100A11 (REG)
UNKNOWN
CTTM
VIM
HSDL2
SERPINB1
HGNL
GALECTIN-3
NUCLEAR MEMBRANE
KPNB1 (Nuclear-CYt TRANSPORT)
EXOS C4 (rRNA PROCESSING)
LMN2 (NUCLEAR LAMININ)
RNABP2 (TRAFFICKING)
TPR (PORE SELECTION)
RNA (TRANSLATION)
mRNA
RARS
DHX9 (HELICASE)
DDX19 (HELICASE)
HNRNPU (RIBONUCLEASE)
ILF2 (TF IL2)
ILF3
LARS (tRNa)
ELAVL1 (RNA BIND)
AARS (tRNA ALANYL)
TARS (tRNA THREON)
HARS (tRNA SYNTH)
SSB (RNA MET)
KARS (tRNA LYSINE)
PCBP2 (RELATED TO ALOX)
PTBP1 (RNA MET)
DDX5 (RNA MET)
RIBOSOMES
Amino acid chain (protein)
Amino acid
tRNA
Large subunit
Codon
mRNA
Small subunit
PROTEIN
RPS7
RPS11A
RPS 18
RPS 15
RPS 18
RPS 18A
RPS 34
RPS 5
RPS 7A
LARS (tRNA)
40S
60S
NACA
KARS
MARS
NCL (RIB MATURATIO)
FBL (PRE-RIB RNA)
METABOLISM
CAD (PIRIDINES)
AKR1B1 (ALC-GLU)
ENO1 (GLYCOLITIC ENZ)
GOT2 (UREA-TCA)
FH (PYR-LACTATE)
MDH2 (MAL-OXALACE)
MAT2A (ADO-MET)
APOA1 (HDL)
APRT (AMP -> Pi)
FASN (FATTY ACIDS)
CBR1 (GLUTATIONE)
SECRETED
GRN
GOLGI APPARATUS
CCT3 (CHAP)
FKBP4 (FOLDING)
HSP90B1 (CHAP)
HSPA1B
TCP1 (CHAP)
CCT5 (CHAP)
CCT6A (CHAP)
PLIN3
ENDOPLASMIC RETICULUM
CCT3 (CHAP)
FKBP4 (FOLDING)
SERPINH1 (CHAP)
HSP90B1 (CHAP)
HSPA1B
RPNI
POR (E DON)
GANAB (GLU REN)
PLOD3 (LY CON)
TCP1 (CHAP)
CCT5 (CHAP)
CCT6A (CHAP)
DDOST (CHAP)
PRKCSH (GLU)
HSP90
PLIN3
MITOCHONDRIA
ATAD3B (STEM CELL)
TUFM (TRANSLATION)
HADHB (FATTY ACIDS)
VDAC1 (E TRANS)
EIF4AE (TF SPLICING)
DDX5 (DEAD)
SLC25A (ADP -> ATP OUT)
AIFM1 (APOP)
GOT2 (UREA-TCA)
ATP5A1 (ATP SYNT)
ATP5C1 (ATP SYNT)
FH (MALATE-FUMARATE)
HM6CL (KETONES)
MDH2 (MAL-OXALA)
LDHB (PYR-LACTATE)
PRDX3 (ANTIOX)
HSP90
RECICLYING-TRANSPORT (IN-OUT)
DYNC1H1 (MICROT ATPAse)
CKAP4 (CYTOSK)
VAT1 (VESICULAR TRANS)
TPM4 (TRANS)
TUBA1C (TUBULIN)
TUBB4B (GTP/ROBO-SLIT SIGN)
YWHAH (MONOXID)
YWHAG (MONOXID)
RAF1 (PKC BIND)
FABP5 (FATTY ACID TRANS)
GDI2 (GDP METAB)
BST2 (HIV)
SCARB2 (INCTIONS)
AHNAK (MM ORGANIZ)
NPEPPS (AMINOPEP)
ACTα/ACTβ
ARPC4 (ACTIN NUCLEAR)
ANXA4 (CA DEP P-LIP)
CLTC (TRAF)
FLOT1 (ADAPTOR)
HSPB1 (HSP-NUCL)
MAP4 (MICROT)
MYH9 (MYOSIN)
S100A11 (REG)
RAB7A (TRAF)
SERPINB6 (SER PROT INH)
STATHRIN (P-PROT)
VAPBC (ADAPTOR)
YWHAE
YWHAQ
YWHA2
RAF (PKC)
IghG1 (MM TRAF)
UBIQUITIN
UBE2N (DNA REPAIR)
RPS14
RPS16
RPS2
RPS23
RPS3
RPS8
RDLP2
RPL13A
RPL14
RPL22
RDL3
RDL4
RPL7
RPL9
40S
60S
PSMD3 (STRUCT)
PSMA4 (STRUCT)
PSMB1 (STRUCT)
PSMB5 (STRUCT)
RPNI (UB-NASC)
MEMBRANE
Cx43
VAT-1 (VESICULAR TRANS)
TLN1 (LINK ACTIN MM)
SCARB2 (JUNCTION)
AHNAK (MM ORG)
MTDH (ADESION)
NPEPPS (AMINOPEP)
HSPA1B (HSP)
DDX5 (DEAD)
ATP1A1 (Na/K GRAD)
ACTA1 (ACTIN)
ACTB (ACTIN)
ANXA4 (Ca DEP P-LIP)
DBN1 (ADAPTOR)
EZR
FLNB (ADAPTOR)
LRO7 (ADAPTOR)
MSN (ADAPTOR)
PLEC (ADAPTOR)
SPTAN1 (ADAPTOR)
VAPB (ADAPTOR)
VCL (VINCULIN)
SPTBN1 (ADAPTOR)
SLC3A2 (AA)
CALM1A (K)
PPM16 (PHOSPATASE)

Figure 7.3. Schematic representation of all the Cx43 binding proteins detected after AA treatment, coimmunoprecipitation and subsequent proteomics. Proteins binding to Cx43 were immunoprecipitated from Hela stably transfected Cx43-CFP cells treated with AA for 24 hours. Proteins were classified in 13 families (nuclear, nuclear membrane, mRNA, ribosomal, metabolic, secreted, Golgi apparatus, endoplasmic reticulum, mitochondrial, recycling-transport, ubiquitin, and membrane related proteins, plus unknown proteins), according to their functional role and to their location described in GeneCards human gene database and literature data. Nuclear, membrane nuclear and mRNA related proteins (in the frame) were excluded because they do not physiologically bind to Cx43. Their detection was due to the mechanical disruption of the nuclear membrane during the procced of the samples. Downregulated proteins are indicated in red, upregulated in green.

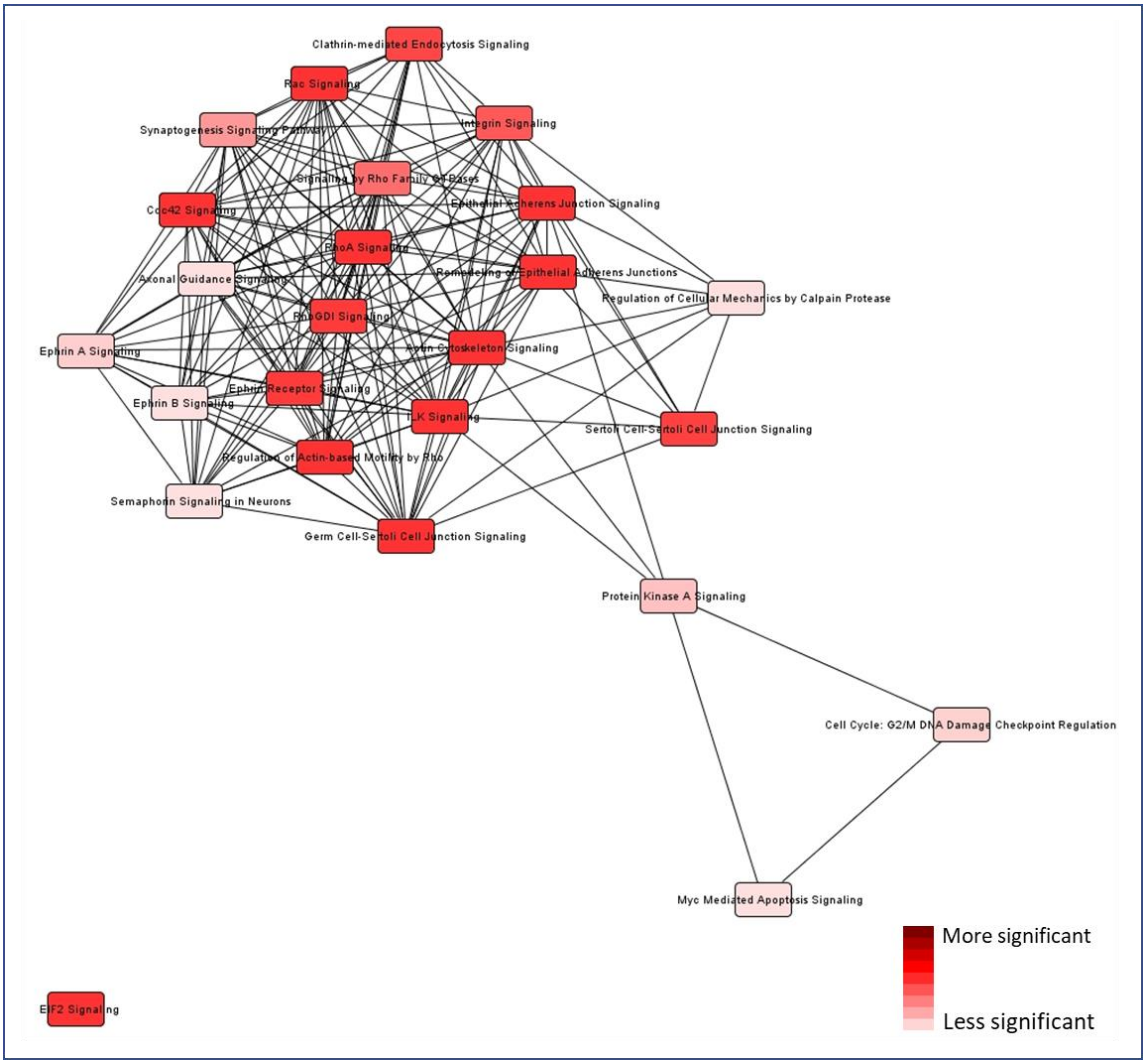

Figure 7.4. Network overlapping of the canonical pathways triggered by the up-regulated recycling-transport, mitochondrial and membrane related proteins after sulfatide treatment. Proteins binding to Cx43 were immunoprecipitated from Hela stably transfected Cx43-CFP cells treated with sulfatide for 24 hours and analyzed by proteomics. The up-regulated proteins related to the recycling-transport, the mitochondrial and the membrane pathways were selected to build a specific molecular network using the Ingenuity Pathway Analysis software. The network overlapping showed the canonical pathways identified in our experimental system. Each pathway was indicated as a single "node" colored proportionally to the Fisher's Exact Test p-value, where brighter red meant more significant. A line connected two pathways when at least one data set molecule was common between them.

Results suggest that the top canonical pathways include integrin-linked kinase (ILK) signaling, actin cytoskeleton signaling, remodeling of epithelial adherens junctions and EIF2 signaling. These pathways are involved in cellular morphology, assembly, organization, and movement.

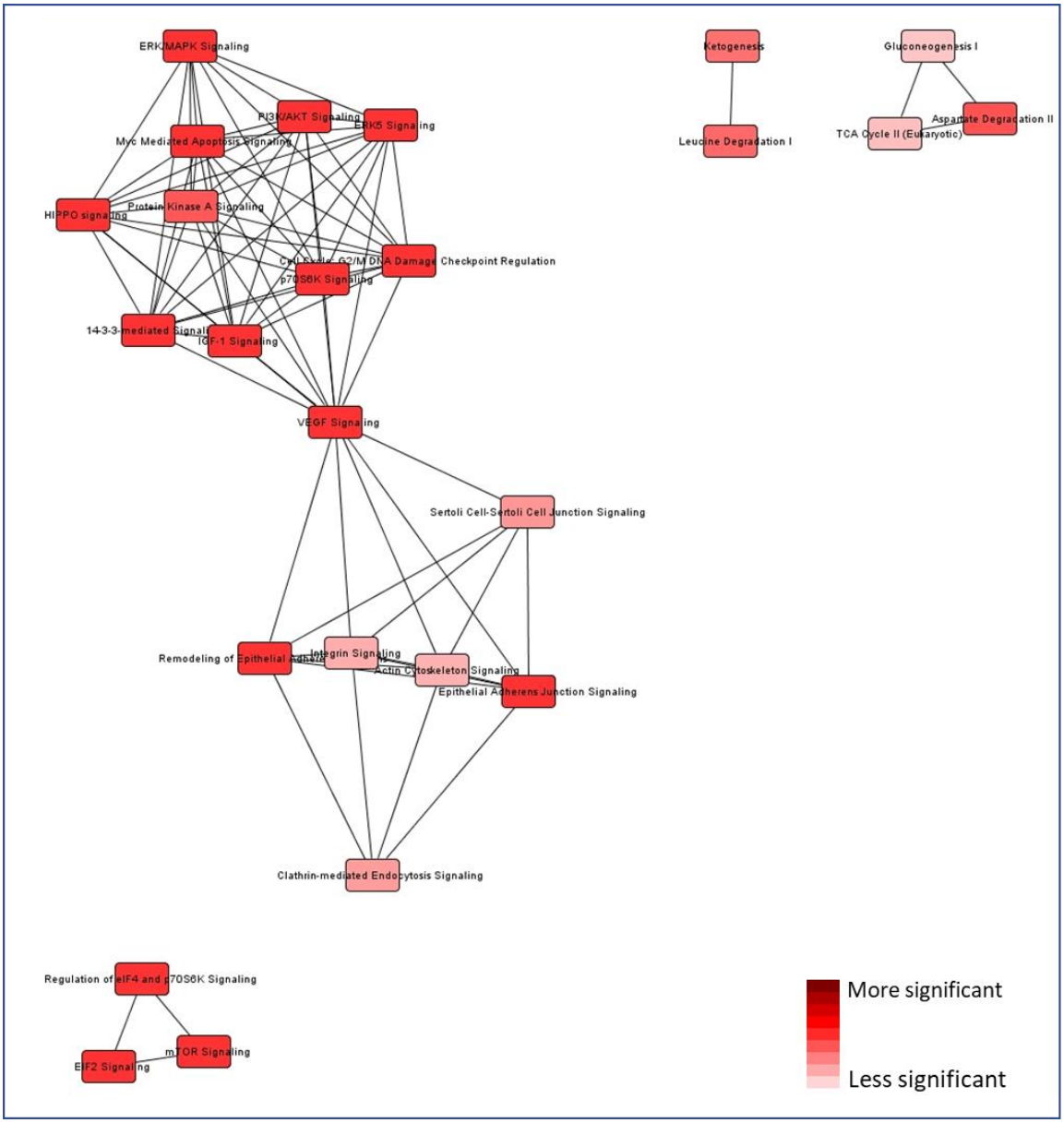

Figure 7.5. Network overlapping of the canonical pathways triggered by the up-regulated recycling-transport, the mitochondrial and the membrane related proteins after AA treatment. Proteins binding to Cx43 were immunoprecipitated from Hela stably transfected Cx43-CFP cells treated with AA for 24 hours and analyzed by proteomics. The up-regulated proteins related to the recycling-transport, the mitochondrial and the membrane pathways were selected to build a specific molecular network using the Ingenuity Pathway Analysis software. The network of overlapping showed the canonical pathways identified in our experimental system. Each pathway was indicated as a single "node" colored proportionally to the Fisher's Exact Test p-value, where brighter red meant

more significant. A line connected two pathways when at least one data set molecule was common between them.

Results suggest that the top canonical pathways are: EIF2 signaling, cell cycle G2/M DNA damage checkpoint regulator, Myc mediated apoptotic signaling, remodeling of epithelial adherent junctions, ERK5 signaling. These pathways are involved in protein synthesis, RNA damage and repair, cellular assembly and organization, protein trafficking, and cell death and survival.

Chapter 8: General discussion and future directions

HIV infection is a major public health concern, affecting around 40 million people in the world (https://www.who.int/news-room/fact-sheets/detail/hiv-aids). Current drugs to treat HIV-infected people are not a cure even they induce immune reconstitution (Perelson et al. 1997). Although, most HIV-infected patients under cART show a normal CD4 count, a low to undetectable viral load and an increased life-expectancy, they develop symptoms of accelerated aging including HIV-associated neurocognitive disorders (HAND) (Saylor et al. 2016). Neurological disorders affect more that the half of HIV-infected individuals and the mechanisms by which HIV induces HAND in the current cART era is unknown.
HIV persists due to the presence of viral reservoirs in different anatomical compartments (Svicher et al. 2014). Moreover, upon cART interruption, the virus rebounds from all the anatomical compartments in which viral reservoirs are resident (De Scheerder et al. 2019).

Currently, there is not a reliable method to detect viral reservoirs, as well as it is unknown in which cells HIV genome is integrated and the size of these cells. In addition, it is unclear the mechanism related to neuroHIV. Thus, this thesis tried to address these two major problems.

As we describe in the general introduction, there are not reliable methods to detect viral reservoirs in the tissues. In this thesis, we outlined a microscopy strategy that can be used for the reliable identification, localization, and quantification of viral reservoirs in the tissues and blood of HIV-infected individuals. This methodology is based on a multi probe and antigen detection system using a DNA probe targeting the HIV-Nef sequence, an mRNA probe targeting HIV Nef mRNA, and detecting HIV proteins and cellular markers using the traditional antibody-based technology. For this analysis, we used human brain tissues provided by NNTC collected from uninfected and HIV-infected patients after 2 hours of death to avoid molecular and tissue disruption. Infected patients were under cART for long time showing normal CD4 count and low to undetectable viral load (see Table 2, Chapter 2). Lymph nodes from the same patients were used as a control for the presence of the viral reservoirs. Through our strategy, we confirmed that the brain is an anatomical compartment for viral reservoirs (Balcom et al. 2019) and that a small population microglia/macrophages and a smaller population of astrocytes are the major reservoirs within the brain (Clayton et al. 2017, Li G. H. et al. 2016) in the current cART era. Nevertheless, not all microglia/macrophages and astrocytes were infected with HIV,

suggesting that an unknown mechanism of selection is used for specific niches within the brain that have a higher susceptibility to HIV infection. Moreover, literature data of the pre-cART era indicated that the percentage of macrophages and astrocytes with HIV-integrated DNA is higher compared to our analysis (Castellano et al. 2017, Churchill et al. 2009). Through our system, we identified that around 0.014% and 0.0035% cells in human brain tissue sections of HIV-infected individuals, showing HIV-integrated DNA, were macrophages/microglia and astrocytes, respectively. As expected, not all of these cells expressed HIV mRNA and few of them synthetized viral proteins. Despite effective cART, we demonstrated that HIV replication persists in particular areas of the brain. Interestingly, the low numbers of viral reservoirs into the brain cannot explain the damage detected in HIV-infected patients. But we demonstrated that viral reservoirs can synthetize HIV proteins that can diffuse or be secreted and be taken up by neighboring uninfected cells. This is the first scientific data demonstrating a local synthesis of viral proteins in the brain of HIV-infected individuals under cART. Several laboratories using animal models such as humanized mouse models and non-human primates (Hanna et al. 1998, Hansen et al. 2009, Nesbit and Schwartz 2002, Yamada et al. 2015) have shown a consistent synthesis of HIV proteins that is not representative of what we observed in human brain tissues, where HIV proteins synthesis is not systemic but localized. Nevertheless, the basal synthesis of HIV proteins can validate the theory of HIV protein neurotoxicity that has discussed for many years and that implicates HIV proteins in the progression of neuroHIV (Kovalevich and Langford 2012, Mocchetti et al. 2012, Wallace 2006). Thus, we demonstrated that viral reservoirs contribute to the bystander damage by secretion of HIV proteins.

To characterize viral reservoirs, we measured the metabolism of these cells based on our recent paper (Castellano et al. 2019). We identified that HIV-infected astrocytes do not behave as latently HIV-infected microglia/macrophages. This, it may be due to the low percentage (~5%) of HIV-infected astrocytes in cultures or because they really have a different metabolic profile. Nevertheless, we demonstrated that microglia/macrophages and astrocytes have a common link with glutamine/glutamate metabolism. Even though, HIV-infected microglia/macrophages use glutamine/glutamate as a major source of energy (Castellano et al. 2019), HIV-infected astrocytes released a large amount of

glutamine/glutamate in the media (Eugenin and Berman 2007). Future studies will elucidate whether HIV-infected astrocytes are the real glutamine/glutamate donors.

Considering that our results for viral reservoirs identification and reservoirs metabolism indicate minimal changes, this do not correlate with the significant neurocognitive impairment that affect HIV-infected individuals. Our recent data indicates that HIV-infected individuals under cART display circulating lipid altered metabolism (Velasquez et al. 2019). In addition, existing literature data revealed that HIV dysregulates lipids causing fat accumulation in the body (Bernasconi et al. 2002, Martinez E. et al. 2001) and dyslipidemia in the blood (Finkelstein et al. 2015, Souza et al. 2013). Importantly, HAND, as well as other neurodegenerative diseases, has been linked to lipid dysregulation (Bandaru et al. 2013), but a real examination of structural and signaling lipids in the brain of HIV-infected individuals under cART and developing neurocognitive impairment is missing. In this thesis, we analyzed lipid distribution in the brain of HIV-infected individuals by MALDI-MSI and we demonstrated the structural lipids of the grey and the white matters did not change in HIV condition, proving that the grey and white matter are not compromised in the cART era. Other neurodegenerative diseases showed significant changes in lipid distribution and an important structural damage (Hussain et al. 2019). For our analysis, we used the same tissue sections where we identified few viral reservoirs with HIV-integrated DNA, minimal expression of viral mRNA and viral proteins but with HIV proteins bystander release. We identified a significant dysregulation of sulfatide in large areas of the brain. Although, sulfatide is the major component of the myelin sheet (Schmitt et al. 2015), so it is relatively abundant in the white matter, its relative intensity was elevated in HIV condition. Our analysis needs to be expanded in order to show if sulfatide increase is due to an over production in the white matter or to a lysosomal storage disorder. Even though we do not know the mechanism of release of sulfatide, we showed that lipid dysregulation involves several subclasses of sulfatide and large areas of the brain, despite the virus is minimally replicated and the number of viral reservoirs is low. If HAND is compared with Alzheimer's (AD) and Parkinson's diseases (PD) several differences appear. First, sulfatide increases in the white matter of HIV-infected patients rather than in the grey matter as observed in PD's patients (Cheng et al. 2003) or being reduced in both grey and white matter as observed in AD condition (Han et al. 2002). Second, in HAND

we did not detect significative alterations for structural membrane phospholipids, whereas in AD and PD conditions cholesterol and phospholipid alterations determine a significant CNS structural compromise (Hussain et al. 2019). These results may correlate with MRI data for HIV-infected brain showing reduction in brain volume but not structural disruption of the brain regions (Alakkas et al. 2019, Ances et al. 2012). This suggest that in the current cART era neuronal apoptosis is not the major mechanism triggered by HIV, but neuronal pruning (Ru and Tang 2017) can be a reasonable explanation for the reversible and flexible symptoms of the common milder forms of HAND. For all these reasons, we proposed sulfatide as a potential biomarker of HAND. For future directions, we intend to expand our research to a larger number of human brain tissues from cART suppressed HIV-infected individuals with different kind of cognitive impairment, we need to analyze different areas of the brain and isolate specific areas by Laser Capture Microdissection (LCM) to quantify the amount of sulfatide.

Tissue reservoirs are not entirely silent, we identified a bystander release of HIV proteins that compromise a bigger area of the brain and we demonstrated that several viral proteins participate in sulfatide secretion *in vitro*. Evaluating sulfatide secretion in the media of human primary astrocytes and differentiated SH-SY5Y neuroblastoma cell co-cultures, we showed that Gp120, Nef, Vif or Vpr increased its secretion. Even though the mechanism of release of sulfatide is unknown, a minimal amount of viral proteins can amply toxicity by sulfatide release. Then, we plan to reproduce the same experiment using connexin43 (Cx43) or pannexin-1 (Panx-1) blockers. This is because other bioactive lipids such as PGE_2 can be released by these channels (Velasquez et al. 2019). Or we can consider potentially other sources of secretion such as exoxomes (Fruhbeis et al. 2012).

One of the key finding of our laboratory is that HIV Tat, that is express in the brain of HIV-infected patients under cART, upregulates Cx43 expression in astrocytes (Berman et al. 2016). Hence, we have investigated extracellular sulfatide effects on human primary astrocytes, differentiated neurons, and Hela cells stably transfected with Cx43-CFP. We used astrocytes because they highly express Cx43, and our previous publication demonstrated that HIV-infected astrocytes induced bystander apoptosis of uninfected cells. Cx43 GJs are maintained between HIV-infected cells and uninfected cells in order to transfer toxic signals such as IP_3 and calcium and extend survival of HIV-infected cells

(Eugenin and Berman 2007, 2013, Eugenin et al. 2011). Recently, unpublished data from our laboratory demonstrated that Nef can bind to IP_3 receptors and amply the damage induced from the few HIV-infected astrocytes. On another hand, neurons were used to mimic the bystander effect mediated by the HIV-infected astrocytes for other residential cells in CNS (Eugenin et al. 2011, Ton and Xiong 2013). Hela cells were used as a stable system for Cx43 expression to study Cx43 trafficking. In these experiments, we demonstrated that sulfatide increased Cx43 mRNA and protein expression, especially in human primary astrocytes, and regulates the trafficking of Cx43 in Hela cells. This suggests that one of the potential mechanisms used by Tat to induce Cx43 expression is related to sulfatide release in HIV condition.

Moreover, we investigated Cx43 binding proteins after sulfatide stimulation by coimmunoprecipitation and subsequent proteomics in Hela cells stably transfected with Cx43-CFP. Proteomics data revealed that sulfatide regulated three important families of proteins related to recycling-transport, mitochondria and cellular membrane, where Cx43 is mostly localized. Between the recycling-transport proteins, we identify proteins binding to Cx43 involved in an active vesicular transport such as myosin and rab proteins. On another hand, mitochondrial proteins binding Cx43 and upregulated by sulfatide were related to glucose and glutamate/glutamine synthesis, that we analyzed in Chapter 3 and future experiments aim to demonstrate the direct interaction of Cx43 with these specific enzymes in the mitochondria. In addition, we found a particular proteomics profile for Cx43 in the plasma membrane that may result in stabilization of Cx43 by Tat and sulfatide. Although, we choose the Hela cells to perform this analysis because they represent a simple model, future studies intend to characterize Cx43 binding proteins in HIV-infected astrocytes.

Overall, there are major contributions to the HIV field presented in this thesis. First, we have optimized a high throughput technique to identify, localize, and quantify viral reservoirs in blood and in the tissues. We characterized that localized populations of microglia/macrophages and astrocytes create clusters of infected cells. Second, we analyzed that viral reservoirs relay glutamine/glutamate to survive. Third, we identified that HIV-infected patients under cART do not have significative structural changes in grey and white matter, and we presented sulfatide as a potential lipid biomarker of HAND, that

is highly expressed in the white matter. Fourth, we showed that sulfatide secretion is regulated by low concentration of HIV proteins, suggesting that amplification of the damage is controlled by viral proteins through a lipid mediated mechanism. Fifth, we identified a potential mechanism used by Tat to increase Cx43 that is mediated by sulfatide, which increased the expression of Cx43 mRNA and protein. In conclusion, we enlightened new Cx43 partners showing a direct or indirect protein:protein interaction with Cx43 in the recycling-trafficking, membrane and mitochondria compartments.

Although, CNS damage in HIV-positive individuals under cART is multifactorial we provided specific tools and unique data that describe a mechanism of neuronal bystander damage in HAND. Therefore, we proposed sulfatide as a potential biomarker or as a molecular target for preventing or curing HAND in the HIV aviremic population.

References

Abbas W, Herbein G. 2012. Molecular Understanding of HIV-1 Latency. Adv Virol 2012:574967.

Abramov AY, Ionov M, Pavlov E, Duchen MR. 2011. Membrane cholesterol content plays a key role in the neurotoxicity of beta-amyloid: implications for Alzheimer's disease. Aging Cell 10:595-603.

Adibhatla RM, Hatcher JF. 2007. Role of Lipids in Brain Injury and Diseases. Future Lipidol 2:403-422.

Adibhatla RM, Hatcher JF. 2008. Altered lipid metabolism in brain injury and disorders. Subcell Biochem 49:241-268.

Agar NY, Yang HW, Carroll RS, Black PM, Agar JN. 2007. Matrix solution fixation: histology-compatible tissue preparation for MALDI mass spectrometry imaging. Anal Chem 79:7416-7423.

Al-Harthi L. 2012. Interplay between Wnt/beta-catenin signaling and HIV: virologic and biologic consequences in the CNS. J Neuroimmune Pharmacol 7:731-739.

Alakkas A, et al. 2019. White matter damage, neuroinflammation, and neuronal integrity in HAND. J Neurovirol 25:32-41.

Allaman I, Gavillet M, Belanger M, Laroche T, Viertl D, Lashuel HA, Magistretti PJ. 2010. Amyloid-beta aggregates cause alterations of astrocytic metabolic phenotype: impact on neuronal viability. J Neurosci 30:3326-3338.

Allen JS, Damasio H, Grabowski TJ. 2002. Normal neuroanatomical variation in the human brain: an MRI-volumetric study. Am J Phys Anthropol 118:341-358.

Ambrosi C, Ren C, Spagnol G, Cavin G, Cone A, Grintsevich EE, Sosinsky GE, Sorgen PL. 2016. Connexin43 Forms Supramolecular Complexes through Non-Overlapping Binding Sites for Drebrin, Tubulin, and ZO-1. PLoS One 11:e0157073.

Amtul Z, Uhrig M, Rozmahel RF, Beyreuther K. 2011. Structural insight into the differential effects of omega-3 and omega-6 fatty acids on the production of Abeta peptides and amyloid plaques. J Biol Chem 286:6100-6107.

Ances BM, Ortega M, Vaida F, Heaps J, Paul R. 2012. Independent effects of HIV, aging, and HAART on brain volumetric measures. J Acquir Immune Defic Syndr 59:469-477.

Ances BM, et al. 2009. Resting cerebral blood flow: a potential biomarker of the effects of HIV in the brain. Neurology 73:702-708.

Ancuta P, et al. 2008. Microbial translocation is associated with increased monocyte activation and dementia in AIDS patients. PLoS One 3:e2516.

Andersen AB, Law I, Krabbe KS, Bruunsgaard H, Ostrowski SR, Ullum H, Hojgaard L, Lebech A, Gerstoft J, Kjaer A. 2010. Cerebral FDG-PET scanning abnormalities in optimally treated HIV patients. J Neuroinflammation 7:13.

Anderson AM, Lennox JL, Mulligan MM, Loring DW, Zetterberg H, Blennow K, Kessing C, Koneru R, Easley K, Tyor WR. 2017. Cerebrospinal fluid interferon alpha levels correlate with neurocognitive impairment in ambulatory HIV-Infected individuals. J Neurovirol 23:106-112.

Anderson EM, Maldarelli F. 2018. The role of integration and clonal expansion in HIV infection: live long and prosper. Retrovirology 15:71.

Anderson NM, Mucka P, Kern JG, Feng H. 2018. The emerging role and targetability of the TCA cycle in cancer metabolism. Protein Cell 9:216-237.

Andreasson K. 2010. Emerging roles of PGE2 receptors in models of neurological disease. Prostaglandins Other Lipid Mediat 91:104-112.
Andrieu-Abadie N, Gouaze V, Salvayre R, Levade T. 2001. Ceramide in apoptosis signaling: relationship with oxidative stress. Free Radic Biol Med 31:717-728.
Ann HW, et al. 2016. Characteristics of Resting-State Functional Connectivity in HIV-Associated Neurocognitive Disorder. PLoS One 11:e0153493.
Antinori A, et al. 2007. Updated research nosology for HIV-associated neurocognitive disorders. Neurology 69:1789-1799.
Archibald SL, et al. 2014. Brain morphometric correlates of metabolic variables in HIV: the CHARTER study. J Neurovirol 20:603-611.
Ariazi J, et al. 2017. Tunneling Nanotubes and Gap Junctions-Their Role in Long-Range Intercellular Communication during Development, Health, and Disease Conditions. Front Mol Neurosci 10:333.
Ashburner J, Friston KJ. 2000. Voxel-based morphometry--the methods. Neuroimage 11:805-821.
Aslam B, Basit M, Nisar MA, Khurshid M, Rasool MH. 2017. Proteomics: Technologies and Their Applications. J Chromatogr Sci 55:182-196.
Athenstaedt K, Daum G. 2006. The life cycle of neutral lipids: synthesis, storage and degradation. Cell Mol Life Sci 63:1355-1369.
Avdoshina V, et al. 2016. The HIV Protein gp120 Alters Mitochondrial Dynamics in Neurons. Neurotox Res 29:583-593.
Bairwa D, Kumar V, Vyas S, Das BK, Srivastava AK, Pandey RM, Sharma SK, Jagannathan NR, Sinha S. 2016. Case control study: magnetic resonance spectroscopy of brain in HIV infected patients. BMC Neurol 16:99.
Balcom EF, Roda WC, Cohen EA, Li MY, Power C. 2019. HIV-1 persistence in the central nervous system: viral and host determinants during antiretroviral therapy. Curr Opin Virol 38:54-62.
Bandaru VV, et al. 2013. A lipid storage-like disorder contributes to cognitive decline in HIV-infected subjects. Neurology 81:1492-1499.
Bandera A, Taramasso L, Bozzi G, Muscatello A, Robinson JA, Burdo TH, Gori A. 2019. HIV-Associated Neurocognitive Impairment in the Modern ART Era: Are We Close to Discovering Reliable Biomarkers in the Setting of Virological Suppression? Front Aging Neurosci 11:187.
Barre-Sinoussi F, et al. 1983. Isolation of a T-lymphotropic retrovirus from a patient at risk for acquired immune deficiency syndrome (AIDS). Science 220:868-871.
Bartke N, Hannun YA. 2009. Bioactive sphingolipids: metabolism and function. J Lipid Res 50 Suppl:S91-96.
Baslow MH. 2003. N-acetylaspartate in the vertebrate brain: metabolism and function. Neurochem Res 28:941-953.
Batzer MA, Deininger PL. 2002. Alu repeats and human genomic diversity. Nat Rev Genet 3:370-379.
Bednarik DP, Cook JA, Pitha PM. 1990. Inactivation of the HIV LTR by DNA CpG methylation: evidence for a role in latency. EMBO J 9:1157-1164.
Bellingan GJ, Caldwell H, Howie SE, Dransfield I, Haslett C. 1996. In vivo fate of the inflammatory macrophage during the resolution of inflammation: inflammatory

macrophages do not die locally, but emigrate to the draining lymph nodes. J Immunol 157:2577-2585.
Bendani MK, Palluy O, Cook-Moreau J, Beneytout JL, Rigaud M, Vallat JM. 1995. Localization of 12-lipoxygenase mRNA in cultured oligodendrocytes and astrocytes by in situ reverse transcriptase and polymerase chain reaction. Neurosci Lett 189:159-162.
Berman JW, Carvallo L, Buckner CM, Luers A, Prevedel L, Bennett MV, Eugenin EA. 2016. HIV-tat alters Connexin43 expression and trafficking in human astrocytes: role in NeuroAIDS. J Neuroinflammation 13:54.
Bernasconi E, et al. 2002. Abnormalities of body fat distribution in HIV-infected persons treated with antiretroviral drugs: The Swiss HIV Cohort Study. J Acquir Immune Defic Syndr 31:50-55.
Berry KA, Hankin JA, Barkley RM, Spraggins JM, Caprioli RM, Murphy RC. 2011. MALDI imaging of lipid biochemistry in tissues by mass spectrometry. Chem Rev 111:6491-6512.
Bhandari DR, Schott M, Rompp A, Vilcinskas A, Spengler B. 2015. Metabolite localization by atmospheric pressure high-resolution scanning microprobe matrix-assisted laser desorption/ionization mass spectrometry imaging in whole-body sections and individual organs of the rove beetle Paederus riparius. Anal Bioanal Chem 407:2189-2201.
Billah MM, Anthes JC. 1990. The regulation and cellular functions of phosphatidylcholine hydrolysis. Biochem J 269:281-291.
Bishop WR, Bell RM. 1988. Functions of diacylglycerol in glycerolipid metabolism, signal transduction and cellular transformation. Oncogene Res 2:205-218.
Blanc L, Lenaerts A, Dartois V, Prideaux B. 2018. Visualization of Mycobacterial Biomarkers and Tuberculosis Drugs in Infected Tissue by MALDI-MS Imaging. Anal Chem 90:6275-6282.
Blankson JN, Persaud D, Siliciano RF. 2002. The challenge of viral reservoirs in HIV-1 infection. Annu Rev Med 53:557-593.
Bowerman B, Brown PO, Bishop JM, Varmus HE. 1989. A nucleoprotein complex mediates the integration of retroviral DNA. Genes Dev 3:469-478.
Bozzi G, et al. 2019. No evidence of ongoing HIV replication or compartmentalization in tissues during combination antiretroviral therapy: Implications for HIV eradication. Sci Adv 5:eaav2045.
Bracq L, Xie M, Benichou S, Bouchet J. 2018. Mechanisms for Cell-to-Cell Transmission of HIV-1. Front Immunol 9:260.
Bratton DL, Henson PM. 2008. Apoptotic cell recognition: will the real phosphatidylserine receptor(s) please stand up? Curr Biol 18:R76-79.
Brekke EM, Walls AB, Schousboe A, Waagepetersen HS, Sonnewald U. 2012. Quantitative importance of the pentose phosphate pathway determined by incorporation of 13C from [2-13C]- and [3-13C]glucose into TCA cycle intermediates and neurotransmitter amino acids in functionally intact neurons. J Cereb Blood Flow Metab 32:1788-1799.
Brier MR, Wu Q, Tanenbaum AB, Westerhaus ET, Kharasch ED, Ances BM. 2015. Effect of HAART on Brain Organization and Function in HIV-Negative Subjects. J Neuroimmune Pharmacol 10:517-521.
Bruce KD, Zsombok A, Eckel RH. 2017. Lipid Processing in the Brain: A Key Regulator of Systemic Metabolism. Front Endocrinol (Lausanne) 8:60.

Bruner KM, et al. 2016. Defective proviruses rapidly accumulate during acute HIV-1 infection. Nat Med 22:1043-1049.
Buchberger AR, DeLaney K, Johnson J, Li L. 2018. Mass Spectrometry Imaging: A Review of Emerging Advancements and Future Insights. Anal Chem 90:240-265.
Burdo TH, Lentz MR, Autissier P, Krishnan A, Halpern E, Letendre S, Rosenberg ES, Ellis RJ, Williams KC. 2011. Soluble CD163 made by monocyte/macrophages is a novel marker of HIV activity in early and chronic infection prior to and after anti-retroviral therapy. J Infect Dis 204:154-163.
Burdo TH, Weiffenbach A, Woods SP, Letendre S, Ellis RJ, Williams KC. 2013. Elevated sCD163 in plasma but not cerebrospinal fluid is a marker of neurocognitive impairment in HIV infection. AIDS 27:1387-1395.
Bush S, Tebit DM. 2015. HIV-1 Group O Origin, Evolution, Pathogenesis, and Treatment: Unraveling the Complexity of an Outlier 25 Years Later. AIDS Rev 17:147-158.
Butkevich E, Hulsmann S, Wenzel D, Shirao T, Duden R, Majoul I. 2004. Drebrin is a novel connexin-43 binding partner that links gap junctions to the submembrane cytoskeleton. Curr Biol 14:650-658.
Byrd DA, et al. 2011. Neurocognitive impact of substance use in HIV infection. J Acquir Immune Defic Syndr 58:154-162.
Campbell EM, Hope TJ. 2015. HIV-1 capsid: the multifaceted key player in HIV-1 infection. Nat Rev Microbiol 13:471-483.
Cantres-Rosario Y, Plaud-Valentin M, Gerena Y, Skolasky RL, Wojna V, Melendez LM. 2013. Cathepsin B and cystatin B in HIV-seropositive women are associated with infection and HIV-1-associated neurocognitive disorders. AIDS 27:347-356.
Cary DC, Fujinaga K, Peterlin BM. 2016. Molecular mechanisms of HIV latency. J Clin Invest 126:448-454.
Cassol E, Misra V, Morgello S, Gabuzda D. 2013. Applications and limitations of inflammatory biomarkers for studies on neurocognitive impairment in HIV infection. J Neuroimmune Pharmacol 8:1087-1097.
Castellano P, Prevedel L, Eugenin EA. 2017. HIV-infected macrophages and microglia that survive acute infection become viral reservoirs by a mechanism involving Bim. Sci Rep 7:12866.
Castellano P, Prevedel L, Valdebenito S, Eugenin EA. 2019. HIV infection and latency induce a unique metabolic signature in human macrophages. Sci Rep 9:3941.
Cermenati G, Mitro N, Audano M, Melcangi RC, Crestani M, De Fabiani E, Caruso D. 2015. Lipids in the nervous system: from biochemistry and molecular biology to patho-physiology. Biochim Biophys Acta 1851:51-60.
Chaganti JR, Heinecke A, Gates TM, Moffat KJ, Brew BJ. 2017. Functional Connectivity in Virally Suppressed Patients with HIV-Associated Neurocognitive Disorder: A Resting-State Analysis. AJNR Am J Neuroradiol 38:1623-1629.
Chang L, Shukla DK. 2018. Imaging studies of the HIV-infected brain. Handb Clin Neurol 152:229-264.
Chang L, Speck O, Miller EN, Braun J, Jovicich J, Koch C, Itti L, Ernst T. 2001. Neural correlates of attention and working memory deficits in HIV patients. Neurology 57:1001-1007.

Chang L, Wang GJ, Volkow ND, Ernst T, Telang F, Logan J, Fowler JS. 2008. Decreased brain dopamine transporters are related to cognitive deficits in HIV patients with or without cocaine abuse. Neuroimage 42:869-878.
Chauhan A. 2015. Enigma of HIV-1 latent infection in astrocytes: an in-vitro study using protein kinase C agonist as a latency reversing agent. Microbes Infect 17:651-659.
Checkley MA, Luttge BG, Freed EO. 2011. HIV-1 envelope glycoprotein biosynthesis, trafficking, and incorporation. J Mol Biol 410:582-608.
Cheng H, Xu J, McKeel DW, Jr., Han X. 2003. Specificity and potential mechanism of sulfatide deficiency in Alzheimer's disease: an electrospray ionization mass spectrometric study. Cell Mol Biol (Noisy-le-grand) 49:809-818.
Chiang K, Sung TL, Rice AP. 2012. Regulation of cyclin T1 and HIV-1 Replication by microRNAs in resting CD4+ T lymphocytes. J Virol 86:3244-3252.
Chughtai K, Heeren RM. 2010. Mass spectrometric imaging for biomedical tissue analysis. Chem Rev 110:3237-3277.
Churchill MJ, Deeks SG, Margolis DM, Siliciano RF, Swanstrom R. 2016. HIV reservoirs: what, where and how to target them. Nat Rev Microbiol 14:55-60.
Churchill MJ, Wesselingh SL, Cowley D, Pardo CA, McArthur JC, Brew BJ, Gorry PR. 2009. Extensive astrocyte infection is prominent in human immunodeficiency virus-associated dementia. Ann Neurol 66:253-258.
Claypool SM. 2009. Cardiolipin, a critical determinant of mitochondrial carrier protein assembly and function. Biochim Biophys Acta 1788:2059-2068.
Clayton KL, Garcia JV, Clements JE, Walker BD. 2017. HIV Infection of Macrophages: Implications for Pathogenesis and Cure. Pathog Immun 2:179-192.
Clifford DB, Ances BM. 2013. HIV-associated neurocognitive disorder. Lancet Infect Dis 13:976-986.
Coffin J, Swanstrom R. 2013. HIV pathogenesis: dynamics and genetics of viral populations and infected cells. Cold Spring Harb Perspect Med 3:a012526.
Cohen MS, Shaw GM, McMichael AJ, Haynes BF. 2011. Acute HIV-1 Infection. N Engl J Med 364:1943-1954.
Connolly CG, Bischoff-Grethe A, Jordan SJ, Woods SP, Ellis RJ, Paulus MP, Grant I, Translational Methamphetamine ARCG. 2014. Altered functional response to risky choice in HIV infection. PLoS One 9:e111583.
Correa DG, Zimmermann N, Doring TM, Wilner NV, Leite SC, Cabral RF, Fonseca RP, Bahia PR, Gasparetto EL. 2015. Diffusion tensor MR imaging of white matter integrity in HIV-positive patients with planning deficit. Neuroradiology 57:475-482.
Cosenza MA, Zhao ML, Si Q, Lee SC. 2002. Human brain parenchymal microglia express CD14 and CD45 and are productively infected by HIV-1 in HIV-1 encephalitis. Brain Pathol 12:442-455.
Couttas TA, Kain N, Daniels B, Lim XY, Shepherd C, Kril J, Pickford R, Li H, Garner B, Don AS. 2014. Loss of the neuroprotective factor Sphingosine 1-phosphate early in Alzheimer's disease pathogenesis. Acta Neuropathol Commun 2:9.
Cribbs SK, Crothers K, Morris A. 2019. Pathogenesis of HIV-related lung disease: Immunity, infection, and inflammation. Physiol Rev.
Dahabieh MS, Battivelli E, Verdin E. 2015. Understanding HIV latency: the road to an HIV cure. Annu Rev Med 66:407-421.

Dayton AI. 2004. Within you, without you: HIV-1 Rev and RNA export. Retrovirology 1:35.
De Scheerder MA, et al. 2019. HIV Rebound Is Predominantly Fueled by Genetically Identical Viral Expansions from Diverse Reservoirs. Cell Host Microbe 26:347-358 e347.
Denton PW, Sogaard OS, Tolstrup M. 2019. Impacts of HIV Cure Interventions on Viral Reservoirs in Tissues. Front Microbiol 10:1956.
Di Paolo G, De Camilli P. 2006. Phosphoinositides in cell regulation and membrane dynamics. Nature 443:651-657.
Divakaruni AS, Paradyse A, Ferrick DA, Murphy AN, Jastroch M. 2014. Analysis and interpretation of microplate-based oxygen consumption and pH data. Methods Enzymol 547:309-354.
Do T, et al. 2014. Three-dimensional imaging of HIV-1 virological synapses reveals membrane architectures involved in virus transmission. J Virol 88:10327-10339.
Du Pasquier RA, et al. 2013. Marked increase of the astrocytic marker S100B in the cerebrospinal fluid of HIV-infected patients on LPV/r-monotherapy. AIDS 27:203-210.
Dufourc EJ. 2008. Sterols and membrane dynamics. J Chem Biol 1:63-77.
Dusick JR, Glenn TC, Lee WN, Vespa PM, Kelly DF, Lee SM, Hovda DA, Martin NA. 2007. Increased pentose phosphate pathway flux after clinical traumatic brain injury: a [1,2-13C2]glucose labeling study in humans. J Cereb Blood Flow Metab 27:1593-1602.
Eckhardt M. 2008. The role and metabolism of sulfatide in the nervous system. Mol Neurobiol 37:93-103.
Eggers C, et al. 2017. HIV-1-associated neurocognitive disorder: epidemiology, pathogenesis, diagnosis, and treatment. J Neurol 264:1715-1727.
Ellis R, Langford D, Masliah E. 2007. HIV and antiretroviral therapy in the brain: neuronal injury and repair. Nat Rev Neurosci 8:33-44.
Engelman A, Mizuuchi K, Craigie R. 1991. HIV-1 DNA integration: mechanism of viral DNA cleavage and DNA strand transfer. Cell 67:1211-1221.
Eriksson S, et al. 2013. Comparative analysis of measures of viral reservoirs in HIV-1 eradication studies. PLoS Pathog 9:e1003174.
Eugenin EA. 2014. Role of connexin/pannexin containing channels in infectious diseases. FEBS Lett 588:1389-1395.
Eugenin EA, Basilio D, Saez JC, Orellana JA, Raine CS, Bukauskas F, Bennett MV, Berman JW. 2012. The role of gap junction channels during physiologic and pathologic conditions of the human central nervous system. J Neuroimmune Pharmacol 7:499-518.
Eugenin EA, Berman JW. 2007. Gap junctions mediate human immunodeficiency virus-bystander killing in astrocytes. J Neurosci 27:12844-12850.
Eugenin EA, Berman JW. 2013. Cytochrome C dysregulation induced by HIV infection of astrocytes results in bystander apoptosis of uninfected astrocytes by an IP3 and calcium-dependent mechanism. J Neurochem 127:644-651.
Eugenin EA, Clements JE, Zink MC, Berman JW. 2011. Human immunodeficiency virus infection of human astrocytes disrupts blood-brain barrier integrity by a gap junction-dependent mechanism. J Neurosci 31:9456-9465.
Eugenin EA, Gaskill PJ, Berman JW. 2009. Tunneling nanotubes (TNT): A potential mechanism for intercellular HIV trafficking. Commun Integr Biol 2:243-244.

Eugenin EA, King JE, Nath A, Calderon TM, Zukin RS, Bennett MV, Berman JW. 2007. HIV-tat induces formation of an LRP-PSD-95- NMDAR-nNOS complex that promotes apoptosis in neurons and astrocytes. Proc Natl Acad Sci U S A 104:3438-3443.
Eugenin EA, Osiecki K, Lopez L, Goldstein H, Calderon TM, Berman JW. 2006. CCL2/monocyte chemoattractant protein-1 mediates enhanced transmigration of human immunodeficiency virus (HIV)-infected leukocytes across the blood-brain barrier: a potential mechanism of HIV-CNS invasion and NeuroAIDS. J Neurosci 26:1098-1106.
Fabelo N, Martin V, Santpere G, Marin R, Torrent L, Ferrer I, Diaz M. 2011. Severe alterations in lipid composition of frontal cortex lipid rafts from Parkinson's disease and incidental Parkinson's disease. Mol Med 17:1107-1118.
Fadeel B, Xue D. 2009. The ins and outs of phospholipid asymmetry in the plasma membrane: roles in health and disease. Crit Rev Biochem Mol Biol 44:264-277.
Fahy E, Cotter D, Sud M, Subramaniam S. 2011. Lipid classification, structures and tools. Biochim Biophys Acta 1811:637-647.
Fahy E, et al. 2005. A comprehensive classification system for lipids. J Lipid Res 46:839-861.
Farooqui AA, Horrocks LA, Farooqui T. 2007. Modulation of inflammation in brain: a matter of fat. J Neurochem 101:577-599.
Fauci AS, Desrosiers RC. 1997. Pathogenesis of HIV and SIV in Coffin JM, Hughes SH, Varmus HE, eds. Retroviruses. Cold Spring Harbor (NY).
Finkelstein JL, Gala P, Rochford R, Glesby MJ, Mehta S. 2015. HIV/AIDS and lipodystrophy: implications for clinical management in resource-limited settings. J Int AIDS Soc 18:19033.
Finzi D, et al. 1997. Identification of a reservoir for HIV-1 in patients on highly active antiretroviral therapy. Science 278:1295-1300.
Fox MD, Raichle ME. 2007. Spontaneous fluctuations in brain activity observed with functional magnetic resonance imaging. Nat Rev Neurosci 8:700-711.
Freed EO. 1998. HIV-1 gag proteins: diverse functions in the virus life cycle. Virology 251:1-15.
Freed EO, Delwart EL, Buchschacher GL, Jr., Panganiban AT. 1992. A mutation in the human immunodeficiency virus type 1 transmembrane glycoprotein gp41 dominantly interferes with fusion and infectivity. Proc Natl Acad Sci U S A 89:70-74.
Freed EO, Mouland AJ. 2006. The cell biology of HIV-1 and other retroviruses. Retrovirology 3:77.
Frisardi V, Panza F, Seripa D, Farooqui T, Farooqui AA. 2011. Glycerophospholipids and glycerophospholipid-derived lipid mediators: a complex meshwork in Alzheimer's disease pathology. Prog Lipid Res 50:313-330.
Fruhbeis C, Frohlich D, Kramer-Albers EM. 2012. Emerging roles of exosomes in neuron-glia communication. Front Physiol 3:119.
Galloway NL, Doitsh G, Monroe KM, Yang Z, Munoz-Arias I, Levy DN, Greene WC. 2015. Cell-to-Cell Transmission of HIV-1 Is Required to Trigger Pyroptotic Death of Lymphoid-Tissue-Derived CD4 T Cells. Cell Rep 12:1555-1563.
Galvagnion C, Buell AK, Meisl G, Michaels TC, Vendruscolo M, Knowles TP, Dobson CM. 2015. Lipid vesicles trigger alpha-synuclein aggregation by stimulating primary nucleation. Nat Chem Biol 11:229-234.

Ganor Y, et al. 2019. HIV-1 reservoirs in urethral macrophages of patients under suppressive antiretroviral therapy. Nat Microbiol 4:633-644.
Gaskill PJ, Yano HH, Kalpana GV, Javitch JA, Berman JW. 2014. Dopamine receptor activation increases HIV entry into primary human macrophages. PLoS One 9:e108232.
German Advisory Committee Blood SAoPTbB. 2016. Human Immunodeficiency Virus (HIV). Transfus Med Hemother 43:203-222.
Giepmans BN, Moolenaar WH. 1998. The gap junction protein connexin43 interacts with the second PDZ domain of the zona occludens-1 protein. Curr Biol 8:931-934.
Glatz JF. 2015. Lipids and lipid binding proteins: a perfect match. Prostaglandins Leukot Essent Fatty Acids 93:45-49.
Gonzalez-Dominguez R, Garcia-Barrera T, Gomez-Ariza JL. 2014. Combination of metabolomic and phospholipid-profiling approaches for the study of Alzheimer's disease. J Proteomics 104:37-47.
Good CD, Ashburner J, Frackowiak RS. 2001. Computational neuroanatomy: new perspectives for neuroradiology. Rev Neurol (Paris) 157:797-806.
Goto-Inoue N, Hayasaka T, Setou M. 2010. Imaging mass spectrometry of glycolipids. Methods Enzymol 478:287-301.
Goto-Inoue N, Hayasaka T, Zaima N, Setou M. 2011. Imaging mass spectrometry for lipidomics. Biochim Biophys Acta 1811:961-969.
Gottlieb MS, Schroff R, Schanker HM, Weisman JD, Fan PT, Wolf RA, Saxon A. 1981. Pneumocystis carinii pneumonia and mucosal candidiasis in previously healthy homosexual men: evidence of a new acquired cellular immunodeficiency. N Engl J Med 305:1425-1431.
Grennan JT, et al. 2012. Magnitude of virologic blips is associated with a higher risk for virologic rebound in HIV-infected individuals: a recurrent events analysis. J Infect Dis 205:1230-1238.
Griffin DE, Wesselingh SL, McArthur JC. 1994. Elevated central nervous system prostaglandins in human immunodeficiency virus-associated dementia. Ann Neurol 35:592-597.
Guda MR, Labak CM, Omar SI, Asuthkar S, Airala S, Tuszynski J, Tsung AJ, Velpula KK. 2019. GLUT1 and TUBB4 in Glioblastoma Could be Efficacious Targets. Cancers (Basel) 11.
Guest J, Garg M, Bilgin A, Grant R. 2013. Relationship between central and peripheral fatty acids in humans. Lipids Health Dis 12:79.
Guha D, Mukerji SS, Chettimada S, Misra V, Lorenz DR, Morgello S, Gabuzda D. 2019. Cerebrospinal fluid extracellular vesicles and neurofilament light protein as biomarkers of central nervous system injury in HIV-infected patients on antiretroviral therapy. AIDS 33:615-625.
Hammoud DA, Endres CJ, Chander AR, Guilarte TR, Wong DF, Sacktor NC, McArthur JC, Pomper MG. 2005. Imaging glial cell activation with [11C]-R-PK11195 in patients with AIDS. J Neurovirol 11:346-355.
Han X. 2007. Potential mechanisms contributing to sulfatide depletion at the earliest clinically recognizable stage of Alzheimer's disease: a tale of shotgun lipidomics. J Neurochem 103 Suppl 1:171-179.

Han X, D MH, McKeel DW, Jr., Kelley J, Morris JC. 2002. Substantial sulfatide deficiency and ceramide elevation in very early Alzheimer's disease: potential role in disease pathogenesis. J Neurochem 82:809-818.
Han X, Gross RW. 2003. Global analyses of cellular lipidomes directly from crude extracts of biological samples by ESI mass spectrometry: a bridge to lipidomics. J Lipid Res 44:1071-1079.
Hancock SE, Friedrich MG, Mitchell TW, Truscott RJ, Else PL. 2017. The phospholipid composition of the human entorhinal cortex remains relatively stable over 80 years of adult aging. Geroscience 39:73-82.
Hanna Z, Kay DG, Rebai N, Guimond A, Jothy S, Jolicoeur P. 1998. Nef harbors a major determinant of pathogenicity for an AIDS-like disease induced by HIV-1 in transgenic mice. Cell 95:163-175.
Hannun YA, Obeid LM. 1995. Ceramide: an intracellular signal for apoptosis. Trends Biochem Sci 20:73-77.
Hannun YA, Obeid LM. 2008. Principles of bioactive lipid signalling: lessons from sphingolipids. Nat Rev Mol Cell Biol 9:139-150.
Hansen SG, et al. 2009. Effector memory T cell responses are associated with protection of rhesus monkeys from mucosal simian immunodeficiency virus challenge. Nat Med 15:293-299.
Harezlak J, et al. 2011. Persistence of HIV-associated cognitive impairment, inflammation, and neuronal injury in era of highly active antiretroviral treatment. AIDS 25:625-633.
Harris AL. 2001. Emerging issues of connexin channels: biophysics fills the gap. Q Rev Biophys 34:325-472.
Harris AL. 2007. Connexin channel permeability to cytoplasmic molecules. Prog Biophys Mol Biol 94:120-143.
Harris JL, Choi IY, Brooks WM. 2015. Probing astrocyte metabolism in vivo: proton magnetic resonance spectroscopy in the injured and aging brain. Front Aging Neurosci 7:202.
Haughey NJ, Cutler RG, Tamara A, McArthur JC, Vargas DL, Pardo CA, Turchan J, Nath A, Mattson MP. 2004. Perturbation of sphingolipid metabolism and ceramide production in HIV-dementia. Ann Neurol 55:257-267.
Hayasaka T, Goto-Inoue N, Zaima N, Kimura Y, Setou M. 2009. Organ-specific distributions of lysophosphatidylcholine and triacylglycerol in mouse embryo. Lipids 44:837-848.
Hayasaka T, Goto-Inoue N, Zaima N, Shrivas K, Kashiwagi Y, Yamamoto M, Nakamoto M, Setou M. 2010. Imaging mass spectrometry with silver nanoparticles reveals the distribution of fatty acids in mouse retinal sections. J Am Soc Mass Spectrom 21:1446-1454.
Hazleton JE, Berman JW, Eugenin EA. 2010. Novel mechanisms of central nervous system damage in HIV infection. HIV AIDS (Auckl) 2:39-49.
He X, Huang Y, Li B, Gong CX, Schuchman EH. 2010. Deregulation of sphingolipid metabolism in Alzheimer's disease. Neurobiol Aging 31:398-408.
Heaton RK, et al. 2010. HIV-associated neurocognitive disorders persist in the era of potent antiretroviral therapy: CHARTER Study. Neurology 75:2087-2096.
Hemelaar J. 2012. The origin and diversity of the HIV-1 pandemic. Trends Mol Med 18:182-192.

Hiener B, et al. 2017. Identification of Genetically Intact HIV-1 Proviruses in Specific CD4(+) T Cells from Effectively Treated Participants. Cell Rep 21:813-822.
Hoffmann T, Dorrestein PC. 2015. Homogeneous matrix deposition on dried agar for MALDI imaging mass spectrometry of microbial cultures. J Am Soc Mass Spectrom 26:1959-1962.
Holman AG, Mefford ME, O'Connor N, Gabuzda D. 2010. HIVBrainSeqDB: a database of annotated HIV envelope sequences from brain and other anatomical sites. AIDS Res Ther 7:43.
Hong JH, Kang JW, Kim DK, Baik SH, Kim KH, Shanta SR, Jung JH, Mook-Jung I, Kim KP. 2016. Global changes of phospholipids identified by MALDI imaging mass spectrometry in a mouse model of Alzheimer's disease. J Lipid Res 57:36-45.
Honke K. 2013. Biosynthesis and biological function of sulfoglycolipids. Proc Jpn Acad Ser B Phys Biol Sci 89:129-138.
Hooijmans CR, Kiliaan AJ. 2008. Fatty acids, lipid metabolism and Alzheimer pathology. Eur J Pharmacol 585:176-196.
Hu WS, Hughes SH. 2012. HIV-1 reverse transcription. Cold Spring Harb Perspect Med 2.
Huot N, Bosinger SE, Paiardini M, Reeves RK, Muller-Trutwin M. 2018. Lymph Node Cellular and Viral Dynamics in Natural Hosts and Impact for HIV Cure Strategies. Front Immunol 9:780.
Hussain G, et al. 2019. Lipids as biomarkers of brain disorders. Crit Rev Food Sci Nutr:1-24.
Hussain G, Schmitt F, Loeffler JP, Gonzalez de Aguilar JL. 2013. Fatting the brain: a brief of recent research. Front Cell Neurosci 7:144.
Hutter G, et al. 2009. Long-term control of HIV by CCR5 Delta32/Delta32 stem-cell transplantation. N Engl J Med 360:692-698.
Ishizaka A, Sato H, Nakamura H, Koga M, Kikuchi T, Hosoya N, Koibuchi T, Nomoto A, Kawana-Tachikawa A, Mizutani T. 2016. Short Intracellular HIV-1 Transcripts as Biomarkers of Residual Immune Activation in Patients on Antiretroviral Therapy. J Virol 90:5665-5676.
Ishizuka I. 1997. Chemistry and functional distribution of sulfoglycolipids. Prog Lipid Res 36:245-319.
Jackson SN, Baldwin K, Muller L, Womack VM, Schultz JA, Balaban C, Woods AS. 2014. Imaging of lipids in rat heart by MALDI-MS with silver nanoparticles. Anal Bioanal Chem 406:1377-1386.
Jacotot E, et al. 2000. The HIV-1 viral protein R induces apoptosis via a direct effect on the mitochondrial permeability transition pore. J Exp Med 191:33-46.
Jaeger LB, Nath A. 2012. Modeling HIV-associated neurocognitive disorders in mice: new approaches in the changing face of HIV neuropathogenesis. Dis Model Mech 5:313-322.
Jayappa KD, Ao Z, Yao X. 2012. The HIV-1 passage from cytoplasm to nucleus: the process involving a complex exchange between the components of HIV-1 and cellular machinery to access nucleus and successful integration. Int J Biochem Mol Biol 3:70-85.
Jenkins GM, Frohman MA. 2005. Phospholipase D: a lipid centric review. Cell Mol Life Sci 62:2305-2316.

Jensen BK, Roth LM, Grinspan JB, Jordan-Sciutto KL. 2019. White matter loss and oligodendrocyte dysfunction in HIV: A consequence of the infection, the antiretroviral therapy or both? Brain Res 1724:146397.
Jones RB, Walker BD. 2016. HIV-specific CD8(+) T cells and HIV eradication. J Clin Invest 126:455-463.
Justice A, Sullivan L, Fiellin D, Veterans Aging Cohort Study Project T. 2010. HIV/AIDS, comorbidity, and alcohol: can we make a difference? Alcohol Res Health 33:258-266.
Kaiser P, Joshi SK, Kim P, Li P, Liu H, Rice AP, Wong JK, Yukl SA. 2017. Assays for precise quantification of total (including short) and elongated HIV-1 transcripts. J Virol Methods 242:1-8.
Kallianpur AR, et al. 2019. Cerebrospinal Fluid Ceruloplasmin, Haptoglobin, and Vascular Endothelial Growth Factor Are Associated with Neurocognitive Impairment in Adults with HIV Infection. Mol Neurobiol 56:3808-3818.
Kamat A, Lyons JL, Misra V, Uno H, Morgello S, Singer EJ, Gabuzda D. 2012. Monocyte activation markers in cerebrospinal fluid associated with impaired neurocognitive testing in advanced HIV infection. J Acquir Immune Defic Syndr 60:234-243.
Kaneko N, Hwang JY, Gertner M, Pontarelli F, Zukin RS. 2014. Casein kinase 1 suppresses activation of REST in insulted hippocampal neurons and halts ischemia-induced neuronal death. J Neurosci 34:6030-6039.
Kanmogne GD, Kennedy RC, Grammas P. 2002. HIV-1 gp120 proteins and gp160 peptides are toxic to brain endothelial cells and neurons: possible pathway for HIV entry into the brain and HIV-associated dementia. J Neuropathol Exp Neurol 61:992-1000.
Karas M, Kruger R. 2003. Ion formation in MALDI: the cluster ionization mechanism. Chem Rev 103:427-440.
Karn J, Stoltzfus CM. 2012. Transcriptional and posttranscriptional regulation of HIV-1 gene expression. Cold Spring Harb Perspect Med 2:a006916.
Kaul M, Lipton SA. 2006. Mechanisms of neuroimmunity and neurodegeneration associated with HIV-1 infection and AIDS. J Neuroimmune Pharmacol 1:138-151.
Kearns A, Gordon J, Burdo TH, Qin X. 2017. HIV-1-Associated Atherosclerosis: Unraveling the Missing Link. J Am Coll Cardiol 69:3084-3098.
Kelesidis T, Currier JS. 2014. Dyslipidemia and cardiovascular risk in human immunodeficiency virus infection. Endocrinol Metab Clin North Am 43:665-684.
Kielian T. 2008. Glial connexins and gap junctions in CNS inflammation and disease. J Neurochem 106:1000-1016.
Kihara A. 2012. Very long-chain fatty acids: elongation, physiology and related disorders. J Biochem 152:387-395.
Kim M, Hosmane NN, Bullen CK, Capoferri A, Yang HC, Siliciano JD, Siliciano RF. 2014. A primary CD4(+) T cell model of HIV-1 latency established after activation through the T cell receptor and subsequent return to quiescence. Nat Protoc 9:2755-2770.
Kim YK, Mbonye U, Hokello J, Karn J. 2011. T-cell receptor signaling enhances transcriptional elongation from latent HIV proviruses by activating P-TEFb through an ERK-dependent pathway. J Mol Biol 410:896-916.
Klaver B, Berkhout B. 1994. Comparison of 5' and 3' long terminal repeat promoter function in human immunodeficiency virus. J Virol 68:3830-3840.
Kolter T. 2012. Ganglioside biochemistry. ISRN Biochem 2012:506160.

Kornberg MD, Bhargava P, Kim PM, Putluri V, Snowman AM, Putluri N, Calabresi PA, Snyder SH. 2018. Dimethyl fumarate targets GAPDH and aerobic glycolysis to modulate immunity. Science 360:449-453.
Kosicek M, Hecimovic S. 2013. Phospholipids and Alzheimer's disease: alterations, mechanisms and potential biomarkers. Int J Mol Sci 14:1310-1322.
Kovalevich J, Langford D. 2012. Neuronal toxicity in HIV CNS disease. Future Virol 7:687-698.
Kwong PD, Wyatt R, Robinson J, Sweet RW, Sodroski J, Hendrickson WA. 1998. Structure of an HIV gp120 envelope glycoprotein in complex with the CD4 receptor and a neutralizing human antibody. Nature 393:648-659.
Lafeuillade A, Stevenson M. 2011. The search for a cure for persistent HIV reservoirs. AIDS Rev 13:63-66.
Lamers SL, et al. 2016. HIV DNA Is Frequently Present within Pathologic Tissues Evaluated at Autopsy from Combined Antiretroviral Therapy-Treated Patients with Undetectable Viral Loads. J Virol 90:8968-8983.
Landgraf RR, Prieto Conaway MC, Garrett TJ, Stacpoole PW, Yost RA. 2009. Imaging of lipids in spinal cord using intermediate pressure matrix-assisted laser desorption-linear ion trap/Orbitrap MS. Anal Chem 81:8488-8495.
Langford TD, Letendre SL, Larrea GJ, Masliah E. 2003. Changing patterns in the neuropathogenesis of HIV during the HAART era. Brain Pathol 13:195-210.
Larder BA, Darby G, Richman DD. 1989. HIV with reduced sensitivity to zidovudine (AZT) isolated during prolonged therapy. Science 243:1731-1734.
Lassmann H, Hickey WF. 1993. Radiation bone marrow chimeras as a tool to study microglia turnover in normal brain and inflammation. Clin Neuropathol 12:284-285.
Lee CH, Olson P, Evans RM. 2003. Minireview: lipid metabolism, metabolic diseases, and peroxisome proliferator-activated receptors. Endocrinology 144:2201-2207.
Leite SC, Correa DG, Doring TM, Kubo TT, Netto TM, Ferracini R, Ventura N, Bahia PR, Gasparetto EL. 2013. Diffusion tensor MRI evaluation of the corona radiata, cingulate gyri, and corpus callosum in HIV patients. J Magn Reson Imaging 38:1488-1493.
Lemp GF, et al. 1990. Projections of AIDS morbidity and mortality in San Francisco. JAMA 263:1497-1501.
Leopold J, Popkova Y, Engel KM, Schiller J. 2018. Recent Developments of Useful MALDI Matrices for the Mass Spectrometric Characterization of Lipids. Biomolecules 8.
Li B, Zhang Y, Ge J, Liu K, Li P. 2018. Sample preparation for mass spectrometry imaging of leaf tissues: a case study on analyte delocalization. Anal Bioanal Chem 410:7449-7456.
Li GH, Henderson L, Nath A. 2016. Astrocytes as an HIV Reservoir: Mechanism of HIV Infection. Curr HIV Res 14:373-381.
Li X, Olson C, Lu S, Kamasawa N, Yasumura T, Rash JE, Nagy JI. 2004. Neuronal connexin36 association with zonula occludens-1 protein (ZO-1) in mouse brain and interaction with the first PDZ domain of ZO-1. Eur J Neurosci 19:2132-2146.
Lin A, Ross BD, Harris K, Wong W. 2005. Efficacy of proton magnetic resonance spectroscopy in neurological diagnosis and neurotherapeutic decision making. NeuroRx 2:197-214.
Liu X, Shah A, Gangwani MR, Silverstein PS, Fu M, Kumar A. 2014. HIV-1 Nef induces CCL5 production in astrocytes through p38-MAPK and PI3K/Akt pathway and utilizes NF-kB, CEBP and AP-1 transcription factors. Sci Rep 4:4450.

Liu Y, Liu H, Kim BO, Gattone VH, Li J, Nath A, Blum J, He JJ. 2004. CD4-independent infection of astrocytes by human immunodeficiency virus type 1: requirement for the human mannose receptor. J Virol 78:4120-4133.
Lo J. 2011. Dyslipidemia and lipid management in HIV-infected patients. Curr Opin Endocrinol Diabetes Obes 18:144-147.
Loisel-Meyer S, et al. 2012. Glut1-mediated glucose transport regulates HIV infection. Proc Natl Acad Sci U S A 109:2549-2554.
Lopez GH, Ilincheta de Boschero MG, Castagnet PI, Giusto NM. 1995. Age-associated changes in the content and fatty acid composition of brain glycerophospholipids. Comp Biochem Physiol B Biochem Mol Biol 112:331-343.
Loreck DJ, Galarraga J, Van der Feen J, Phang JM, Smith BH, Cummins CJ. 1987. Regulation of the pentose phosphate pathway in human astrocytes and gliomas. Metab Brain Dis 2:31-46.
Luberto C, Haley JD, Del Poeta M. 2019. Imaging with mass spectrometry, the next frontier in sphingolipid research? A discussion on where we stand and the possibilities ahead. Chem Phys Lipids 219:1-14.
Lusic M, Marini B, Ali H, Lucic B, Luzzati R, Giacca M. 2013. Proximity to PML nuclear bodies regulates HIV-1 latency in CD4+ T cells. Cell Host Microbe 13:665-677.
Ly A, Ragionieri L, Liessem S, Becker M, Deininger SO, Neupert S, Predel R. 2019. Enhanced Coverage of Insect Neuropeptides in Tissue Sections by an Optimized Mass-Spectrometry-Imaging Protocol. Anal Chem 91:1980-1988.
Mahboobi SH, Javanpour AA, Mofrad MR. 2015. The interaction of RNA helicase DDX3 with HIV-1 Rev-CRM1-RanGTP complex during the HIV replication cycle. PLoS One 10:e0112969.
Malik S, Theis M, Eugenin EA. 2017. Connexin43 Containing Gap Junction Channels Facilitate HIV Bystander Toxicity: Implications in NeuroHIV. Front Mol Neurosci 10:404.
Margolis DM. 2011. Histone deacetylase inhibitors and HIV latency. Curr Opin HIV AIDS 6:25-29.
Marlink R. 1996. Lessons from the second AIDS virus, HIV-2. AIDS 10:689-699.
Martin N, Welsch S, Jolly C, Briggs JA, Vaux D, Sattentau QJ. 2010. Virological synapse-mediated spread of human immunodeficiency virus type 1 between T cells is sensitive to entry inhibition. J Virol 84:3516-3527.
Martinez AD, Saez JC. 1999. Arachidonic acid-induced dye uncoupling in rat cortical astrocytes is mediated by arachidonic acid byproducts. Brain Res 816:411-423.
Martinez E, et al. 2001. Risk of lipodystrophy in HIV-1-infected patients treated with protease inhibitors: a prospective cohort study. Lancet 357:592-598.
Masini E, et al. 2008. Ceramide: a key signaling molecule in a Guinea pig model of allergic asthmatic response and airway inflammation. J Pharmacol Exp Ther 324:548-557.
Massanella M, Yek C, Lada SM, Nakazawa M, Shefa N, Huang K, Richman DD. 2018. Improved assays to measure and characterize the inducible HIV reservoir. EBioMedicine 36:113-121.
Mbonye U, Karn J. 2014. Transcriptional control of HIV latency: cellular signaling pathways, epigenetics, happenstance and the hope for a cure. Virology 454-455:328-339.
McCutchan FE. 2006. Global epidemiology of HIV. J Med Virol 78 Suppl 1:S7-S12.
McNally GA. 2019. HIV and Cancer: An Overview of AIDS-Defining and Non-AIDS-Defining Cancers in Patients With HIV. Clin J Oncol Nurs 23:327-331.

Mdanda S, Ntshangase S, Singh SD, Naicker T, Kruger HG, Baijnath S, Govender T. 2019. Mass spectrometric investigations into the brain delivery of abacavir, stavudine and didanosine in a rodent model. Xenobiotica:1-10.
Menger RF, Stutts WL, Anbukumar DS, Bowden JA, Ford DA, Yost RA. 2012. MALDI mass spectrometric imaging of cardiac tissue following myocardial infarction in a rat coronary artery ligation model. Anal Chem 84:1117-1125.
Merrill AH, Jr., Schmelz EM, Dillehay DL, Spiegel S, Shayman JA, Schroeder JJ, Riley RT, Voss KA, Wang E. 1997. Sphingolipids--the enigmatic lipid class: biochemistry, physiology, and pathophysiology. Toxicol Appl Pharmacol 142:208-225.
Mesa-Herrera F, Taoro-Gonzalez L, Valdes-Baizabal C, Diaz M, Marin R. 2019. Lipid and Lipid Raft Alteration in Aging and Neurodegenerative Diseases: A Window for the Development of New Biomarkers. Int J Mol Sci 20.
Mitchell BI, Laws EI, Ndhlovu LC. 2019. Impact of Myeloid Reservoirs in HIV Cure Trials. Curr HIV/AIDS Rep 16:129-140.
Mocchetti I, Bachis A, Avdoshina V. 2012. Neurotoxicity of human immunodeficiency virus-1: viral proteins and axonal transport. Neurotox Res 21:79-89.
Mohamed M, Barker PB, Skolasky RL, Sacktor N. 2018. 7T Brain MRS in HIV Infection: Correlation with Cognitive Impairment and Performance on Neuropsychological Tests. AJNR Am J Neuroradiol 39:704-712.
Mohamed MA, Barker PB, Skolasky RL, Selnes OA, Moxley RT, Pomper MG, Sacktor NC. 2010. Brain metabolism and cognitive impairment in HIV infection: a 3-T magnetic resonance spectroscopy study. Magn Reson Imaging 28:1251-1257.
Mok HP, Lever AM. 2007. Chromatin, gene silencing and HIV latency. Genome Biol 8:228.
Moss AR, Bacchetti P. 1989. Natural history of HIV infection. AIDS 3:55-61.
Mourez T, Simon F, Plantier JC. 2013. Non-M variants of human immunodeficiency virus type 1. Clin Microbiol Rev 26:448-461.
Nakagawa F, May M, Phillips A. 2013. Life expectancy living with HIV: recent estimates and future implications. Curr Opin Infect Dis 26:17-25.
Nath A. 2002. Human immunodeficiency virus (HIV) proteins in neuropathogenesis of HIV dementia. J Infect Dis 186 Suppl 2:S193-198.
Nesbit CE, Schwartz SA. 2002. In vitro and animal models of human immunodeficiency virus infection of the central nervous system. Clin Diagn Lab Immunol 9:515-524.
Ntshangase S, Mdanda S, Naicker T, Kruger HG, Govender T, Baijnath S. 2019. Rilpivirine as a potential candidate for the treatment of HIV-associated neurocognitive disorders (HAND). J Mol Histol 50:295-303.
Ojo JO, Algamal M, Leary P, Abdullah L, Mouzon B, Evans JE, Mullan M, Crawford F. 2018. Disruption in Brain Phospholipid Content in a Humanized Tau Transgenic Model Following Repetitive Mild Traumatic Brain Injury. Front Neurosci 12:893.
Okafo G, Prevedel L, Eugenin E. 2017. Tunneling nanotubes (TNT) mediate long-range gap junctional communication: Implications for HIV cell to cell spread. Sci Rep 7:16660.
Okazaki T, Bielawska A, Bell RM, Hannun YA. 1990. Role of ceramide as a lipid mediator of 1 alpha,25-dihydroxyvitamin D3-induced HL-60 cell differentiation. J Biol Chem 265:15823-15831.
Oliveira MF, et al. 2017. Early Antiretroviral Therapy Is Associated with Lower HIV DNA Molecular Diversity and Lower Inflammation in Cerebrospinal Fluid but Does Not Prevent

the Establishment of Compartmentalized HIV DNA Populations. PLoS Pathog 13:e1006112.
Olsen ASB, Faergeman NJ. 2017. Sphingolipids: membrane microdomains in brain development, function and neurological diseases. Open Biol 7.
Orellana JA, Saez JC, Bennett MV, Berman JW, Morgello S, Eugenin EA. 2014. HIV increases the release of dickkopf-1 protein from human astrocytes by a Cx43 hemichannel-dependent mechanism. J Neurochem 128:752-763.
Padmapriyadarsini C, et al. 2017. Factors affecting high-density lipoprotein cholesterol in HIV-infected patients on nevirapine-based antiretroviral therapy. Indian J Med Res 145:641-650.
Paine MRL, Liu J, Huang D, Ellis SR, Trede D, Kobarg JH, Heeren RMA, Fernandez FM, MacDonald TJ. 2019. Three-Dimensional Mass Spectrometry Imaging Identifies Lipid Markers of Medulloblastoma Metastasis. Sci Rep 9:2205.
Palacios-Prado N, et al. 2013. Intracellular magnesium-dependent modulation of gap junction channels formed by neuronal connexin36. J Neurosci 33:4741-4753.
Palmer CS, et al. 2014. Increased glucose metabolic activity is associated with CD4+ T-cell activation and depletion during chronic HIV infection. AIDS 28:297-309.
Park ES, Lee JH, Hong JH, Park YK, Lee JW, Lee WJ, Lee JW, Kim KP, Kim KH. 2014. Phosphatidylcholine alteration identified using MALDI imaging MS in HBV-infected mouse livers and virus-mediated regeneration defects. PLoS One 9:e103955.
Park JY, Pillinger MH, Abramson SB. 2006. Prostaglandin E2 synthesis and secretion: the role of PGE2 synthases. Clin Immunol 119:229-240.
Pasternak AO, Berkhout B. 2018. What do we measure when we measure cell-associated HIV RNA. Retrovirology 15:13.
Pau AK, George JM. 2014. Antiretroviral therapy: current drugs. Infect Dis Clin North Am 28:371-402.
Paulick MG, Bertozzi CR. 2008. The glycosylphosphatidylinositol anchor: a complex membrane-anchoring structure for proteins. Biochemistry 47:6991-7000.
Pence BD, Yarbro JR. 2018. Aging impairs mitochondrial respiratory capacity in classical monocytes. Exp Gerontol 108:112-117.
Perelson AS, Essunger P, Cao Y, Vesanen M, Hurley A, Saksela K, Markowitz M, Ho DD. 1997. Decay characteristics of HIV-1-infected compartments during combination therapy. Nature 387:188-191.
Persaud D, Gay H, Ziemniak C, Chen YH, Piatak M, Jr., Chun TW, Strain M, Richman D, Luzuriaga K. 2013. Absence of detectable HIV-1 viremia after treatment cessation in an infant. N Engl J Med 369:1828-1835.
Petersen RC, et al. 2016. Association of Elevated Amyloid Levels With Cognition and Biomarkers in Cognitively Normal People From the Community. JAMA Neurol 73:85-92.
Petravic J, Rasmussen TA, Lewin SR, Kent SJ, Davenport MP. 2017. Relationship between Measures of HIV Reactivation and Decline of the Latent Reservoir under Latency-Reversing Agents. J Virol 91.
Pidoux G, Gerbaud P, Dompierre J, Lygren B, Solstad T, Evain-Brion D, Tasken K. 2014. A PKA-ezrin-Cx43 signaling complex controls gap junction communication and thereby trophoblast cell fusion. J Cell Sci 127:4172-4185.
Pinzone MR, O'Doherty U. 2018. Measuring integrated HIV DNA ex vivo and in vitro provides insights about how reservoirs are formed and maintained. Retrovirology 15:22.

Pomerantz RJ. 2004. Effects of HIV-1 Vpr on neuroinvasion and neuropathogenesis. DNA Cell Biol 23:227-238.
Posse de Chaves E, Sipione S. 2010. Sphingolipids and gangliosides of the nervous system in membrane function and dysfunction. FEBS Lett 584:1748-1759.
Prevedel L, Ruel N, Castellano P, Smith C, Malik S, Villeux C, Bomsel M, Morgello S, Eugenin EA. 2019. Identification, Localization, and Quantification of HIV Reservoirs Using Microscopy. Curr Protoc Cell Biol 82:e64.
Prideaux B, ElNaggar MS, Zimmerman M, Wiseman JM, Li X, Dartois V. 2015a. Mass spectrometry imaging of levofloxacin distribution in TB-infected pulmonary lesions by MALDI-MSI and continuous liquid microjunction surface sampling. Int J Mass Spectrom 377:699-708.
Prideaux B, et al. 2015b. The association between sterilizing activity and drug distribution into tuberculosis lesions. Nat Med 21:1223-1227.
Procopio FA, et al. 2015. A Novel Assay to Measure the Magnitude of the Inducible Viral Reservoir in HIV-infected Individuals. EBioMedicine 2:874-883.
Puebla C, Retamal MA, Acuna R, Saez JC. 2017. Regulation of Connexin-Based Channels by Fatty Acids. Front Physiol 8:11.
Purohit V, Rapaka R, Shurtleff D. 2011. Drugs of abuse, dopamine, and HIV-associated neurocognitive disorders/HIV-associated dementia. Mol Neurobiol 44:102-110.
Radmark O, Samuelsson B. 2009. 5-Lipoxygenase: mechanisms of regulation. J Lipid Res 50 Suppl:S40-45.
Ramadan S, Lin A, Stanwell P. 2013. Glutamate and glutamine: a review of in vivo MRS in the human brain. NMR Biomed 26:1630-1646.
Rash JE, Yasumura T, Dudek FE, Nagy JI. 2001. Cell-specific expression of connexins and evidence of restricted gap junctional coupling between glial cells and between neurons. J Neurosci 21:1983-2000.
Real F, Sennepin A, Arrigucci R, Zhu A, Sannier G, Zheng J, Xu L, Massé JM, Greffe S, Cazabat M, Donoso M, Delobel P, Izopet J, Eugenin EA, Gennaro ML, Rouveix E, Cramer Bordé E, Bomsel M. In press. Platelets from cART-suppressed HIV-infected patients with poor CD4+ T cell recovery carry infectious HIV. Science Translational Medicine.
Reeves JD, Piefer AJ. 2005. Emerging drug targets for antiretroviral therapy. Drugs 65:1747-1766.
Retamal MA, Cortes CJ, Reuss L, Bennett MV, Saez JC. 2006. S-nitrosylation and permeation through connexin 43 hemichannels in astrocytes: induction by oxidant stress and reversal by reducing agents. Proc Natl Acad Sci U S A 103:4475-4480.
Rodriguez-Sinovas A, Ruiz-Meana M, Denuc A, Garcia-Dorado D. 2018. Mitochondrial Cx43, an important component of cardiac preconditioning. Biochim Biophys Acta Biomembr 1860:174-181.
Roth MJ, Schwartzberg PL, Goff SP. 1989. Structure of the termini of DNA intermediates in the integration of retroviral DNA: dependence on IN function and terminal DNA sequence. Cell 58:47-54.
Rouach N, Avignone E, Meme W, Koulakoff A, Venance L, Blomstrand F, Giaume C. 2002. Gap junctions and connexin expression in the normal and pathological central nervous system. Biol Cell 94:457-475.

Royal W, 3rd, Zhang L, Guo M, Jones O, Davis H, Bryant JL. 2012. Immune activation, viral gene product expression and neurotoxicity in the HIV-1 transgenic rat. J Neuroimmunol 247:16-24.
Ru W, Tang SJ. 2017. HIV-associated synaptic degeneration. Mol Brain 10:40.
Russell RA, Chojnacki J, Jones DM, Johnson E, Do T, Eggeling C, Padilla-Parra S, Sattentau QJ. 2017. Astrocytes Resist HIV-1 Fusion but Engulf Infected Macrophage Material. Cell Rep 18:1473-1483.
Sadowski I, Hashemi FB. 2019. Strategies to eradicate HIV from infected patients: elimination of latent provirus reservoirs. Cell Mol Life Sci 76:3583-3600.
Sailasuta N, et al. 2012. Change in brain magnetic resonance spectroscopy after treatment during acute HIV infection. PLoS One 7:e49272.
Sami Saribas A, Cicalese S, Ahooyi TM, Khalili K, Amini S, Sariyer IK. 2017. HIV-1 Nef is released in extracellular vesicles derived from astrocytes: evidence for Nef-mediated neurotoxicity. Cell Death Dis 8:e2542.
Sanford R, Fernandez Cruz AL, Scott SC, Mayo NE, Fellows LK, Ances BM, Collins DL. 2017. Regionally Specific Brain Volumetric and Cortical Thickness Changes in HIV-Infected Patients in the HAART Era. J Acquir Immune Defic Syndr 74:563-570.
Sathekge M, McFarren A, Dadachova E. 2014. Role of nuclear medicine in neuroHIV: PET, SPECT, and beyond. Nucl Med Commun 35:792-796.
Saylor D, Dickens AM, Sacktor N, Haughey N, Slusher B, Pletnikov M, Mankowski JL, Brown A, Volsky DJ, McArthur JC. 2016. HIV-associated neurocognitive disorder--pathogenesis and prospects for treatment. Nat Rev Neurol 12:234-248.
Scheller C, et al. 2010. Increased dopaminergic neurotransmission in therapy-naive asymptomatic HIV patients is not associated with adaptive changes at the dopaminergic synapses. J Neural Transm (Vienna) 117:699-705.
Schmitt S, Castelvetri LC, Simons M. 2015. Metabolism and functions of lipids in myelin. Biochim Biophys Acta 1851:999-1005.
Schober Y, Guenther S, Spengler B, Rompp A. 2012. High-resolution matrix-assisted laser desorption/ionization imaging of tryptic peptides from tissue. Rapid Commun Mass Spectrom 26:1141-1146.
Schousboe A, Waagepetersen HS. 2005. Role of astrocytes in glutamate homeostasis: implications for excitotoxicity. Neurotox Res 8:221-225.
Schwamborn K, Caprioli RM. 2010. Molecular imaging by mass spectrometry--looking beyond classical histology. Nat Rev Cancer 10:639-646.
Schwartz C, Bouchat S, Marban C, Gautier V, Van Lint C, Rohr O, Le Douce V. 2017. On the way to find a cure: Purging latent HIV-1 reservoirs. Biochem Pharmacol 146:10-22.
Seeley EH, Caprioli RM. 2008. Molecular imaging of proteins in tissues by mass spectrometry. Proc Natl Acad Sci U S A 105:18126-18131.
Seneviratne HK, Hendrix CW, Fuchs EJ, Bumpus NN. 2018. MALDI Mass Spectrometry Imaging Reveals Heterogeneous Distribution of Tenofovir and Tenofovir Diphosphate in Colorectal Tissue of Subjects Receiving a Tenofovir-Containing Enema. J Pharmacol Exp Ther 367:40-48.
Sengupta S, Siliciano RF. 2018. Targeting the Latent Reservoir for HIV-1. Immunity 48:872-895.
Sharp PM, Hahn BH. 2011. Origins of HIV and the AIDS pandemic. Cold Spring Harb Perspect Med 1:a006841.

Shaw GM, Hunter E. 2012. HIV transmission. Cold Spring Harb Perspect Med 2.
Shi W, Zhou L, Peng X, Ren H, Wang Q, Shan F, Zhang Z, Liu L, Shi Y. 2019. HIV-infected patients with opportunistic pulmonary infections misdiagnosed as lung cancers: the clinicoradiologic features and initial application of CT radiomics. J Thorac Dis 11:2274-2286.
Shugars DC, Wild CT, Greenwell TK, Matthews TJ. 1996. Biophysical characterization of recombinant proteins expressing the leucine zipper-like domain of the human immunodeficiency virus type 1 transmembrane protein gp41. J Virol 70:2982-2991.
Sickmann HM, Schousboe A, Fosgerau K, Waagepetersen HS. 2005. Compartmentation of lactate originating from glycogen and glucose in cultured astrocytes. Neurochem Res 30:1295-1304.
Siliciano JD, Kajdas J, Finzi D, Quinn TC, Chadwick K, Margolick JB, Kovacs C, Gange SJ, Siliciano RF. 2003. Long-term follow-up studies confirm the stability of the latent reservoir for HIV-1 in resting CD4+ T cells. Nat Med 9:727-728.
Simon F, Mauclere P, Roques P, Loussert-Ajaka I, Muller-Trutwin MC, Saragosti S, Georges-Courbot MC, Barre-Sinoussi F, Brun-Vezinet F. 1998. Identification of a new human immunodeficiency virus type 1 distinct from group M and group O. Nat Med 4:1032-1037.
Soderberg M, Edlund C, Kristensson K, Dallner G. 1991. Fatty acid composition of brain phospholipids in aging and in Alzheimer's disease. Lipids 26:421-425.
Solan JL, Lampe PD. 2007. Key connexin 43 phosphorylation events regulate the gap junction life cycle. J Membr Biol 217:35-41.
Sorgen PL, Trease AJ, Spagnol G, Delmar M, Nielsen MS. 2018. Protein(-)Protein Interactions with Connexin 43: Regulation and Function. Int J Mol Sci 19.
Souza SJ, Luzia LA, Santos SS, Rondo PH. 2013. Lipid profile of HIV-infected patients in relation to antiretroviral therapy: a review. Rev Assoc Med Bras (1992) 59:186-198.
Stein J, Storcksdieck Genannt Bonsmann M, Streeck H. 2016. Barriers to HIV Cure. HLA 88:155-163.
Stoffel W, Bosio A. 1997. Myelin glycolipids and their functions. Curr Opin Neurobiol 7:654-661.
Straub AC, et al. 2011. Compartmentalized connexin 43 s-nitrosylation/denitrosylation regulates heterocellular communication in the vessel wall. Arterioscler Thromb Vasc Biol 31:399-407.
Suh J, et al. 2014. Progressive increase in central nervous system immune activation in untreated primary HIV-1 infection. J Neuroinflammation 11:199.
Sundquist WI, Krausslich HG. 2012. HIV-1 assembly, budding, and maturation. Cold Spring Harb Perspect Med 2:a006924.
Svicher V, Ceccherini-Silberstein F, Antinori A, Aquaro S, Perno CF. 2014. Understanding HIV compartments and reservoirs. Curr HIV/AIDS Rep 11:186-194.
Takahashi T, Suzuki T. 2012. Role of sulfatide in normal and pathological cells and tissues. J Lipid Res 53:1437-1450.
Tan NK, Carrington D, Pope CF. 2018. Verification of the Roche cobas((R)) 6800 PCR 200 microl and 500 microl protocols for the quantification of HIV-1 RNA, HBV DNA and HCV RNA and evaluation with COBAS((R)) Ampliprep/COBAS((R)) TaqMan((R)) assays. J Med Microbiol 67:1711-1717.

Tedaldi EM, Minniti NL, Fischer T. 2015. HIV-associated neurocognitive disorders: the relationship of HIV infection with physical and social comorbidities. Biomed Res Int 2015:641913.
Tekeste SS, Wilkinson TA, Weiner EM, Xu X, Miller JT, Le Grice SF, Clubb RT, Chow SA. 2015. Interaction between Reverse Transcriptase and Integrase Is Required for Reverse Transcription during HIV-1 Replication. J Virol 89:12058-12069.
Thevenin AF, Kowal TJ, Fong JT, Kells RM, Fisher CG, Falk MM. 2013. Proteins and mechanisms regulating gap-junction assembly, internalization, and degradation. Physiology (Bethesda) 28:93-116.
Thevenin AF, Margraf RA, Fisher CG, Kells-Andrews RM, Falk MM. 2017. Phosphorylation regulates connexin43/ZO-1 binding and release, an important step in gap junction turnover. Mol Biol Cell 28:3595-3608.
Thomas T, Jordan K, Simek J, Shao Q, Jedeszko C, Walton P, Laird DW. 2005. Mechanisms of Cx43 and Cx26 transport to the plasma membrane and gap junction regeneration. J Cell Sci 118:4451-4462.
Thompson KA, Cherry CL, Bell JE, McLean CA. 2011. Brain cell reservoirs of latent virus in presymptomatic HIV-infected individuals. Am J Pathol 179:1623-1629.
Timilsina U, Gaur R. 2016. Modulation of apoptosis and viral latency - an axis to be well understood for successful cure of human immunodeficiency virus. J Gen Virol 97:813-824.
Tomaras GD, Haynes BF. 2009. HIV-1-specific antibody responses during acute and chronic HIV-1 infection. Curr Opin HIV AIDS 4:373-379.
Ton H, Xiong H. 2013. Astrocyte Dysfunctions and HIV-1 Neurotoxicity. J AIDS Clin Res 4:255.
Turner BG, Summers MF. 1999. Structural biology of HIV. J Mol Biol 285:1-32.
Urbanelli L, Buratta S, Tancini B, Sagini K, Delo F, Porcellati S, Emiliani C. 2019. The Role of Extracellular Vesicles in Viral Infection and Transmission. Vaccines (Basel) 7.
Valcour VG, et al. 2013. HIV DNA reservoir increases risk for cognitive disorders in cART-naive patients. PLoS One 8:e70164.
Vallari A, et al. 2011. Confirmation of putative HIV-1 group P in Cameroon. J Virol 85:1403-1407.
Valle-Casuso JC, et al. 2019. Cellular Metabolism Is a Major Determinant of HIV-1 Reservoir Seeding in CD4(+) T Cells and Offers an Opportunity to Tackle Infection. Cell Metab 29:611-626 e615.
van den Dries L, Claassen MAA, Groothuismink ZMA, van Gorp E, Boonstra A. 2017. Immune activation in prolonged cART-suppressed HIV patients is comparable to that of healthy controls. Virology 509:133-139.
van der Windt GJ, Chang CH, Pearce EL. 2016. Measuring Bioenergetics in T Cells Using a Seahorse Extracellular Flux Analyzer. Curr Protoc Immunol 113:3 16B 11-13 16B 14.
van Meer G, Voelker DR, Feigenson GW. 2008. Membrane lipids: where they are and how they behave. Nat Rev Mol Cell Biol 9:112-124.
Van Zijl PC, Barker PB. 1997. Magnetic resonance spectroscopy and spectroscopic imaging for the study of brain metabolism. Ann N Y Acad Sci 820:75-96.
Vance JE, Steenbergen R. 2005. Metabolism and functions of phosphatidylserine. Prog Lipid Res 44:207-234.
Vanhamel J, Bruggemans A, Debyser Z. 2019. Establishment of latent HIV-1 reservoirs: what do we really know? J Virus Erad 5:3-9.

Vassallo M, et al. 2013. Relevance of lipopolysaccharide levels in HIV-associated neurocognitive impairment: the Neuradapt study. J Neurovirol 19:376-382.
Vejar S, Oyarzun JE, Retamal MA, Ortiz FC, Orellana JA. 2019. Connexin and Pannexin-Based Channels in Oligodendrocytes: Implications in Brain Health and Disease. Front Cell Neurosci 13:3.
Velasquez S, Prevedel L, Valdebenito S, Gorska AM, Golovko M, Khan N, Geiger J, Eugenin EA. 2019. Circulating levels of ATP is a biomarker of HIV cognitive impairment. EBioMedicine:102503.
Vigneswaran S, Rojas JH, Garvey L, Taylor-Robinson S, Winston A. 2015. Differences in the variability of cerebral proton magnetic resonance spectroscopy (1H-MRS) measurements within three HIV-infected cohorts. Neuroradiol J 28:545-554.
Villanelo F, Escalona Y, Pareja-Barrueto C, Garate JA, Skerrett IM, Perez-Acle T. 2017. Accessing gap-junction channel structure-function relationships through molecular modeling and simulations. BMC Cell Biol 18:5.
Visseaux B, Damond F, Matheron S, Descamps D, Charpentier C. 2016. Hiv-2 molecular epidemiology. Infect Genet Evol 46:233-240.
von Bartheld CS, Bahney J, Herculano-Houzel S. 2016. The search for true numbers of neurons and glial cells in the human brain: A review of 150 years of cell counting. J Comp Neurol 524:3865-3895.
Wall ME, Otey C, Qi J, Banes AJ. 2007. Connexin 43 is localized with actin in tenocytes. Cell Motil Cytoskeleton 64:121-130.
Wallace DR. 2006. HIV neurotoxicity: potential therapeutic interventions. J Biomed Biotechnol 2006:65741.
Wang GJ, Chang L, Volkow ND, Telang F, Logan J, Ernst T, Fowler JS. 2004. Decreased brain dopaminergic transporters in HIV-associated dementia patients. Brain 127:2452-2458.
Williams DW, Eugenin EA, Calderon TM, Berman JW. 2012. Monocyte maturation, HIV susceptibility, and transmigration across the blood brain barrier are critical in HIV neuropathogenesis. J Leukoc Biol 91:401-415.
Williams DW, Veenstra M, Gaskill PJ, Morgello S, Calderon TM, Berman JW. 2014. Monocytes mediate HIV neuropathogenesis: mechanisms that contribute to HIV associated neurocognitive disorders. Curr HIV Res 12:85-96.
Wong JK, Yukl SA. 2016. Tissue reservoirs of HIV. Curr Opin HIV AIDS 11:362-370.
Wright PW, Heaps JM, Shimony JS, Thomas JB, Ances BM. 2012. The effects of HIV and combination antiretroviral therapy on white matter integrity. AIDS 26:1501-1508.
Xicota L, et al. 2019. Multi-omics signature of brain amyloid deposition in asymptomatic individuals at-risk for Alzheimer's disease: The INSIGHT-preAD study. EBioMedicine 47:518-528.
Yamada E, Yoshikawa R, Nakano Y, Misawa N, Koyanagi Y, Sato K. 2015. Impacts of humanized mouse models on the investigation of HIV-1 infection: illuminating the roles of viral accessory proteins in vivo. Viruses 7:1373-1390.
Yang HC, et al. 2009. Small-molecule screening using a human primary cell model of HIV latency identifies compounds that reverse latency without cellular activation. J Clin Invest 119:3473-3486.
Yeager M, Nicholson BJ. 1996. Structure of gap junction intercellular channels. Curr Opin Struct Biol 6:183-192.

Yilmaz A, Blennow K, Hagberg L, Nilsson S, Price RW, Schouten J, Spudich S, Underwood J, Zetterberg H, Gisslen M. 2017. Neurofilament light chain protein as a marker of neuronal injury: review of its use in HIV-1 infection and reference values for HIV-negative controls. Expert Rev Mol Diagn 17:761-770.
Yin H, et al. 2013. Role of mitochondria in programmed cell death mediated by arachidonic acid-derived eicosanoids. Mitochondrion 13:209-224.
Young AC, Yiannoutsos CT, Hegde M, Lee E, Peterson J, Walter R, Price RW, Meyerhoff DJ, Spudich S. 2014. Cerebral metabolite changes prior to and after antiretroviral therapy in primary HIV infection. Neurology 83:1592-1600.
Yu RK, Tsai YT, Ariga T, Yanagisawa M. 2011. Structures, biosynthesis, and functions of gangliosides--an overview. J Oleo Sci 60:537-544.
Yuan L, Liu A, Qiao L, Sheng B, Xu M, Li W, Chen D. 2015. The relationship of CSF and plasma cytokine levels in HIV infected patients with neurocognitive impairment. Biomed Res Int 2015:506872.
Yuan L, Wei F, Zhang X, Guo X, Lu X, Su B, Zhang T, Wu H, Chen D. 2017. Intercellular Adhesion Molecular-5 as Marker in HIV Associated Neurocognitive Disorder. Aging Dis 8:250-256.
Zaima N, Hayasaka T, Goto-Inoue N, Setou M. 2009. Imaging of metabolites by MALDI mass spectrometry. J Oleo Sci 58:415-419.
Zajonc DM, Kronenberg M. 2009. Carbohydrate specificity of the recognition of diverse glycolipids by natural killer T cells. Immunol Rev 230:188-200.
Zimmerman M, Blanc L, Chen PY, Dartois V, Prideaux B. 2018. Spatial Quantification of Drugs in Pulmonary Tuberculosis Lesions by Laser Capture Microdissection Liquid Chromatography Mass Spectrometry (LCM-LC/MS). J Vis Exp.